Computational and Mathematical Methods in Medicine

Mathematical Modeling and Control of Infectious Diseases

Lead Guest Editor: Gul Zaman
Guest Editors: Il H. Jung, Delfim F. M. Torres, and Anwar Zeb

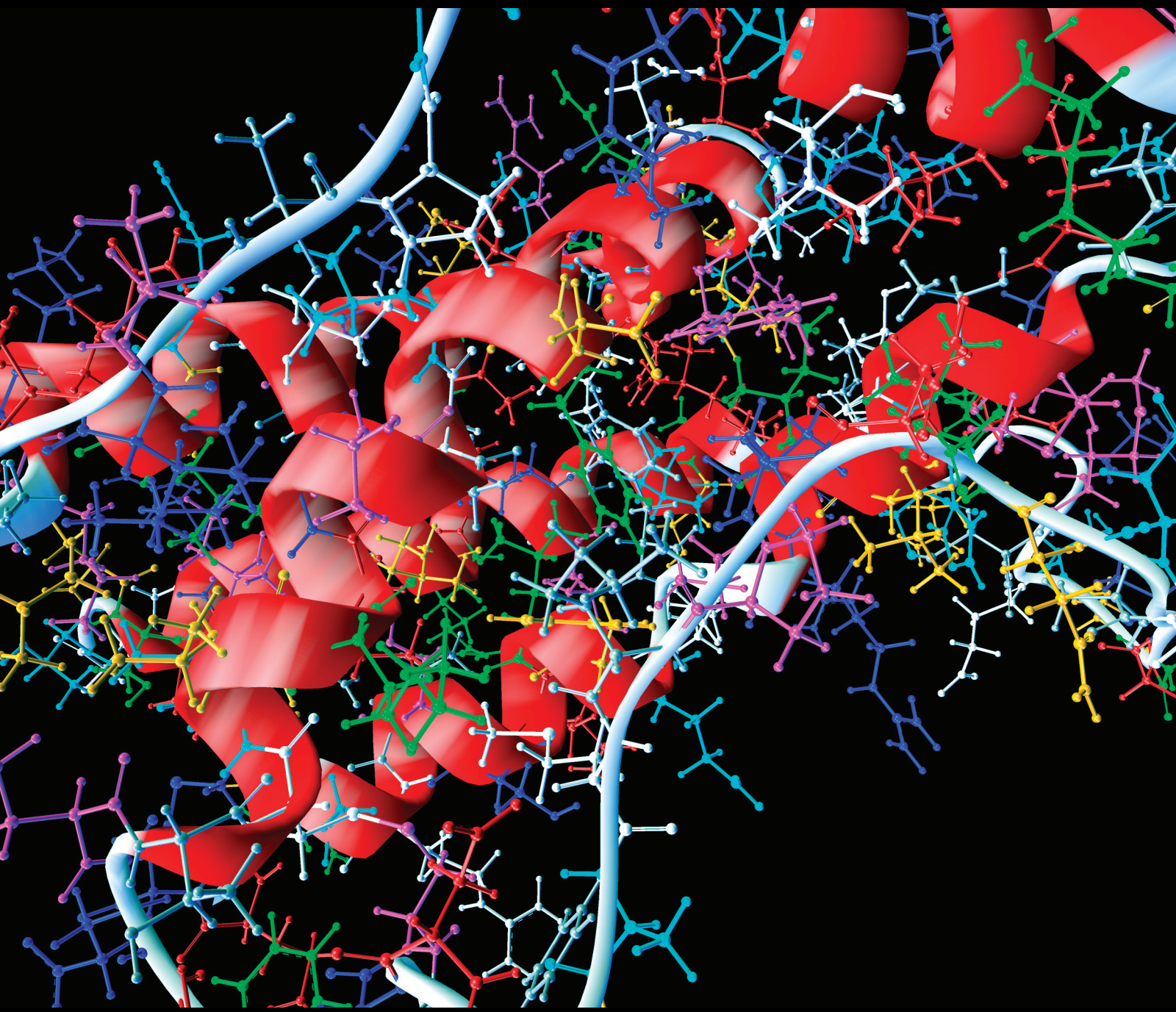

Mathematical Modeling and Control of Infectious Diseases

Computational and Mathematical Methods in Medicine

Mathematical Modeling and Control of Infectious Diseases

Lead Guest Editor: Gul Zaman
Guest Editors: Il H. Jung, Delfim F. M. Torres, and Anwar Zeb

Editorial Board

Contents

Hindawi
Computational and Mathematical Methods in Medicine
Volume 2017, Article ID 7149154, 1 page
https://doi.org/10.1155/2017/7149154

Editorial
Mathematical Modeling and Control of Infectious Diseases

Gul Zaman,[1] Il H. Jung,[2] Delfim F. M. Torres,[3] and Anwar Zeb[4]

[1]*Department of Mathematics, University of Malakand, Chakdara, Pakistan*
[2]*Department of Mathematics, Pusan National University, San 30, Busan 609-735, Republic of Korea*
[3]*Department of Mathematics and CIDMA, University of Aveiro, Aveiro, Portugal*
[4]*Department of Mathematics, COMSATS Institute of Information Technology, Abbottabad, Pakistan*

Correspondence should be addressed to Gul Zaman; gzaman@uom.edu.pk

Received 14 November 2017; Accepted 15 November 2017; Published 7 December 2017

Mathematical modeling has become a valuable tool for the analysis of dynamics of infectious disease and for the support of control strategies development in recent years. This work highlights the conceptual ideas and mathematical tools needed for infectious diseases modeling. The main convergence of this was on the dynamics of infectious diseases, the analysis of transmission patterns in various populations, and methods to assess the effectiveness of control strategies such as HIV, childhood infections, influenza, and vector borne infections. It was concerned with qualitative behaviors of infectious disease model. The qualitative behavior of model includes positivity, uniqueness, local stability, global stability, bifurcation analysis, control of diseases, and existence of solutions. This study provided a platform for the discussion of the major research challenges and achievements on qualitative behaviors of infectious diseases and their control. Due to the availability of a lot of applications of this study, many authors contributed.

G. R. Phaijoo and D. B. Gurung demonstrated that dengue is spreading in new areas due to people movement. They considered a multipatch model to assess the impact of temperature and human movement on the transmission dynamics of dengue disease. Dynamics of vector and host populations are investigated with different human movement rates and different temperature levels.

N. Pipatsart et al. discussed adaptive random network models to describe human behavioral change during epidemics and performed stochastic simulations of SIR epidemic models on adaptive random networks.

C. Burgess et al. derived risk-based immunization by deployment to polio-endemic regions, which is sufficient to prevent transmission among both deployed and nondeployed US military populations.

T. Tilahun et al. analyzed a compartmental nonlinear deterministic mathematical model for the typhoid fever outbreak and optimal control strategies in a community with varying population.

L. Worden et al. extended an approximation technique of the long-term behavior of a supercritical stochastic epidemic model, using the WKB approximation and a Hamiltonian phase space, to the subcritical case.

S. Anis et al. discussed some of the genetic properties on the basis of algebra.

Finally, A. Miao et al. proposed a stochastic SIR model with vertical transmission and vaccination. They showed that large noise can lead to the extinction of infectious diseases, which is conducive to epidemic diseases control.

Gul Zaman
Il H. Jung
Delfim F. M. Torres
Anwar Zeb

Hindawi
Computational and Mathematical Methods in Medicine
Volume 2017, Article ID 1093045, 8 pages
https://doi.org/10.1155/2017/1093045

Research Article

Posterior Estimates of Dynamic Constants in HIV Transmission Modeling

Yingqing Chen,[1] Renee Dale,[2] Hongyu He,[3] and Quoc-Anh T. Le[3]

[1]*Fred Hutchinson Cancer Research Center, Seattle, WA, USA*
[2]*Department of Biological Sciences, Louisiana State University, Baton Rouge, LA 70803, USA*
[3]*Department of Mathematics, Louisiana State University, Baton Rouge, LA 70803, USA*

Correspondence should be addressed to Hongyu He; hhe@lsu.edu

Received 28 April 2017; Accepted 4 October 2017; Published 7 November 2017

Academic Editor: Anwar Zeb

In this paper, we construct a linear differential system in both continuous time and discrete time to model HIV transmission on the population level. The main question is the determination of parameters based on the posterior information obtained from statistical analysis of the HIV population. We call these parameters dynamic constants in the sense that these constants determine the behavior of the system in various models. There is a long history of using linear or nonlinear dynamic systems to study the HIV population dynamics or other infectious diseases. Nevertheless, the question of determining the dynamic constants in the system has not received much attention. In this paper, we take some initial steps to bridge such a gap. We study the dynamic constants that appear in the linear differential system model in both continuous and discrete time. Our computations are mostly carried out in Matlab.

1. Introduction

Patients infected with Human Immunodeficiency Virus (HIV) are very likely to develop Acquired Immunodeficiency Disease Syndrome- (AIDS-) related diseases that are usually fatal if not treated with effective antiretroviral therapies. Since the discovery of HIV in 1983, an efficacious vaccine is yet to be developed to fight the deadly virus. Although highly active antiretroviral therapies (HAART) invented in mid-1990s have saved millions of lives and deterred the disease progression of those infected, HIV infection remains a public health threat. Reducing the risk of HIV transmission is of top priority.

One particular challenge in HIV prevention is its long period of latency period. The average time of an HIV infected patient to become symptomatic with AIDS-related diseases can be more than 10 years [1]. In the sexual transmission of HIV, many of the HIV infected patients may not be aware of their HIV infection status, and the virus continues spreading to their HIV negative partners. Therefore, an in-depth understanding of HIV transmission is the key to successful HIV prevention.

HIV dynamics have long been studied in the field of mathematical epidemiology using linear and nonlinear models [2, 3]. The classic model in epidemiology is the SIR model, which considers the dynamics of the susceptible, infected, and recovered populations [4]. This model is not useful for HIV dynamics, as there is no recovered population. An extension of this is the SEIR model, which includes the population of individuals who are exposed but not yet infected. The period between exposure and infectiousness in HIV lasts about two to four weeks [1]. Since a recovered population does not exist, we can consider this period to have a negligible effect on population dynamics.

Hierarchical models are common in HIV modeling due to the high correlation between risky behavior and HIV incidence [5]. In this paper we will incorporate risk indirectly by considering diagnosed and undiagnosed populations. Intuitively, diagnosed individuals would modify their behavior relative to their behavior prior to the diagnosis.

In this paper, we shall form two models: a continuous time linear differential model and a discrete time differential model. These models are the most fundamental among their

kinds. The focus will then be given to determination of the parameter estimates, the dynamic constants in these models. As we will show in this paper, the estimates of the dynamic constants depend on the type of model as well as the qualitative properties of the models.

There are two important dynamic constants in our model, namely, the transmission rates for diagnosed HIV population and for undiagnosed HIV population. One important finding in our study is that the transmission rates for the diagnosed and undiagnosed infected populations are comparable. This leads to our conclusion that the transmission rates should be attached to different groups of susceptibles based on their risk level.

2. General Nonlinear Differential Model

One of the frequently used mathematical models for HIV population dynamics can be described as follows. Let $S(t)$ be the susceptibles. We divide the HIV positive population into two groups: N_0 is the populations that are unaware of the infection; N_1 is the populations that are aware of the infection. Let ϵ_i be the mortality rate for the group N_i. Let r be the growth rate of the susceptibles. Let γ_0 be the transmission rate of N_0 group and let γ_1 be the transmission rate of N_1 group. Then we have the following nonlinear differential equations:

$$\begin{aligned}
\frac{dS(t)}{dt} &= S(t)\left(r - \gamma_0 N_0(t) - \gamma_1 N_1(t)\right);\\
\frac{dN_0(t)}{dt} &= \left(1-\beta\right)\gamma_1 N_1(t) S(t) + \gamma_0 N_0 S(t) - \delta N_0\\
&\quad - \epsilon_0 N_0;\\
\frac{dN_1(t)}{dt} &= \beta\gamma_1 N_1(t) S(t) + \delta N_0 - \epsilon_1 N_1.
\end{aligned} \tag{1}$$

Here $\gamma_1 N_1(t)S(t)$ counts for those who are infected by group N_1 (per unit time), and among them β is the proportion of those who are aware of their infection. The constant δ denotes the rate of the HIV positive population in N_0 group who become aware of their infection (per unit time). So there is a flow of $\delta N_0(t)$ from group N_0 to N_1 once a member from N_0 finds out his/her infection through HIV testing.

Many variations of this nonlinear dynamic model have been considered and appeared in the literature to study the HIV population dynamics. For example, in [6], mortality rate of the susceptibles is considered and appears in the differential equation of $S(t)$. In addition, the parameters are allowed to change but are *piecewise* constant.

In our differential equation model, we have a few constants: β, δ, γ_0, γ_1, ϵ_0, and ϵ_1. These constants essentially determine the qualitative and quantitative properties of the mathematical model. We shall call these constants the *dynamic constants* of the model. Notice that some of the constants, like γ_i, may have prior estimates, based on the data collected directly from the groups N_i and S. Some of the constants, like ϵ_i, will have posterior estimates. The constants δ, β may have prior estimates. Our main focus here is to give posterior estimates of these constants.

We shall remark here that the dynamic constants are model-dependent. This might not be obvious. Even though many of them can be estimated statistically without reference to any models, applying these estimates directly to the model may be problematic, as we shall see in the next section. In this paper, we take some initial steps to estimate the model-based dynamic constants.

3. Linear Differential Model and Preliminary Discussions

We shall now build a simpler linear model. The main assumption is that the susceptible population is a lot larger than N_0 and N_1. The change of susceptible population, due to HIV infection, is quite small, comparing with the overall size of susceptible. Therefore, we may ignore the dynamics of susceptible population, by assuming that the susceptible population is a constant. This more or less justifies the use of linear system only involving N_0 and N_1.

Let us start with the HIV transmission rate estimates by Pinkerton [7]. The estimates of transmission rates are

$$\begin{aligned}
\gamma_0 &\cong 0.0927,\\
\gamma_1 &\cong 0.0268.
\end{aligned} \tag{2}$$

γ_i are estimated in terms of infection transmitted per person per year. Since the overall susceptible population is a lot larger that N_i, we can assume that HIV transmission events are proportional to the size of N_1 and N_0. Based on this hypothesis, we may model HIV transmission by linear differential equations:

$$\begin{aligned}
\frac{dN_0}{dt} &= \left(1-\beta\right)\gamma_1 N_1 + \gamma_0 N_0 - \delta N_0 - \epsilon_0 N_0,\\
\frac{dN_1}{dt} &= \beta\gamma_1 N_1 + \delta N_0 - \epsilon_1 N_1.
\end{aligned} \tag{3}$$

The dynamic constants δ and β remain unchanged. It is also known that $\epsilon_1 \cong 1.9\%$ [8]. There is no statistics done on ϵ_0. So we can assume $\epsilon_0 \cong 1.9\%$ as well.

Next, we shall apply the known estimates and study our linear differential model. Notice that β remain unknown at this moment. According to [8], δ is somewhere around 1/4. We may tentatively set $\delta = 1/4$. Utilizing the estimates of dynamic constants directly from [7, 8], let us consider several cases.

3.1. $\beta = 4/5$. We start by assuming that β takes the value of the overall portion of those who are aware of their infection. Now we have the following linear equations:

$$\begin{aligned}
\frac{dN_0}{dt} &= \frac{0.0268}{5}N_1 + 0.0927N_0 - \frac{1}{4}N_0 - 0.019N_0.\\
\frac{dN_1}{dt} &= \frac{0.0268\times 4}{5}N_1 + \frac{1}{4}N_0 - 0.019N_1.
\end{aligned} \tag{4}$$

We found that the two linear independent solutions have growth rate of

$$\lambda_+ = 0.01,$$
$$\lambda_- = -0.18. \tag{5}$$

However, we know that the growth of $N_0 + N_1$ is about 0.048. Hence our assumption $\beta = \eta = 4/5$ is not valid. Even if we ignore the mortality rate, we have

$$\lambda_+ = 0.021,$$
$$\lambda_- = -0.16. \tag{6}$$

This is still far below the estimated 4.8% growth rate.

3.2. $\beta = 1$ or $\beta = 0$. One extreme is that $\beta = 1$, meaning that the population infected by N_1 gets tested and becomes aware of their infection (within the first year). We have

$$\frac{dN_0}{dt} = 0.0927N_0 - \frac{1}{4}N_0 - 0.019N_0,$$
$$\frac{dN_1}{dt} = 0.0268N_1 + \frac{1}{4}N_0 - 0.019N_1. \tag{7}$$

Under this assumption N_0 will decrease at the rate of −0.268, which means that the population N_0 will gradually vanish in a few years. This cannot be true.

Another extreme is that $\beta = 0$, meaning that the population infected by N_1 will be initially unaware of their infection (within the first year). We have

$$\frac{dN_0}{dt} = 0.0268N_1 + 0.0927N_0 - \frac{1}{4}N_0 - 0.019N_0,$$
$$\frac{dN_1}{dt} = \frac{1}{4}N_0 - 0.019N_1. \tag{8}$$

We have

$$\lambda_+ = 0.016,$$
$$\lambda_- = -0.211. \tag{9}$$

The overall HIV population growth will be less than 0.016. This is quite small comparing with the estimate that the growth rate is about 0.048.

3.3. δ, β Not Fixed. One might conclude that δ must be a much smaller number than 1/4, what we have initially assumed. We let δ and β be unfixed. In this case, we have

$$\frac{dN_0}{dt} = (0.0927 - \delta) N_0 + (1 - \beta)(0.0268) N_1 - 0.019N_0,$$
$$\frac{dN_1}{dt} = 0.0268\beta N_1 + \delta N_0 - 0.019N_1. \tag{10}$$

We have the matrix

$$A = \begin{pmatrix} 0.0927 - \delta - 0.019 & (0.0268)(1 - \beta) \\ \delta & 0.0268\beta - 0.019 \end{pmatrix}. \tag{11}$$

We know the growth rates are controlled by the eigenvalues of A. In particular, we might assume that $\det(A - \lambda) = 0$ with $\lambda = 0.048$. This will guarantee that the dominant term of the solution will grow at the rate of 0.048 (per year). Hence we obtain

$$(0.0257 - \delta)(0.0268\beta - 0.067) = 0.0268(1 - \beta)\delta. \tag{12}$$

Simplifying it, we have

$$1.56\delta + 0.0268\beta \cong 0.067. \tag{13}$$

Since $0 \le \beta \le 1$, we find that $0.043 \ge \delta \ge 0.0258$. This suggests that there are between 2% to 5% of N_0 getting tested. This percentage seems to be too low comparing with the CDC estimate of about 25%.

We shall remark that our discussion is based on the estimates that $\gamma_0 = 0.0927$ and $\gamma_1 = 0.0268$ [7]. As we have seen, directly using these estimates as dynamic constants in differential equation modeling will be inadequate to produce the right kind of outcomes and trend. In this paper, we shall discuss posterior estimate of parameters and hope to find some remedy.

4. Posterior Estimate of Parameters

In our earlier discussion, we directly insert the transmission rates from the statistical analysis into the linear differential system. The result is not satisfactory. It is desirable to estimate the transmission rates that will produce the right kind of outcome from the linear differential system model. Let us recall the CDC data from 2007 to 2013 (in thousands) [8].

We first simplify our notation. Let $\mathbf{N} = \binom{N_1}{N_0}$. We rewrite our linear system as

$$\frac{d\mathbf{N}}{dt} = \mathbf{M}\mathbf{N}(t), \tag{14}$$

where

$$\mathbf{M} = \begin{pmatrix} \beta\gamma_1 - \epsilon_1 & \delta \\ (1 - \beta)\gamma_1 & \gamma_0 - \delta - \epsilon_0 \end{pmatrix}. \tag{15}$$

The general solution to this system is

$$\mathbf{N}(t) = \mathbf{P} \exp \lambda_1 t + \mathbf{Q} \exp \lambda_2 t. \tag{16}$$

Here λ_1, λ_2 are eigenvalues of M. They can be both real or complex. There is also a degenerate case $\lambda_1 = \lambda_2$ that we do not treat here. The behavior of the linear differential system is quite different in these two cases. It is not surprising that we need to use two different methods to estimate the matrix $\mathbf{M}$.

4.1. λ_1, λ_2 Real: Simple Curve Fitting. We try a global optimization curve fitting using Matlab. We have

$$\mathbf{N}(t) = \begin{pmatrix} 14.12 \\ 79.86 \end{pmatrix} \exp -0.1919t + \begin{pmatrix} 892.3 \\ 115.57 \end{pmatrix} \exp 0.0273t. \tag{17}$$

Let $\mathbf{A} = \begin{pmatrix} 14.12 & 892.3 \\ 79.86 & 115.57 \end{pmatrix}$. Then

$$\mathbf{M} \cong \mathbf{A}\begin{pmatrix} -0.1919 & 0 \\ 0 & 0.0273 \end{pmatrix}\mathbf{A}^{-1} = \begin{pmatrix} 0.032 & -0.040 \\ 0.0291 & -0.197 \end{pmatrix}. \tag{18}$$

Notice that the dominant term $\begin{pmatrix} 892.3 \\ 115.57 \end{pmatrix} \exp 0.0273t$ suggested the overall rate of growth of HIV infected population grows at the rate close to 2.73%. This seems to be reasonable. But δ, the rate of flow of population from N_0 to N_1, is estimated at −4%. This is completely off the mark. One remedy is that we first estimate the dominant term and then estimate the remainder.

4.2. λ_1, λ_2 Real: Dominant Term Estimate. Suppose that $\lambda_2 < \lambda_1$. Then $\mathbf{P} \exp \lambda_1 t$ is the dominant term. We shall have

$$\|\mathbf{N}(t)\| \cong \|\mathbf{P}\| \exp \lambda_1 t. \tag{19}$$

Now

$$\|\mathbf{N}(t)\| = [947.3, 973.3, 997.1, 1021.1, 1044.3, 1069.4, 1092.5]. \tag{20}$$

Using curve $F(t) = ae^{\lambda t}$ to fit this data, we obtain

$$a = 927.7, \quad \lambda = 0.0236. \tag{21}$$

4.3. λ_1 Dominant, λ_2 Real. Now we can assume $\lambda_1 = 0.0236$ and use curve fitting to find λ_2, $\mathbf{P}$, and $\mathbf{Q}$. We have

$$\mathbf{P} = \begin{pmatrix} 922.1 \\ 115.9 \end{pmatrix}, \quad \mathbf{Q} = \begin{pmatrix} -20.4 \\ 77.6 \end{pmatrix}, \tag{22}$$

and $\lambda_2 = -0.172$, $\lambda_1 = 0.0236$. It follows that

$$\mathbf{M} = \begin{pmatrix} \beta\gamma_1 - \epsilon_1 & \delta \\ (1-\beta)\gamma_1 & \gamma_0 - \delta - \epsilon_0 \end{pmatrix} = \begin{pmatrix} 0.0173 & 0.0498 \\ 0.0238 & -0.1656 \end{pmatrix}. \tag{23}$$

We derive that $\gamma_1 - \epsilon_1 \cong 0.041$ and $\delta \cong 0.05$. These parameters seem to be reasonable. However, $\gamma_0 - \epsilon_0 = 0.0498 - 0.1656 = -0.1158$. Hence γ_0 will be a negative number which is not possible.

4.4. λ_1, λ_2 Complex with Fixed Real Part. Suppose that λ_1 and λ_2 are complex. Then λ_1 and λ_2 are conjugate to each other. In particular, the real part of λ, $\Re(\lambda_1) = \Re(\lambda_2)$ should be approximately 0.0236. Write $\lambda_1 = \lambda_0 + i\mu$. We should have

$$\mathbf{N}(t) = \mathbf{P} \exp \lambda_0 t \cos \mu t + \mathbf{Q} \exp \lambda_0 t \sin \mu t, \tag{24}$$

where μ is sometimes called a phase constant. A simple curve fitting shows that

$$\mathbf{P} = \begin{pmatrix} 904.12 \\ 182.7 \end{pmatrix}, \quad \mathbf{Q} = \begin{pmatrix} -117 \\ 420 \end{pmatrix} \tag{25}$$

and $\lambda_0 = 0.0236$ and $\mu = -0.017$. Hence

$$M \cong [\mathbf{P}, \mathbf{Q}]\begin{pmatrix} 0.0236 & 0.017 \\ -0.017 & 0.0236 \end{pmatrix}[\mathbf{P}, \mathbf{Q}]^{-1} = \begin{pmatrix} 0.0187 & 0.0325 \\ -0.0089 & -0.0285 \end{pmatrix}. \tag{26}$$

Let us see what this tells us. We have

$$\mathbf{M} = \begin{pmatrix} \beta\gamma_1 - \epsilon_1 & \delta \\ (1-\beta)\gamma_1 & \gamma_0 - \delta - \epsilon_0 \end{pmatrix} = \begin{pmatrix} 0.0187 & 0.0325 \\ -0.0089 & -0.0285 \end{pmatrix}, \tag{27}$$

$$\gamma_1 - \epsilon_1 = 0.0187 - 0.0089 \cong 0.01, \quad \gamma_0 - \epsilon_0 = 0.004, \quad \delta = 0.0325.$$

This roughly says that there are about 3.25% of N_0 that become aware of their infection every year. The annual transmission rate for N_1 is 2.9%. The annual transmission rate for N_0 is 2.3%.

4.5. λ_1, λ_2 Complex. We finally use Matlab global optimization to fit the data in the curve

$$\mathbf{N}(t) = \mathbf{P} \exp \lambda_0 t \cos \mu t + \mathbf{Q} \exp \lambda_0 t \sin \mu t. \tag{28}$$

We obtain $\lambda_0 = 0.0088$, $\mu = -0.036$,

$$\mathbf{P} = \begin{pmatrix} 902.4 \\ 184 \end{pmatrix}, \quad \mathbf{Q} = \begin{pmatrix} -476.3 \\ 149.5 \end{pmatrix}. \tag{29}$$

Hence we obtain the estimate

$$\mathbf{M} \cong \begin{pmatrix} 902.4 & -476.3 \\ 184 & 149.5 \end{pmatrix}\begin{pmatrix} 0.0088 & 0.036 \\ -0.036 & 0.0088 \end{pmatrix}\begin{pmatrix} 902.4 & -476.3 \\ 184 & 149.5 \end{pmatrix}^{-1} = \begin{pmatrix} -0.0065 & 0.1684 \\ -0.0091 & 0.0241 \end{pmatrix}. \tag{30}$$

Now we have

$$\begin{aligned} \beta\gamma_1 - \epsilon_1 &\cong -0.0065, \\ \delta &\cong 0.1684, \\ (1-\beta)\,\gamma_1 &\cong -0.0091, \\ \gamma_0 - \delta - \epsilon_0 &\cong 0.0241. \end{aligned} \tag{31}$$

It follows that

$$\begin{aligned} \gamma_1 &\cong \epsilon_1 - 0.0156 \cong 0.0034, \\ \gamma_0 &= 0.193 + \epsilon_1 \cong 0.21. \end{aligned} \tag{32}$$

So γ_1 is neglectable and γ_0 is about 21%. This again makes the model invalid.

4.6. Discussion. In this section, we choose dynamics constants to fit the temporal data. We have found that these dynamic constants depend on the qualitative properties of the model. Yet, none of the dynamic constants we choose match perfectly with the existing estimates. One reason is that yearly data is not suitable for a continuous time model. Therefore, we shall explore the discrete time model.

5. Discrete Dynamic Model

We may regard $\mathbf{N}_t$ $(t = 1, 2, 3, 4, 5, 6, 7)$ as a discrete time dynamical system. Let us assume that this discrete dynamics is defined by a transition matrix $\mathbf{T}$:

$$\mathbf{N}_{t+1} = \mathbf{T}\mathbf{N}_t. \tag{33}$$

In principle, based on our earlier discussion,

$$\mathbf{T} = \mathbf{I} + \begin{pmatrix} \beta\gamma_1 - \epsilon_1 & \delta \\ (1-\beta)\,\gamma_1 & \gamma_0 - \delta - \epsilon_0 \end{pmatrix}. \tag{34}$$

Now we would like to estimate $\mathbf{T}$.

5.1. Basic Estimates. The easiest way to find $\mathbf{T}$ is by considering the following matrix equations:

$$\left[\mathbf{N}_i \mathbf{N}_{i+1}\right] = \mathbf{T}\left[\mathbf{N}_{i-1}\mathbf{N}_i\right]. \tag{35}$$

For example, for $i = 2$, we will have

$$\begin{pmatrix} 956.9 & 982.4 \\ 178.1 & 170.6 \end{pmatrix} = \mathbf{T}\begin{pmatrix} 929.3 & 956.9 \\ 183.7 & 178.1 \end{pmatrix}. \tag{36}$$

Then we find the following estimate of $\mathbf{T}$:

$$\begin{gathered} \begin{pmatrix} 0.9775 & 0.2641 \\ -0.0370 & 1.1568 \end{pmatrix} \\ \begin{pmatrix} 1.0118 & 0.0800 \\ 0.0302 & 0.7959 \end{pmatrix} \\ \begin{pmatrix} 0.9922 & 0.1928 \\ 0.0370 & 0.7563 \end{pmatrix} \\ \begin{pmatrix} 1.0481 & -0.1482 \\ 0.0318 & 0.7880 \end{pmatrix} \\ \begin{pmatrix} 0.9427 & 0.5214 \\ 0.0639 & 0.5844 \end{pmatrix}. \end{gathered} \tag{37}$$

We can see some consistency among these transition matrices. For example, the $(2, 1)$-th entry has been around 3%. This translates into

$$(1-\beta)\,\gamma_1 \cong 3\%. \tag{38}$$

This is the rate of transmission for group N_1. It seems to be consistent with the estimate of [7].

5.2. (Arithmetic) Average Estimate of $\mathbf{T}$. Now we may average all $\mathbf{T}$'s and obtain

$$\mathbf{T} \cong \begin{pmatrix} 0.9945 & 0.1820 \\ 0.0252 & 0.8163 \end{pmatrix}. \tag{39}$$

Hence

$$\begin{aligned} \mathbf{M} &= \begin{pmatrix} \beta\gamma_1 - \epsilon_1 & \delta \\ (1-\beta)\,\gamma_1 & \gamma_0 - \delta - \epsilon_0 \end{pmatrix} \\ &= \begin{pmatrix} -0.0055 & 0.1820 \\ 0.0252 & -0.1837 \end{pmatrix}. \end{aligned} \tag{40}$$

Our estimate yields that $\delta \cong 18\%$; in other words, about 18% of those unaware of their infection will become aware of their infection next year. We also have

$$\gamma_0 - \epsilon_0 = \delta + (\gamma_0 - \delta - \epsilon_0) = -0.0017. \tag{41}$$

If the mortality rate ϵ_0 is set to be 0.019, then we have $\gamma_0 = 0.017$. Similarly, we have

$$\gamma_1 - \epsilon_1 = \beta\gamma_1 - \epsilon_1 + (1-\beta)\,\gamma_1 \cong 0.02. \tag{42}$$

If the mortality rate ϵ_1 is set to be 0.019, then we have $\gamma_1 = 0.039$. This suggests that the transmission rate of N_1 group is twice as large as the transmission rate of N_0 group. There may be some truth to it. However, we believe that this estimate is off the mark due to the reason that $[\mathbf{N}_i\mathbf{N}_{i+1}]$ are correlated with each other. Hence each estimate $\mathbf{T}$ will be biased. We shall correct this and give a more robust estimate later.

5.3. Least Square Estimate of **T**. Perhaps a good way to estimate **T** is the least square method. We write

$$\left[\mathbf{N}_2\mathbf{N}_3\cdots\mathbf{N}_7\right] = \mathbf{T}\left[\mathbf{N}_1\mathbf{N}_2\cdots\mathbf{N}_6\right]. \tag{43}$$

Applying the least square method, we find that the least square solution to **T** is

$$\begin{pmatrix} 1.0013 & 0.1406 \\ 0.0245 & 0.8350 \end{pmatrix}. \tag{44}$$

This estimate seems to be better than the arithmetic average, in the sense that, irregularities will have smaller effect on the least square solution. Because we can reorder $\mathbf{N}_i$'s and the least square solution does not change, we also avoid the pitfall that $\mathbf{N}_i$ and $\mathbf{N}_{i+1}$ are correlated. We have our posterior estimates:

$$\begin{aligned} \mathbf{M} &\cong \begin{pmatrix} \beta\gamma_1 - \epsilon_1 & \delta \\ (1-\beta)\gamma_1 & \gamma_0 - \delta - \epsilon_0 \end{pmatrix} \\ &= \begin{pmatrix} 0.0013 & 0.1406 \\ 0.0245 & -0.1650 \end{pmatrix}. \end{aligned} \tag{45}$$

This estimate is similar to the arithmetic average we just computed. The dynamic constant estimates will be very similar. We shall then look for a solution that is more robust. One particular reason that the least square estimate is not satisfactory is that there are additional relations like

$$\mathbf{N}_{i+k} = \mathbf{T}^k\mathbf{N}_i \tag{46}$$

that least square method does not take into consideration. In other words, $\mathbf{T}^2$, $\mathbf{T}^3$ can also be estimated and shall be taken into consideration when we estimate **T**. We shall offer one remedy that avoids this issue.

5.4. A More Robust Estimate. One of the problems with our estimate is that $\mathbf{N}_i$ and $\mathbf{N}_{t+1}$ are correlated to each other. As a remedy, we pick $\mathbf{N}_1$ and $\mathbf{N}_6$ as far from each other as possible. We observe that

$$\mathbf{T}\left[\mathbf{N}_1\mathbf{N}_6\right] = \left[\mathbf{N}_2\mathbf{N}_7\right]. \tag{47}$$

We compute

$$\mathbf{T} = \left[\mathbf{N}_2\mathbf{N}_7\right]\left[\mathbf{N}_1\mathbf{N}_6\right]^{-1} = \begin{pmatrix} 0.9965 & 0.1681 \\ 0.023 & 0.8533 \end{pmatrix}. \tag{48}$$

Then

$$\begin{aligned} \mathbf{M} &= \begin{pmatrix} \beta\gamma_1 - \epsilon_1 & \delta \\ (1-\beta)\gamma_1 & \gamma_0 - \delta - \epsilon_0 \end{pmatrix} \\ &\cong \begin{pmatrix} -0.0035 & 0.1681 \\ 0.023 & -0.1467 \end{pmatrix}. \end{aligned} \tag{49}$$

We have

$$\begin{aligned} \delta &\cong 0.1681, \\ \gamma_0 - \epsilon_0 &\cong 0.0214, \\ \gamma_1 - \epsilon_1 &\cong 0.0195. \end{aligned} \tag{50}$$

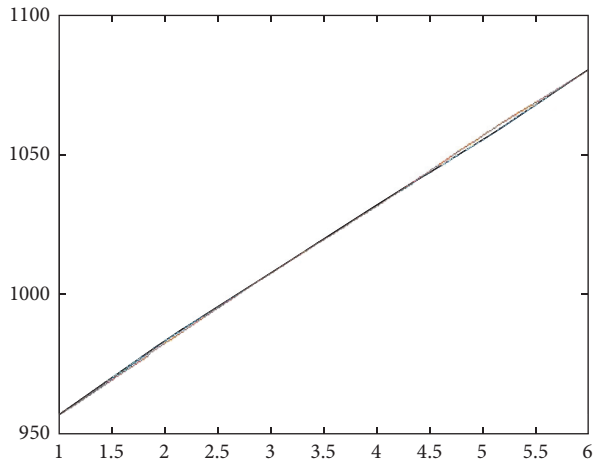

Figure 1: Comparison of $\mathbf{TN}_t$ and $\mathbf{N}_{t+1}$: N_1 group.

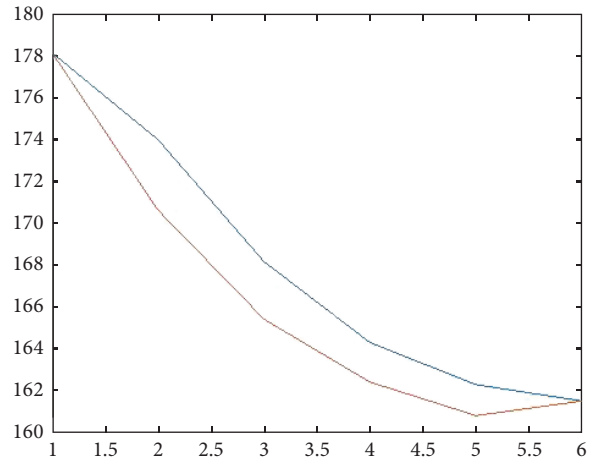

Figure 2: Comparison of $\mathbf{TN}_t$ and $\mathbf{N}_{t+1}$: N_0 group.

5.5. Discussion. This estimate of **M** is quite consistent with the least square estimate. Our estimate seems to suggest that the transmission rates for N_0 and N_1 may be in the similar range. By [8], assume that $\epsilon_0 = \epsilon_1 = 0.019$. We have

$$\begin{aligned} \gamma_1 &= 0.0385, \\ \gamma_0 &= 0.04, \\ \delta &= 0.185; \\ \beta &= \frac{\beta\gamma_1}{\gamma_1} = \frac{0.019 - 0.0035}{0.0385} = 0.4. \end{aligned} \tag{51}$$

Every year about 18.5% of those unaware of their HIV positiveness become aware of their infection due to testing. About 40% of those infected by N_1 group become aware of their infection. This seems to be consistent with some of the observations in [7], with one exception; namely, in our estimates, the transmission rates for N_1 and N_0 are very close. Figures 1 and 2 show the difference between $\mathbf{TN}_t$ and $\mathbf{N}_{t+1}$.

5.6. Arithmetic Average versus Geometric Average. Now we may state our problem in greater generality. Given a temporal

Table 1: Population of undiagnosed individuals with HIV from 2007 to 2013.

Year	Diagnosed	Undiagnosed	Percentage of total
2007	929.3	183.777	16.5
2008	956.9	178.1165	15.7
2009	982.4	170.6282	14.8
2010	1007.6	165.3507	14.1
2011	1031.6	162.4248	13.6
2012	1057.2	160.7760	13.2
2013	1080.5	161.46	13.0

Source: [8].

vector $\mathbf{N}(t)$, suppose that $\mathbf{N}(t+1) = \mathbf{T}\mathbf{N}(t)$ with transitional matrix $\mathbf{T}$. How should one estimate the matrix $\mathbf{T}$?

As we discussed earlier, we can use least squares with the equations

$$\mathbf{N}(t+1) = \mathbf{T}\mathbf{N}(t). \tag{52}$$

The least square estimate of $\mathbf{T}$, in some sense, is very similar to the arithmetic mean of the transitional matrix $\mathbf{T}$. But what makes better sense is a geometric mean. More precisely, we have to take into consideration that

$$\mathbf{N}(t+k) = \mathbf{T}^k\mathbf{N}(t). \tag{53}$$

Suppose that $\mathbf{T}_t$ is the transitional matrix at time t. Then a good estimate of $\mathbf{T}$ should be the "geometric average" of $\mathbf{T}_t$. For scalars, one can define the geometric average of $p_1, p_2, \ldots, p_n$ to be the nth root of $\prod p_i$. But matrix multiplications are not commutative and one cannot define the geometric average of matrices. It remains a challenging problem to define computationally a geometric mean of $\mathbf{T}_t$.

5.7. Roots Estimate. Tentatively, we may define the geometric mean by taking roots. For example, we may now consider

$$\mathbf{T}^2\left[\mathbf{N}_1\mathbf{N}_4\right] = \left[\mathbf{N}_3\mathbf{N}_6\right]. \tag{54}$$

Then

$$\mathbf{T} \cong \begin{pmatrix} 1.0038 & 0.1277 \\ 0.0228 & 0.8443 \end{pmatrix}, \qquad \mathbf{M} \cong \begin{pmatrix} 0.0038 & 0.1277 \\ 0.0228 & -0.1557 \end{pmatrix}. \tag{55}$$

We can also consider

$$\mathbf{T}^4\left[\mathbf{N}_1\mathbf{N}_3\right] = \left[\mathbf{N}_5\mathbf{N}_7\right]. \tag{56}$$

We have

$$\mathbf{T} = \begin{pmatrix} 1.0008 & 0.1430 \\ 0.0301 & 0.8011 \end{pmatrix}, \qquad \mathbf{M} \cong \begin{pmatrix} 0.0008 & 0.143 \\ 0.0301 & -0.2 \end{pmatrix}. \tag{57}$$

Both estimates of $\mathbf{T}$ are consistent with the least square estimate and the estimates in the previous section. Above all, all our estimates point to the same range of transmission rates for both N_0 and N_1.

6. Concluding Remarks

Now we shall compare our dynamic constant estimates in the linear differential model in continuous time and in discrete time.

In the continuous time model, we obtain the transmission rate ϵ_1 of about 4% for the N_1 group, those who were aware of their HIV infection. Nevertheless, δ the rate of flow from N_0 to N_1 due to HIV testing turned out to be too low and ϵ_0 often came out to be negative, which cannot be the case. The best results are obtained when we assume the two eigenvalues are complex. In this case

$$\gamma_1 \cong 0.029, \qquad \delta \cong 0.0325, \qquad \gamma_0 \cong 0.023. \tag{58}$$

Yet δ seems to be quite low. According to the CDC report [8], δ is estimated at about 25%.

There are various reasons why our dynamic constants are inconsistent with known estimates. Firstly, the CDC data we use tends to underestimate the N_0 and N_1 population sizes, particularly in more recent years. The CDC estimates the sizes of the populations infected with HIV by back calculation. The estimates for any given year will increase as new diagnoses are obtained. HIV may go undiagnosed for up to 10 years without causing the death of the patient (Table 1) [5]. Depending on the stage of the disease, the individual will be counted as undiagnosed for a number of years prior to the diagnosis. This causes the estimates of the population sizes to be smaller than the actual size of the population. A new estimate of the HIV prevalence agrees with this conclusion [9]. Although this new estimate is more conservative than the back calculation method, it may still underestimate the N_0 population. Both estimates show a downward trend in the data, but this is likely to be erased as more individuals are diagnosed in the later stages of the disease.

Secondly, our computations assume that the susceptible population is much larger than the infected population. However, failing to obtain the right estimates suggests that opposite may be true—the susceptible population could be much smaller. HIV infection is overrepresented in some subpopulations, such as men who have sex with men (MSM) [1]. This subpopulation is only about 5% of the US population, or approximately 15 million individuals. Not all MSM can

be considered to have equal risk of contracting the disease, and since over 1 million individuals are currently living with the disease, the susceptible population may be comparable to the size of the infected population. For this reason, any differential system model of the HIV transmission must include the susceptible population.

The discrete dynamics model seems to be most robust against the bias caused by back calculation and the size of the susceptibles. By ignoring the 2013 year's data, we are able to determine the transmission rates as

$$\begin{aligned} \gamma_1 &\cong 0.0385, \\ \gamma_0 &\cong 0.04. \end{aligned} \tag{59}$$

Also $\delta \cong 0.184$, not too different from the CDC estimate 0.25. We see that the dynamic constants in the discrete time model are less affected by the underestimation caused by back calculation. It is also true that the relative size of susceptibles has less effect on the discrete time model than on the continuous time model.

Finally, our estimates of the transmission rates for diagnosed and undiagnosed HIV population are relatively close. This is very different from the previous estimate, where the transmission rate of the undiagnosed population is about 4 times as high as the diagnosed population [7]. This implies that the transmission rates should be attached to the susceptible population. It makes sense to divide the susceptible population into groups depending on the possible transmission rates for them. We shall pursue this in a different paper.

Conflicts of Interest

The authors declare no conflicts of interest regarding the publication of this paper.

Acknowledgments

This research is partially supported by the NIH R01 Grant AI12125903.

References

[1] CDC HIV Risk Reduction Tool. https://wwwn.cdc.gov/hivrisk/what_is/stages_hiv_infection.html.

[2] R. M. Anderson and R. M. May, "Population biology of infectious diseases: part I," *Nature*, vol. 280, no. 5721, pp. 361–367, 1979.

[3] R. M. May and R. M. Anderson, "Population biology of infectious diseases: part II," *Nature*, vol. 280, no. 5722, pp. 455–461, 1979.

[4] W. O. Kermack and A. G. McKendrick, "A contribution to the mathematical theory of epidemics," *Proceedings of the royal society a: mathematical, physical and engineering sciences*, vol. 115, no. 772, p. 700, 1927.

[5] Centers for Disease Control and Prevention. HIV Surveillance Report, vol. 27. http://www.cdc.gov/hiv/library/reports/hiv-surveillance.html,2015.

[6] F. Bozkurt and F. Paker, "Mathematical Modelling of HIV epidemic and stability analysis," *Advances in Differential Equations*, vol. 95, 2014.

[7] S. D. Pinkerton, "HIV Transmission rate modeling: A primer, review, and extension," *AIDS and Behavior*, vol. 16, no. 4, pp. 791–796, 2012.

[8] Centers for Disease Control and Prevention, "Monitoring selected national HIV prevention and care objectives by using HIV surveillance data United States and 6 dependent areas," *HIV Surveillance Supplemental Report 2016*, vol. 4, 2014.

[9] R. Song, H. I. Hall, T. A. Green, C. L. Szwarcwald, and N. Pantazis, "Using CD4 Data to Estimate HIV Incidence, Prevalence, and Percent of Undiagnosed Infections in the United States," *Journal of Acquired Immune Deficiency Syndromes*, vol. 74, no. 1, pp. 3–9, 2017.

Hindawi
Computational and Mathematical Methods in Medicine
Volume 2017, Article ID 1747134, 9 pages
https://doi.org/10.1155/2017/1747134

Research Article

Modeling Impact of Temperature and Human Movement on the Persistence of Dengue Disease

Ganga Ram Phaijoo and Dil Bahadur Gurung

Department of Natural Sciences (Mathematics), School of Science, Kathmandu University, Dhulikhel, Kavre, Nepal

Correspondence should be addressed to Ganga Ram Phaijoo; gangaram@ku.edu.np

Received 15 April 2017; Revised 5 June 2017; Accepted 8 August 2017; Published 19 September 2017

Academic Editor: Gul Zaman

Dengue is a vector-borne infectious disease endemic in many parts of the world. The disease is spreading in new places due to human movement into the dengue disease supporting areas. Temperature is the major climatic factor which affects the biological processes of the mosquitoes and their interaction with the viruses. In the present work, we propose a multipatch model to assess the impact of temperature and human movement in the transmission dynamics of dengue disease. The work consists of system of ordinary differential equations that describe the transmission dynamics of dengue disease between humans and mosquitoes. Human population is divided into four classes: susceptible, exposed, infectious, and recovered. Mosquito population is divided into three classes: susceptible, exposed, and infectious. Basic reproduction number $\mathscr{R}_0$ of the model is obtained using Next-Generation Matrix method. The qualitative analysis of the model is made in terms of the basic reproduction number. Parameters used in the model are considered temperature dependent. Dynamics of vector and host populations are investigated with different human movement rates and different temperature levels. Numerical results show that proper management of human movement between patches helps reducing the burden of dengue disease. It is also seen that the temperature affects the transmission dynamics of the disease significantly.

1. Introduction

Dengue disease is a vector-borne viral infection that usually occurs in tropical and subtropical countries. Nowadays, the disease has been recognized in over 100 countries and an estimated 50–100 million dengue cases occur annually. The disease is threatening about 40% of the world's population [1]. The disease is transmitted by the bites of infected mosquitoes named *Aedes aegypti* and *Aedes albopictus*. Four serologically different viruses *DEN* 1–*DEN* 4 cause the disease. Infection from one serotype grants life-long immunity to that strain and also shows temporary cross-immunity to the others. However, ultimately the recovered patient will become more susceptible to the other three forms [2, 3]. We assume that the infectivity of the mosquitoes ends with their death since they have a short lifespan.

Mathematical modeling has become an interesting tool for the understanding of epidemic diseases and to propose strategies to control the transmission of the disease. In 1927, Kermack and McKendrick developed an SIR model to describe epidemic diseases [4]. The model is being followed by many researchers to investigate the transmission dynamics of infectious diseases with some modifications. Esteva and Vargas proposed the SIR model to address dengue disease transmission considering constant and variable human populations [5, 6]. Since then many mathematical models have been proposed to study different aspects of dengue disease transmission. Authors [7, 8] discussed the role of awareness in controlling dengue disease transmission. Pinho et al. used a mathematical model for dengue disease transmission analysis comparing two dengue epidemics [9]. Authors [10–14] focused on incubation period to study dengue disease transmission. Sardar et al. discussed a mathematical model of dengue disease transmission with memory. They incorporated memory in the model by using a fractional differential operator [15].

Dengue infections are sensitive to the climate. Changing climate factors affect the potential for the geographic spread and future dengue disease. One of the principal determinants of *Aedes* mosquitoes' survival is temperature which has been associated with seasonal changes. The temperature plays an important role in the life cycle and behavior of the mosquitoes. So, mathematical studies have been made to understand the role of temperature in transmission dynamics of dengue disease. Brady et al. modeled *Aedes aegypti* and *Aedes albopictus* survival at different temperature levels in laboratory and field settings [16]. Liu-Helmersson et al. studied the vectorial capacity of *Aedes aegypti* and made investigations on the effects of temperature and implications for global dengue epidemic potential [17]. Polwiang discussed the seasonal basic reproduction number of dengue and impacts of climate on transmission of the disease [18].

Travel and transport contribute to the spread of infectious diseases like dengue in new places. So, one of the major factors contributing to the reemergence of infectious diseases is human movement from one place to the other. They help the disease in expanding their geographic range. Many mathematical models are proposed to address the impact of movement of humans and dispersal of vectors in the transmission dynamics of infectious diseases. Wang and Zhao discussed an epidemic model in patchy environment to describe the dynamics of disease spread among patches due to population dispersal [19]. An epidemic model was proposed by Wang and Mulone to describe the dynamics of disease spread between two patches due to population dispersal. They proved that reproduction number is a threshold of the uniform persistence and disappearance of the disease [20]. Arino and van den Driessche gave some analytical results for a model that describes the propagation of a disease in a population of individuals who travel between n patches [21]. Hsieh et al. proposed a multipatch epidemic model to study the impact of travel of humans on the spread of disease between patches with different level of disease prevalence [22]. Cosner et al. investigated the effects of human movement on the persistence of vector-borne diseases [23]. Dynamics of malaria disease was studied in patchy environment by Auger et al. They generalized Ross-Macdonald model to n-patches to describe the transmission dynamics of the disease [24]. Lee and Castillo-Chavez [25] and Phaijoo and Gurung [26] discussed dengue disease transmission dynamics in patchy environment.

Temperature influences dengue disease dynamics by affecting dynamics of mosquitoes and vector host interactions. Dengue disease has been spreading rapidly to new areas via human movement. So, in the present work, we propose a multipatch SEIR-SEI model of dengue disease considering the temperature dependent model parameters to study the impact of temperature and movement of humans on the persistence of dengue disease. We have considered different temperature levels and different movement rates in different patches. Basic reproduction number of the individual patches and a combined basic reproduction number are computed. Local stability of disease-free equilibrium point is proved by basic reproduction number.

2. Model Description and Formulation

The total human (host) population in each patch is subdivided into the classes: susceptible S_i^h, exposed E_i^h, infectious I_i^h, and recovered R_i^h. Mosquito (vector) population is subdivided into the classes: susceptible S_i^v, exposed E_i^v, and infectious I_i^v, $i = 1, 2, 3, \ldots, n$. Recovered class in the mosquito population is not considered due to their short lifespan.

The recruitment rate of host population is A_i^h. Susceptible hosts get infected by infectious vectors at the rate $b_i\beta_i^h I_i^v/N_i^h$, where b_i is the biting rate and β_i^h is the transmission probability from vector to host. The exposed host becomes infectious at the rate ν_i^h after developing the symptoms. Infectious host recovers at the rate γ_i^h. Host dies naturally with the rate d_i^h. In case of vector population, susceptible vector gets infected by interaction with infectious hosts at the rate $b_i\beta_i^v I_i^h/N_i^h$. The exposed vector becomes infectious at the rate ν_i^v developing the symptoms of the disease. d_i^v is the natural death rate of vectors.

Here, the model parameters b_i, β_i^h, β_i^v, d_i^v, and ν_i^v are temperature dependent. The temperature dependency relations are discussed below [17, 18]:

$$
\begin{aligned}
&b_i(T) = 0.0043T + 0.0943 \quad \left(21^\circ\mathrm{C} \le T \le 32^\circ\mathrm{C}\right),\\
&\beta_i^v(T) = \begin{cases} 0.0729T - 0.9037 & \left(12.4^\circ\mathrm{C} \le T \le 26.1^\circ\mathrm{C}\right),\\ 1, & \left(26.1^\circ\mathrm{C} < T < 32.5^\circ\mathrm{C}\right),\end{cases}\\
&\beta_i^h(T) = 0.001044T(T - 12.286)\sqrt{32.461 - T},\\
&\qquad\qquad \left(12.286^\circ\mathrm{C} < T < 32.461^\circ\mathrm{C}\right),\\
&\nu_i^v(T) = 4 + e^{5.15 - 0.123T}, \quad \left(12^\circ\mathrm{C} < T < 36^\circ\mathrm{C}\right),\\
&d_i^v(T) = 0.8692 - 0.159T + 0.01116T^2 - 3.408\times 10^{-4}T^3\\
&\qquad + 3.809\times 10^{-6}T^4, \quad \left(10.54^\circ\mathrm{C} \le T \le 33.41^\circ\mathrm{C}\right).
\end{aligned}
\tag{1}
$$

We consider human movement between the patches. Human of patch i moves to patch j at the rate m_{ji}^C and the human of patch j moves to patch i at the rate m_{ij}^C. Here $i, j = 1, 2, 3, \ldots, n$ and C represents S, E, I, and R, respectively for susceptible, exposed, infectious, and recovered human movement rates.

The system of ordinary differential equations describing the present multipatch model [22] is given by

$$
\begin{aligned}
\frac{dS_i^h}{dt} &= A_i^h - \frac{b_i\beta_i^h}{N_i^h}S_i^h I_i^v + \sum_{j=1}^{n} m_{ij}^S S_j^h - \sum_{j=1}^{n} m_{ji}^S S_i^h - d_i^h S_i^h,\\
\frac{dE_i^h}{dt} &= \frac{b_i\beta_i^h}{N_i^h}S_i^h I_i^v + \sum_{j=1}^{n} m_{ij}^E E_j^h - \sum_{j=1}^{n} m_{ji}^E E_i^h\\
&\quad - \left(\nu_i^h + d_i^h\right)E_i^h,
\end{aligned}
$$

$$\begin{aligned}
\frac{dI_i^h}{dt} &= \nu_i^h E_i^h + \sum_{j=1}^{n} m_{ij}^I I_j^h - \sum_{j=1}^{n} m_{ji}^I I_i^h - \left(\gamma_i^h + d_i^h\right) I_i^h,\\
\frac{dR_i^h}{dt} &= \gamma_i^h I_i^h + \sum_{j=1}^{n} m_{ij}^R R_j^h - \sum_{j=1}^{n} m_{ji}^R R_i^h - d_i^h R_i^h,\\
\frac{dS_i^v}{dt} &= A_i^v - \frac{b_i \beta_i^v}{N_i^h} S_i^v I_i^h - d_i^v S_i^v,\\
\frac{dE_i^v}{dt} &= \frac{b_i \beta_i^v}{N_i^h} S_i^v I_i^h - \left(\nu_i^v + d_i^v\right) E_i^v,\\
\frac{dI_i^v}{dt} &= \nu_i^v E_i^v - d_i^v I_i^v,\\
&\qquad \left(i, j = 1, 2, 3, \ldots, n,\ i \neq j\right),
\end{aligned} \tag{2}$$

where

$$\begin{aligned}
&S_i^h(t) + E_i^h + I_i^h(t) + R_i^h(t) = N_i^h(t),\\
&\left(\text{Total host population of patch } i \text{ in time } t\right),\\
&S_i^v(t) + E_i^v + I_i^v(t) = N_i^v(t),\\
&\left(\text{Total vector population of patch } i \text{ in time } t\right).
\end{aligned} \tag{3}$$

3. Equilibrium Point and Stability Analysis

In this section, we find disease-free equilibrium (DFE) of the system of (2) and discuss its stability. An equilibrium is said to be disease-free if there is no infective population in both host and vector populations.

Theorem 1. *Model (2) has a unique disease-free equilibrium.*

Proof. In disease-free situation, $S_i^h = S_i^{h*} > 0$, $S_i^v = S_i^{v*} > 0$ and other variables $E_i^h = 0$, $E_i^v = 0$, $I_i^h = 0$, $I_i^v = 0$, and $R_i^h = 0$ for $i = 1, 2, 3, \ldots, n$.

System of (2) for host population in disease-free situation can be written as

$$XS^{h*} = A^h, \tag{4}$$

where

$$X = \operatorname{diag}\left(d_i^h + \sum_{j=1}^{n} m_{ji}^S\right) - M^S,$$

$$M^S = \begin{bmatrix} 0 & m_{12}^S & \cdots & m_{1n}^S \\ m_{21}^S & 0 & \cdots & m_{2n}^S \\ \vdots & \vdots & \ddots & \vdots \\ m_{n1}^S & m_{n2}^S & \cdots & 0 \end{bmatrix},$$

$$A^h = \left[A_1^h, A_2^h, \ldots, A_n^h\right]^T,$$

$$S^h = \left[S_1^{h*}, S_2^{h*}, \ldots, S_n^{h*}\right]^T. \tag{5}$$

System of (2) for vector population in disease-free situation can be written as

$$YS^{v*} = A^v, \tag{6}$$

where

$$\begin{aligned}
Y &= \operatorname{diag}\left(d_i^v\right),\\
S^v &= \left[S_1^{v*}, S_2^{v*}, \ldots, S_n^{v*}\right]^T,\\
A^v &= \left[A_1^v, A_2^v, \ldots, A_n^v\right]^T.
\end{aligned} \tag{7}$$

Since the matrix X has all off-diagonal entries negative and each column sum is positive, X is nonsingular M-matrix. Matrix X is irreducible as the matrix has nonzero diagonal elements. So, X must have positive inverse [27]. Hence, the system of (4) has a unique solution $S^{h*} = X^{-1}A^h > 0$.

Again, matrix Y is a diagonal matrix with positive diagonal elements. So, Y^{-1} exists with positive diagonal elements. Hence, the system of (6) has a unique solution $S^{v*} = Y^{-1}A^v$ and system (2) has a unique disease-free equilibrium. □

Basic Reproduction Number. When a typical infective is introduced into a completely susceptible population, the expected number of new infections produced by this single infective during its infectious period is called basic reproduction number.

To find the mathematical expression for the basic reproduction number, we order the variables related to the infections by $E_1^h, E_2^h, \ldots, E_n^h, E_1^v, E_2^v, \ldots, E_n^v, I_1^h, I_2^h, \ldots, I_n^h, I_1^v, I_2^v, \ldots, I_n^v$. We use Next-Generation Matrix method [28, 29] to find transmission matrix, F, and transition matrix, V, and we find basic reproduction number $\mathscr{R}_0$ as

$$\mathscr{R}_0 = \rho\left\{FV^{-1}\right\}. \tag{8}$$

For the system of (2),

$$F = \begin{bmatrix} 0 & 0 & 0 & \operatorname{diag}\left(\dfrac{b_i \beta_i^h}{N_i^h} S_i^{h*}\right) \\ 0 & 0 & \operatorname{diag}\left(\dfrac{b_i \beta_i^h}{N_i^h} S_i^{v*}\right) & 0 \\ 0 & 0 & 0 & 0 \\ 0 & 0 & 0 & 0 \end{bmatrix}, \tag{9}$$

$$V = \begin{bmatrix} V_{11} & 0 & 0 & 0 \\ 0 & V_{22} & 0 & 0 \\ V_{31} & 0 & V_{33} & 0 \\ 0 & V_{42} & 0 & V_{44} \end{bmatrix}.$$

Here,

$$V_{11} = \begin{bmatrix} \sum_{j\neq 1} m_{j1}^E + \nu_1^h + d_1^h & -m_{12}^E & \cdots & -m_{1n}^E \\ -m_{21}^E & \sum_{j\neq 2} m_{j2}^E + \nu_2^h + d_2^h & \cdots & -m_{2n}^E \\ \vdots & \vdots & \ddots & \vdots \\ -m_{n1}^E & -m_{n2}^E & \cdots & \sum_{j\neq n} m_{jn}^E + \nu_n^h + d_n^h \end{bmatrix},$$

$$V_{22} = \operatorname{diag}\left(\nu_i^v + d_i^v\right),$$

$$V_{31} = \operatorname{diag}\left(-\nu_i^h\right),$$

$$V_{33} = \begin{bmatrix} \sum_{j\neq 1} m_{j1}^I + \gamma_1^h + d_1^h & -m_{12}^I & \cdots & -m_{1n}^I \\ -m_{21}^I & \sum_{j\neq 2} m_{j2}^I + \gamma_2^h + d_2^h & \cdots & -m_{2n}^I \\ \vdots & \vdots & \ddots & \vdots \\ -m_{n1}^I & -m_{n2}^I & \cdots & \sum_{j\neq n} m_{jn}^I + \gamma_n^h + d_n^h \end{bmatrix},$$

$$V_{42} = \operatorname{diag}\left(-\nu_i^v\right),$$

$$V_{44} = \operatorname{diag}\left(d_i^v\right). \tag{10}$$

Matrices V_{11} and V_{33} are irreducible nonnegative M-matrices. So, V_{11}^{-1} and V_{33}^{-1} exist. Also, V_{22}, V_{31}, V_{42}, and V_{44} are diagonal matrices. So, their inverses exist. Hence, V^{-1} exists and basic reproduction number, $\mathscr{R}_0$, is given by

$$\mathscr{R}_0 = \rho\left\{FV^{-1}\right\}. \tag{11}$$

Theorem 2 (local stability). *The disease-free equilibrium point of the system of (2) is locally asymptotically stable if $\mathscr{R}_0 < 1$ and unstable if $\mathscr{R}_0 > 1$.*

Proof. Jacobian matrix for the system of (2) at disease-free equilibrium is given by

$$\zeta = \begin{bmatrix} A & B \\ 0 & F - V \end{bmatrix}. \tag{12}$$

Matrix ζ is triangular matrix. So, the stability of the system of (2) depends on matrices A and $F-V$. Matrix A can be written as

$$A = \begin{bmatrix} -X & 0 \\ 0 & -Y \end{bmatrix}. \tag{13}$$

Matrices X and Y (defined in Theorem 1) are nonsingular M-matrices. So, the matrix A has eigenvalues with negative real parts [27]. Hence, the stability of model (2) depends on the matrix $F - V$ only. Here, matrix F is nonnegative matrix and V is a nonsingular M-matrix. So, the matrix will have eigenvalues with negative real parts if $\rho\{FV^{-1}\} < 1$ [29]; that is, $\mathscr{R}_0 < 1$. Thus, the disease-free equilibrium is locally asymptotically stable if $\mathscr{R}_0 < 1$. If $\mathscr{R}_0 > 1$, then $s(F-V) > 0$. Which shows that at least one eigenvalue lies in right half plane. So, the disease-free equilibrium is unstable if $\mathscr{R}_0 > 1$. □

When only the two patches are taken into the consideration, the basic reproduction $\mathscr{R}_0$ is given by

$$\mathscr{R}_0 = \sqrt{\frac{1}{2}\left(m_1\mathscr{R}_{01}^2 + m_2\mathscr{R}_{02}^2\right) + \frac{1}{2}\sqrt{\left(m_1\mathscr{R}_{01}^2 + m_2\mathscr{R}_{02}^2\right)^2 - 4m_3\mathscr{R}_{01}^2\mathscr{R}_{02}^2}}, \tag{14}$$

where

$$\mathscr{R}_{01} = \sqrt{\frac{b_1^2 S_1^{h*} S_1^{v*} \beta_1^h \beta_1^v \nu_1^h \nu_1^v}{d_1^v N_1^{h^2}\left(d_1^h + m_{21}^I + \gamma_1^h\right)\left(d_1^h + m_{21}^E + \nu_1^h\right)\left(d_1^v + \nu_1^v\right)}},$$

$$\mathscr{R}_{02} = \sqrt{\frac{b_2^2 S_2^{h*} S_2^{v*} \beta_2^h \beta_2^v \nu_2^h \nu_2^v}{d_2^v N_2^{h^2}\left(d_2^h + m_{12}^I + \gamma_2^h\right)\left(d_2^h + m_{12}^E + \nu_2^h\right)\left(d_2^v + \nu_2^v\right)}},$$

$$m_1 = \frac{g_1 n_1\left(m_{12}^I m_{21}^E \nu_2^h + \nu_1^h g_2 n_2\right)}{\nu_1^h\left(-m_{12}^I m_{21}^I + g_1 g_2\right)\left(-m_{12}^E m_{21}^E + n_1 n_2\right)},$$

$$m_2 = \frac{g_2 n_2\left(m_{12}^E m_{21}^I \nu_1^h + g_1 n_1 \nu_2^h\right)}{\nu_2^h\left(-m_{12}^I m_{21}^I + g_1 g_2\right)\left(-m_{12}^E m_{21}^E + n_1 n_2\right)},$$

$$m_3 = \frac{g_1 n_1 g_2 n_2}{\left(m_{12}^I \nu_1^h + g_3 d_2^h + g_3 \gamma_2^h + g_2 d_1^h\right)\left(m_{12}^E \nu_1^h + n_3 d_2^h + n_3 \nu_2^h + n_2 d_1^h\right)},$$

$$g_1 = d_1^h + m_{21}^I + \gamma_1^h,$$

$$g_2 = d_2^h + m_{12}^I + \gamma_2^h,$$

$$g_3 = m_{21}^I + \gamma_1^h$$

$$n_1 = d_1^h + m_{21}^E + \nu_1^h,$$

$$n_2 = d_2^h + m_{21}^E + \nu_2^h,$$

$$n_3 = m_{21}^E + \nu_1^h. \tag{15}$$

Here, $\mathscr{R}_{01}$ is the basic reproduction number of patch 1 and $\mathscr{R}_{02}$ is the basic reproduction number of patch 2.

4. Simulations and Discussion

Temperature plays a significant role in the transmission dynamics of dengue disease. Small change in temperature can affect whole dynamics of the disease. Human movement from one place to the other helps spreading disease into new areas and influences the prevalence of the disease. Thus, both temperature and human movement have a significant influence on the transmission dynamics of dengue disease.

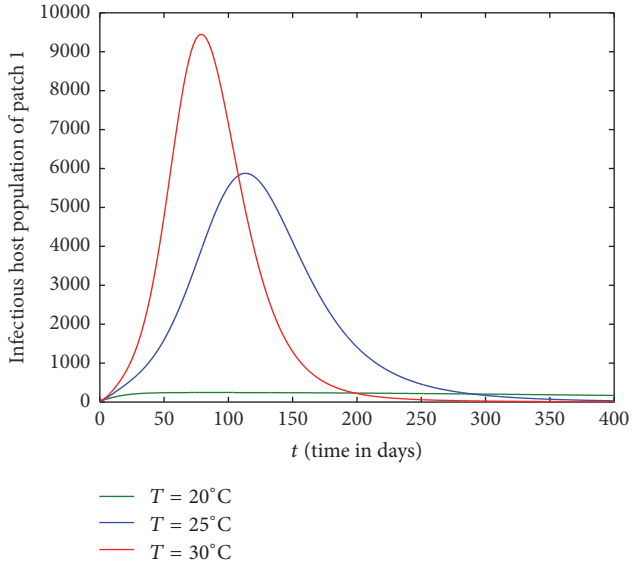

Figure 1: Dynamics of infectious hosts of patch 1 without host movement between the patches.

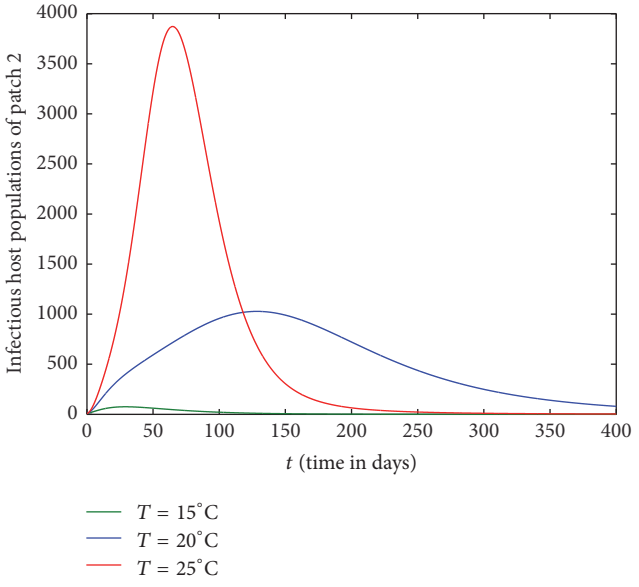

Figure 2: Dynamics of infectious hosts of patch 2 without host movement between the patches.

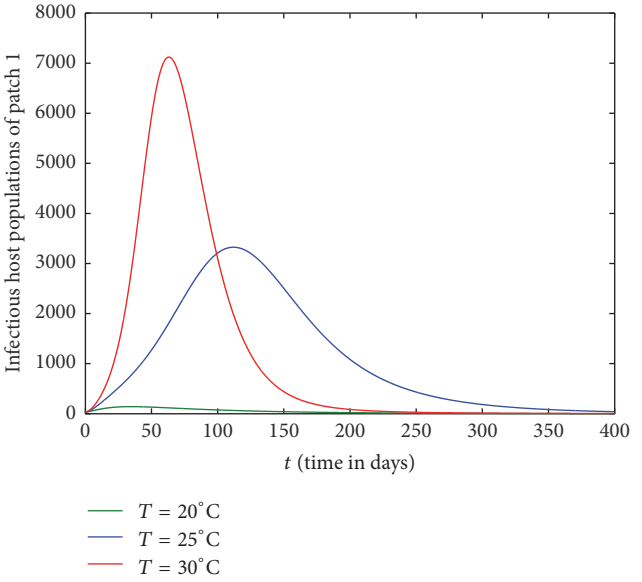

Figure 3: Dynamics of infectious hosts of patch 1 with host movement between patches.

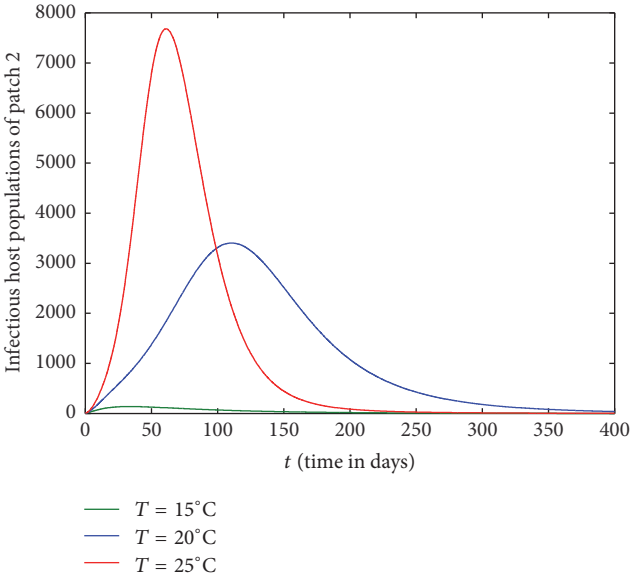

Figure 4: Dynamics of infectious hosts of patch 2 with host movement between patches.

For the simulation purpose, the following data are used: $N_1^h = 50000, d_1^h = d_2^h = 0.00004029, \nu_1^h = \nu_1^h = 0.1667, \gamma_1^h = \gamma_2^h = 0.0714, N_2^h = 20000$. The parameters b_i, β_i^h, β_i^v, d_i^v, ν_i^v are considered temperature dependent following [17].

Figures 1–4 are drawn with different temperature levels to investigate the dynamics of infectious hosts of patch 1 and patch 2. Figures 1 and 2 are drawn when there is no human movement between the patches. Here, patch 1 is high disease prevalent compared to patch 2. With the human movement, it is seen that infectious host population is decreased in patch 1 and the population is increased in patch 2. Thus, the human movement can cause the low endemic patch to be high endemic and high endemic patch to be low endemic patch (Figures 1–4). Also, the figures show that the burden of disease is increased with temperature. Again, the number of infectious hosts is seen increasing initially due to interaction of hosts with infectious vectors. Afterwards the number is seen decreased due to recovery from the disease and natural death of hosts (Figures 1–4).

Figures 5 and 6 show the impact of movement of infectious and susceptible hosts, respectively, on basic reproduction number $\mathcal{R}_0$. Infectious host can infect the mosquitoes of

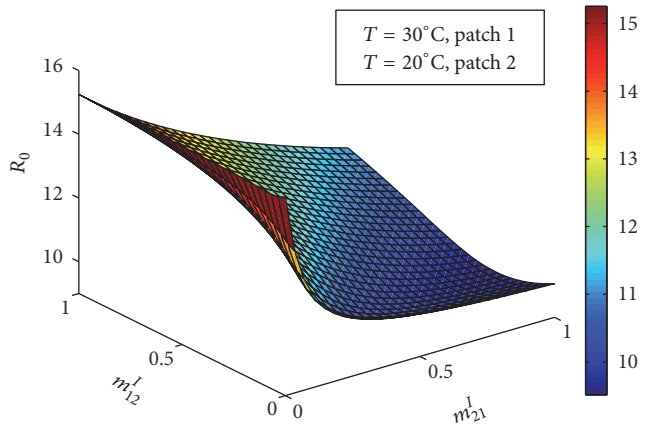

Figure 5: Combined basic reproduction number against m^I_{21} and m^I_{12}.

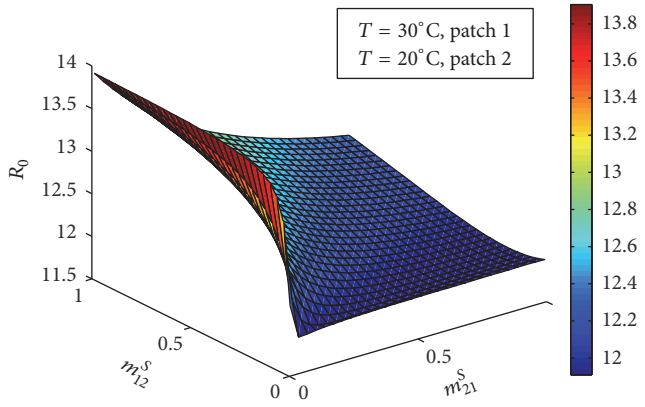

Figure 6: Combined basic reproduction number against m^S_{21} and m^S_{12}.

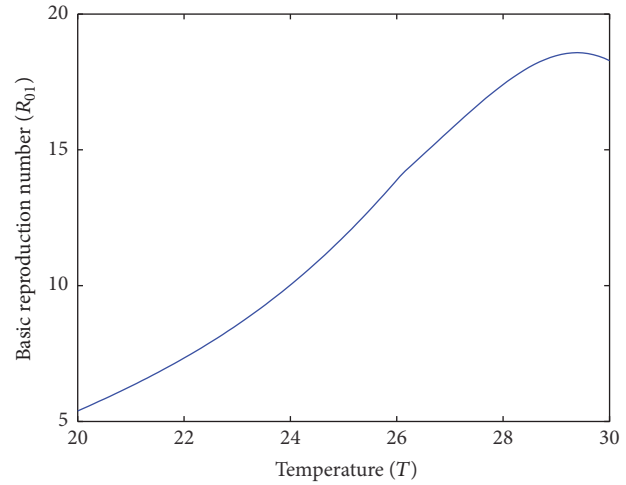

Figure 7: Basic reproduction number of patch 1 without host movement.

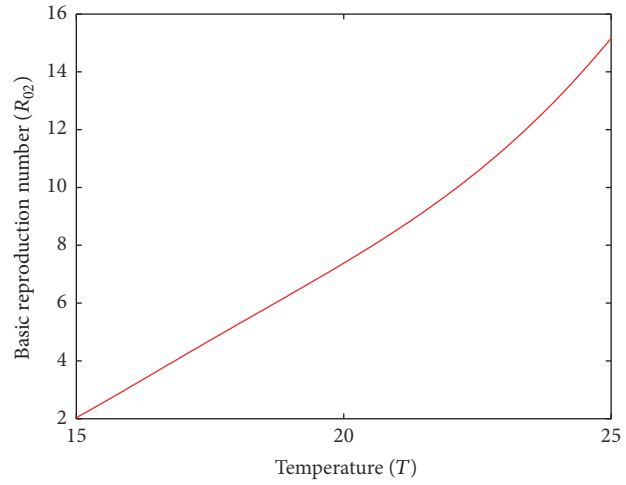

Figure 8: Basic reproduction number of patch 2 without host movement.

the patch where the hosts are travelling and the susceptible hosts can get infected of the disease from the mosquitoes of the patch where the hosts have travelled. It is observed that movement of both infectious and susceptible hosts from low prevalent patch to the high prevalent patch increases the endemic level of the disease. But their movement from high prevalent patch to the low prevalent patch decreases the endemic level of the disease.

Temperature has a significant influence on basic reproduction number (Figures 7 and 8). In patch 1, the prevalence of disease is seen increasing with temperature and the maximum disease prevalence has occurred at 29.3°C temperature as in [17]. In case of patch 2 where average temperature range is 15°C to 25°C, disease prevalence increases with the increase in temperature and the maximum disease prevalence has occurred at 25°C.

4.1. Dynamics with Unidirectional Movement. In this section, we investigate the impact of host movement in one direction only with different temperature levels. Figures 9–12 show the dynamics of infectious host population of patch 1 and patch 2 when there is host movement from patch 1 to patch 2 only or patch 2 to patch 1 only. When the hosts from patch 2 are not allowed to move to patch 1 (Figures 9 and 10), burden of disease is decreased in patch 1 and increased in patch 2. When the hosts from patch 1 are restricted to travel to patch 2, the burden of disease is increased in patch 1 and decreased in patch 2 (Figures 11 and 12). In each case, the dynamics of infectious hosts are seen temperature dependent. Disease prevalence is observed increasing with temperature. Thus, movement of hosts can cause the patch to be less disease prevalent (Figures 9 and 12) and more disease prevalent (Figures 10 and 11).

When only the hosts from patch 2 are allowed to move to patch 1, basic reproduction number of patch 1 increases and that of patch 2 decreases with the increase in movement rate (Figure 13). Also, basic reproduction number of patch 1 decreases and that of patch 2 increases when only the hosts from patch 1 are allowed to move to patch 2 (Figure 14). So,

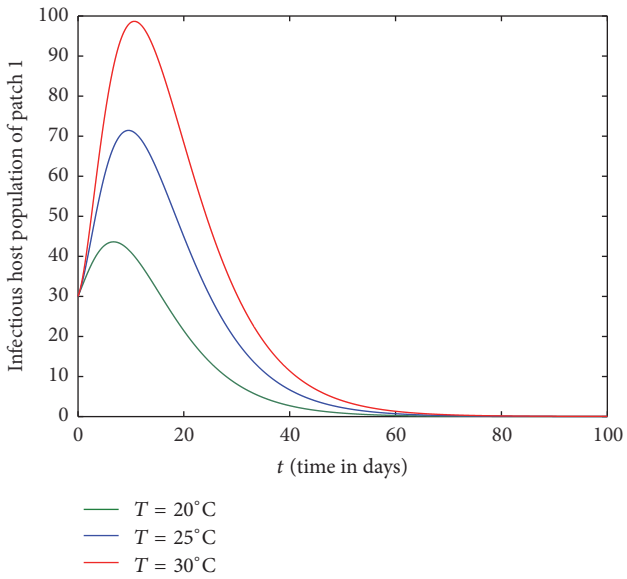

Figure 9: Dynamics of infectious hosts of patch 1 without host movement from patch 2 to patch 1.

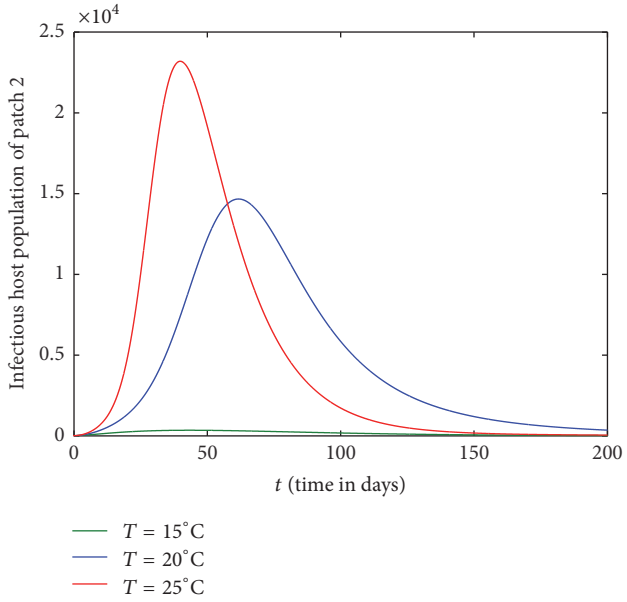

Figure 10: Dynamics of infectious hosts of patch 2 without host movement from patch 2 to patch 1.

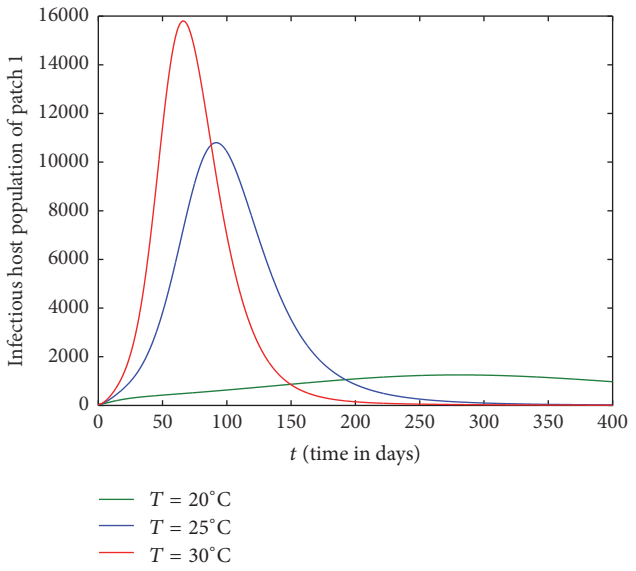

Figure 11: Dynamics of infectious hosts of patch 1 without host movement from patch 1 to patch 2.

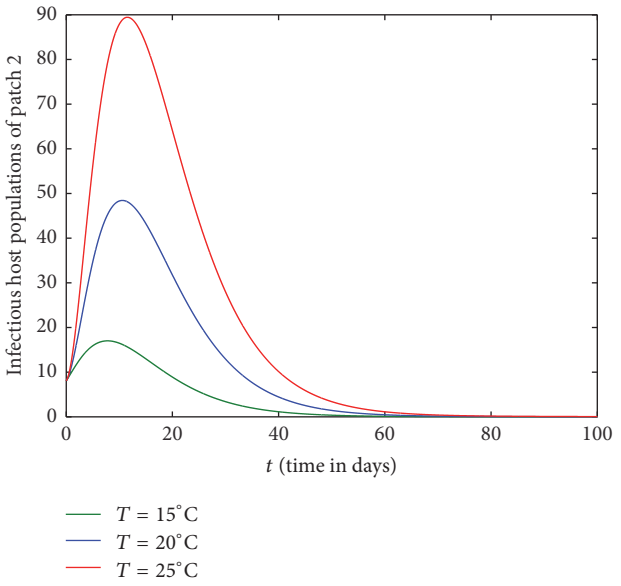

Figure 12: Dynamics of infectious hosts of patch 2 without host movement from patch 1 to patch 2.

the host population can be moved from one patch to the other to bring the disease under control.

5. Conclusion

Temperature plays a significant role in dynamics of dengue disease transmission. It affects the lifecycle and biting behavior of mosquitoes. Human movements contribute in spreading the disease in new places. We have proposed multipatch model of dengue disease with the human movement between patches considering temperature dependent model parameters. In the present work, we explored the impact of temperature and host movement between patches on the transmission dynamics of dengue disease. We have investigated the stability of disease-free equilibrium point. It is observed that the point is locally asymptotically stable when basic reproduction number $\mathscr{R}_0 < 1$ and unstable when $\mathscr{R}_0 > 1$. Simulated results show that basic reproduction number depends on temperature and host movement. The prevalence of disease can increase or decrease with temperature and mobility of hosts from one patch to the other. Present work shows that the burden of the disease can be reduced by managing the host movement and the temperature can enhance

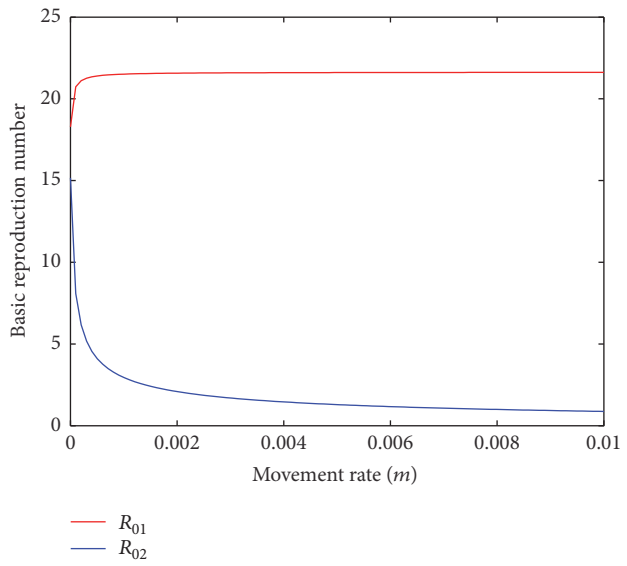

FIGURE 13: Basic reproduction numbers of patch 1 and patch 2 against movement rate, $m = m_{12}^S = m_{12}^E = m_{12}^I$, without host movement from patch 1 to patch 2.

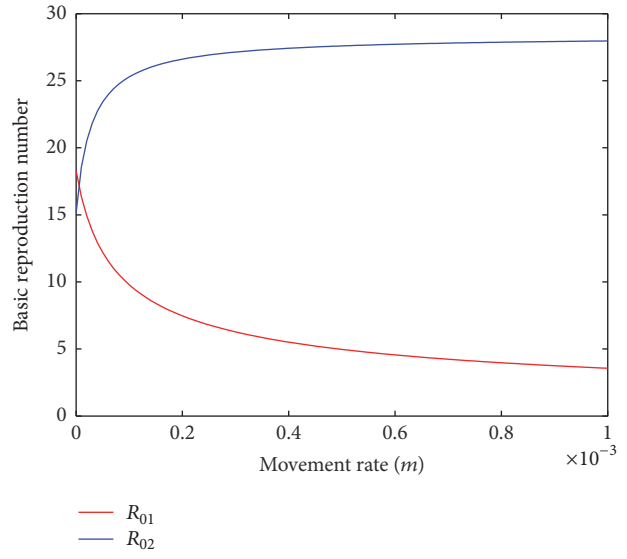

FIGURE 14: Basic reproduction numbers of patch 1 and patch 2 against movement rate, $m = m_{21}^S = m_{21}^E = m_{21}^I$, without host movement from patch 2 to patch 1.

the strength of the disease. These pieces of information can be helpful to the concerned authorities to bring dengue disease under control.

Conflicts of Interest

The authors declare that there are no conflicts of interest regarding the publication of this paper.

References

[1] *Global strategy for dengue prevention and control 2012-2020*, World Health Organization, 2012.

[2] N. M. Ferguson, C. A. Donnelly, and R. M. Anderson, "Transmission dynamics and epidemiology of dengue: Insights from age-stratified sero-prevalence surveys," *Philosophical Transactions of the Royal Society B: Biological Sciences*, vol. 354, no. 1384, pp. 757–768, 1999.

[3] D. J. Gubler, "Dengue and dengue hemorrhagic fever," *Clinical Microbiology Reviews*, vol. 11, no. 3, pp. 480–496, 1998.

[4] W. O. Kermack and A. G. McKendrick, "A contribution to the mathematical theory of epidemics," *Proceedings of the Royal Society A*, vol. 115, no. 772, pp. 700–721, 1927.

[5] L. Esteva and C. Vargas, "Analysis of a dengue disease transmission model," *Mathematical Biosciences*, vol. 150, no. 2, pp. 131–151, 1998.

[6] L. Esteva and C. Vargas, "A model for dengue disease with variable human population," *Journal of Mathematical Biology*, vol. 38, no. 3, pp. 220–240, 1999.

[7] S. Gakkhar and N. C. Chavda, "Impact of Awareness on the Spread of Dengue Infection in Human Population," *Applied Mathematics*, vol. 04, no. 08, pp. 142–147, 2013.

[8] G. R. Phaijoo and D. B. Gurung, "Mathematical model of dengue disease transmission dynamics with control measures," *Journal of Advances in Mathematics and Computer Science*, vol. 23, no. 3, pp. 1–12, 2017.

[9] S. T. Pinho, C. P. Ferreira, L. Esteva, F. R. Barreto, V. C. Morato e Silva, and M. G. Teixeira, "Modelling the dynamics of dengue real epidemics," *Philosophical Transactions of the Royal Society of London. Series A. Mathematical, Physical and Engineering Sciences*, vol. 368, no. 1933, pp. 5679–5693, 2010.

[10] M. Chan and M. A. Johansson, "The Incubation Periods of Dengue Viruses," *PLoS ONE*, vol. 7, no. 11, Article ID e50972, 2012.

[11] P. Pongsumpun, "Transmission model for dengue disease with and without the effect of extinsic incubation period," *KMITL Science and Technology Journal*, vol. 6, pp. 74–82, 2006.

[12] P. Pongsumpun, "Mathematical model of dengue disease with the incubation period of virus," *World Academy of Science, Engineering and Technology*, vol. 44, pp. 328–332, 2008.

[13] S. Side and M. S. M. Noorani, "SEIR model for transmission of dengue fever in selangor Malaysia," *International Journal of Modern Physics*, vol. 9, pp. 380–389, 2012.

[14] S. Side and S. M. Noorani, "A SIR model for spread of dengue fever disease (simulation for South Sulawesi, Indonesia and Selangor, Malaysia)," *World Journal of Modelling and Simulation*, vol. 9, no. 2, pp. 96–105, 2013.

[15] T. Sardar, S. Rana, and J. Chattopadhyay, "A mathematical model of dengue transmission with memory," *Communications in Nonlinear Science and Numerical Simulation*, vol. 22, no. 1-3, pp. 511–525, 2015.

[16] O. J. Brady, M. A. Johansson, C. A. Guerra et al., "Modelling adult Aedes aegypti and Aedes albopictus survival at different temperatures in laboratory and field settings," *Parasites and Vectors*, vol. 6, no. 1, article no. 351, 2013.

[17] J. Liu-Helmersson, H. Stenlund, A. Wilder-Smith, and J. Rocklöv, "Vectorial capacity of *Aedes aegypti*: effects of temperature and implications for global dengue epidemic potential," *PLoS ONE*, vol. 9, no. 3, Article ID e89783, 2014.

[18] S. Polwiang, "The seasonal reproduction number of dengue fever: Impacts of climate on transmission," *PeerJ*, vol. 2015, no. 7, Article ID e1069, 2015.

[19] W. Wang and X.-Q. Zhao, "An epidemic model in a patchy environment," *Mathematical Biosciences*, vol. 190, no. 1, pp. 97–112, 2004.

[20] W. Wang and G. Mulone, "Threshold of disease transmission on a patch environment," *Journal of Mathematical Analysis and Applications*, vol. 285, no. 1, pp. 321–335, 2003.

[21] J. Arino and P. van den Driessche, "A multi-city epidemic model," *Mathematical Population Studies. An International Journal of Mathematical Demography*, vol. 10, no. 3, pp. 175–193, 2003.

[22] Y.-H. Hsieh, P. van den Driessche, and L. Wang, "Impact of travel between patches for spatial spread of disease," *Bulletin of Mathematical Biology*, vol. 69, no. 4, pp. 1355–1375, 2007.

[23] C. Cosner, J. C. Beier, R. S. Cantrell et al., "The effects of human movement on the persistence of vector-borne diseases," *Journal of Theoretical Biology*, vol. 258, no. 4, pp. 550–560, 2009.

[24] P. Auger, E. Kouokam, G. Sallet, M. Tchuente, and B. Tsanou, "The Ross-Macdonald model in a patchy environment," *Mathematical Biosciences*, vol. 216, no. 2, pp. 123–131, 2008.

[25] S. Lee and C. Castillo-Chavez, "The role of residence times in two-patch dengue transmission dynamics and optimal strategies," *Journal of Theoretical Biology*, vol. 374, pp. 152–164, 2015.

[26] G. R. Phaijoo and D. B. Gurung, "Mathematical Study of Dengue Disease Transmission in Multi-Patch Environment," *Applied Mathematics*, vol. 07, no. 14, pp. 1521–1533, 2016.

[27] A. Berman and R. J. Plemmons, *Nonnegative Matrices in Mathematical Sciences*, Academic Press, New York, NY, USA, 1979.

[28] O. Diekmann, J. A. P. Heesterbeek, and J. A. J. Metz, "On the definition and computation of the basic reproduction ratio R_0 in models for infectious diseases in heterogeneous populations," *Journal of Mathematical Biology*, vol. 28, no. 4, pp. 365–382, 1990.

[29] P. van den Driessche and J. Watmough, "Reproduction numbers and sub-threshold endemic equilibria for compartmental models of disease transmission," *Mathematical Biosciences*, vol. 180, pp. 29–48, 2002.

Hindawi
Computational and Mathematical Methods in Medicine
Volume 2017, Article ID 2403851, 11 pages
https://doi.org/10.1155/2017/2403851

Research Article

Stochastic Models of Emerging Infectious Disease Transmission on Adaptive Random Networks

Navavat Pipatsart,[1] Wannapong Triampo,[1,2,3] and Charin Modchang[1,2,3]

[1]*Department of Physics, Faculty of Science, Mahidol University, Bangkok 10400, Thailand*
[2]*Centre of Excellence in Mathematics, CHE, Bangkok 10400, Thailand*
[3]*Thailand Center of Excellence in Physics, CHE, 328 Si Ayutthaya Road, Bangkok 10400, Thailand*

Correspondence should be addressed to Charin Modchang; cmodchang@gmail.com

Received 14 March 2017; Accepted 15 August 2017; Published 17 September 2017

Academic Editor: Delfim F. M. Torres

We presented adaptive random network models to describe human behavioral change during epidemics and performed stochastic simulations of SIR (susceptible-infectious-recovered) epidemic models on adaptive random networks. The interplay between infectious disease dynamics and network adaptation dynamics was investigated in regard to the disease transmission and the cumulative number of infection cases. We found that the cumulative case was reduced and associated with an increasing network adaptation probability but was increased with an increasing disease transmission probability. It was found that the topological changes of the adaptive random networks were able to reduce the cumulative number of infections and also to delay the epidemic peak. Our results also suggest the existence of a critical value for the ratio of disease transmission and adaptation probabilities below which the epidemic cannot occur.

1. Introduction

Within few decades, numerous studies on infectious disease transmission using the network theory have been carried out. Networks provide a mathematical platform for the interpretation of the interaction between individuals or populations and are especially useful when each individual is assumed to be in direct contact only with a small proportion of the population [1–5]. Network models tend to be very powerful tools that provide understanding of the disease transmission in human populations and allow the assumptions of either social or sexual contacts [6]. However, the vast majority of infectious disease transmission models on networks employed static networks [7]. The static network structure does not change over time and such models ignore the effect of individual's behavioral change due to the infection. On the other hand, there are studies that implemented rules on dynamical network structures that opened the possibility of network adaptation. These rules help to generate complex network models and are also expected to reflect some real-world networks [8–13].

Recent studies brought forth characteristic rules of networks that adapted the network structure more dynamically by responding to the infection status of individuals [14–16]. These dynamic networks took into account the fact that individuals tend to respond to the emerging infectious disease transmission by avoiding contacts with infected individuals. Such rewiring of local contacts can have a strong impact on the dynamics of an infectious disease transmission as shown in a study of a complicated mutual interplay between network adaptation dynamics and the dynamics of individual states. There are two popular closely related adaptive rules of the network: the first rule allows susceptible individuals to temporarily disconnect their contacts with infectious individuals [17] and the other allows susceptible individuals to avoid contact with the infectious individuals by rewiring their network connections [18]. This has revealed new perspectives onto effects on concurrent partnerships [19, 20] and on structure changing patterns [21]. A definition of dynamic networks was given stating that such networks are regulated by a feedback loop between the dynamics of node's state and

interaction in a network and the coevolution or adaptation of the networks [22].

Most studies on infectious disease transmission using adaptive networks are deterministic. Admittedly, the implementation of such models is easier, but they are insufficient to explain some fluctuating dynamics in real-world systems [23]. Deterministic models provide exactly the same results given the same initial conditions. However, we would not expect to observe exactly the same people becoming infected at exactly the same time. In contrast, infectious disease modeling using the adaptive networks takes into account the fluctuations or noise by considering interactions between individuals. Clearly, there is an important element of chance and stochastic models are concerned with approximating this random or probabilistic element. In general, chance will play the most important role whenever the number of infectious individuals is relatively small, which can happen when the population size is small. It is especially important that stochasticity is taken into account and incorporated into the network model.

However, there is no comparative study about effect of these two adaptive rules to the infectious disease transmission in population yet. The main goals of this work is not only to model networks representing individuals in a population that tend to respond to the emergence of an infectious disease and incorporate two different specific patterns of behavioral change regarding the interaction between individuals in a population but also to investigate the interplay between infectious disease dynamics and network adaptation dynamics by using stochastic simulations in order to gain insight into infectious disease transmission in real-world system.

2. Network Models

2.1. Construction of Static Random Network. In our model, we represented an individual human by a node and a potential disease-causing interaction between two individuals by a link. The $G(n, p)$ random network was constructed from a finite set of n nodes with $n(n-1)/2$ possible pairs. Each pair of nodes was then randomly chosen to be connected with a probability p, where the number of nodes n and independent probability p are fixed. We defined the initial structure of random network at each simulation run by setting the initial structure as a $G(n, p)$ random network. The number of individuals in this system was fixed at $n = 1{,}000$ nodes. We expected a low frequency of the disease-causing contact between two individuals henceforth, comprising a small proportion of the population and represented by a low probability $p = 0.01$.

2.2. Infectious Disease Transmission on Networks. According to the *SIR* epidemic model mechanism, an individual human was represented as a node amongst a finite and fixed number of individuals in a population and the potential disease-causing contact between two individuals as a link. Two nodes were assigned as neighbors, if connected by a link. A node neither could be linked to itself nor shares more than one link with another node. At any time, each node has only one specific state, namely, the susceptible state (S), the infectious state (I), or the recovered state (R). This model is appropriate for a disease that spreads through human populations by direct contact between infectious individuals and susceptible individuals, such as influenza. We also assumed that recovered individual confers lifelong immunity. In this paper we will consider only diseases of this type. Diseases that are endemic because they propagate on time scales comparable to or slower than the rate of turnover of the population or because they confer only temporary immunity are not well represented by this model.

For the $S \rightarrow I$ transition, an infectious disease can be transmitted, if a given infectious node shares links with other susceptible nodes. We denoted this link as SI-link. Those susceptible neighbors were then infected with probability ϕ per SI-link and per time-step. In addition, the more the contacts a susceptible node has with infectious nodes, the higher the chance to become infected simply is because a pathogen can be transmitted from many infected individuals. Hence, we calculated the infection probability λ of each node individually as follows:

$$\lambda = 1 - \left(1 - \phi\right)^{k_{SI}}, \tag{1}$$

where k_{SI} is the number of SI-links that is connected to that node. The $I \rightarrow R$ transition implies that infected nodes can independently self-recover with a recovery probability η. In contrast to the $S \rightarrow I$ transition, the $I \rightarrow R$ transition is not influenced by SI-links. The initial conditions were set as follow: (1) The entire nodes in the network are in susceptible state. (2) A single node is randomly chosen to become the first infectious node.

When an infectious disease spreads on a social network, humans tend to respond to the emergence of an epidemic by avoiding contacts with infected individuals. Such rewiring of the local connections can have a strong effect on the dynamics of the disease, which in turn influences the rewiring process. Thus, a complicated mutual interaction between network adaptation dynamics and the dynamics of disease transmission emerges (Figure 1). In our network, such nodes with reconnecting or rewiring ability were called adaptive nodes. It shall be noted that only susceptible nodes are capable of such adaptation once being at risk of infection. Hence, the network adaptation concerned the ability of susceptible nodes to adapt as to avoid contact with infectious nodes. In addition, these behavioral changes can lead to the isolation of infected nodes and then again affects the behavioral changes of susceptible nodes. Consequently, there is interplay between the changing state of nodes and the changing interaction of nodes at any time of infectious disease transmission on the network. This provides a feedback loop between the infectious disease dynamics and network adaptation dynamics of the network as illustrated in Figure 1. These networks including feedback loops are defined as coevolution networks or adaptive networks [24].

Thus, this feedback loop is dependent on the existence of a pathogen, which can trigger node state changes and altered interaction of nodes. This feedback loop then determines the outcome of the infectious disease transmission on the network, which is either invasion or disappearance of the

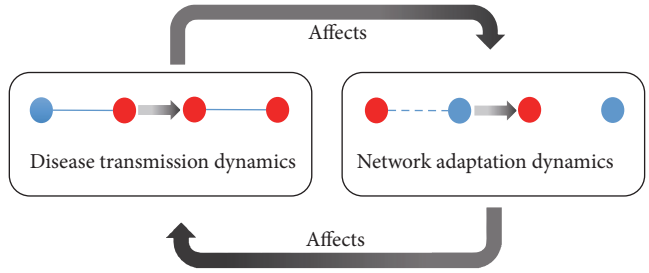

Figure 1: Schematic diagram of the feedback loop between the infectious disease dynamics and network adaptation dynamics of an adaptive network. Blue and red nodes represent susceptible and infectious nodes, respectively. Solid and dot lines represent network links and links that will be cut due to network adaptation dynamics, respectively.

pathogen. At any given time of the ongoing infectious disease transmission on an adaptive network, both changing states of nodes and their interaction have potential to occur. The dynamics also lead to a new perspective that cannot be observed using a static network model. There are two types of adaptive networks in this work, which are described in the following.

Type I Adaptive Random Network. In this model, the adaptive and susceptible nodes have the feature to protect themselves by temporarily disconnecting each of their *SI*-link between infectious neighboring nodes with probability ω_{I} at any time-step. The destroyed links are then reconnected when the neighboring nodes transform into recovered nodes, as shown in Figure 2.

In this way, every susceptible node has a constant and equal chance to disconnect each of their *SI*-links and then also reconnects the formerly destroyed links at every time-step. Therefore, the number of links, m in this network, is changed in accordance with the time-steps. Type I adaptation in an adaptive random network represents a real-world situation given the assumption of effective quarantine of infected people during epidemics and the later release after their recovery from infection.

Type II Adaptive Random Network. The network adaptation dynamics of this model allows adapting susceptible nodes to protect themselves by rewiring their links. The adaptive and susceptible nodes disconnect their *SI*-links with the infectious nodes with probability ω_{II} for every *SI*-link at each time-step. This rule of rewiring is basically similar to the type I adaptive network; however, instead of reconnecting with the former neighbors, other susceptible or recovered state nodes will be randomly chosen to establish new links immediately after successful disconnection of the previous *SI*-links. The chosen nodes are prohibited to link with themselves and their current neighboring nodes. We define this behavioral change as rewiring of the links and denote ω_{II} as the rewiring probability.

However, every susceptible node in this model does not memorize their prior destroyed links and their abandoned neighbors. Consequently, adaptive and susceptible nodes can either reconnect to the abandoned neighboring nodes or any other nodes at later time-step as shown in Figure 3.

Table 1: The value range of the parameters that were used for the simulation.

Time, t	1–100
Disease transmission ratio, χ	1.5–5.0
Recovery probability, η	0.2
Destruction probability, ω_{I}	0.0–0.7
Rewiring probability, ω_{II}	0.0–0.7

At any time-step, the adaptive and susceptible nodes responded to the disease transmission by rewiring their links, but the number of links m remained constant. On the other hands, the behavioral change of individual nodes in regard to the avoidance of contact with infected individual nodes is determined by destruction probability ω_{I} and rewiring probability ω_{II} for the type I adaptive random network and the type II adaptive random network, respectively. The value range of both the epidemic and the network adaptation probabilities are shown in Table 1. All simulations were performed using the standard kinetic Monte Carlo algorithm and were simulated using MATLAB software.

3. Results

3.1. Infectious Disease Transmission on Type I Adaptive Random Networks. This section presents the results of the investigations on the behavior of the infectious disease transmission on type I adaptive random network upon variation of the network adaptation probability or more precisely the destruction probability ω_{I}. We assigned other parameters according to Table 1. Then, we have allowed the chosen infected node to transmit the pathogen across its *SI*-links. We investigated the disease transmission over a period of 100 time-steps and varied ω_{I} from 0 to 0.7, while keeping ratio $\chi \equiv \phi/\eta$ constant (Figure 4). Colored labeling of the fraction of infectious nodes was applied to facilitate the illustration. Figure 4(a) shows the results for $\chi = 2.0$. We found that the pathogen failed to invade the population. A minor occurrence of an infectious fraction can be observed, if $\omega_{\mathrm{I}} < 0.3$. The infectious fraction tended to be decreased in case of the static network model ($\omega_{\mathrm{I}} = 0$).

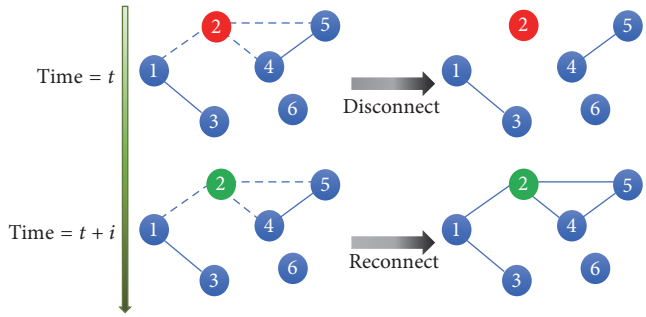

FIGURE 2: Schematic illustration of the adaptation process of type I adaptive network. At time t, the susceptible nodes 1, 4, and 5 can disconnect their SI-links, namely, $(1, 2)$, $(2, 4)$, and $(2, 5)$ links, with the probability ω_I. At time $t + i$, when the node 2 recovers from the disease, the disconnected links will be reconnected. Blue, red, and green nodes represent susceptible, infectious, and recovered nodes, respectively. Dot lines represent links that are disconnected and then reconnected.

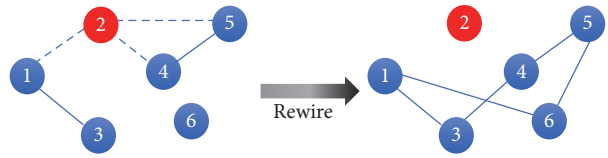

FIGURE 3: Schematic illustration of the adaptation process of type II adaptive network. In this figure, nodes 1, 4, and 5, can cut their $(1, 2)$, $(2, 4)$, and $(2, 5)$ links with the probability ω_{II}. The node that decided to cut its SI-link will immediately choose a new noninfectious node to connect with. Blue, red, and green nodes represent susceptible, infectious, and recovered nodes, respectively. Dot lines represent SI-links.

The effect of the network adaptation probability is more obvious, if the pathogen has a higher potential to be transmitted as show in Figure 4(b). We can see that the appearance of the infectious fraction tended to be delayed with increasing ω_I to the point of its disappearance for ω_I exceeding 0.50. Independent of the delay, the infectious fraction tended to last until stationary state of the network at similar time-steps and measured an average period of appearance of 47 time-steps. The appearance of the infectious fraction in Figure 4(c) followed previous patterns observing the delay in association with an increasing value of ω_I and a fixed $\chi = 4.0$. The infectious fractions occurred at time-steps 6, 7, 7, 8, 10, 13, and 20 for $\omega_I = 0.1$, 0.2, 0.3, 0.4, 0.5, and 0.6, respectively, and then decayed until stationary state. The fractions of infectious nodes tended to be reduced in case of the static network model. The average period of the appearance was 41 time-steps ranging from 33 to 52 time-steps for values of ω_I ranging between 0 and 0.55. The period of appearance measured 45 time-steps in case of $\omega_I = 0.60$. These results led us to realize that the successful disease invasion did depend not only on the network adaptation probability, which is a parameter of individual behavioral change, but also on the disease transmission ratio χ, which is a parameter of the infectious disease, too. More precisely, the infectious disease can invade the population for specific values of both ω_I and χ.

Figure 4(d) shows the time evolution of the fraction of infected nodes and the appearance of invasion of the disease for the entire range of ω_I while χ was fixed at 5.0. Therefore, this model tends to speed up the disease transmission but reaches the stationary state at similar time-points when compared to previous results. On the other hand, the periods of appearance tend to be increased with an increasing value of ω_I, except for $\omega_I = 0.7$. We noticed that infectious fraction began to appear and the commencement of the stationary state was slightly delayed with increasing ω_I. In the same way, the infectious fractions tended to decline in the static network model with increasing ω_I until their disappearance using an appropriate value of ω_I. Also, the periods of appearance of the infectious fractions tended to increase with increasing ω_I and could be reduced by choosing an appropriate value of ω_I. It must be noted that the behavioral change of individuals as modeled in the type I adaptive random network is reflected by network adaptation dynamics and may have caused the reduction in numbers of infectious people in a population. Also, such dynamics can protect susceptible individuals from infection by avoiding contact with infectious people. The higher the chance of avoidance, the lower the number of infectious individuals in that population. In this way, the destruction probability ω_I can be interpreted as the chance of susceptible individual to detect infected neighbors in a local population. Thus, ω_I is a parameter to determine behavior of individual.

The results show that the infectious disease can invade the population, if the pathogen transmission is probable despite a 70-percent chance of any susceptible individual in the population to avoid contact with infected individuals. Furthermore, the behavioral change of susceptible individuals as represented by the network adaptation dynamics in type I adaptive random networks has potential to reduce the number of infected people prospectively but also can lead to a delay in the epidemic peak time. In this way, the individual behavior may lead to a prolonged disease spread in that population.

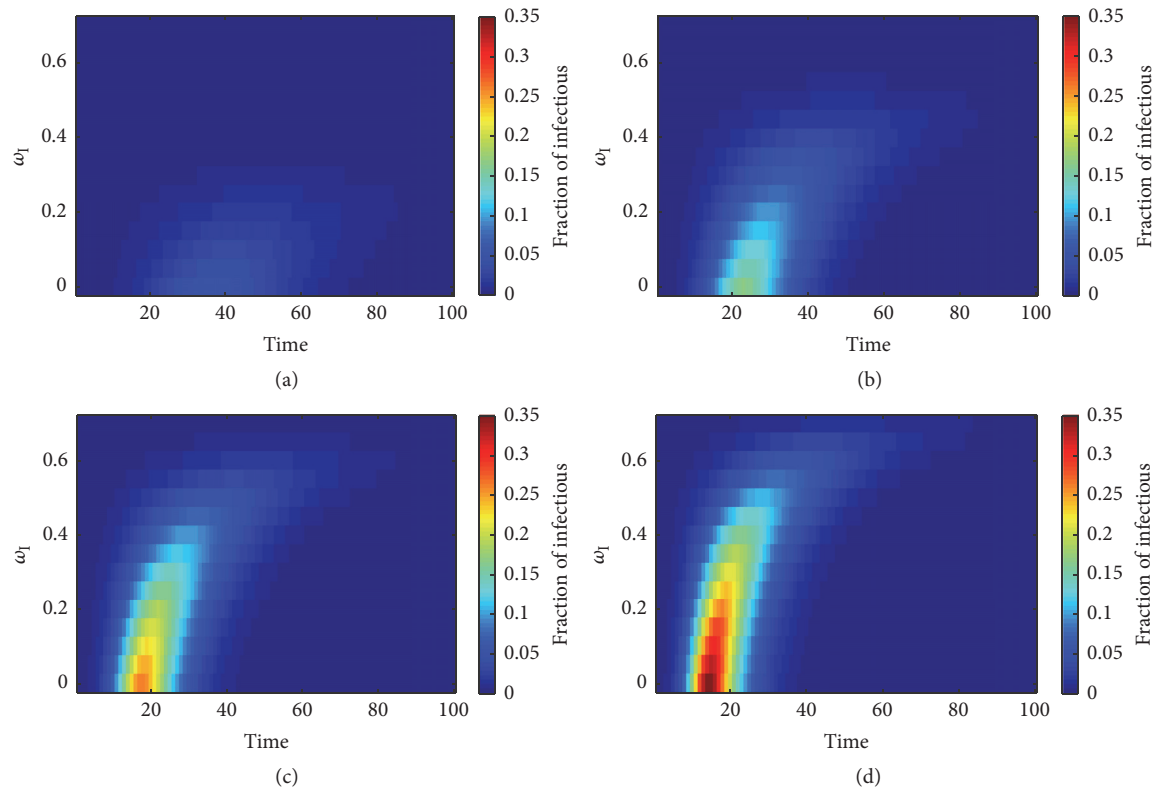

Figure 4: Profile of the infectious disease's prevalence plotted against time and destruction probability ω_I on the type I adaptive random network. The ratio $\chi \equiv \phi/\eta$ was varied as (a) $\chi = 2.0$, (b) $\chi = 3.0$, (c) $\chi = 4.0$, and (d) $\chi = 5.0$. Grids correspond to the average of over 5,000 simulations.

3.2. Infectious Disease Transmission on Type II Adaptive Random Networks. Thereafter, we studied the infectious disease transmission in another adaptive network model, namely, the type II adaptive random network, by using the equivalent conditions as in the previous section to investigate the effect of network adaptation dynamics on the infectious disease transmission. Figure 5(a) shows the time evolution of fractions of infectious nodes with varying ω_{II} and fixed $\chi = 2.0$. The appearance of the infectious fractions is clearly visible (colored pixels against blue background) in case of the static network model and type II adaptive random network for $\omega_{II} = 0.05$. This corresponds to the results in a previous section. This stands in contrast to the behavior of the type I network, which produced disease invasion only for a network adaptation probability less than 0.3. Figure 5(b) shows the time evolution of infectious fractions for $\chi = 3.0$. Infectious fractions appeared for $\omega_{II} \leq 0.2$ and tended to be increased with proceeding time-steps arriving at an epidemic peak and then decayed to zero at stationary state. In case of the static network model, the infectious fraction tended to decrease dramatically. In the case of adaptive networks, the infectious fraction decreased with an increasing ω_{II} until its disappearance for $\omega_{II} > 0.2$. The time-steps of occurrence of the infectious fractions tended to be delayed with an increasing ω_{II} and infectious fractions remained in the network for an average period of 46 time-steps. In this case, the period of appearance was similar to the simulation results of the type I adaptive network measuring 40–45 time-steps. Nevertheless, the fraction of infected nodes was always lower when compared to the type I adaptive network under equivalent conditions.

Moreover, Figure 5(c) shows the simulation result for $\chi = 4.0$. The results followed previous patterns observing delayed occurrence of the infectious fraction, but its period tended to be increased with an increasing ω_{II}. However, the stationary state of infectious fractions tended to be delayed for higher values of ω_{II}. The time evolution of the infectious fraction became obvious for $\omega_{II} \leq 0.30$. We noticed a shift in the limitation of occurrence of the infectious fractions when the disease transmission ratio χ was increased by 0.5 points. This might be due to the interplay between the network adaptation probability and the disease transmission ratio. Moreover, the average period of appearance of infectious fractions tended to be decreased by about 6 time-steps when compare to the previous results.

In addition, Figure 5(d) shows the simulation results for $\chi = 5.0$. Infectious fractions appeared, if the rewiring probability ω_{II} ranged between 0 and 0.4. Fractions and also the network stationary state tended to be delayed with the increase in ω_{II}. The period of appearance of infectious fractions tended to increase with the increase in ω_{II} except in case of $\omega_{II} = 0.40$, which measured only 22 time-steps. This might be due to the observation of a large fluctuation. Consequently, the infectious fractions as simulated for the type II adaptive

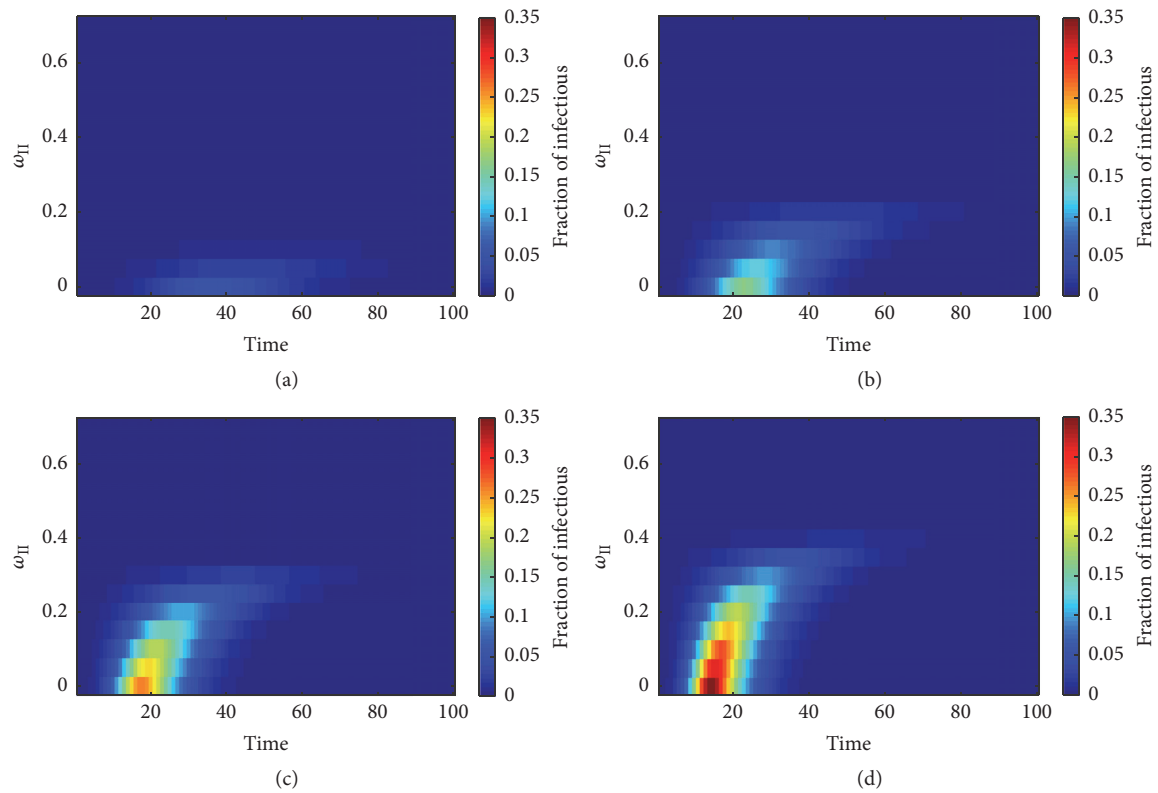

FIGURE 5: Profile of the infectious disease's prevalence plotted against time and destruction probability ω_{II} on the type II adaptive random network. The probability ratio χ was varied as (a) $\chi = 2.0$, (b) $\chi = 3.0$, (c) $\chi = 4.0$, and (d) $\chi = 5.0$. Grids correspond to the average of over 5,000 simulations.

random network were less obvious than in case of the type I network under same parameter conditions. Particularly, when the network adaptation probability was above 0.4, the infectious disease failed to invade the population in case of the type II network for every value of χ, whereas succeeded in all ranges of χ, in case of type I network simulations. The infectious fractions in the type II case tended to occur later but remained longer when compared to the type I network for equivalent parameters.

Furthermore, we observed that the infectious disease transmission in the adaptive networks was less frequent when compared to the static network simulations in regard to an increasing value of the network adaptation probability. For the infectious disease transmission in type I adaptive random networks, susceptible nodes continued to forsake their infectious neighboring nodes. To follow the thought, we can assume an increasing number of isolated infected nodes. Relations have reformed when the infected nodes have recovered. Similar to the infectious disease transmission on type II adaptive random networks, susceptible nodes continued to change connections by seeking contact with noninfectious nodes upon linkage with infectious neighboring nodes. This contributes to a form of community, which excludes any infected nodes. This particular behavior may well reduce the numbers of disease transmissions and yet also delays the period of disease transmissions. Moreover, in contrast to type I, type II adaptive networks comprise a more sensitive topology in regard to the network adaptation probability. It is meant that it can reduce the number of infections but delays the disease transmission and remission. We explain this with the remaining and more frequent paths of pathogen transmission in the type I adaptive network than can be found in type II networks, despite the destructions of numerous infection paths.

3.3. Effects of Network Adaptation Probability to the Infectious Disease Transmission on Adaptive Random Networks. In order to understand the effects of network adaptation probabilities on the infectious disease transmission, we plotted the number of links and the number of *SI*-links of both types of adaptive networks against time as shown in Figure 6; the figure shows the simulation result based on varying values of the disease transmission ratio χ ranging from 2.0 to 5.0. As described in previous sections, we have learned that the number of links in the type II adaptive random network is constant due to the topology of the network adaptation dynamics. The number of initial links counted 5,094 links. Figure 6 shows the time evolution of links of the type I and the type II adaptive random networks where χ was set to 2.0. The number of links in the type I network was reduced for $\omega_I \leq 0.20$. At time-steps 43, 49, and 53, 34, 38, and 23 links were disconnected for $\omega_I = 0.1$, 0.2, and 0.3, respectively, as show in Figure 6(a). In addition, there are 338, 189, and 75 *SI*-links in the type I network at time-steps 43, 48, and 53 for

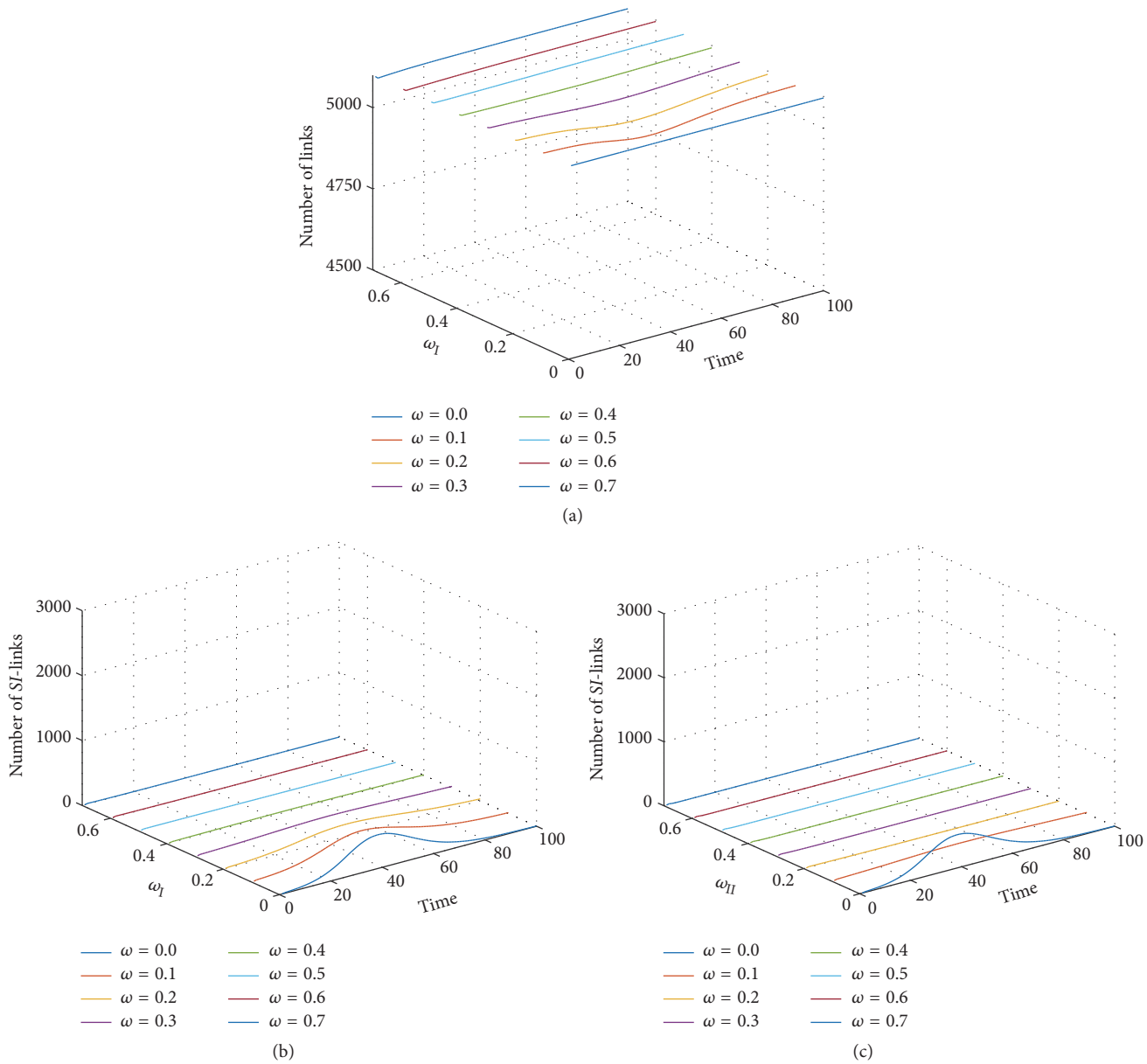

FIGURE 6: Profile of time evolution of the number of links in type I adaptive random networks (a), the number of SI-links in type I adaptive random networks (b), and the number of SI-links in type II adaptive random networks (c) ($\chi = 2.0$).

$\omega_I = 0.1$, 0.2, and 0.3, respectively, as shown in Figure 6(b). We noticed that these time-steps are correlated with each other and coincided with epidemic peaking calling them epidemic peak time. Previous results showed that the infectious disease failed to invade for $\omega_I = 0.30$ which might be correlated with the number of disconnected SI-links. Furthermore, the time evolution of SI-links in the type II adaptive random network is shown in Figure 6(c). We observed that almost all of the SI-links were rewired before the pathogen was transmitted. This may have had effect on the invasion of infectious disease in the type II network and may have contributed to the failure of invasion.

Further support of the obtained pattern of results provides the time evolutions of the number of links in the type I model and the number of SI-links in the type I and type II network models for $\chi = 5.0$ as shown in Figure 7. The number of disconnected links tended to be slightly increased when compared to the previous results. In addition, the number of SI-links of both the type I and II networks was also comparatively higher.

According to our results, the change of interaction based on the network adaptation dynamics had strong effect on the reduction of the number of SI-links. Choosing an appropriate value for the network adaptation probability was crucial for the failure of the infectious disease invasion due to the destruction or rewiring of most SI-links before the pathogen could be transmitted. The number of disconnected links depended on the number of SI-links in the network. It was

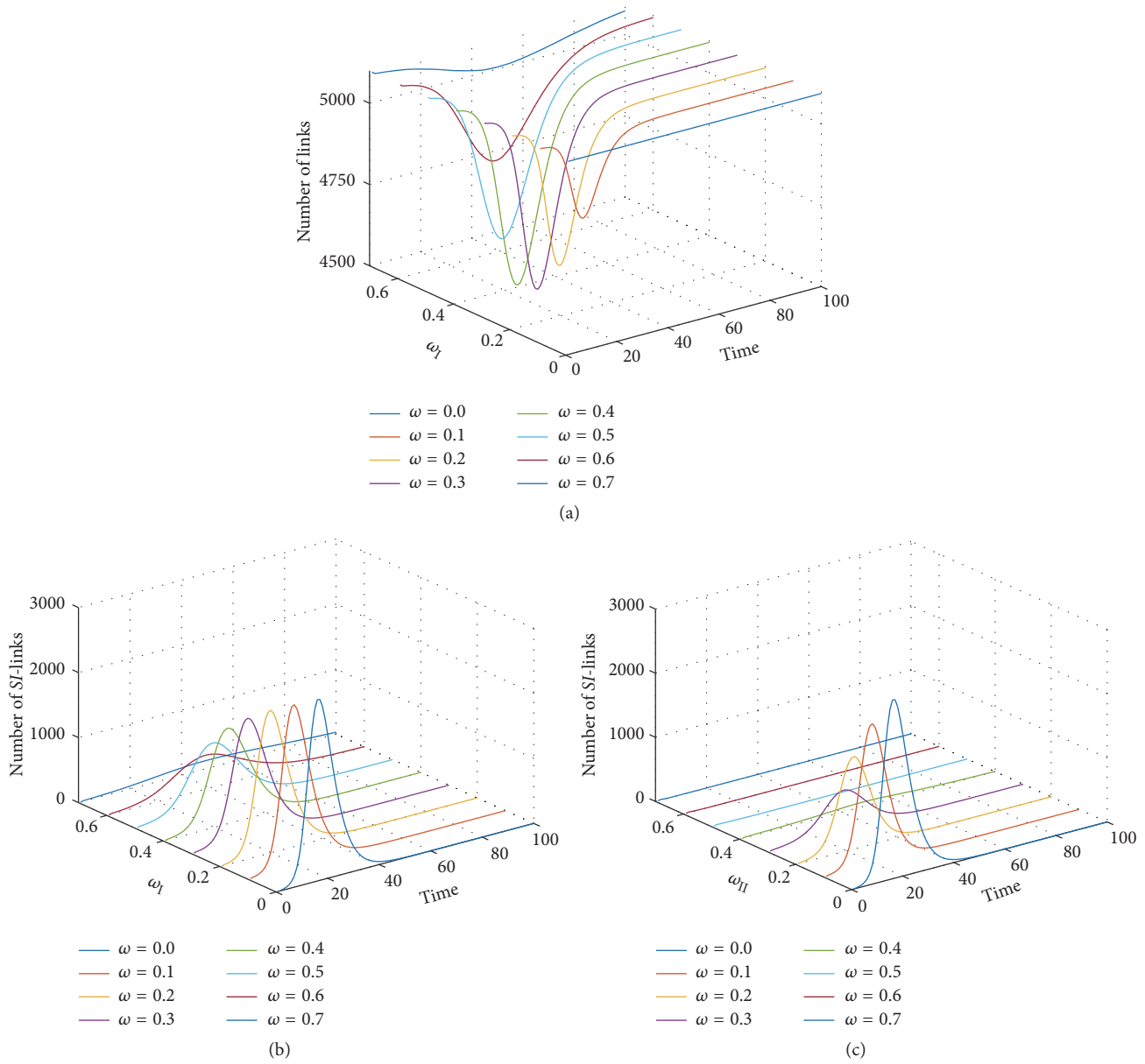

FIGURE 7: Profile of time evolution of the number of links in type I adaptive random networks (a), the number of SI-links in type I adaptive random networks (b), and the number of SI-links in type II adaptive random networks (c) ($\chi = 5.0$).

found that the higher the network adaptation probability, the higher the fraction of disconnected SI-links. Consequently, this provided a way to think about the failure phenomenon of infectious disease invasion even if it has a high capacity of transmission.

3.4. Interplay between Network Adaptation Probability and Disease Transmission Ratio and Its Effect on the Infectious Disease Transmission on Adaptive Random Networks. In this work, we also studied the interplay between the varied values of the network adaptation probability and the disease transmission ratio in the 2 types of adaptive networks. We observed that in the previous sections an increase of the infectious fraction reaches its peak at the epidemic peak time and then decayed to zero at the stationary state after an appropriate period of time-steps. More precisely, keeping the disease transmission ratio χ constant and increasing the network adaptation probabilities ω_{I} and ω_{II} affected the epidemic peak time and the infectious fraction at epidemic peak time by delaying the time of occurrence and reducing the fraction nodes. On the other hand, it hastened the time of epidemic peaking, if the network adaptation probabilities ω_{I} and ω_{II} were fixed and the disease transmission ratio χ was increased. We observed competition between the values of ω_{I} and ω_{II} and χ affecting the incidence of epidemic peaking of the infectious fraction by increasing χ but decreasing ω_{I} and ω_{II}. We plotted the infectious fraction against the disease transmission ratio and the network adaptation probability

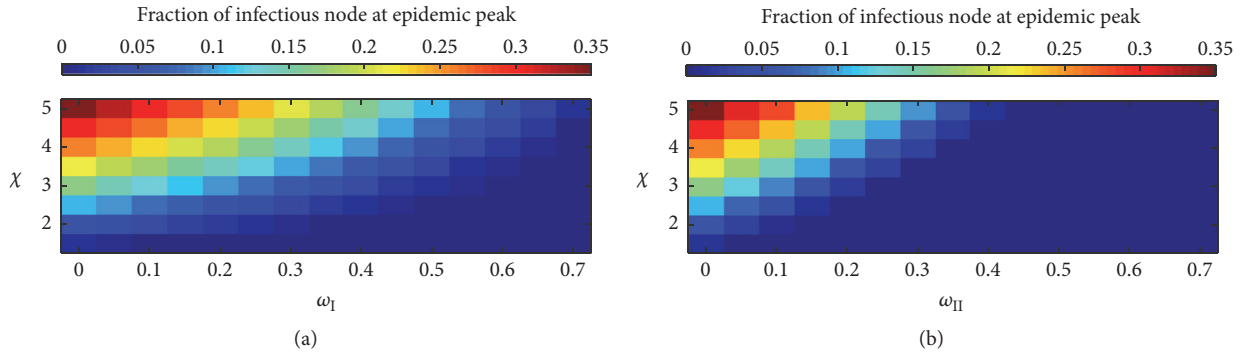

FIGURE 8: Profile of the infectious fraction at the epidemic peak time as function of the network adaptation probabilities ω_I and ω_{II} and the disease transmission ratio χ of type I adaptive random network (a) and type II adaptive random network (b).

to obtain more understanding of the interplay between these probabilities. From the results in previous sections, we observe that the epidemic peak time was dramatically delayed in case of the static network simulations. Figure 8 shows the infectious fraction at epidemic peak time-steps in cases of the type I and II network models. We observe a tentatively decrease of the infectious fraction at epidemic peak time in the static type I network but a dramatically decrease in case of simulations of the type II network with an increasing value of the network adaptation probability. The pattern of the colored grids tended to behave in a linear fashion with an increase in ω_I and ω_{II} and χ in both cases of type I and II network models. In this way, there is a connection line between dark blue grids and nondark blue grids. It refers to a critical value below which the infectious disease is considered to fail its invasion. This led us to the description of the threshold phenomenon.

Consequently, the epidemic peak time of the type I adaptive network occurs earlier and its infectious fraction at epidemic peak time is larger than similar simulations using the type II adaptive network.

The results tell that the interplay between the network adaptation probability and the disease transmission ratio affects the epidemic peak time, the infectious fraction at the epidemic peak time, and also the cumulative number of infection cases at stationary state R_∞ as shown in Figure 9. The cumulative number of infection cases at stationary state, R_∞, for calculations with the static random network ranged from 0.14 to 0.85 and the disease transmission ratio χ ranged between 1.5 and 5.0. In this set of results, a basically similar pattern was observed between both the type I and II network models. More precisely, the number dramatically decreased with an increasing network adaptation probability but dramatically increased with an increasing disease transmission ratio. We learned that the infectious disease is expected to fail invasiveness, if there are less than 10 cumulative cases of infection at stationary state. The threshold phenomenon then occurred for appropriate probabilities in both cases of type I and II network models. Hence, the threshold condition for the type I network was a destruction probability ω_I in range of 0.3 to 0.55 and a disease transmission ratio χ less than 3 with a 3.95 slope. Interestingly, the threshold condition for the type II networks was fulfilled for the entire range of the ratio between the rewiring probability ω_{II} and the disease transmission ratio χ measuring a slope of 8.65. In any cases of the emerging infectious disease transmission, the number of cumulative case fractions in the type I adaptive random network is higher than in the type II adaptive random network.

Finally, we investigated the relative cumulative cases of type I and type II adaptive random networks at equivalent conditions as shown in Figure 10. This exhibits a difference of interplay between network adaptation probability and the disease transmission ratio. We plotted the relative cumulative cases against the network adaptation probabilities ω_I and ω_{II} and the disease transmission ratio χ. The curve tended to increase with increasing ω_I and ω_{II} along the χ-axis but obviously vanished for ω_I and ω_{II} exceeding the value of 0.6. In addition, there was a high ratio number between cumulative cases of type I and type II adaptive network for ω_I and ω_{II} ranging between 0.4 and 0.6, because it was below the threshold condition of type II adaptive network in these cases.

Moreover, with an appropriate value setting of χ and ω_I and ω_{II} the infectious disease failed to invade the population. This led us to the threshold conditions for these models in which other parameters and structures of the initial network condition were fixed. The threshold parameter is supposed to intersect between dark blue and semidark blue grids and to be a function of both χ and ω_I and ω_{II}. In addition, the topology of network adaptation dynamics in the type II adaptive random network reduced more effectively the disease transmissions than the topology of network adaptation dynamics in the type I adaptive network. In contrast to the type II adaptive random network, the number of links in the type I adaptive random network changed over time, due to the destroyed links of the susceptible nodes. This effect reduced the average degree of nodes in such networks. The epidemic peak time was shown to exhibit a maximum number of destroyed SI-links and was always equal to the epidemic peak time of infectious fraction, because there was a maximum number of SI-links at that time, while the susceptible nodes attempted to disconnect their SI-links until reaching the stationary state. Consequently, we may argue that if the emerging infectious disease has a high transmissibility, the individuals in the population must increase their chance to avoid contact with

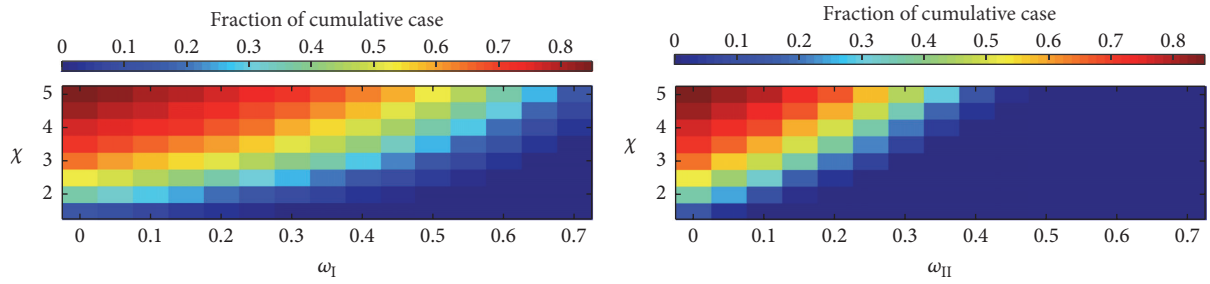

FIGURE 9: Profile of the cumulative cases as function of the network adaptation probabilities ω_{I} and ω_{II} and the disease transmission ratio χ of type I adaptive random network (a) and type II adaptive random network (b).

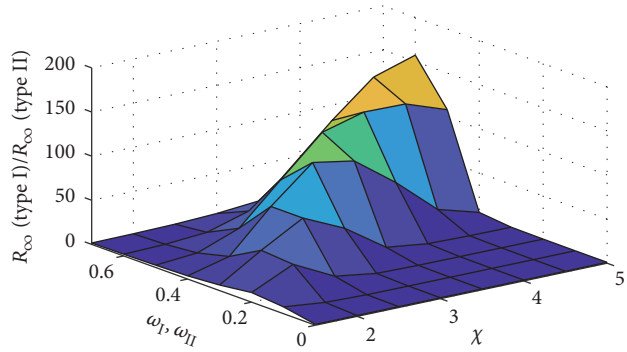

FIGURE 10: Profile of relative cumulative cases of type I and type II adaptive network against network adaptation probabilities ω_{I} and ω_{II} and epidemic characteristic ratio χ. R_∞ is the number of recovered individuals at the equilibrium.

infected individuals in order to protect the population from the invasion.

4. Conclusion

In this research, the modeling of adaptive random networks was studied. We concluded that the topology of network adaptation dynamics may have strong effect on reducing the infectious disease transmission on respective network models. The number of cumulative cases of infection at stationary state was affected by both epidemic parameters and adaptive parameters. The networks with adaptation dynamics such as the type II adaptive random network are more effective in reducing the final epidemic spread when compared with the type I adaptive random network. Moreover, the results suggested the occurrence of a threshold phenomenon independence of choices of appropriate values of respective network parameters.

Disclosure

The study's sponsors have no role in the study design; collection, analysis, and interpretation of data; the writing of the manuscript; and the decision to submit the manuscript for publication.

Conflicts of Interest

The authors declare that there are no conflicts of interest.

Acknowledgments

This research is supported by the Centre of Excellence in Mathematics, the Commission on Higher Education, Thailand, the Thailand Center of Excellence in Physics (ThEP), and the Thailand Research Fund under Grant no. TRG5880157.

References

[1] G. P. Garnett and R. M. Anderson, "Sexually transmitted diseases and sexual behavior: Insights from mathematical models," *Journal of Infectious Diseases*, vol. 174, no. 2, pp. S150–S161, 1996.

[2] J. J. Potterat, R. B. Rothenberg, and S. Q. Muth, "Network structural dynamics and infectious disease propagation," *International Journal of STD and AIDS*, vol. 10, no. 3, pp. 182–185, 1999.

[3] A. S. Klovdahl, "Networks and pathogens," *Sexually Transmitted Diseases*, vol. 28, no. 1, pp. 25–28, 2001.

[4] B. Szendroi and G. Csányi, "Polynomial epidemics and clustering in contact networks," *Proceedings of the Royal Society B: Biological Sciences*, vol. 271, no. 5, pp. S364–S366, 2004.

[5] I. A. Doherty, N. S. Padian, C. Marlow, and S. O. Aral, "Determinants and consequences of sexual networks as they affect the spread of sexually transmitted infections," *Journal of Infectious Diseases*, vol. 191, supplement 1, pp. S42–S54, 2005.

[6] M. J. Keeling and P. Rohani, *Modeling Infectious Diseases in Humans and Animals*, Princeton University Press, New Jersey, NJ, USA, 2008.

[7] M. J. Keeling and K. T. D. Eames, "Networks and epidemic models," *Journal of the Royal Society Interface*, vol. 2, no. 4, pp. 295–307, 2005.

[8] R. Pastor-Satorras and A. Vespignani, "Epidemic spreading in scale-free networks," *Physical Review Letters*, vol. 86, no. 14, pp. 3200–3203, 2001.

[9] M. Kuperman and G. Abramson, "Small world effect in an epidemiological model," *Physical Review Letters*, vol. 86, no. 13, pp. 2909–2912, 2001.

[10] M. Barahona and L. M. Pecora, "Synchronization in small-world systems," *Physical Review Letters*, vol. 89, no. 5, Article ID 054101, 2002.

[11] K. Klemm and V. M. Eguíluz, "Highly clustered scale-free networks," *Physical Review E - Statistical, Nonlinear, and Soft Matter Physics*, vol. 65, no. 3, Article ID 036123, 036123 pages, 2002.

[12] M. E. Newman, "Spread of epidemic disease on networks," *Physical Review E. Statistical, Nonlinear, and Soft Matter Physics*, vol. 66, no. 1, Article ID 016128, 016128, 11 pages, 2002.

[13] M. E. Newman, "Mixing patterns in networks," *Physical Review E: Statistical, Nonlinear, and Soft Matter Physics*, vol. 67, no. 2, 2003.

[14] S. Bornholdt and T. Rohlf, "Topological evolution of dynamical networks: global criticality from local dynamics," *Physical Review Letters*, vol. 84, no. 26, pp. 6114–6117, 2000.

[15] H. Ebel, J. Davidsen, and S. Bornholdt, "Dynamics of social networks," *Complexity*, vol. 8, no. 2, pp. 24–27 (2003), 2002.

[16] P. Holme and G. Ghoshal, "Dynamics of networking agents competing for high centrality and low degree," *Physical Review Letters*, vol. 96, no. 9, Article ID 098701, 2006.

[17] T. Gross, C. J. D. D'Lima, and B. Blasius, "Epidemic dynamics on an adaptive network," *Physical Review Letters*, vol. 96, no. 20, Article ID 208701, 2006.

[18] I. Tunc, M. S. Shkarayev, and L. B. Shaw, "Epidemics in adaptive social networks with temporary link deactivation," *Journal of Statistical Physics*, vol. 151, no. 1-2, pp. 355–366, 2013.

[19] C. T. Bauch, "A versatile ODE approximation to a network model for the spread of sexually transmitted diseases," *Journal of Mathematical Biology*, vol. 45, no. 5, pp. 375–395, 2002.

[20] K. T. Eames and M. J. Keeling, "Monogamous networks and the spread of sexually transmitted diseases," *Mathematical Biosciences*, vol. 189, no. 2, pp. 115–130, 2004.

[21] C. Kamp, "Untangling the interplay between epidemic spread and transmission network dynamics," *PLoS Computational Biology*, vol. 6, no. 11, e1000984, 9 pages, 2010.

[22] N. Geard, "Adaptive networks: theory, models and applications," in *Artificial Life*, T. Gross and H. Sayama, Eds., vol. 16, pp. 329–331, Springer-Verlag, 2010.

[23] L. B. Shaw and I. B. Schwartz, "Fluctuating epidemics on adaptive networks," *Physical Review E. Statistical, Nonlinear, and Soft Matter Physics*, vol. 77, no. 6, Article ID 066101, 066101, 10 pages, 2008.

[24] T. Gross and B. Blasius, "Adaptive coevolutionary networks: a review," *Journal of the Royal Society Interface*, vol. 5, no. 20, pp. 259–271, 2008.

Hindawi
Computational and Mathematical Methods in Medicine
Volume 2017, Article ID 7981645, 12 pages
https://doi.org/10.1155/2017/7981645

Research Article

Modelling Risk to US Military Populations from Stopping Blanket Mandatory Polio Vaccination

Colleen Burgess,[1,2] Andrew Burgess,[2] and Kellie McMullen[3]

[1]*Ramboll Environ, Inc., Amherst, MA, USA*
[2]*MathEcology, LLC, Phoenix, AZ, USA*
[3]*Naval Health Research Center, San Diego, CA, USA*

Correspondence should be addressed to Colleen Burgess; cburgess@ramboll.com
and Kellie McMullen; kellie.l.mcmullen2.mil@mail.mil

Received 27 April 2017; Accepted 8 June 2017; Published 14 September 2017

Academic Editor: Delfim F. M. Torres

Objectives. Transmission of polio poses a threat to military forces when deploying to regions where such viruses are endemic. US-born soldiers generally enter service with immunity resulting from childhood immunization against polio; moreover, new recruits are routinely vaccinated with inactivated poliovirus vaccine (IPV), supplemented based upon deployment circumstances. Given residual protection from childhood vaccination, risk-based vaccination may sufficiently protect troops from polio transmission. *Methods.* This analysis employed a mathematical system for polio transmission within military populations interacting with locals in a polio-endemic region to evaluate changes in vaccination policy. *Results.* Removal of blanket immunization had no effect on simulated polio incidence among deployed military populations when risk-based immunization was employed; however, when these individuals reintegrated with their base populations, risk of transmission to nondeployed personnel increased by 19%. In the absence of both blanket- and risk-based immunization, transmission to nondeployed populations increased by 25%. The overall number of new infections among nondeployed populations was negligible for both scenarios due to high childhood immunization rates, partial protection against transmission conferred by IPV, and low global disease incidence levels. *Conclusion.* Risk-based immunization driven by deployment to polio-endemic regions is sufficient to prevent transmission among both deployed and nondeployed US military populations.

1. Introduction

Polio is a viral disease that invades the nervous system and can cause paralysis in a matter of hours, though most poliovirus infections are asymptomatic [1]. There are 3 wild poliovirus (WPV) types, two of which have not been detected globally since 2012 [2]. Polio infection in immunocompetent individuals leads to immunity, although immunity induced by one serotype does not protect against the other two [3]. There are 2 vaccines against polio: inactivated poliovirus vaccine (IPV) and oral poliovirus vaccine (OPV). Successful vaccination with either formulation provides at least partial protection from infection and full disease immunity in approximately 7 days [4].

After IPV immunization, antibodies are produced in the blood in response to the inactivated virus, protecting the individual from disease; however, viral replication in the gut is still possible, with the potential for asymptomatic transmission to the community [5]. IPV-induced antibodies decrease over time, and some adults vaccinated as children may lack a detectable antibody.

In contrast, OPV induces mucosal immunity in the gastrointestinal tract, which is important for community protection [6], and provides long-term immunity against both disease and transmission. Yet, "the oral vaccine often fails in developing countries and in rare cases the vaccine virus itself leads to paralysis" [7]. OPV can also lead to the circulation of a vaccine-induced virus, shed for 1–3 weeks following primary vaccination and easily transmitted within and outside the household. While this shedding is widely accepted as inducing protection or boosting immunity in contacts [3],

it can also contribute to the spread of circulating vaccine-derived poliovirus (cVDPV) [6], particularly in settings with weak routine immunization coverage in otherwise polio-free countries [8].

Due to these risks, most developed countries have switched from OPV to IPV [9]. However, for developing countries where polio is endemic or the risk of importation is high, the benefits of OPV outweigh the risks, and, for now, OPV remains the vaccine of choice [3]. The ultimate goal is to eliminate OPV vaccination and switch to IPV-only immunization, thus eliminating the risk of cVDPV altogether. As of November 2016, 173 countries now include IPV in their routine immunizations; the remaining World Health Organization (WHO) member countries are on schedule to introduce IPV by the end of 2016 [10].

Today, WPV remains endemic in 3 countries—Pakistan, Afghanistan, and Nigeria [11]. While WPVs circulate in these areas, "the rest of the world must continue to keep polio vaccination levels very high, due to the risk of outbreaks among susceptible people in polio-free countries" [12]. Response to polio circulation in developing areas such as these generally involves the use of OPV, and "each response round comes with a substantial and uncertain amount of secondary OPV infection" [4], which are of particular risk to deployed US soldiers with incomplete or waning protection against poliomyelitis transmission.

In the United States, children currently receive 3 routine doses of IPV at 2 months, 4 months, and 6–18 months, and a booster at 4–6 years [13]. As a result, US-born soldiers generally enter military service with a high level of immunity to disease, though this may wane over time. The military actively vaccinates all recruits against a number of diseases including polio; "these vaccines are further supplemented, based on occupational and deployment circumstances of the recruits" [14]. However, in countries with insufficient vaccination and/or active viral circulation, contact with local populations puts US warfighters at risk for transmission of both WPV and cVDPV. This is particularly the case since

> [although] militaries primarily engage in traditional major combat operations, they are increasingly involved in humanitarian assistance missions. Such missions permit extensive interaction with the local populace and environment, greatly increasing the chance of acquiring locally endemic infectious diseases and necessitating the management of diseases in the local populace that are not traditionally seen in military personnel [15].

Thus, while blanket vaccination of all soldiers may be epidemiologically redundant and cause unnecessary expenditure of resources, risk-based vaccination driven by travel to polio-endemic areas can be appropriate. However, evaluating multiple vaccination strategies once deployment is underway may result in higher-than-necessary disease incidence and cost in an effort to control transmission. In lieu of this, predictive modelling of polio transmission allows for the exploration of vaccination strategies through simulation of multiple scenarios and their outcomes prior to putting troops and mission objectives at risk.

In recent years, published mathematical models for polio transmission have focused primarily on the role of OPV in attaining eradication of the disease. Several mathematical models have also explored vaccine-derived polioviruses [16–18], and additional analyses have addressed the impact of asymptomatic infection [19–22]. Kalkowska et al. [20, 21] explored the possibility of silent transmission of WPV in populations with high IPV coverage, emphasizing that "IPV-based protection alone might not provide sufficient population immunity to prevent poliovirus transmission after an importation" [20] and acknowledging the need to "consider the role of previously-vaccinated or infected individuals (i.e., partially infectible individuals) who remain immune to paralytic disease, but not to reinfection, and their potential participation in silent transmission of the virus" [21]. Most recently, Koopman et al. [22] modelled the interaction between waning immunity and the duration of silent circulation of polio and found that expanding beyond childhood immunization to vaccinate a portion of the adult population could have a significant impact on asymptomatic transmission.

Each of these modelling studies focuses on issues among multigenerational populations with varying levels of immunization coverage and background immunity; none have addressed the unique circumstances affecting polio transmission in highly mobile military populations, which experience conditions that directly affect the spread of disease, both beneficially and detrimentally. US soldiers are vaccinated against polio at recruitment and again prior to deployment to at-risk areas; however, immunization with IPV may leave troops at risk of VDPV or subject to asymptomatic transmission. Quantifying this risk is crucial to evaluating the elimination of mandatory blanket polio vaccination and switching to a solely risk-based vaccination policy.

Mathematical models can be immensely useful in examining the impact of vaccines on disease transmission and are frequently used to inform response policy. For deployed military populations, these models can also evaluate the relative change in transmission risk associated with multiple vaccination scenarios by employing data on specific demographics, epidemiology, and the effects of timing of response. For this analysis, we modified an existing military-specific model system to accommodate polio transmission and vaccination to maximize the achievement of deployed mission objectives, while minimizing the possibility of transmission to troops both abroad and at home.

2. Methods

2.1. Population Structure. The military population structure for this study was built upon previous analyses [23]. The simulated deployed population consisted of 4 subpopulations defined by interaction with the local population, ranging from negligible to high levels of daily contact. Deployed soldiers were assumed to be posted to a long-standing base

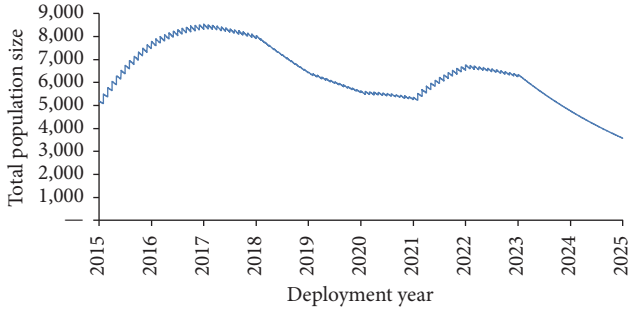

Figure 1: Change in deployed population size over the 10-year duration of the deployment action [23].

within the host country, with well-established water purification and food safety systems to minimize environmental disease transmission. Social mixing was presumed to be mainly within-unit and homogeneous, with between-unit mixing occurring at lower levels.

The 10-year simulated deployment period began in 2015, with individual soldiers rotating annually. In- and outbound rotation rates (b_{IN} and b_{OUT}) varied over the 10-year period to allow for force increase and decrease (see Figure 1) and a daily casualty rate (μ) accounted for removal of individuals for reasons other than rotation or polio-related disease. See Burgess et al. [23] for additional population details.

The local population was modelled without structure and based on the demographic characteristics of Afghanistan as estimated by the United Nations Population Division [24]. Mixing among locals was homogeneous within the simulated geographic region. Local birth and nonpolio death rates varied annually [24], and a polio-specific death rate (μ_{POLIO}) was applied to infected individuals. OPV immunization of locals was set to historic reported coverage rates (ρ) up to 2013 (the most recent year for which data was available at the time of model development) [25] and held constant at the 2013 rate for the remainder of the simulation period.

2.2. Transmission Model. Polio transmission was modelled as a modified compartmental Susceptible-Exposed-Infected-Removed model (1) (see Figure 2 and Tables 1 and 2) employing structured ordinary differential equations. Transmission of polio occurred via direct contact between susceptible and infected individuals, with random case importation boosting infection levels stochastically throughout the simulation.

$$\begin{aligned}
\frac{dS_i}{dt} &= b_{\text{IN}i}\left(1-\text{protect}_i\right)N_i \\
&\quad -\left(\rho_i+\beta_i+\mu_i+b_{\text{OUT}i}\right)S_i, \\
\frac{dS_{Pi}}{dt} &= b_{\text{IN}i}\text{protect}_i N_i+\Omega R_i-\left(\pi_s\beta_i+\mu_i+b_{\text{OUT}i}\right)S_{Pi}, \\
\frac{dE_i}{dt} &= \beta_i S_i-\left(\iota+\mu_i+b_{\text{OUT}i}\right)E_i, \\
\frac{dE_{Pi}}{dt} &= \pi_s\beta_i S_{Pi}-\left(\iota_p+\mu_i+b_{\text{OUT}i}\right)E_{Pi}, \\
\frac{dI_i}{dt} &= \iota E_i-\left(\gamma+\mu_{\text{POLIO}}+\mu_i+b_{\text{OUT}i}\right)I_i, \\
\frac{dI_{Pi}}{dt} &= \iota_p E_{Pi}-\left(\gamma_p+\mu_i+b_{\text{OUT}i}\right)I_{Pi}, \\
\frac{dR_i}{dt} &= \rho_i S_i+\gamma I_i+\gamma_p I_{Pi}-\left(\Omega+\mu_i+b_{\text{OUT}i}\right)R_i, \\
\frac{dN_i}{dt} &= \left(b_{\text{IN}i}-b_{\text{OUT}i}-\mu_i\right)N_i-\mu_{\text{POLIO}}I_i.
\end{aligned} \tag{1}$$

Table 1: Variable definitions for polio transmission model.

Variable	Definition
S_i	Number of unprotected susceptible individuals in subpopulation i
S_{Pi}	Number of partially protected susceptible individuals in subpopulation i
E_i	Number of unprotected exposed individuals in subpopulation i
E_{Pi}	Number of partially protected exposed individuals in subpopulation i
I_i	Number of unprotected infected individuals in subpopulation i
I_{Pi}	Number of partially protected infected individuals in subpopulation i
R_i	Number of recovered or removed individuals in subpopulation i
N_i	Total population size in subpopulation i

To establish endemicity, polio transmission among locals was simulated for a burn-in period of 35 years prior to the arrival of the deployed military population in 2015. Simulated, combined symptomatic and asymptomatic incidence during this burn-in phase was validated against reported paralytic polio cases as recorded by the WHO [34], adjusted to account for the widely accepted 10% proportion of cases that are symptomatic [28]. Validation was performed qualitatively and visually, comparing adjusted historical data to the output of multiple stochastic model iterations under baseline parameter assumptions. Simulated local cases fit well with historical data for 1980–2014 (data missing for 1992–1994 and 1996), in terms of both magnitude and frequency of peaks (Figure 3).

Individuals entered population either via birth (locals) with full susceptibility (S) or via inward rotation (military) with partial susceptibility (S_p) defined by childhood immunization, blanket immunization upon recruitment, and/or booster immunization prior to deployment (see Scenario Construction). Following an incubation period of 3-4 days (ι or ι_p, depending on immune status), exposed individuals (E, E_p) progressed to infection lasting 27 days (Υ) (range: 27-28 days) for unprotected individuals (I) or 9 days (Υ_p) (range: 9–25 days) for partially protected individuals (I_p), who were 20% (π_i) (range: 20–90%) as infectious as fully

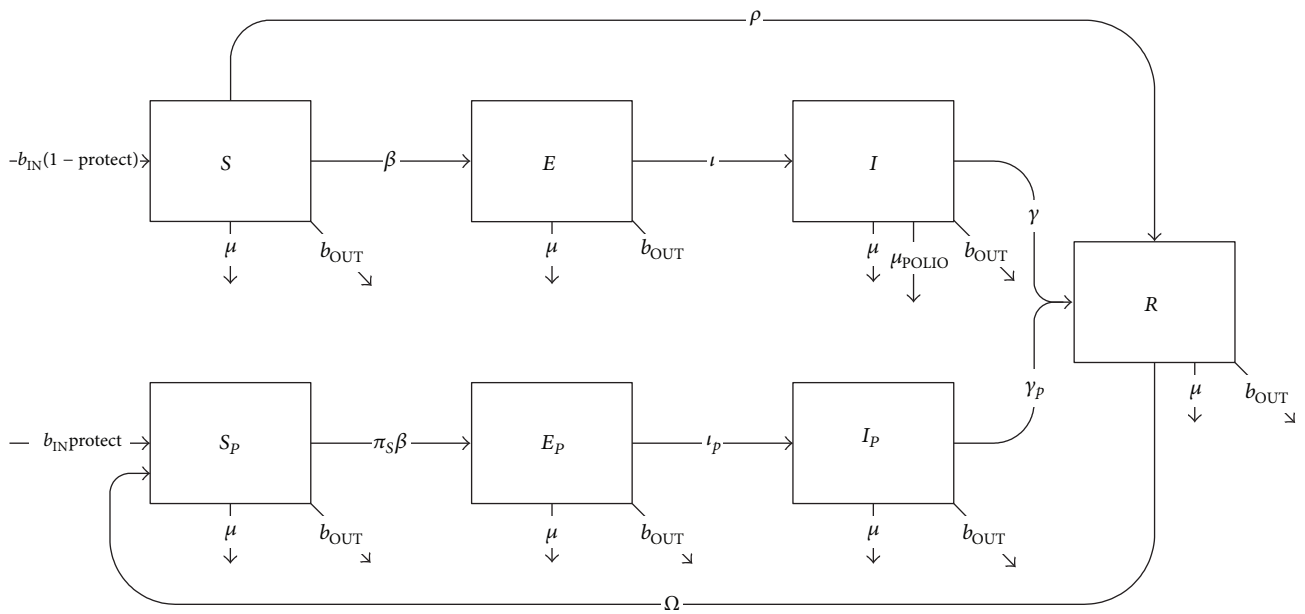

Figure 2: Schematic diagram of polio transmission with both OPV (ρ) and IPV (S_p) immunization and waning immunity.

Table 2: Parameter definitions for polio transmission model for military (MIL) and local (LOC) populations.

Parameter	Definition	Value (range)	Source
b_{INi}	Daily inbound rotation rate (MIL)/birth rate (LOC) for subpopulation i	[Array]	
b_{OUTi}	Daily outbound rotation rate (MIL)/background death rate (LOC) for subpopulation i	[Array]	
μ_i	Daily background casualty rate for subpopulation i (MIL)	[Array]	
protect_i	Daily proportion of inbound population with preexisting partial protection for subpopulation i (MIL)	[Array]	
ρ_i	Daily (OPV) vaccination rate for subpopulation i (LOC)	[Array]	
β_i	Effective polio transmission rate for subpopulation i	[Function]	
π_s	Relative susceptibility of S_p individuals	0.2 (0.2–0.9)	[26]
$1/\iota$	Duration of latent period for unprotected individuals	3 d (3-4 d)	[26, 27]
$1/\iota_p$	Duration of latent period for partially protected individuals	4 d (3-4 d)	[26, 27]
$1/\gamma$	Duration of infectious period for unprotected individuals	27 d (27-28 d)	[26]
$1/\gamma_p$	Duration of infectious period for partially protected individuals	9 d (9–25 d)	[26]
μ_{POLIO}	Polio mortality rate	0.22 (0.02–0.30)	[28]
Ω	1/duration of OPV or disease-induced immunity	$1/(365 * 20)$	(See text)
seas	Seasonal variation in polio transmission	[Function]	
σ	Proportional change in polio transmission due to seasonality	0.15	[21]
χ	Polio attack rate	20/100,000 (0.1/1,000,000–6.8/100,000)	[29–32]
C_{ij}	Daily contact rate between subpopulations i and j	[Array]	[23]
π_i	Relative infectiousness of I_p individuals	0.2 (0.2–0.9)	[26, 33]
symp	Proportion of unprotected polio cases that are symptomatic	0.1	[28]
importrisk	Probability of polio case importation from outside population	0.001	(See text)
importampl	Amplitude of polio case importation from outside population	2/100,000	(See text)

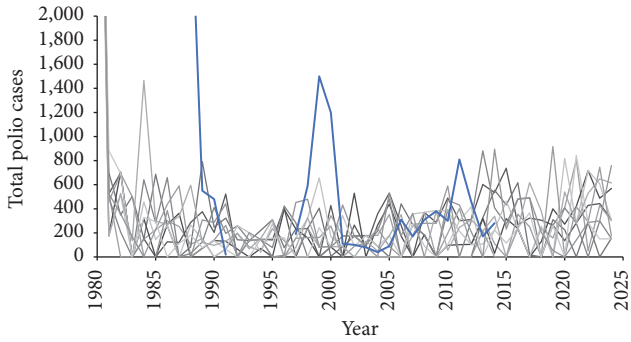

FIGURE 3: Qualitative comparison between simulated (gray lines) and historical (blue line) polio cases (symptomatic + asymptomatic) for the local population over a sample of 10 random simulations.

unprotected infected persons. Recovered individuals (R) possessed immunity to both transmission and disease for a period of 20 years ($1/\Omega$) (see discussion of uncertainty), after which only immunity to disease was retained and individuals entered (or reentered) the partially susceptible (S_p) class.

Ten percent (symp) of cases in nonimmune, infected individuals presented with symptoms, with the remainder being subclinical; all infections in partially protected individuals were assumed to be asymptomatic. Polio-related mortality affected only symptomatically infected individuals.

Polio transmission was driven by an attack rate (χ) of 20 cases per 100,000 population (range: 0.1/1,000,000–20/100,000) with seasonal forcing (seas), allowing for both high- and low-transmission periods within the year. Transmission was further impacted by stochastic case importation with 0.1% probability (importrisk) and amplitude of 1/10th the attack rate (importampl) (see discussion of uncertainty):

$$\begin{aligned} \text{seas} &= 1 + \sigma\left(\cos\left(\frac{2\pi t}{365}\right)\right), \\ \beta_i &= \left(\text{seas} * \chi * \sum C_{ij}\left(\frac{I_j + \pi_i I_{Pj}}{N_j}\right)\right) \\ &\quad + \text{import}, \\ \text{import} &= \begin{cases} \text{importampl} & \text{if rand} < \text{importrisk} \\ 0 & \text{if rand} \geq \text{importrisk}, \end{cases} \end{aligned} \tag{2}$$

where rand $\sim U(0,1)$.

2.3. Sensitivity and Uncertainty Analyses. Sensitivity and uncertainty analyses were performed on 21 model parameters, with outcomes measured in terms of total symptomatic and asymptomatic polio cases and mean annual incidence among military and local populations.

Total military cases and annual incidence showed direct sensitivity to the relative susceptibility (π_s) of partially protected individuals (S_p). Since the significant majority of the military population falls into the S_p category, as a result of IPV immunization, it is logical that increased relative susceptibility in these individuals results in more cases overall. In contrast, transmission among locals was dramatically less sensitive to π_s, since the only S_p individuals within the local population included those who were previously infected and recovered and for whom enough time had passed that preexisting immunity from recovery waned.

Local annual disease incidence was significantly sensitive to the polio death rate (μ_{POLIO}); higher mortality results in fewer polio cases, as a result of an overall decrease in individuals participating in transmission. As IPV immunization is assumed to confer at least partial protection, the bulk of polio cases within deployed troops are asymptomatic and, thus, not affected by disease-related death rates.

The duration of the infectious period ($1/\Upsilon_p$) for partially protected, infected individuals (I_p) significantly affected total military cases and annual incidence, reflecting that a shorter infectious period among I_p resulted in lower transmission and, therefore, fewer subsequent polio cases. The impact on local populations was dramatically lower due to the smaller fraction of locals falling within the I_p category.

Local incidence was inversely affected by changes in the duration of OPV- or disease-induced immunity ($1/\Omega$), that is, longer-lasting immunity resulted in fewer local cases overall. There was no significant impact on military polio incidence; however, since these individuals were not immunized with OPV, the overall deployment period was not long enough to allow for waning of postrecovery immunity to occur.

The level of residual protection resulting from childhood IPV immunization (childhood) had a moderate impact on polio transmission within military populations in simulations within which no other polio vaccination was administered. In the presence of either blanket or booster vaccination (or both), variation in childhood residual protection had no impact on military polio transmission, since the more recent adult immunization overrode any effects due to vaccination occurring early in life.

Uncertainty in case importation (importrisk and importampl) had a dramatic impact on polio incidence in both military and local populations, overriding even variation in the polio attack rate (χ). This mirrors on-the-ground experience with polio eradication efforts. In the absence of new cases entering into an area, adequate routine immunization can halt the local transmission of polio; however, small levels of case importation can spark outbreaks even in immunized regions.

2.4. Scenario Construction. To evaluate the hypothesis that residual immunity from childhood vaccination, combined with risk-based deployment vaccination, is sufficient to protect troops from polio transmission, 3 military IPV scenarios were tested:

(1) Blanket immunization at recruitment + booster immunization at deployment + residual childhood protection (Scenario 1, baseline).

(2) (Blanket immunization terminated in 2015) + booster immunization at deployment + residual childhood protection (Scenario 2).

(3) (Blanket immunization terminated in 2015) + residual childhood protection only (Scenario 3).

As of 2013, the US childhood IPV vaccination coverage rate was approximately 93% [25]; that is, 93% of children aged 1–4 years have received 3 routine doses of IPV. The Centers for Disease Control and Prevention's Pink Book [28] indicates that IPV efficacy after 3 doses is approximately 99% (efficacy), and immunity against disease is "probably lifelong"; while there is some debate regarding waning protection, few studies have been performed to evaluate this. To determine residual adult protection resulting from childhood immunization, we developed a waning curve based on data provided by Lapinleimu and Stenvik [35], which describe the change in detectable polio antibodies over time in individuals in Finland where IPV is the only implemented vaccination. From this data, we extrapolated a relationship between detectable antibodies and years since the most recent IPV booster, defined as a function of age. Based on the 2012 Demographics Profile of the Military Community [36], the average age of the active duty force is 28.7 years; when combined with the childhood IPV coverage rate and applied to the waning immunity curve, on average 92% of soldiers still possess detectable antibodies resulting from childhood IPV immunization (childhood).

The childhood IPV coverage rate accounts for both philosophical and medical exemptions to vaccination, including impaired immune status, allergies to vaccine components, or history of vaccine-associated adverse events. Within the 2012-2013 school year, medical exemptions for childhood vaccinations (not specific to polio) ranged from 0.1 to 1.6% (median 0.3%), and nonmedical exemptions ranged from 0.2 to 6.4% (median 1.5%) [37]. While immunization exemptions are allowed for military service members, "noncompliance with immunization requirements may adversely impact deployability, assignment, or international travel," and "[nonmedical] exemptions may be revoked, in accordance with service-specific policies and procedures, if the individual and/or unit are at imminent risk of exposure to a disease for which an immunization is available" [38].

For this analysis, we assumed that military exemption rates sit at the low-end of the range for childhood vaccination exemptions, yielding an overall military IPV exemption rate (exemption) of 0.3% (range 0.3–8.0%, median 1.8%), with the inclusion of a 75% proportional reduction (dfact) in exemption rate (range 0–100%) for deploying personnel.

Military IPV effective coverage rates for blanket and booster immunization were calculated as follows:

$$\begin{aligned} \text{blanket} &= (1 - \text{exemption}) * \text{efficacy}, \\ \text{boost} &= (1 - (\text{dfact} * \text{exemption})) * \text{efficacy}. \end{aligned} \tag{3}$$

For Scenarios 2 and 3, blanket immunization upon recruitment was halted in 2015; those individuals recruited prior to 2015 would have relatively recent immunity, while those recruited in 2015 or later would have immunity resulting only from deployment booster immunization (Scenario 2) or residual immunity from childhood immunization (Scenario 3). Thus, for these two scenarios, at any point in time from 2015 through the end of the simulation, there would always be a blend of blanket- and nonblanket-immunized individuals in the deployed population.

As of 2006 [39], accession rates within branches of the US military ranged from 13% for the Air Force to 19% for the Army (accession). For Scenarios 2 and 3, the proportion of service members protected by blanket immunization administered prior to 2015 ($B(t)$) was defined as a recursive function diluted by the accession rate:

$$B(t) = \left(1 - \frac{\text{accession}}{365}\right) * B(t-1). \tag{4}$$

The net protection level of the military population from prior blanket immunization combined with residual immunity from childhood immunization was, therefore, given as a maximum function, which decayed to no lower than the childhood protection level:

$$\begin{aligned} N(t) = \max\big((B(t) * \text{blanket}) \\ + [(1 - B(t)) * \text{childhood}], \text{childhood}\big). \end{aligned} \tag{5}$$

This resulted in a drop in overall protection from 98.7% to 93.0% over the 10-year deployment period.

Scenario-specific parameters are provided in Table 3, and final scenario definitions for deployed and nondeployed military personnel are given in Table 4.

Each scenario was run for 1500 simulations to account for stochasticity in polio case importation. Model outputs were measured as total deployed symptomatic and asymptomatic polio cases and average annual incidence (included both symptomatic and asymptomatic cases) for deployed military and local populations.

3. Results

For all scenarios, local disease dynamics remained fairly consistent across all simulations, tracking with historical cases prior to 2015, then sustaining low endemicity driven by case importation to the end of the simulation period (Figures 4(a)–4(c)).

Similarly, there was insignificant change in polio dynamics among deployed military populations between Scenarios 1 and 2, with a slight increase in infections under Scenario 3 (Figures 5(a)–5(c)).

Stochasticity associated with case importation caused variation between simulation results for total cases and average annual polio incidence for all 3 scenarios (Figures 6(a)–6(d)). This variation was relatively small; however, and data points were generally well-clustered around mean values.

Dropping blanket immunization but maintaining predeployment booster immunization had negligible effect on simulated deployed military cases and incidence. Dropping both blanket and predeployment immunizations yielded a 5% increase in polio cases and annual incidence among deployed populations over the baseline scenario of blanket immunization (Table 5). Local annual incidence was not significantly affected by changes in military immunization

Table 3: Parameter definitions for scenario calculations.

Parameter	Definition	Value (range)	Source
efficacy	IPV vaccine efficacy (MIL)	99% (50–100%)	[28]
childhood	Residual protection level from childhood IPV vaccination	0.92 (0.0–1.0)	Calculated from [25, 35]
exemption	Overall military vaccination exemption rate (medical + administrative)	0.003 (0.003–0.08)	Calculated from [37]
dfact	Proportional reduction in exemption rate for deployed personnel (versus nondeployed)	0.75 (0.0–1.0)	(Estimated)
blanket	IPV blanket vaccine coverage (when implemented) for all military personnel upon accession	(Function)	
boost	IPV boost vaccine coverage (when implemented) for deploying personnel	(Function)	
accession	Military accession rate	0.19 (0.13–0.19)	[39]
B	Proportion of military population covered by blanket vaccination prior to 2015	(Function)	
N	Overall protection of military population from blanket vaccination prior to 2015 and residual childhood immunity	(Function)	

Table 4: Scenario definitions for deployed and nondeployed military personnel.

	Protection levels (protect)	
	Deployed personnel	Nondeployed personnel
Scenario 1 (baseline)	blanket	blanket
Scenario 2 (booster)	boost	$N(t)$
Scenario 3 (childhood)	$N(t)$	$N(t)$

strategies, with any variation resulting only from model stochasticity, which indicated that transmission from military to local populations was not an important issue at these levels of military protection.

The total number of symptomatic and asymptomatic polio cases in the deployed military population remained less than one for all 3 immunization scenarios, though fractional cases were still utilized in the calculation of incidence rates. Though frequently undetectable in the field, asymptomatic cases were included in the case-count and incidence calculations to provide a measure of the potential for silent transmission.

For nondeployed personnel, dropping blanket immunization resulted in a decrease in polio disease protection from 99% to 93%. Since IPV vaccination confers full protection from disease but only partial (model assumption: 20%) protection from transmission, this yielded an increase in overall susceptibility to transmission among the nondeployed population from 21% to 26%.

Combining nondeployed susceptibility levels with the average annual polio incidence among deployed populations for each scenario allowed for estimation of the risk of new polio infections within nondeployed personnel due to mixing with infected soldiers returning from deployment. For the blanket immunization scenario (Scenario 1), the risk of new polio infections resulting from reintegrating infected soldiers was predicted to be 0.000504/1,000,000. For Scenario 2—where blanket immunization was terminated but predeployment booster was still employed—the simulated risk of new polio infections increased from 0.000504/1,000,000 to 0.000624/1,000,000 after 10 years without blanket vaccination. For Scenario 3—where both blanket and booster immunizations were terminated—simulated risk of new polio infections among nondeployed personnel increased from 0.000546/1,000,000 to 0.000676/1,000,000 (Table 6) over the same 10-year period.

4. Discussion and Conclusions

Mathematical models can help guide preventive medicine policy, resulting in healthier and protected populations. This analysis employed a mathematical model for the transmission of polio within deployed military populations interacting with local populations in an endemic setting. Results from model simulations described the potential benefits of protecting these troops via routine blanket immunization, predeployment booster immunization, and residual protection resulting from childhood vaccination.

In the absence of blanket immunization on recruitment, immunity to polio disease among *nondeployed* personnel defaults gradually to residual protection resulting from childhood immunization, and the percentage of this population susceptible to transmission increases. Although the removal of simulated blanket immunization had no noticeable effect on polio incidence among *deployed* personnel subject to predeployment booster immunization, the risk of transmission to nondeployed personnel mixing with deployed soldiers reintegrating with base populations increased by 19%. In the absence of predeployment booster immunization, risk of transmission to nondeployed populations increased by 25% over the baseline scenario.

Though the increased percentage in transmission resulting from dropping blanket immunization was nonzero, the

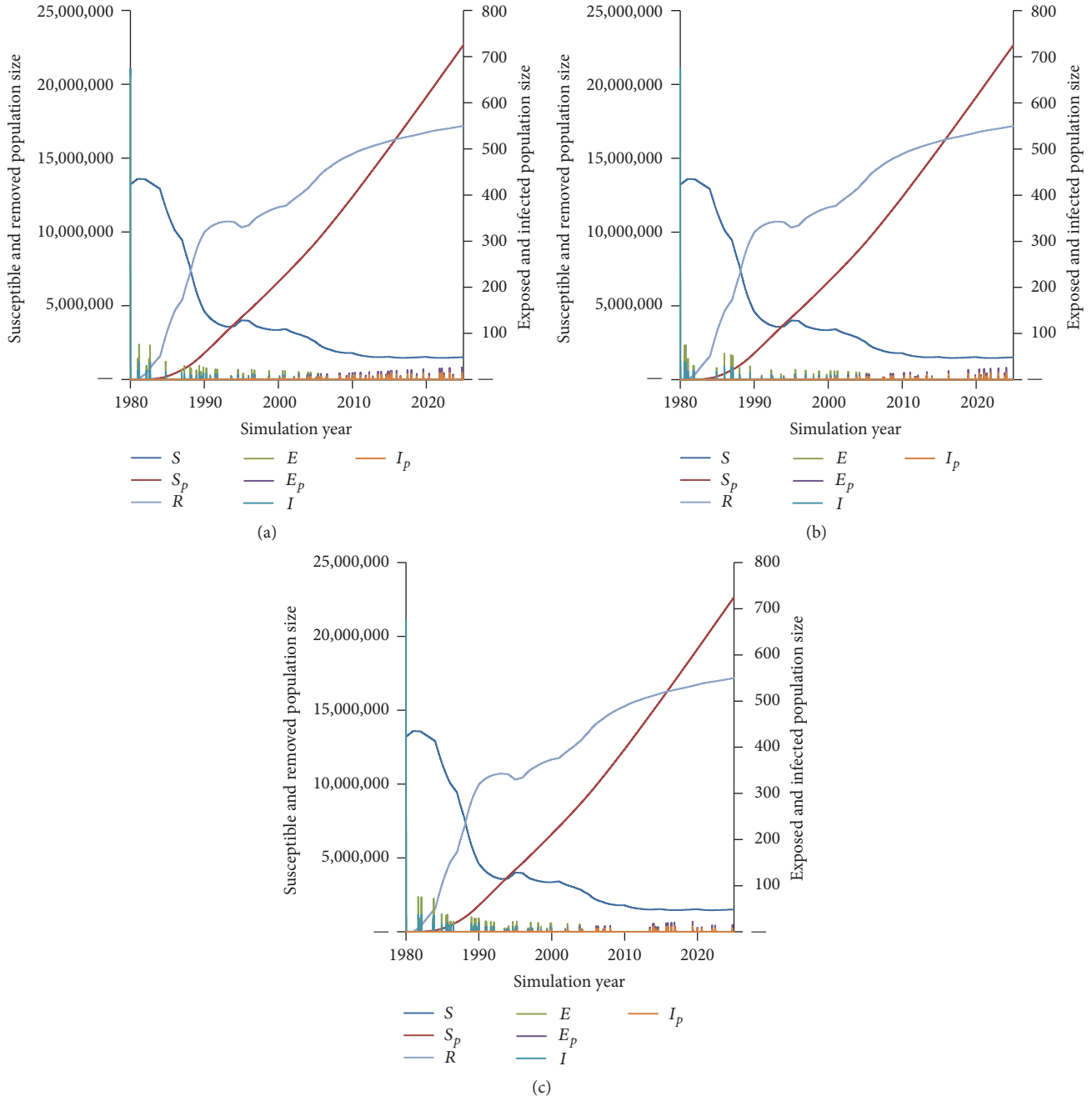

Figure 4: Polio disease dynamics among local populations under military immunization Scenarios (a) 1 (blanket + booster + residual childhood), (b) 2 (booster + residual childhood), and (c) 3 (residual childhood).

Table 5: Median total polio cases and average annual incidence with percentage of change over baseline for deployed military and local populations under 3 military immunization scenarios.

Scenario	Total cases (military)		Average annual incidence	
	Symptomatic	Asymptomatic	Military	Local
1	0.076	0.687	0.012/1000	0.022/1000
2	0.076 (+0%)	0.687 (+0%)	0.012/1000 (+0.2%)	0.022/1000 (+0.8%)
3	0.080 (+5%)	0.721 (+5%)	0.013/1000 (+5.4%)	0.022/1000 (+0.1%)

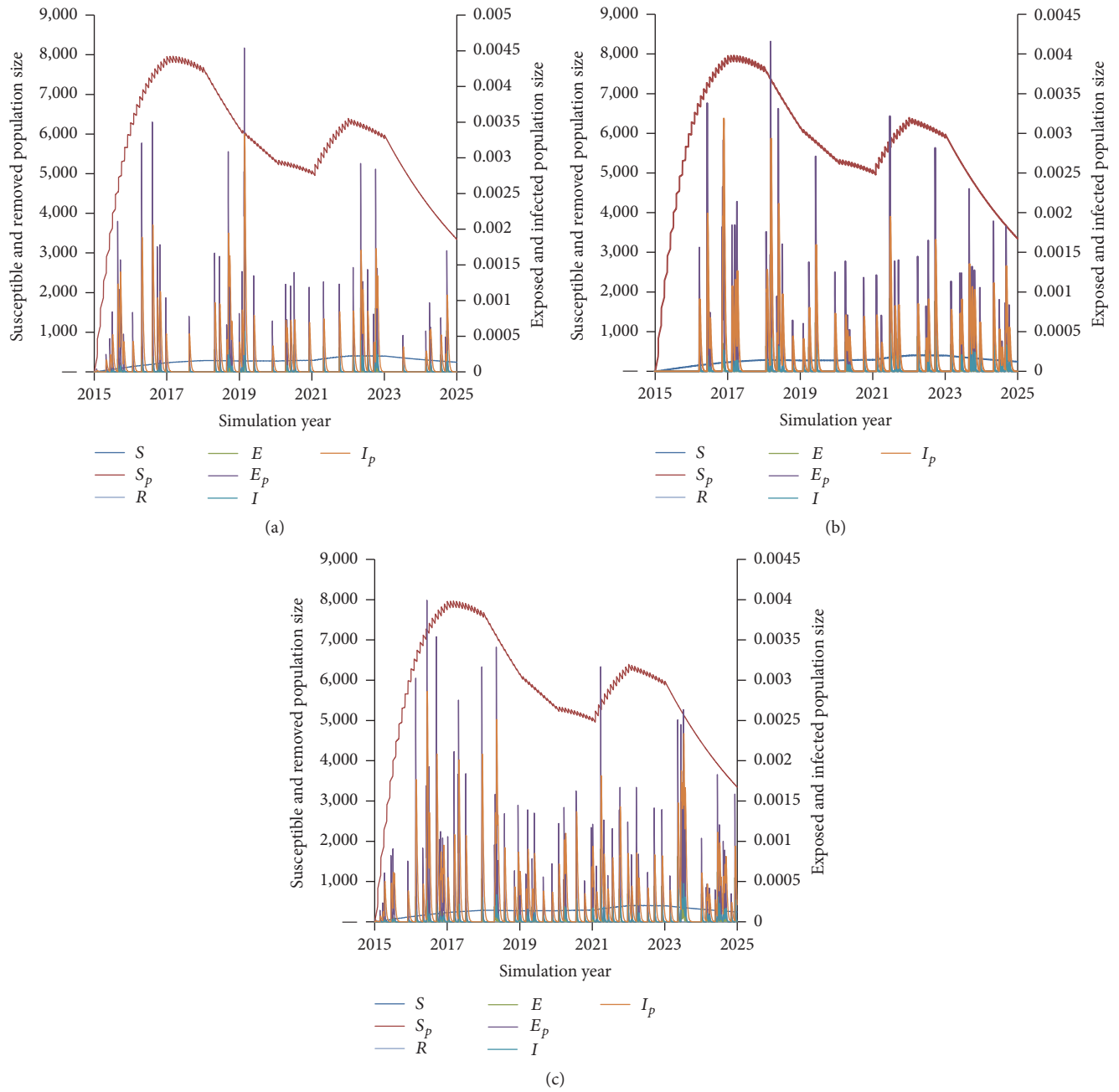

FIGURE 5: Polio disease dynamics among deployed military populations under military immunization Scenarios (a) 1 (blanket + booster + residual childhood), (b) 2 (booster + residual childhood), and (c) 3 (residual childhood).

TABLE 6: Modelled risk of new polio infections among nondeployed service members as a result of infected soldiers reintegrating upon return from deployment.

Scenario	% protected from disease (deployed)	Average annual incidence (nondeployed)	% protected from disease (nondeployed)	% susceptible to transmission (nondeployed)	Risk of new infections (nondeployed)
1	99%	1.2/100,000	99%	21%	0.000504/1,000,000
2	99%	1.2/100,000	99% ↘ 93%	21% ↗ 26%	0.000504/1,000,000 ↗ 0.000624/1,000,000
3	99% ↘ 93%	1.3/100,000	99% ↘ 93%	21% ↗ 26%	0.000546/1,000,000 ↗ 0.000676/1,000,000

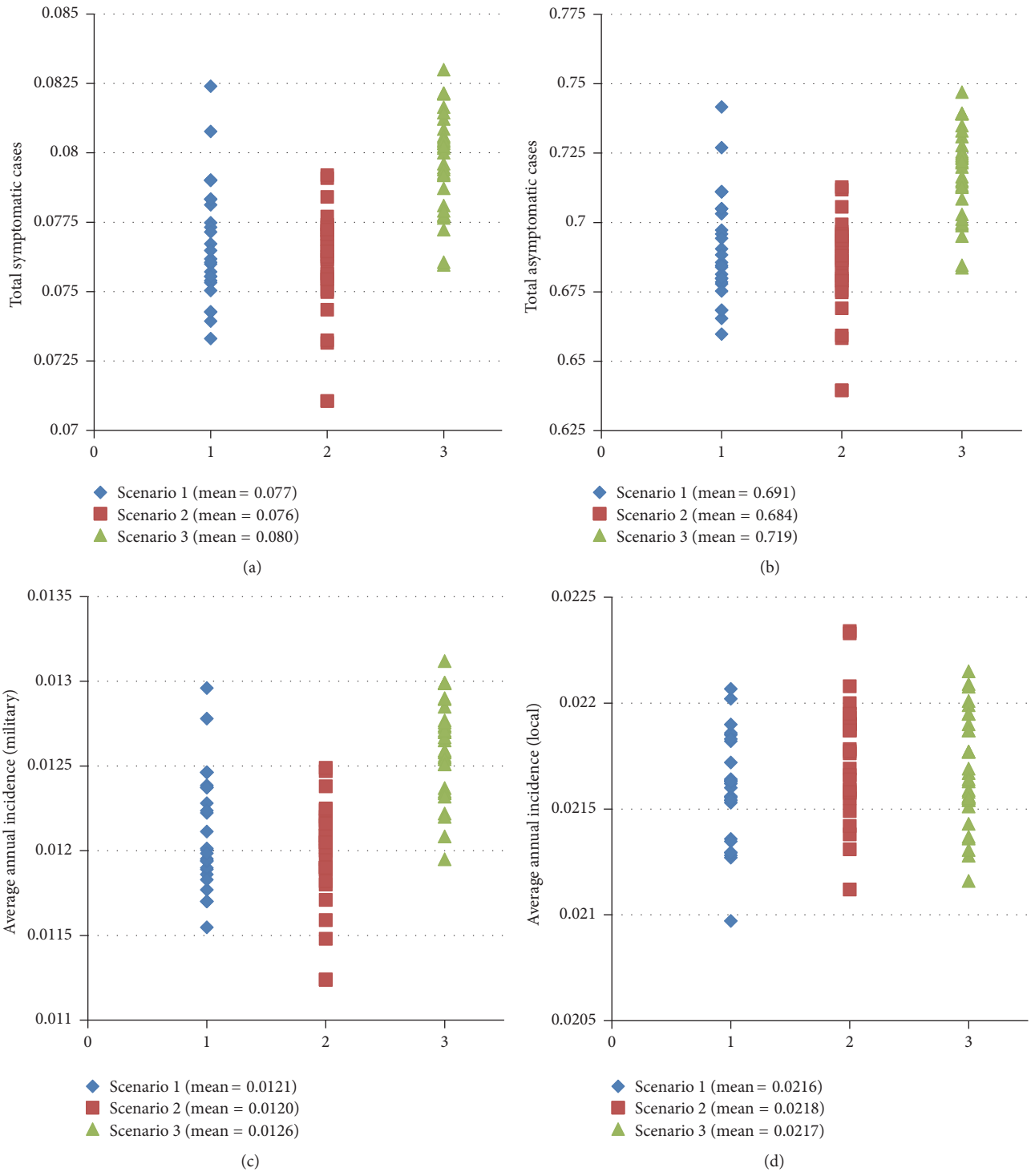

Figure 6: Distribution over 1500 simulations per scenario of (a) total symptomatic polio cases in deployed military populations; (b) total asymptomatic polio cases in deployed military populations; (c) average annual polio incidence in deployed military populations; and (d) average annual polio incidence in local populations under 3 military immunization scenarios.

overall risk of new infections among both deployed and nondeployed service members was extremely low, resulting from the combination of high US childhood immunization coverage rates, conferment of partial protection against polio transmission by IPV, and low disease incidence levels globally. At this range of risk, the likelihood of importation of polio cases among deployed soldiers, and subsequent spread to their nondeployed counterparts, is exceptionally small even in the absence of blanket immunization.

Given preexisting protection resulting from routine childhood vaccination, predeployment booster of service members driven by travel to polio-endemic regions is

sufficient to prevent additional transmission among both deployed and nondeployed populations based on these results. Blanket mandatory polio vaccination of Department of Defense service members appears to be epidemiologically redundant, and dropping this routine immunization will not adversely affect troop readiness or mission objectives.

Disclosure

Kellie McMullen is a military service member (or employee of the US Government). This work was prepared as part of the official duties. Title 17, USC §105, provides that "copyright protection under this title is not available for any work of the United States Government." Title 17, USC §101, defines a US Government work as work prepared by a military service member or employee of the US Government as part of that person's official duties. Report no. 17-XX is supported by the Military Vaccine Agency under Work Unit no. N1415. The views expressed in this article are those of the authors and do not necessarily reflect the official policy or position of the Department of the Navy, Department of the Army, Department of the Air Force, Department of Veterans Affairs, Department of Defense, or the US Government. This work is approved for public release; distribution is unlimited.

Conflicts of Interest

The authors declare they have no conflicts of interest.

Acknowledgments

This work was funded by the Military Vaccine Agency, US Government Work (17 USC 105), and NHRC Contract no. N62645-15-F-1002. The authors wish to thank LCDR Lori N. Perry for her assistance with this contract and manuscript.

References

[1] World Health Organization, "Poliomyelitis, Fact Sheet No. 114," 2017, http://www.who.int/mediacentre/factsheets/fs114/en/index.html.

[2] Global Polio Eradication Initiative, "Data and monitoring: Polio this week as of 2 March 2016," 2016, http://www.polioeradication.org/Dataandmonitoring/Poliothis-week.aspx.

[3] World Health Organization, "Polio vaccines and polio immunization in the pre-eradication era: WHO position paper," *Weekly Epidemiological Record*, vol. 85, pp. 213–228, 2010.

[4] K. M. Thompson, R. J. Duintjer Tebbens, and M. A. Pallansch, "Evaluation of response scenarios to potential polio outbreaks using mathematical models," *Risk Analysis*, vol. 26, no. 6, pp. 1541–1556, 2006.

[5] Global Polio Eradication Initiative, "Fact Sheet: Vaccine-derived poliovirus," 2015, http://www.polioeradication.org/Portals/0/Document/Polioandprevention/CVDPVFactSheet-March2015.pdf.

[6] D. J. Wood, R. W. Sutter, and W. R. Dowdle, "Stopping poliovirus vaccination after eradication: Issues and challenges," *Bulletin of the World Health Organization*, vol. 78, no. 3, pp. 347–357, 2000.

[7] M. Eichner and K. P. Hadeler, "Deterministic models for the eradication of poliomyelitis: Vaccination with the inactivated (IPV) and attenuated (OPV) polio virus vaccine," *Mathematical Biosciences*, vol. 127, no. 2, pp. 149–166, 1995.

[8] World Health Organization, "Statement on the 8th IHR Emergency Committee meeting regarding the international spread of poliovirus," http://www.who.int/mediacentre/news/statements/2016/8th-IHR-emergency-committee-polio/en/.

[9] R. J. D. Tebbens, M. A. Pallansch, O. M. Kew, V. M. Cáceres, R. W. Sutter, and K. M. Thompson, "A dynamic model of poliomyelitis outbreaks: Learning from the past to help inform the future," *American Journal of Epidemiology*, vol. 162, no. 4, pp. 358–372, 2005.

[10] World Health Organization, "Status updates on country planning for IPV introduction," http://www.who.int/entity/immunization/diseases/poliomyelitis/endgame_objective2/IPV_2016_November.pptx?ua=1.

[11] Global Polio Eradication Initiative, "This Week: Polio this week as of 12 April 2017," http://polioeradication.org/polio-today/polio-now/this-week.

[12] H. Rahmandad, K. Hu, R. J. D. Tebbens, and K. M. Thompson, "Development of an individual-based model for polioviruses: Implications of the selection of network type and outcome metrics," *Epidemiology and Infection*, vol. 139, no. 6, pp. 836–848, 2011.

[13] Centers for Disease Control and Prevention, "Vaccines and preventable diseases: polio vaccination," http://www.cdc.gov/vaccines/vpd-vac/polio/default.htm.

[14] V. Kak, "Infections in Confined Spaces: Cruise Ships, Military Barracks, and College Dormitories," *Infectious Disease Clinics of North America*, vol. 21, no. 3, pp. 773–784, 2007.

[15] C. K. Murray and L. L. Horvath, "An approach to prevention of infectious diseases during military deployments," *Clinical Infectious Diseases*, vol. 44, no. 3, pp. 424–430, 2007.

[16] R. J. D. Tebbens, M. A. Pallansch, J.-H. Kim et al., "Oral poliovirus vaccine evolution and insights relevant to modeling the risks of circulating vaccine-derived polioviruses (cVDPVs)," *Risk Analysis*, vol. 33, no. 4, pp. 680–702, 2013.

[17] M. R. Behrend, H. Hu, K. R. Nigmatulina, and P. Eckhoff, "A quantitative survey of the literature on poliovirus infection and immunity," *International Journal of Infectious Diseases*, vol. 18, pp. 4–13, 2014.

[18] J.-H. Kim and S.-H. Rho, "Transmission dynamics of oral polio vaccine viruses and vaccine-derived polioviruses on networks," *Journal of Theoretical Biology*, vol. 364, pp. 266–274, 2015.

[19] K. M. Thompson, M. A. Pallansch, R. J. D. Tebbens, S. G. Wassilak, and S. L. Cochi, "Modeling population immunity to support efforts to end the transmission of live polioviruses," *Risk Analysis*, vol. 33, no. 4, pp. 647–663, 2013.

[20] D. A. Kalkowska, R. J. Duintjer Tebbens, I. Grotto et al., "Modeling options to manage type 1 wild poliovirus imported into Israel in 2013," *Journal of Infectious Diseases*, vol. 211, no. 11, pp. 1800–1812, 2015.

[21] D. A. Kalkowska, R. J. D. Tebbens, M. A. Pallansch, S. L. Cochi, S. G. Wassilak, and K. M. Thompson, "Modeling undetected live poliovirus circulation after apparent interruption of transmission: Implications for surveillance and vaccination," *BMC Infectious Diseases*, vol. 15, no. 1, 66 pages, 2015.

[22] J. Koopman, C. Henry, J. Park, M. Eisenberg, E. Ionides, and J. Eisenberg, "Dynamics affecting the risk of silent circulation when oral polio vaccination is stopped," *Epidemics*, 2017.

[23] C. Burgess, A. Peace, R. Everett, B. Allegri, and P. Garman, "Computational modeling of interventions and protective thresholds to prevent disease transmission in deploying populations," *Computational and Mathematical Methods in Medicine*, Article ID 785752, Art. ID 785752, 17 pages, 2014.

[24] "United Nations, Department of Economic and Social Affairs, Population Division, World Population Prospects, the 2015 Revision," http://esa.un.org/unpd/wpp/DVD.

[25] World Health Organization, "WHO/UNICEF estimates of national routine immunization coverage, 2013 revision," http://www.who.int/immunization/monitoring_surveillance/data/en/.

[26] R. J. Duintjer Tebbens, M. A. Pallansch, D. A. Kalkowska, S. G. F. Wassilak, S. L. Cochi, and K. M. Thompson, "Characterizing poliovirus transmission and evolution: Insights from modeling experiences with wild and vaccine-related polioviruses," *Risk Analysis*, vol. 33, no. 4, pp. 703–749, 2013.

[27] I. Blake and K. O'Reilly, "Approaches to modeling, parameter estimation, and policy guidance during the endgame," in *Proceedings of the Workshop on Analyzing the Polio Eradication Endgame*, Seattle, WA, USA, July 2015.

[28] Centers for Disease Control and Prevention, *Epidemiology and Prevention of Vaccine-Preventable Diseases*, Public Health Foundation, Washington D.C, Wash, USA, 13th edition, 2015.

[29] N. Nathanson and O. M. Kew, "From emergence to eradication: the epidemiology of poliomyelitis deconstructed," *American Journal of Epidemiology*, vol. 172, no. 11, pp. 1213–1229, 2010.

[30] H. E. Jenkins, R. B. Aylward, A. Gasasira et al., "Implications of a circulating vaccine-derived poliovirus in Nigeria," *New England Journal of Medicine*, vol. 362, pp. 2360–2369, 2010.

[31] D. R. Prevots, M. L. Ciofi Degli Atti, A. Sallabanda et al., "Outbreak of paralytic poliomyelitis in Albania, 1996: high attack rate among adults and apparent interruption of transmission following nationwide mass vaccination," *Clinical Infectious Diseases*, vol. 26, no. 2, pp. 419–425, 1998.

[32] J. R. Paul and D. M. Horstmann, "A survey of poliomyelitis virus antibodies in French Morocco," *The American journal of tropical medicine and hygiene*, vol. 4, no. 3, pp. 512–524, 1955.

[33] H. Jafari, J. M. Deshpande, R. W. Sutter et al., "Efficacy of inactivated poliovirus vaccine in India," *Science*, vol. 345, no. 6199, pp. 922–925, 2014.

[34] World Health Organization, "Reported cases of selected vaccine preventable diseases (VPDs)," http://www.who.int/entity/immunization/monitoring_surveillance/data/incidence_series.xls?ua=1.

[35] K. Lapinleimu and M. Stenvik, "Experiences with polio vaccination and herd immunity in Finland," *Developments in Biological Standardization*, vol. 47, pp. 241–246, 1981.

[36] Anonymous, "2012 Demographics Profile of the Military Community. Office of the Deputy Assistant Secretary of Defense (Military Community and Family Policy)," http://download.militaryonesource.mil/12038/MOS/Reports/2012_Demographics_Report.pdf.

[37] Centers for Disease Control and Prevention, "Vaccination coverage among children in kindergarten – United States, 2012-13 school year," *Morbidity and Mortality Weekly Report*, vol. 62, no. 30, pp. 607–612, 2013.

[38] Headquarters Departments of the Army, the Navy, the Air Force, and the Coast Guard, Medical Services, "Immunizations and chemoprophylaxis for the prevention of infectious disease," 2013, http://www.apd.army.mil/jw2/xmldemo/r40_562/main.asp.

[39] Congress of the United States Congressional Budget Office, "Recruiting, retention, and future levels of military personnel," October 2006, https://www.cbo.gov/sites/default/files/cbofiles/ftpdocs/76xx/doc7626/10-05-recruiting.pdf.

Hindawi
Computational and Mathematical Methods in Medicine
Volume 2017, Article ID 2324518, 16 pages
https://doi.org/10.1155/2017/2324518

Research Article

Modelling and Optimal Control of Typhoid Fever Disease with Cost-Effective Strategies

Getachew Teshome Tilahun,[1] Oluwole Daniel Makinde,[2] and David Malonza[3]

[1]*Pan African University Institute of Basic Sciences Technology and Innovation, Nairobi, Kenya*
[2]*Faculty of Military Science, Stellenbosch University, Stellenbosch, South Africa*
[3]*Department of Mathematics, Kenyatta University, Nairobi City, Kenya*

Correspondence should be addressed to Getachew Teshome Tilahun; gmgech@gmail.com

Received 23 February 2017; Revised 19 May 2017; Accepted 22 May 2017; Published 10 September 2017

Academic Editor: Anwar Zeb

We propose and analyze a compartmental nonlinear deterministic mathematical model for the typhoid fever outbreak and optimal control strategies in a community with varying population. The model is studied qualitatively using stability theory of differential equations and the basic reproductive number that represents the epidemic indicator is obtained from the largest eigenvalue of the next-generation matrix. Both local and global asymptotic stability conditions for disease-free and endemic equilibria are determined. The model exhibits a forward transcritical bifurcation and the sensitivity analysis is performed. The optimal control problem is designed by applying Pontryagin maximum principle with three control strategies, namely, the prevention strategy through sanitation, proper hygiene, and vaccination; the treatment strategy through application of appropriate medicine; and the screening of the carriers. The cost functional accounts for the cost involved in prevention, screening, and treatment together with the total number of the infected persons averted. Numerical results for the typhoid outbreak dynamics and its optimal control revealed that a combination of prevention and treatment is the best cost-effective strategy to eradicate the disease.

1. Introduction

According to [1], "infectious diseases are those diseases caused by viruses, bacteria, epiphytes, and parasites such as protozoans or worms that have a potential to spread into the population easily." Typhoid fever is one of the common infectious diseases in human beings that is caused by different species of Salmonella. The most common species of Salmonella that cause typhoid fever are *Salmonella paratyphi A, B, and C* and *Salmonella paratyphi D* [WHO [2]]. "Most of the time typhoid fever is caused by lack of sanitation in which the disease causing bacteria is transmitted by ingestion of contaminated food or water" WHO, 2003. The bacteria are released from the infectious individuals or carriers and then contaminate food or drinking water as a consequence of unsatisfactory hygiene practices. Due to this, typhoid fever is a common disease in developing countries. The data taken from Ethiopia for that past seven years (2009–2015), in Figure 1, indicate that in each year the disease is increasing in alarming rate. Mathematical models have great benefits for describing the dynamics of infectious disease. Moreover, it plays a significant role in predicting suitable control strategies and analyzing and ranking their cost-effectiveness (for example, see Okosun and Makinde [3–7]). Very essential research results on the transmission dynamics of typhoid have come out in the last decade; for instance, see Adetunde [8], Mushayabasa and Bhunu [9], Moffat et al. (2014), Steady et al. (2014), Adeboye and Haruna [10], Omame et al. [11], Khan et al. [12], and Akinyi et al. [13]. All of the above studies reveal an important result for typhoid fever dynamics by considering different countries situation. But we have identified that till now there is no study that has been done to investigate the typhoid fever dynamics with the application of optimal control methods and cost-effectiveness analysis of the applied control strategies.

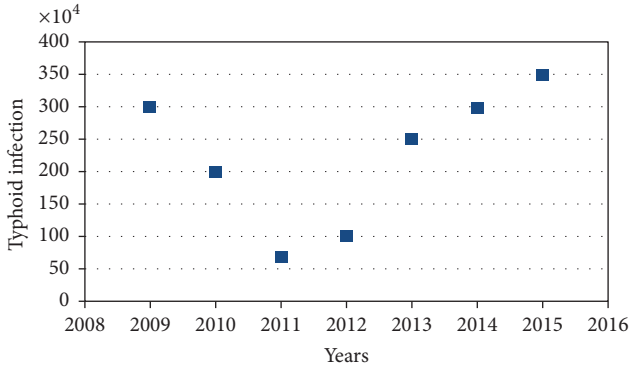

Figure 1: Reported cases of typhoid in Ethiopia for the past seven years.

In view of the above, we developed a deterministic mathematical model to investigate the dynamics of typhoid fever with optimal control strategies and also we investigated the cost-effectiveness of the implemented control strategies.

2. Model Description and Formulation

The model considers human population as well as bacteria population (B_c). The human population at time t is divided into four subclasses. *Susceptible* (S): this class includes those individuals who are at risk for developing an infection from typhoid fever disease. *Infected* (I): this class includes all individuals who are showing the symptom of the disease. *Carrier* (C): this is a person who is colonized by the bacterium *Salmonella typhi* without showing any obvious signs of disease and who is a potential source of infection to others by contaminating foods and water carelessly during preparation and handling. *Recovered* (R): this class includes all individuals that have recovered from the disease and got temporary immunity. The susceptible class is increased by birth or emigration at a rate of Λ and also from recovered class by losing temporary immunity with δ rate. Susceptible individuals will get typhoid causing bacteria when they take foods or waters which is contaminated by Salmonella bacteria. The force of infection of the model is $\lambda = B_c v/(K + B_c)$, where v is ingestion rate, K is the concentration of Salmonella bacteria in foods or waters, and $B_c/(K + B_c)$ is the probability of individuals in consuming foods or drinks contaminated with typhoid causing bacteria. After the susceptible individuals got the typhoid causing bacteria, they have probability of joining carrier with ρ rate or being a member of infective with $1 - \rho$ rate. The infected subclass is increased from carrier subclass by θ screening rate. Those individuals in the infected subclass can get treatment and join recovered subclass with a rate of β. The recovered subclass also increases with individuals who came from carrier class by getting natural immunity with a rate of ϕ. In all human subclasses, μ is the natural death rate of individuals, but in the infective class α is the disease causing death rate. The model assumed the bacteria population in contaminated foods and waters, where carriers and infectives can contribute to increasing the number of bacteria population in foods and waters without proper sanitation with a discharge rate of σ_1 and σ_2, respectively. We consider μ_b to be the death rate of Salmonella bacteria and all the described parameters are nonnegative.

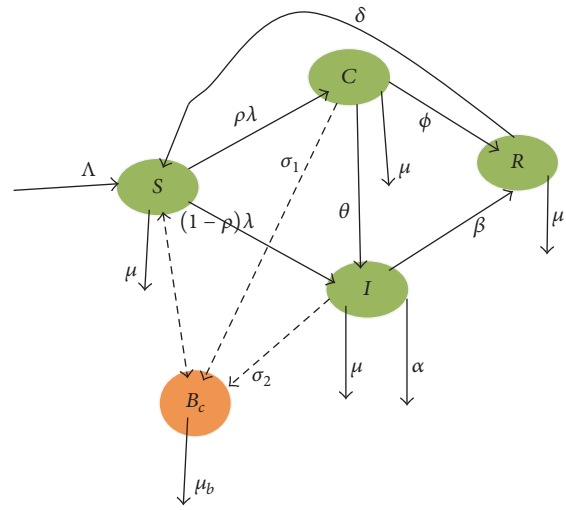

Figure 2: Flow diagram of the model.

The above model description is represented Figure 2.

Figure 2 can be written in five systems of differential equations.

$$\begin{aligned}
\frac{dS}{dt} &= \Lambda + \delta R - (\mu + \lambda) S, \\
\frac{dC}{dt} &= \rho\lambda S - (\sigma_1 + \theta + \mu + \phi) C, \\
\frac{dI}{dt} &= (1 - \rho)\lambda S + \theta C - (\sigma_2 + \beta + \mu + \alpha) I, \\
\frac{dR}{dt} &= \beta I + \phi C - (\mu + \delta) R, \\
\frac{dB_c}{dt} &= \sigma_1 C + \sigma_2 I - \mu_b B_c,
\end{aligned} \tag{1}$$

where $\lambda = B_c v/(K + B_c)$, with initial condition $S(0) = S_0$, $C(0) = C_0$, $I(0) = I_0$, $R(0) = R_0$, and $B_c(0) = B_{c0}$.

3. The Model Analysis

3.1. Invariant Region. We obtained the invariant region, in which the model solution is bounded. To do this, first we considered the total human population (N), where $N = S + C + I + R$.

Then, differentiating N both sides with respect to t leads to

$$\frac{dN}{dt} = \frac{dS}{dt} + \frac{dC}{dt} + \frac{dI}{dt} + \frac{dR}{dt}. \tag{2}$$

By combining (1) and (2), we can get

$$\frac{dN}{dt} = \Lambda - \mu N - \alpha I. \tag{3}$$

In the absence of mortality due to typhoid fever disease ($\alpha = 0$), (3) becomes

$$\frac{dN}{dt} \leq \Lambda - \mu N. \tag{4}$$

Integrating both sides of (4),

$$\begin{gathered} \int \frac{dN}{\Lambda - \mu N} \leq \int dt \Longleftrightarrow \\ \frac{-1}{\mu} \ln\left(\Lambda - \mu N\right) \leq t + c \end{gathered} \tag{5}$$

which simplifies into

$$\Lambda - \mu N \geq Ae^{-\mu t}, \tag{6}$$

where A is constant. By applying the initial condition $N(0) = N_0$ in (6), we get $A = \Lambda - \mu N_0$ which upon substitution in (6) yields

$$\Lambda - \mu N \geq \left(\Lambda - \mu N_0\right) e^{-\mu t}. \tag{7}$$

Then by rearranging (7), we can get

$$N \leq \frac{\Lambda}{\mu} - \left[\frac{\Lambda - \mu N_0}{\mu}\right] e^{-\mu t}. \tag{8}$$

As $t \to \infty$ in (8), the population size $N \to \Lambda/\mu$ which implies that $0 \leq N \leq \Lambda/\mu$. Thus, the feasible solution set of the system equation of the model enters and remains in the region:

$$\Omega = \left\{(S, I, C, R) \in \mathfrak{R}_+^4 : N \leq \frac{\Lambda}{\mu}\right\}. \tag{9}$$

Therefore, the basic model is well posed epidemiologically and mathematically. Hence, it is sufficient to study the dynamics of the basic model in Ω.

3.2. Positivity of the Solutions. We assumed that the initial condition of the model is nonnegative, and now we also showed that the solution of the model is also positive.

Theorem 1. *Let* $\Omega = \{(S, C, I, R, B_c) \in \mathfrak{R}_+^5 : S_0 > 0,\ I_0 > 0,\ C_0 > 0,\ R_0 > 0,\ B_{c_0} > 0\}$*; then the solutions of* $\{S, C, I, R, B_c\}$ *are positive for* $t \geq 0$.

Proof. From the system of differential equation (1), let us take the first equation:

$$\begin{gathered} \frac{dS}{dt} = \Lambda + \delta R - \left(\mu + \lambda\right) S \Longrightarrow \\ \frac{dS(t)}{dt} \geq -\left(\mu + \lambda\right) S(t) \Longrightarrow \\ \frac{dS(t)}{S(t)} \geq -\left(\mu + \lambda\right) d(t) \Longrightarrow \\ \int \frac{dS(t)}{S(t)} \geq -\int \left(\mu + \lambda\right) d(t). \end{gathered} \tag{10}$$

Then by solving using separation of variable and applying condition, we obtained

$$S(t) \geq S_0 e^{-(\mu+\lambda)t} \geq 0. \tag{11}$$

And also by taking the second equation of (1), that is,

$$\frac{dC}{dt} = \rho\lambda S - \left(\sigma_1 + \theta + \mu + \phi\right) C, \tag{12}$$

it is true that

$$\begin{gathered} \frac{dC}{dt} \geq -\left(\sigma_1 + \theta + \mu + \phi\right) C \Longrightarrow \\ \frac{dC}{C} \geq -\left(\sigma_1 + \theta + \mu + \phi\right) d(t) \Longrightarrow \\ \int \frac{dC}{C} \geq -\int \left(\sigma_1 + \theta + \mu + \phi\right) dt. \end{gathered} \tag{13}$$

Then by solving using separation of variable and applying initial condition gives;

$$\therefore C(t) \geq C_0 e^{-(\mu+\phi)t} \geq 0. \tag{14}$$

Similarly we took the third equation of (1) which is;

$$\frac{dI(t)}{dt} = \left(1 - \rho\right)\lambda S + \theta C - \left(\sigma_2 + \beta + \mu + \alpha\right) I \tag{15}$$

it is true that

$$\begin{gathered} \frac{dI}{dt} \geq -\left(\sigma_2 + \beta + \mu + \alpha\right) I \Longrightarrow \\ \frac{dI}{I} \geq -\left(\sigma_2 + \beta + \mu + \alpha\right) d(t) \Longrightarrow \\ \int \frac{dI}{I} \geq -\int \left(\sigma_2 + \beta + \mu + \alpha\right) d(t). \end{gathered} \tag{16}$$

After solving using technique of separation of variable and then applying initial condition, the following is obtained:

$$\therefore I(t) \geq I_0 e^{-(\sigma_2+\beta+\mu+\alpha)t} \geq 0. \tag{17}$$

We took the fourth equation of (1) which is

$$\begin{gathered} \frac{dR}{dt} = \beta I + \phi C - \left(\mu + \delta\right) R \Longrightarrow \\ \frac{dR}{dt} \geq -\left(\mu + \delta\right) R \Longrightarrow \end{gathered}$$

$$\frac{dR}{R} \geq -(\mu+\delta)\,d(t) \Longrightarrow$$
$$\int \frac{dR}{R(t)} \geq -\int (\mu+\delta)\,d(t)$$
$$\therefore R(t) \geq R_0 e^{-(\mu+\delta)t} \geq 0. \tag{18}$$

Finally we took the fifth equation of (1),

$$\frac{dB_c}{dt} = \sigma_1 C + \sigma_2 I - \mu_b B_c \Longrightarrow$$
$$\frac{dB_c}{dt} \geq -\mu_b B_c \Longrightarrow$$
$$\frac{dB_c}{B_c(t)} \geq -(\mu_b)\,d(t) \Longrightarrow \tag{19}$$
$$\int \frac{dB_c}{B_c} \geq -\int (\mu_b)\,d(t)$$
$$\therefore B_c \geq B_{c_0} e^{-(\mu_b)t} \geq 0.$$

This completes the proof of the theorem. □

Therefore, the solution of the model is positive.

3.3. The Disease-Free Equilibrium (DFE). To find the disease-free equilibrium (DFE), we equated the right hand side of model (1) to zero, evaluating it at $C = I = 0$ and solving for the noninfected and noncarrier state variables. Therefore, the disease-free equilibrium $E_0 = (\Lambda/\mu, 0, 0, 0, 0)$.

3.4. The Basic Reproductive Number ($\mathfrak{R}_0$). In this section, we obtained the threshold parameter that governs the spread of a disease which is called the basic reproduction number which is determined. To obtain the basic reproduction number, we used the next-generation matrix method so that it is the spectral radius of the next-generation matrix [15].

The model equations are rewritten starting with newly infective classes:

$$\frac{dC}{dt} = \rho\lambda S - (\sigma_1 + \theta + \mu + \phi)\,C,$$
$$\frac{dI}{dt} = (1-\rho)\,\lambda S + \theta C - (\sigma_2 + \beta + \mu + \alpha)\,I, \tag{20}$$
$$\frac{dB_c}{dt} = \sigma_1 C + \sigma_2 I - \mu_b B_c.$$

Then by the principle of next-generation matrix, we obtained

$$f = \begin{bmatrix} \rho\left(\dfrac{B_c \nu}{K + B_c}\right) S \\ (1-\rho)\left(\dfrac{B_c \nu}{K + B_c}\right) S \end{bmatrix},$$
$$\nu = \begin{bmatrix} (\sigma_1 + \theta + \mu + \phi)\,C \\ (\sigma_2 + \beta + \mu + \alpha)\,I - \theta C \\ -(\sigma_1 C + \sigma_2 I - \mu_b B_c) \end{bmatrix}. \tag{21}$$

The Jacobian matrices of f and ν evaluated at DFE are given by F and V, respectively, such that

$$F = \begin{bmatrix} 0 & 0 & \rho\dfrac{\Lambda\nu}{\mu K} \\ 0 & 0 & (1-\rho)\dfrac{\Lambda\nu}{\mu K} \\ 0 & 0 & 0 \end{bmatrix},$$
$$V = \begin{bmatrix} (\sigma_1 + \theta + \mu + \phi) & 0 & 0 \\ -\theta & (\sigma_2 + \beta + \mu + \alpha) & 0 \\ -\delta_1 & -\delta_2 & \mu_b \end{bmatrix}. \tag{22}$$

The inverse of V is obtained and given by

$$V^{-1} = \begin{bmatrix} \dfrac{1}{k_1} & 0 & 0 \\ \dfrac{\theta}{k_1 k_2} & \dfrac{1}{k_2} & 0 \\ \dfrac{\theta\sigma_2 + \sigma_1 k_2}{k_1 k_2 \mu_b} & \dfrac{\sigma_2}{k_2 \mu_b} & \dfrac{1}{\mu_b} \end{bmatrix}, \tag{23}$$

where $k_1 = (\sigma_1 + \theta + \mu + \phi)$ and $k_2 = (\sigma_2 + \beta + \mu + \alpha)$.

Then,

$$FV^{-1} = \begin{bmatrix} \dfrac{\rho\Lambda\nu(\theta\sigma_2 + \sigma_1 k_2)}{\mu K k_1 k_2 \mu_b} & \dfrac{\rho\Lambda\nu\sigma_2}{\mu K k_2 \mu_b} & \dfrac{\rho\Lambda\nu}{\nu K \mu_b} \\ \dfrac{(1-\rho)\Lambda\nu(\theta\sigma_2 + \sigma_1 k_2)}{\mu K k_1 k_2 \mu_b} & \dfrac{(1-\rho)\Lambda\nu\sigma_2}{\mu K k_2 \mu_b} & \dfrac{(1-\rho)\Lambda\nu}{\nu K \mu_b} \\ 0 & 0 & 0 \end{bmatrix}. \tag{24}$$

The characteristic equation of FV^{-1} is obtained as

$$\lambda^2 \left(\rho\frac{\Lambda\nu(\theta\sigma_2 + \sigma_1 k_2)}{\mu K k_1 k_2 \mu_b} + (1-\rho)\right)\frac{\Lambda\nu\sigma_2}{\mu K k_2 \mu_b} = 0. \tag{25}$$

The eigenvalues of FV^{-1} are

$$\lambda_1 = \lambda_2 = 0,$$
$$\lambda_3 = \rho\frac{\Lambda\nu(\theta\sigma_2 + \sigma_1 k_2)}{\mu K k_1 k_2 \mu_b} + (1-\rho)\frac{\Lambda\nu\sigma_2}{\mu K k_2 \mu_b}. \tag{26}$$

The dominant eigenvalue of FV^{-1} is λ_3.

Therefore, the basic reproduction number ($\mathfrak{R}_0$) after substituting k_1 and k_2 is given by

$$\mathfrak{R}_0 = \left[\rho\frac{(\theta\sigma_2 + \sigma_1(\sigma_2 + \beta + \mu + \alpha))}{(\sigma_1 + \theta + \mu + \phi)} + (1-\rho)\sigma_2\right] \cdot \frac{\Lambda\nu}{\mu K(\sigma_2 + \beta + \mu + \alpha)\mu_b}. \tag{27}$$

3.5. Local Stability of Disease-Free Equilibrium

Proposition 2. *The disease-free equilibrium point is locally asymptotically stable if $\mathfrak{R}_0 < 1$ and unstable if $\mathfrak{R}_0 > 1$.*

Proof. To proof this theorem first we obtain the Jacobian matrix of system (1) at the disease-free equilibrium E_0 as follows:

$$J_{E_0} = \begin{bmatrix} -\mu & 0 & 0 & \delta & \frac{\nu\Lambda}{K\mu} \\ 0 & -(\sigma_1 + \theta + \mu + \phi) & 0 & 0 & \frac{\rho\nu\Lambda}{\mu K} \\ 0 & \theta & -(\sigma_2 + \beta + \mu + \alpha) & 0 & \frac{(1-\rho)\nu\Lambda}{\mu K} \\ 0 & \phi & \beta & -(\mu + \delta) & 0 \\ 0 & \sigma_1 & \sigma_2 & 0 & -\mu_b \end{bmatrix}. \tag{28}$$

From the Jacobian matrix of (28), we obtained a characteristic polynomial:

$$(-\lambda - \mu)(-\lambda - (\mu + \delta))\left(\lambda^3 + L_1\lambda^2 + L_2\lambda + L_3\right) = 0, \tag{29}$$

where

$$\begin{aligned} L_1 &= \sigma_2 + \beta + 2\mu + \alpha + \sigma_1 + \phi + \theta + \mu_b, \\ L_2 &= \mu_b(\sigma_2 + \beta + 2\mu + \alpha + \sigma_1 + \phi + \theta) \\ &\quad + (\sigma_2 + \beta + \mu + \alpha)(\sigma_1 + \mu + \phi + \theta) \\ &\quad - (\rho\sigma_1 + (1-\rho)\sigma_2)\frac{\nu\Lambda}{\mu K}, \\ L_3 &= \mu_b(\sigma_2 + \beta + \mu + \alpha)(\sigma_1 + \mu + \phi + \theta)(1 - \mathfrak{R}_0). \end{aligned} \tag{30}$$

From (29) clearly, we see that

$$\begin{aligned} -\lambda - \mu &= 0, \\ \text{or } -\lambda - (\mu + \delta) &= 0, \\ \text{or } \lambda^3 + L_1\lambda^2 + L_2\lambda + L_3 &= 0 \\ &\Downarrow \\ \lambda_1 &= -\mu < 0, \\ \lambda_2 &= -(\mu + \delta) < 0. \end{aligned} \tag{31}$$

For the last expression, that is,

$$\lambda^3 + L_1\lambda^2 + L_2\lambda + L_3 = 0, \tag{32}$$

we applied Routh-Hurwitz criteria. By the principle of Routh-Hurwitz criteria, (32) has strictly negative real root if and only if $L_1 > 0$, $L_3 > 0$, and $L_1L_2 > L_3$.

Obviously we see that L_1 is positive because it is a sum of positive variables, but L_3 to be positive $1 - \mathfrak{R}_0$ must be positive, which leads to $\mathfrak{R}_0 < 1$. Therefore, DFE will be locally asymptotically stable if and only if $\mathfrak{R}_0 < 1$. □

3.6. Global Stability of DFE

Theorem 3. *The disease-free equilibrium is globally asymptotically stable in the feasible region Ω if $\mathfrak{R}_0 < 1$.*

Proof. To proof this theorem, we first developed a Lyapunov function, technically.

$$L = \left[\frac{\theta\sigma_2 + \sigma_1k_2}{k_1}\right]C + \sigma_2I + k_2B_c, \tag{33}$$

where $k_1 = \sigma_1 + \theta + \mu + \phi$ and $k_2 = \sigma_2 + \beta + \mu + \alpha$

Then differentiating L both sides leads to

$$\frac{dL}{dt} = \left[\frac{\theta\sigma_2 + \sigma_1k_2}{k_1}\right]\frac{dC}{dt} + \sigma_2\frac{dI}{dt} + k_2\frac{dB_c}{dt}. \tag{34}$$

Substituting expression for dC/dt, dI/dt, and dB_c/dt from (1) to (34) results in

$$\begin{aligned} \frac{dL}{dt} &= \left[\frac{\theta\sigma_2 + \sigma_1k_2}{k_1}\right]\rho\lambda S - (\sigma_1 + \theta + \mu + \phi)C \\ &\quad + \sigma_2((1-\rho)\lambda S + \theta C - (\sigma_2 + \beta + \mu + \alpha)I) \\ &\quad + k_2(\sigma_1C + \sigma_2I - \mu_bB_c). \end{aligned} \tag{35}$$

By collecting like terms of (35),

$$\begin{aligned} \frac{dL}{dt} &= \left[\rho\frac{\theta\sigma_2 + \sigma_1k_2}{k_1} + (1-\rho)\sigma_2\right]\lambda S \\ &\quad + (\theta\sigma_2 - \theta\sigma_2 - \sigma_1k_2)C - \sigma_2k_2I \\ &\quad + k_2(\sigma_1C + \sigma_2I - \mu_bB_c). \end{aligned} \tag{36}$$

Equation (36) can be simplified as

$$\frac{dL}{dt} = \left[\rho\frac{\theta\sigma_2 + \sigma_1 k_2}{k_1} + (1-\rho)\sigma_2\right]\lambda S - k_2\mu_b B_c). \quad (37)$$

Equation (37) can be written as interims of $\mathfrak{R}_0$,

$$\frac{dL}{dt} = \left(\mathfrak{R}_0\mu_b k_2\frac{\mu K}{\Lambda\nu}\right)\lambda S - k_2\mu_b B_c). \quad (38)$$

At $S = S_0 = \Lambda/\mu$, (38) becomes

$$\frac{dL}{dt} \le (\mathfrak{R}_0 - 1)\, k_2\mu_b B_c. \quad (39)$$

So $dL/dt \le 0$ if $\mathfrak{R}_0 \le 1$. Furthermore, $dL/dt = 0 \Leftrightarrow B_c = 0$ which leads to $C = I = 0$ or $\mathfrak{R}_0 = 1$.

Hence, L is Lyapunov function on Ω and the largest compact invariant set in $\{(S, C, I, R, B_c) \in \Omega,\ dL/dt = 0\}$ is the singleton $(S_0, 0, 0, 0, 0)$.

Therefore, by LaSalle's invariance principle (LaSalle [16]), every solution to equations of model (1) with initial conditions in Ω which approaches the disease-free equilibrium at t (time) tends to infinity ($t \to \infty$) whenever $\mathfrak{R}_0 \le 1$. Hence, the disease-free equilibrium is globally asymptotically stable. □

3.7. The Endemic Equilibrium. The endemic equilibrium is denoted by $E^* = (S^*, C^*, I^*, R^*, B_c^*)$ and it occurs when the disease persists in the community. To obtain it, we equate all the model equations (1) to zero. Then we obtain

$$\begin{aligned}
S^* &= \frac{\Lambda(\sigma_2+\mu+\alpha+\beta)(\sigma_1+\mu+\theta+\phi)(\mu+\delta)}{(\mu+\lambda^*) - \beta\lambda^*\delta((1-\rho)(\sigma_1+\mu+\theta+\phi)+\rho\theta) - \delta\phi\rho\lambda^*(\sigma_2+\mu+\beta+\alpha)},\\
C^* &= \frac{\rho\lambda^*\Lambda(\sigma_2+\mu+\alpha+\beta)(\mu+\delta)}{(\mu+\lambda^*) - \beta\lambda^*\delta((1-\rho)(\sigma_1+\mu+\theta+\phi)+\rho\theta) - \delta\phi\rho\lambda^*(\sigma_2+\mu+\beta+\alpha)},\\
I^* &= \frac{(\mathfrak{R}_0 K(\sigma_1+\mu+\theta+\phi)(\sigma_2+\mu+\beta+\alpha)\mu\mu_b - \sigma_1\rho\Lambda\nu(\sigma_2+\mu+\beta+\alpha))(\mu+\delta)}{\mu K\sigma_2 + \nu\sigma_2 - \beta\delta\mathfrak{R}_0 K(\sigma_1+\mu+\theta+\phi)(\sigma_2+\mu+\beta+\alpha)\mu\mu_b + \beta\delta\sigma_1(\sigma_2+\mu+\beta+\alpha)\Lambda\nu - \delta\sigma_2\phi\rho\nu(\sigma_2+\mu+\beta+\alpha)},\\
R^* &= \frac{\beta I^* + \phi C^*}{\mu+\delta},\\
B_c^* &= \frac{\lambda^*\Lambda(\mu+\lambda^*)[\sigma_1\rho(\sigma_2+\mu+\alpha+\beta)+\sigma_2(1-\rho)(\sigma_1+\mu+\theta+\phi)+\rho\theta]}{\mu_b[\mu+\lambda^*) - \beta\lambda\delta((1-\rho)(\sigma_1+\mu+\theta+\phi)+\rho\theta) - \delta\phi\rho\lambda^*(\sigma_2+\mu+\beta+\alpha)]}.
\end{aligned} \quad (40)$$

When we substitute the expression for B_c^* into the force of infection, that is, $\lambda^* = B_c^*\nu/(K + B_c^*)$, we obtained a characteristic polynomial of force of infection,

$$p(\lambda^*) = D_1\lambda^{*2} + D_2\lambda^* = 0, \quad (41)$$

where $D_1 = 1+\mathfrak{R}_0(\sigma_2+\mu+\alpha+\beta)(\sigma_1+\mu+\theta+\phi)(\mu+\delta)\mu\mu_b K + (\beta\delta((1-\rho)(\sigma_1+\mu+\theta+\phi)+\rho\theta) + \delta\phi\rho(\sigma_2+\mu+\alpha+\beta))$, $D_2 = (1-\mathfrak{R}_0)(\mu+\delta)\mu$.

Clearly, $D_1 > 0$ and $D_2 \ge 0$. Whenever $\mathfrak{R}_0 < 1$, $\lambda^* = -D_1/D_2 \le 0$. From this, we see that, for $\mathfrak{R}_0 < 1$, there is no endemic equilibrium for this model.

Therefore, this condition shows that it is not possible for backward bifurcation in the model if $\mathfrak{R}_0 < 1$. When we plot I^* over $\mathfrak{R}_0$ by using the expression for I^* and estimated parameters in Table 2, we got a forward bifurcation (Figure 3).

Lemma 4. *A unique endemic equilibrium point E^* exists and is positive if $\mathfrak{R}_0 > 1$.*

4. Sensitivity Analysis of Model Parameters

On the basic parameters, we carried out sensitivity analysis. This helped us to check and identify parameters that can impact the basic reproductive number. To carry out sensitivity analysis, we followed the technique outlined by [17, 18]. This technique develops a formula to obtain the sensitivity index of all the basic parameters, defined as $\Delta_x^{\mathfrak{R}_0} = (\partial\mathfrak{R}_0/\partial x)(x/\mathfrak{R}_0)$, for x represents all the basic parameters.

For example, the sensitivity index of $\mathfrak{R}_0$ with respect to ν is $\Delta_\nu^{\mathfrak{R}_0} = (\partial\mathfrak{R}_0/\partial\nu)(\nu/R_{\text{eff}}) = 1$. And with respect to the remaining parameters, $\Delta_K^{\mathfrak{R}_0}$, $\Delta_{\sigma_1}^{\mathfrak{R}_0}$, $\Delta_{\sigma_2}^{\mathfrak{R}_0}$, $\Delta_\rho^{\mathfrak{R}_0}$, $\Delta_\mu^{\mathfrak{R}_0}$, $\Delta_{\mu_b}^{\mathfrak{R}_0}$, $\Delta_\alpha^{\mathfrak{R}_0}$, $\Delta_\theta^{\mathfrak{R}_0}$, $\Delta_\beta^{\mathfrak{R}_0}$, and $\Delta_\phi^{\mathfrak{R}_0}$ are obtained and evaluated at $\Lambda = 100$, $\phi = 0.0003$, $\sigma_1 = 0.9$, $\sigma_2 = 0.8$, $\beta = 0.0002$, $\rho = 0.3$, $\mu = 0.0247$, $\mu_b = 0.0001$, $\alpha = 0.052$, $\theta = 0.2$, $\nu = 0.9$, and $K = 50{,}000$. Their sensitivity indices are in Table 1.

4.1. Interpretation of Sensitivity Indices. The sensitivity indices of the basic reproductive number with respect to main parameters are arranged orderly in Table 1. Those

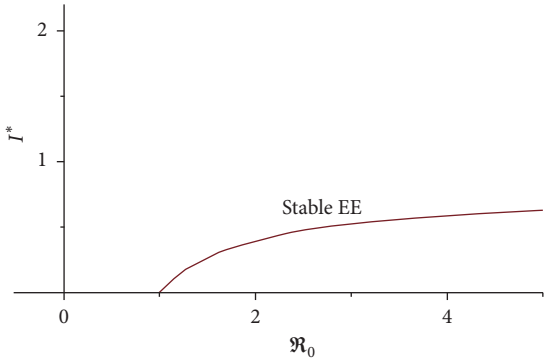

Figure 3: Forward bifurcation of typhoid fever model.

Table 1: Sensitivity indices table.

Parameter symbol	Sensitivity indices
ν	1
K	0.999
σ_1	0.26
σ_2	0.03
ρ	0.00506
μ	−1.028
μ_b	−1
α	−0.0592
θ	0.009
β	−0.00017
ϕ	−0.000089

parameters that have positive indices (ν, K, σ_1, σ_2, and ρ) show that they have great impact on expanding the disease in the community if their values are increasing. Due to the reason that the basic reproduction number increases as their values increase, it means that the average number of secondary cases of infection increases in the community. And also those parameters in which their sensitivity indices are negative (μ, μ_b, α, θ, β, and ϕ) have an influence of minimizing the burden of the disease in the community as their values increase while the others are left constant. And also as their values increase, the basic reproduction number decreases, which leads to minimizing the endemicity of the disease in the community.

5. Extension of the Model into an Optimal Control

In this section, the basic model of typhoid fever is generalized by incorporating three control interventions. The controls are prevention (u_1) (sanitation and proper hygiene controls), treatment (u_2) (treating individuals who developed symptoms of the disease), and screening of carriers (u_3) which helps them to get proper treatment if they are aware of their status.

After incorporating the controls into the basic model of typhoid fever, we get the following state equations:

$$\begin{aligned}
\frac{dS}{dt} &= \Lambda + \delta R - (1-u_1)\lambda S - \mu S,\\
\frac{dC}{dt} &= (1-u_1)\rho\lambda S - (\theta + u_3)C - (\sigma_1 + \phi + \mu)C,\\
\frac{dI}{dt} &= (1-u_1)(1-\rho)\lambda S + (1-u_3)\theta C - (u_2+\beta)I\\
&\quad - (\sigma_2 + \mu + \alpha)I,\\
\frac{dR}{dt} &= (u_2+\beta)I + \phi C - (\mu+\delta)R,\\
\frac{dB_c}{dt} &= \sigma_1 C + \sigma_2 I - \mu_b B_c,
\end{aligned} \tag{42}$$

where $\lambda = B_c\nu/(K + B_c)$.

$\{0 \le u_1 < 1,\ 0 \le u_2 < 1,\ 0 \le u_3 < 1, 0 \le t \le T\}$ is Lebesgue measurable. Our main objective is to obtain the optimal levels of the controls and associated state variables that optimize the objective function. The form of the objective function is taken from [19] and given by

$$J = \min_{u_1,u_2,u_3} \int_0^{t_f} \left(b_1 C + b_2 I + \frac{1}{2}\sum_{i=1}^{3} w_i u_i^2 \right) dt. \tag{43}$$

The coefficients associated with state variables (b_1 and b_2) and with controls (w_i) are positive. Due to the fact that cost is not linear in its condition, we make the cost expression $((1/2)w_i u_i^2)$ quadratic.

As objective function (43) shows, we aimed to minimize the number of carriers, infectives, and costs. That is, we want to get an optimal triple (u_1^*, u_2^*, u_3^*) such that

$J(u_1^*, u_2^*, u_3^*) = \min\{J(u_1, u_2, u_3) \mid u_i \in U\}$, where $U = \{(u_1, u_2, u_3) \mid \text{each } u_i \text{ is measurable with } 0 \le u_i < 1 \text{ for } 0 \le t \le t_f\}$ is the set of acceptable controls.

5.1. Existence of an Optimal Control. The existence of the optimal control can be showed by using an approach of [20]. We have already justified the boundedness of the solution of the basic typhoid fever model. This result can be used to prove the existence of optimal control. For detailed proof, see [20] [Theorem 4.1, p68-69].

5.2. The Hamiltonian and Optimality System. To obtain the Hamiltonian (H), we follow the approach of [21] such that

$$H = \frac{dJ}{dt} + \lambda_1\frac{dS}{dt} + \lambda_2\frac{dC}{dt} + \lambda_3\frac{dI}{dt} + \lambda_4\frac{dR}{dt} + \lambda_5\frac{dB_c}{dt}. \tag{44}$$

That is,

$$\begin{aligned}
H(S, C, I, R, B_c, t) &= L(C, I, u_1, u_2, u_3, t) + \lambda_1\frac{dS}{dt}\\
&\quad + \lambda_2\frac{dC}{dt} + \lambda_3\frac{dI}{dt} + \lambda_4\frac{dR}{dt}\\
&\quad + \lambda_5\frac{dB_c}{dt},
\end{aligned} \tag{45}$$

Table 2: Parameter values for typhoid fever model.

Parameter symbol	Parameter description	Value	Source
ν	Salmonella ingestion rate	0.9	Assumed
K	Concentration of Salmonella bacteria in foods and water	50000	[14]
μ	Human beings natural death rate	0.0247	Assumed
α	Typhoid induced death rate	0.052	Estimated
β	Treatment rate of infectious diseases	0.002	Estimated
σ_1	Discharge rate of Salmonella from carriers	0.9	Gosh et al., 2006
σ_2	Discharge rate of Salmonella from infective	0.8	Assumed
δ	Removal rate from recovered subclass to susceptible subclass	0.000904	Adetunde, 2008
θ	Screening rate of carriers	0.2	Assumed
ϕ	Removal of carriers by natural immunity	0.0003	Assumed
ρ	Probability of susceptible joining carrier state	0.3	Assumed
μ_b	Natural/drug induced death rate of bacteria	0.001	Gosh et al., 2006
Λ	Recruitment of human beings	100	Assumed

where $L(C, I, u_1, u_2, u_3, t) = b_1 C + b_2 I + (1/2)\sum_{i=1}^{3} w_i u_i^2$, λ_1, $\lambda_2, \lambda_3, \lambda_4$, and λ_5 are the adjoint variable functions. To obtain the adjoint variables, we followed the classical result of [21].

Theorem 5. *There exist an optimal control set of u_1, u_2, and u_3 and corresponding solution, S, C, I, R, and B_c, that minimize $J(u_1, u_2, u_3)$ over U. Furthermore, there exist adjoint functions $\lambda_1, \ldots, \lambda_5$ such that*

$$\begin{aligned}
\frac{d\lambda_1}{dt} &= -\lambda_1\left(-\mu - \frac{B_c\nu(1-u_1)}{K+B_c}\right) \\
&\quad - \frac{\lambda_2(1-\rho)(1-u_1)B_c\nu}{K+B_c} - \frac{\lambda_3(1-u_1)\rho\nu B_c}{K+B_c}, \\
\frac{d\lambda_2}{dt} &= -b_1 - \lambda_2(-\theta-u_3) - \lambda_3(1-u_3)\theta - \lambda_4\phi \\
&\quad - \lambda_5(\sigma_1+\phi+\mu), \\
\frac{d\lambda_3}{dt} &= -b_2 - \lambda_3(-u_2-\beta-\sigma_2) - \lambda_4(u_2+\beta) \\
&\quad - \lambda_5(\sigma_2+\mu+\alpha), \\
\frac{d\lambda_4}{dt} &= -\lambda_1\delta - \lambda_4(-\mu-\delta), \\
\frac{d\lambda_5}{dt} &= -\frac{\lambda_1 B_c\nu(1-u_1)s}{(k+B_c)^2} - \lambda_2\left(\frac{(1-u_1)\rho\nu S}{K+B_c}\right. \\
&\quad \left. - \frac{(1-u_1)\rho\nu B - cS}{(K+B_c)^2}\right) - \lambda_3\left(\frac{(1-\rho)(1-u_1)\nu S}{K+B_c}\right. \\
&\quad \left. - \frac{(1-\rho)(1-u_1)B_c\nu S}{(K+B_c)^2}\right) + \lambda_5\mu_b,
\end{aligned} \tag{46}$$

with transversality conditions,

$$\lambda_i(t_f) = 0, \quad i = 1, \ldots, 5. \tag{47}$$

And the characterized control set of (u_1^*, u_2^*, u_3^*) is

$$\begin{aligned}
u_1^*(t) &= \max\left\{0, \right. \\
&\quad \left. \min\left(1, \frac{S(\lambda_2\rho\nu B_c - B_c\rho\nu\lambda_3 + B_c\nu\lambda_3 - \lambda_1 B_c\nu)}{(K+B_c)w_1}\right)\right\}, \\
u_2^*(t) &= \max\left\{0, \min\left(1, \frac{I(\lambda_3-\lambda_4)}{w_2}\right)\right\}, \\
u_3^*(t) &= \max\left\{0, \min\left(1, \frac{C(\lambda_3\theta+\lambda_2)}{w_3}\right)\right\}.
\end{aligned} \tag{48}$$

Proof. To prove this theorem, we used the classical result of [21]. Accordingly, to get the system of adjoint variables, we differentiate the Hamiltonian (45) with respect to each state as follows:

$$\begin{aligned}
\frac{d\lambda_1}{dt} &= -\frac{dH}{dS} = -\lambda_1\left(-\mu - \frac{B_c\nu(1-u_1)}{K+B_c}\right) \\
&\quad - \frac{\lambda_2(1-\rho)(1-u_1)B_c\nu}{K+B_c} - \frac{\lambda_3(1-u_1)\rho\nu B_c}{K+B_c}, \\
\frac{d\lambda_2}{dt} &= -\frac{dH}{dC} = -b_1 - \lambda_2(-\theta-u_3) - \lambda_3(1-u_3)\theta \\
&\quad - \lambda_4\phi - \lambda_5(\sigma_1+\phi+\mu), \\
\frac{d\lambda_3}{dt} &= -\frac{dH}{dI} = -b_2 - \lambda_3(-u_2-\beta-\sigma_2) - \lambda_4(u_2 \\
&\quad + \beta) - \lambda_5(\sigma_2+\mu+\alpha), \\
\frac{d\lambda_4}{dt} &= -\frac{dH}{dR} = -\lambda_1\delta - \lambda_4(-\mu-\delta),
\end{aligned}$$

$$\frac{d\lambda_5}{dt} = -\frac{dH}{dB_c} = -\frac{\lambda_1 B_c \nu (1-u_1) S}{(K+B_c)^2} - \lambda_2 \left(\frac{(1-u_1)\rho\nu S}{K+B_c} - \frac{(1-u_1)\rho\nu B_c S}{(K+B_c)^2} \right) - \lambda_3 \left(\frac{(1-\rho)(1-u_1)\nu S}{K+B_c} - \frac{(1-\rho)(1-u_1) B_c \nu S}{(K+B_c)^2} \right) + \lambda_5 \mu_b. \tag{49}$$

And also for characterization of the optimal control, we used the following partial differential equation:

$$\frac{\partial H}{\partial u_i} = 0 \quad \text{at } u_i = u_i^*, \tag{50}$$

where $i = 1, 2, 3$.

For $i = 1$,

$$\frac{\partial H}{\partial u_1} = 0 \quad \text{at } u_1^* \Downarrow u_1^* = \frac{S(\lambda_2 \rho \nu B_c - B_c \rho \nu \lambda_3 + B_c \nu \lambda_3 - \lambda_1 B_c \nu)}{(K+B_c) w_1}. \tag{51}$$

For $i = 2$,

$$\frac{\partial H}{\partial u_2} = 0 \quad \text{at } u_2^* \Downarrow u_2^* = \frac{I(\lambda_3 - \lambda_4)}{w_2}. \tag{52}$$

For $i = 3$,

$$\frac{\partial H}{\partial u_3} = 0 \quad \text{at } u_3^* \Downarrow u_3^* = \frac{C(\lambda_3 \theta + \lambda_2)}{w_3}. \tag{53}$$

Since $0 < u_i^* < 1$, we can write in a compact notation:

$$u_1^* = \max\left\{0, \min\left(1, \frac{S(\lambda_2 \rho \nu B_c - B_c \rho \nu \lambda_3 + B_c \nu \lambda_3 - \lambda_1 B_c \nu)}{(K+B_c) w_1}\right)\right\},$$
$$u_2^* = \max\left\{0, \min\left(1, \frac{I(\lambda_3 - \lambda_4)}{w_2}\right)\right\},$$
$$u_3^* = \max\left\{0, \min\left(1, \frac{C(\lambda_3 \theta + \lambda_2)}{w_3}\right)\right\}. \tag{54}$$

□

5.3. The Optimality System. It is a system of states (42) and adjoint (46) incorporating with the characterization of the optimal control and initial and transversality conditions. Then we have the following optimality system:

$$\frac{dS}{dt} = \Lambda + \delta R - (1-u_1^*)\lambda S - \mu S,$$
$$\frac{dC}{dt} = (1-u_1{}^*)\rho\lambda S - (\theta + u_3^*) C - (\sigma_1 + \phi + \mu) C,$$
$$\frac{dI}{dt} = (1-u_1^*)(1-\rho)\lambda S + (1-u_3^*)\theta C - (u_2^* + \beta) I - (\sigma_2 + \mu + \alpha) I,$$
$$\frac{dR}{dt} = (u_2^* + \beta) I + \phi C - (\mu + \delta) R,$$
$$\frac{dB_c}{dt} = Q + \sigma_1 C + \sigma_2 I - \mu_b B_c,$$
$$\frac{d\lambda_1}{dt} = -\lambda_1 \left(-\mu - \frac{B_c \nu (1-u_1^*)}{k+B_c} \right) - \frac{\lambda_2 (1-\rho)(1-u_1^*) B_c \nu}{K+B_c} - \frac{\lambda_3 (1-u_1^*)\rho\nu B_c}{K+B_c},$$
$$\frac{d\lambda_2}{dt} = -b_1 - \lambda_2(-\theta - u_3^*) - \lambda_3(1-u_3^*)\theta - \lambda_4\phi - \lambda_5\sigma_1,$$
$$\frac{d\lambda_3}{dt} = -b_2 - \lambda_3(-u_2^* - \beta - (\sigma_2 + \mu + \alpha)) - \lambda_4(u_2^* + \beta) - \lambda_5\sigma_2,$$
$$\frac{d\lambda_4}{dt} = -\lambda_1\delta - \lambda_4(-\mu - \delta),$$
$$\frac{d\lambda_5}{dt} = -\frac{\lambda_1 B_c \nu (1-u_1^*) S}{(K+B_c)^2} - \lambda_2 \left(\frac{(1-u_1^*)\rho\nu S}{K+B_c} - \frac{(1-u_1^*)\rho\nu B - cS}{(K+B_c)^2} \right) - \lambda_3 \left(\frac{(1-\rho)(1-u_1^*)\nu S}{K+B_c} - \frac{(1-\rho)(1-u_1^*) B_c \nu S}{(K+B_c)^2} \right) + \lambda_5 \mu_b, \tag{55}$$
$$\lambda_i(t_f) = 0, \quad i = 1, 2, 3, 4, 5,$$
$$S(0) = S_0,$$
$$C(0) = C_0,$$
$$I(0) = I_0,$$
$$R(0) = R_0,$$
$$B_c(0) = B_{c_0}.$$

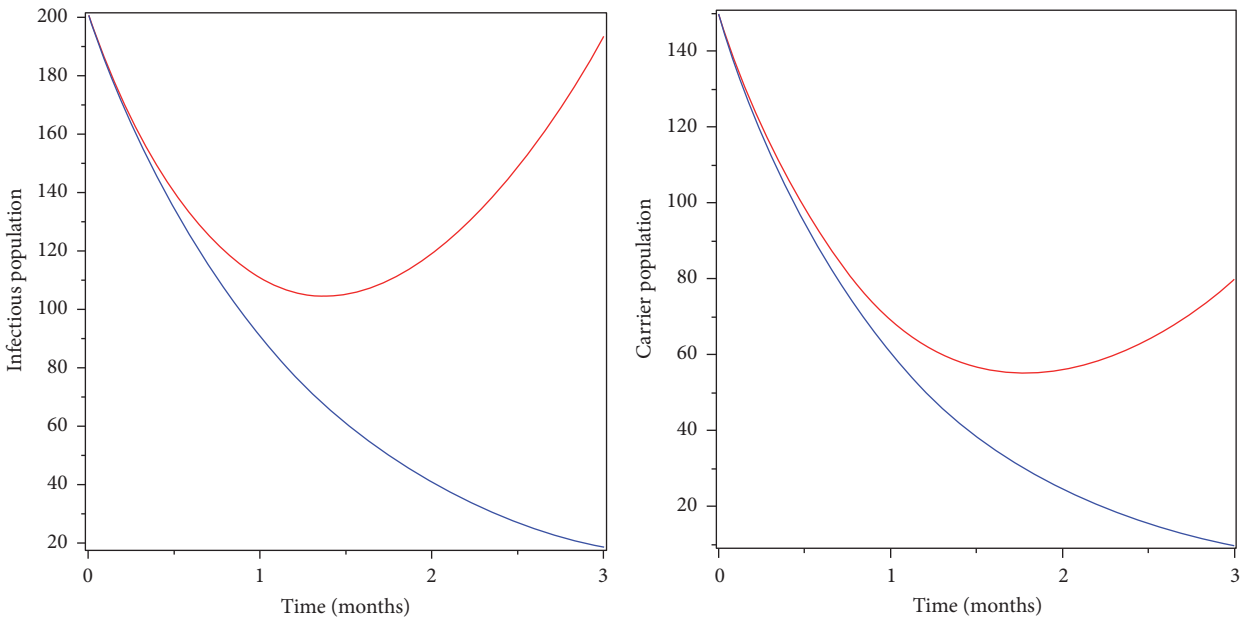

(a) Prevention impact on infectious population

(b) Prevention impact on carrier population

FIGURE 4: Simulations of typhoid fever model with prevention control only.

5.4. Uniqueness of the Optimality System. Since the state and adjoint variables are bounded and also the obtained ordinary differential equations have Lipschitz in their structure, it is possible to show the uniqueness, hence the following theorem.

Theorem 6. *For $t \in [0, t_f]$, the bounded solutions to the optimality system are unique.*

Proof. See [22] for the proof of this theorem. □

6. Numerical Simulations

We perform numerical simulation of the optimality system by using the parameter values given in Table 2.

To obtain optimal solution, we apply iterative technique. By using an advantage of the initial conditions of the state system, we used a forward fourth-order Runge-Kutta method to solve it and also due to the final conditions for the adjoint system, we used a backward fourth-order Runge-Kutta method to solve it. To solve the state initial guess of controls is used and the solution of the state system and the initial guess helps to solve the adjoint system. Each control continues to be updated by combining its previous and characterization values. To repeat the solutions, the updated controls are used. This situation continues until two consecutive iterations are close enough [23].

To examine the impact of each control on eradication of typhoid fever disease, we used the following strategy:

(i) Applying prevention only (u_1) as intervention

(ii) Applying treatment only (u_2) as intervention

(iii) Applying screening only (u_3) as intervention

(iv) Implementing prevention (u_1) and treatment (u_2) intervention

(v) Implementing prevention (u_1) and screening (u_3) intervention

(vi) Implementing treatment (u_2) and screening (u_3) intervention

(vii) Using all the three controls: prevention effort u_1, treatment effort u_2, and also screening u_3

Initial values that we used for simulation of the optimal control are $S(0) = 1000$, $C(0) = 150$, $I(0) = 200$, $R(0) = 300$, and $B_c(0) = 200$ and also coefficients of the state and controls that we used are $b_1 = 25$, $b_2 = 25$, $w_1 = 4$, $w_2 = 3$, and $w_3 = 5$.

6.1. Control with Prevention Only. We simulated the optimality system by incorporating prevention intervention only. Figures 4(a) and 4(b) show the decrease of infectious and carrier population in the specified time. We conclude that prevention that includes sanitation and other techniques is a vital method to reduce typhoid fever infection. The number of individuals who have been with typhoid fever disease before implementation of prevention control has gone down due to disease induced and natural deaths. Therefore, applying optimized prevention control can eradicate typhoid fever disease in the community.

6.2. Control with Treatment Only. We applied treatment only as intervention that is treating individuals who develop

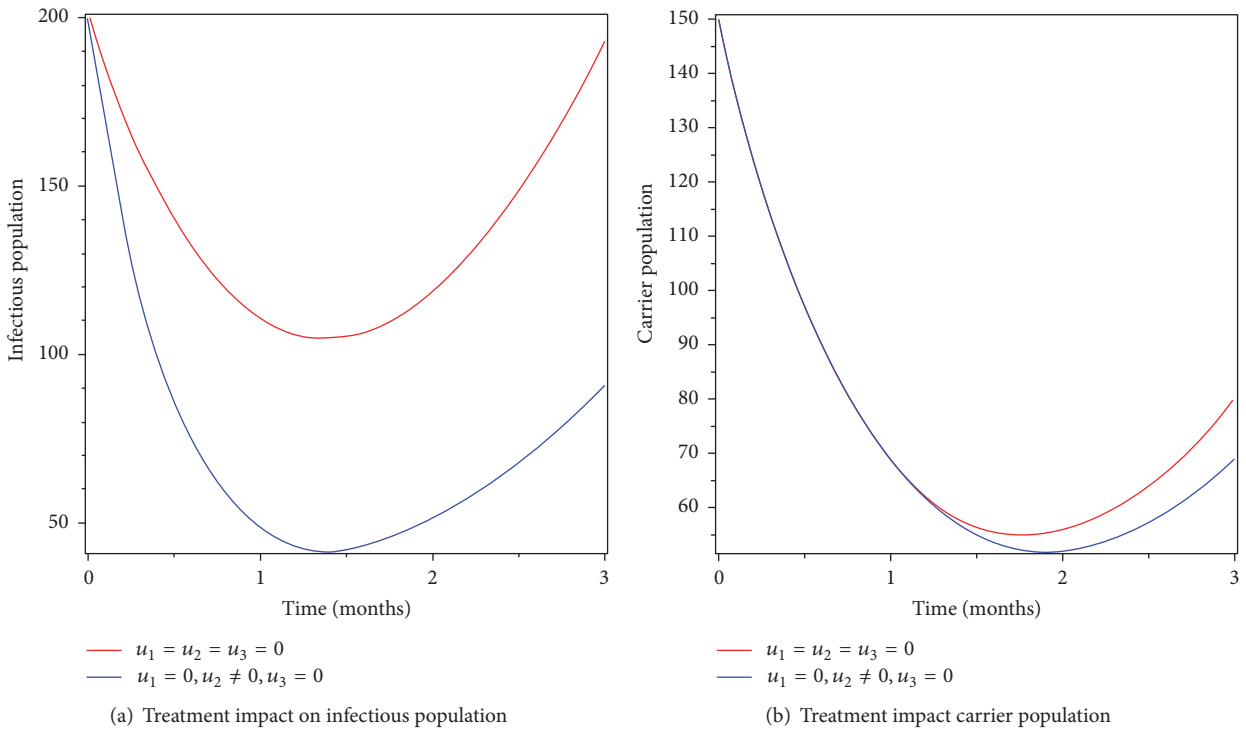

(a) Treatment impact on infectious population

(b) Treatment impact carrier population

FIGURE 5: Simulations of typhoid fever model with treatment control only.

disease symptom. From Figures 5(a) and 5(b), we understand that the number of infectious individuals and carriers decreased when treatment intervention is applied. The number of infectious individuals and carriers did not go to zero over the period of implementation of this intervention strategy. The reason is that due to lack of prevention susceptible individuals still get infected. Therefore, we conclude that applying optimized treatment only as control intervention decreases the burden of the disease but it cannot eradicate typhoid fever disease in the community.

6.3. Control with Screening Only. As we know screening helps carriers to identify their status as they are leaving with the bacteria or not. Therefore, Figures 6(a) and 6(b) show that the infectious and carrier population goes down by screening effort but their number cannot be zero. New infection always appears in the community because the diseases are not prevented and individuals who develop the symptom of the disease are not getting treatment. Therefore, control with screening only reduces the burden in some extent but it is not helpful to eradicate typhoid fever disease totally from the community.

6.4. Control with Prevention and Treatment. We simulate the model using a combination of prevention and treatment as intervention strategy for control of typhoid fever disease in the community. Figures 7(a) and 7(b) clearly show that the infectious and carrier population has gone to zero at the end of the implementation period. Therefore, we conclude that this strategy is effective in eradicating the disease from the community in a specified period of time.

6.5. Control with Prevention and Screening. We simulated the model by incorporating optimized prevention and screening as disease control strategy. Figures 8(a) and 8(b) show that the infectious and carrier population goes to zero at the end of the implementation of intervention time. From this, we can conclude that applying prevention and screening can eradicate the disease even if without treating individuals that have disease symptom. Therefore, applying optimized prevention and screening as intervention strategy will eradicate typhoid fever disease from the community.

6.6. Control with Treatment and Screening. In this strategy, we applied treatment and screening as intervention to control typhoid fever disease. Figures 9(a) and 9(b) show that optimized intervention by treating infectious individuals and screening of carriers decreases the number of infectious and carrier populations but did not go to zero. Therefore, this strategy is not 100% effective in eradicating the disease in the specified period of time.

6.7. Control with Prevention, Treatment, and Screening. In this strategy, we implemented all the three controls (prevention, treatment, and screening) as intervention to eradicate typhoid fever from the community. Figures 10(a) and 10(b) show that the number of infectious individuals and carriers goes to zero at the end of the implementation period. Moreover, Figure 11 shows that the number of Salmonella bacteria population decreased after the implementation of the strategy. Therefore, applying this strategy is effective in eradicating typhoid fever disease form the community in a specified period of time.

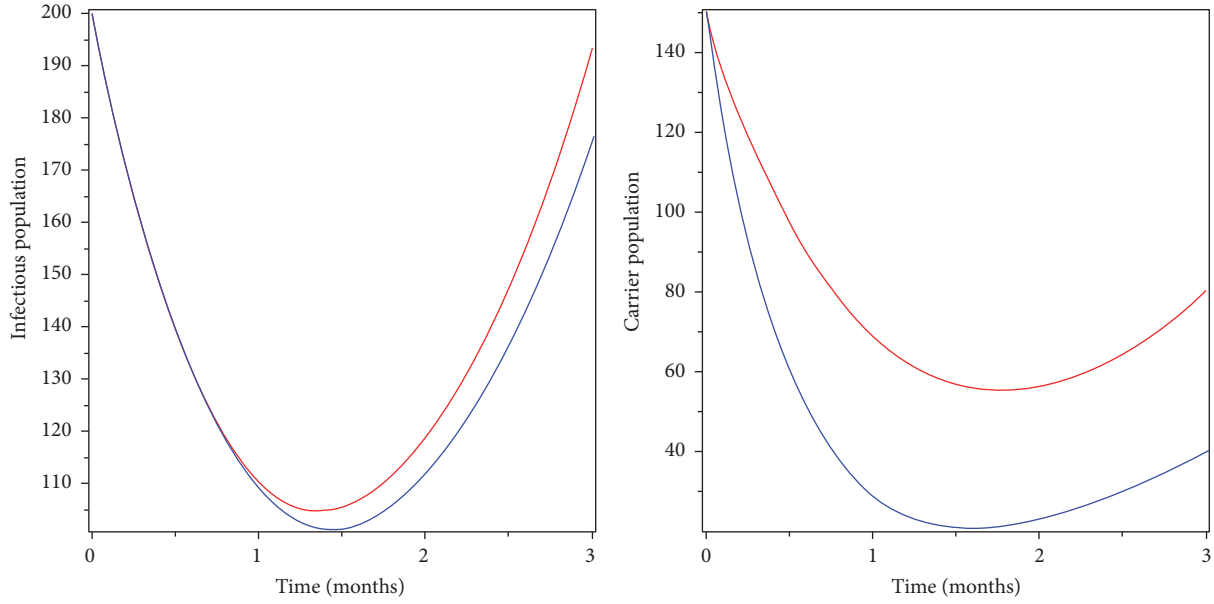

(a) Screening impact on infectious population

(b) Screening only impact on carrier population

Figure 6: Simulations of typhoid fever model with screening control only.

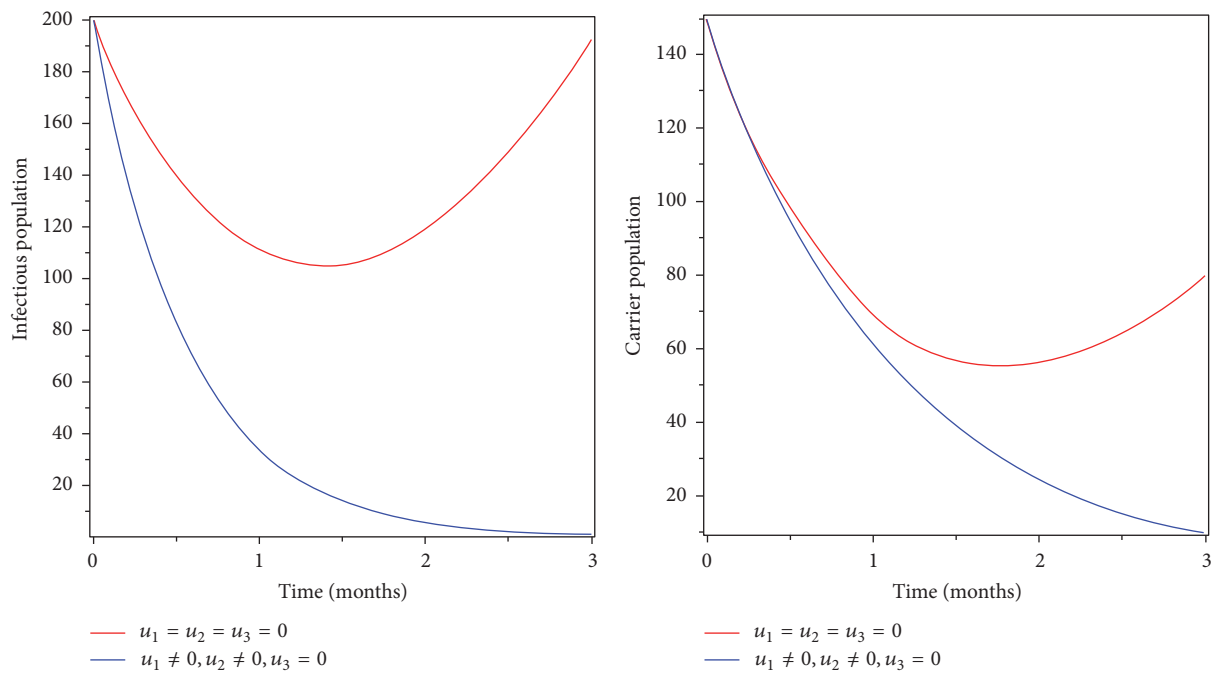

(a) Prevention and treatment impact on infectious individuals

(b) Prevention and treatment impact on carrier

Figure 7: Simulations of typhoid fever model with prevention and treatment controls.

7. Cost-Effectiveness Analysis

In this section, we identified a strategy which is cost-effective compared to other strategies. To achieve this, we used incremental cost-effectiveness ratio (ICER), which is done dividing the difference of costs between two strategies to the difference of the total number of their infections averted. We estimated the total number of infections averted for each strategy by subtracting total infections with control from without control. To get the total cost of each strategy, we used

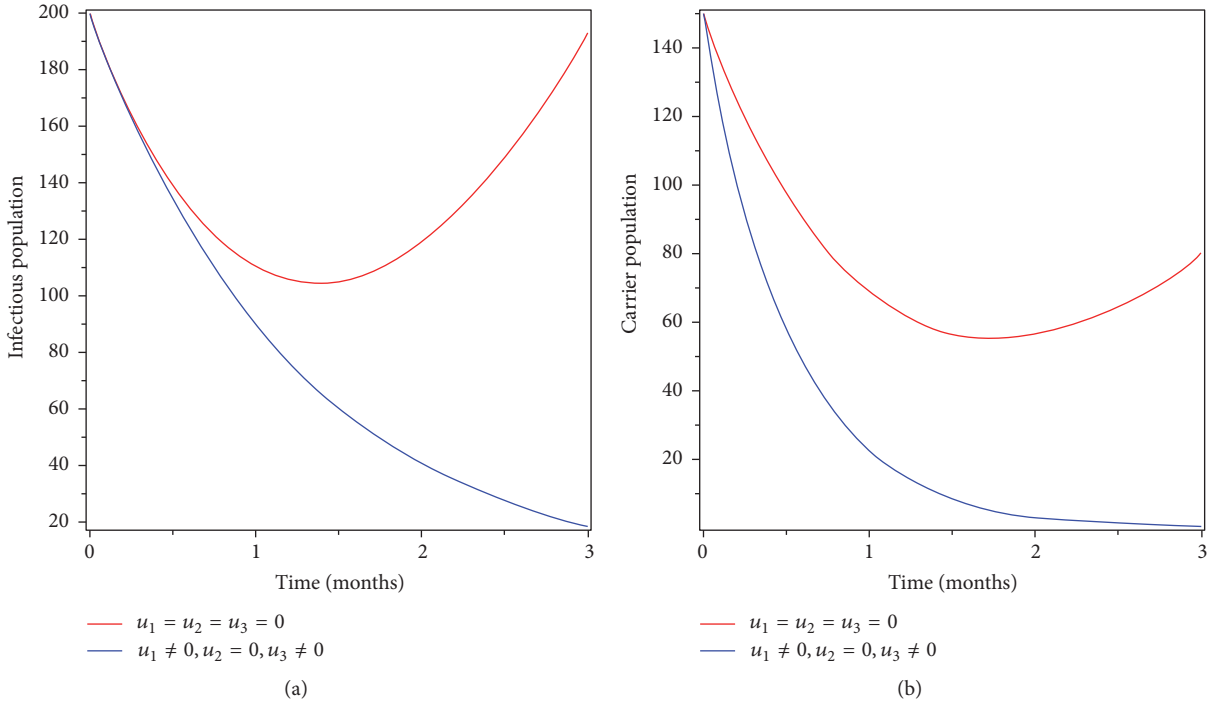

FIGURE 8: Simulations of the typhoid fever model with prevention and screening controls.

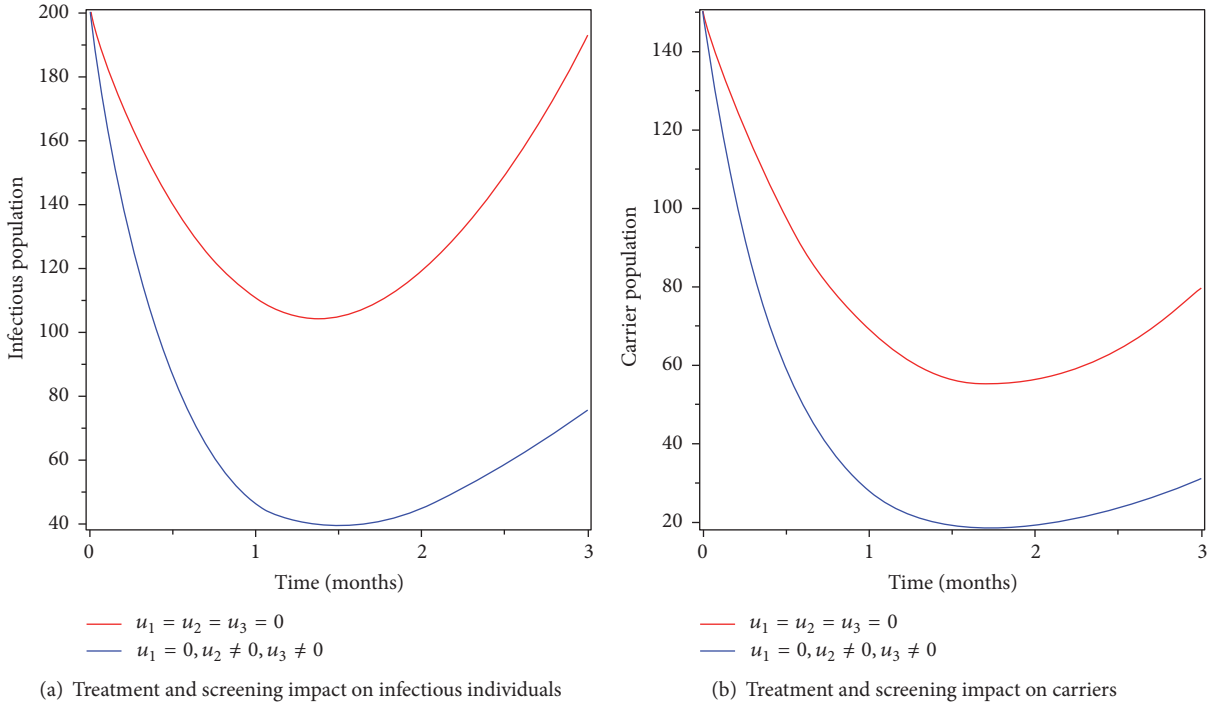

FIGURE 9: Simulations of the typhoid fever model with treatment and screening controls.

their respective cost function ($(1/2)w_1u_1^2$, $(1/2)w_2u_2^2$, and $(1/2)w_3u_3^2$) to calculate over the time of intervention. We did not consider strategies that implement one intervention only, due to the reason that one intervention only is not guaranteed to eradicate the disease totally from the community. Those strategies which incorporate more than one intervention are ordered below to be compared pairwise:

Strategy A (prevention and screening)

Strategy B (treatment and screening)

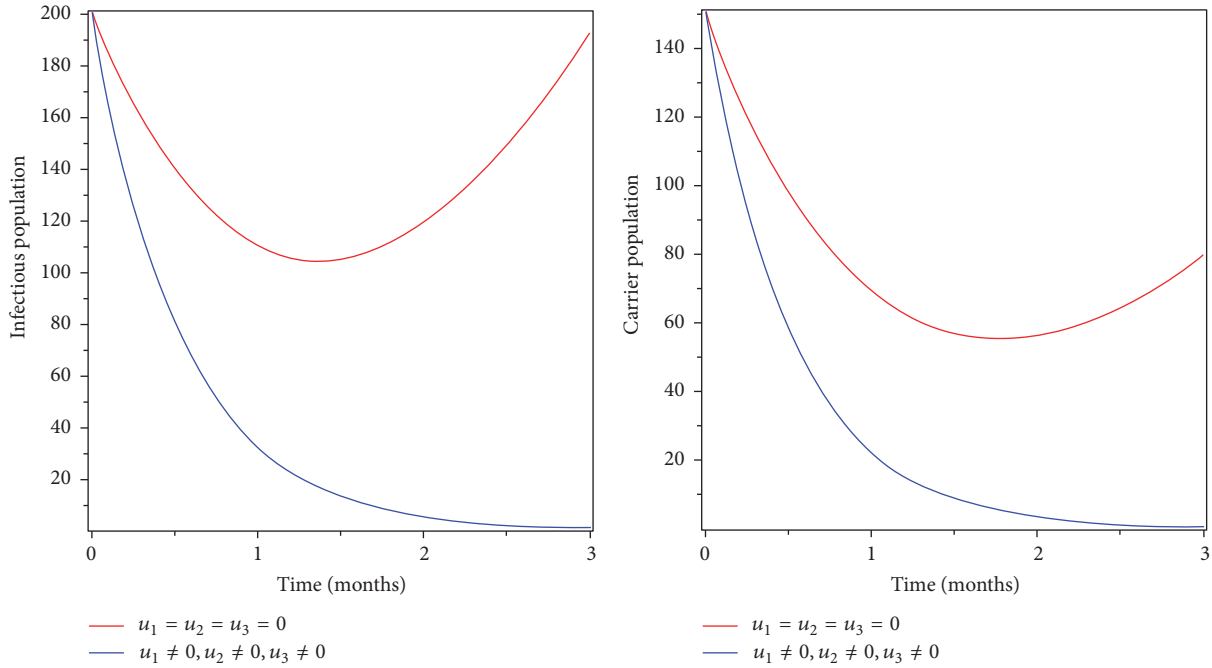

(a) Prevention, treatment, and screening impact on infectious individuals

(b) Prevention, treatment, and screening impact on carriers

Figure 10: Simulations of the typhoid fever model with prevention, treatment, and screening controls.

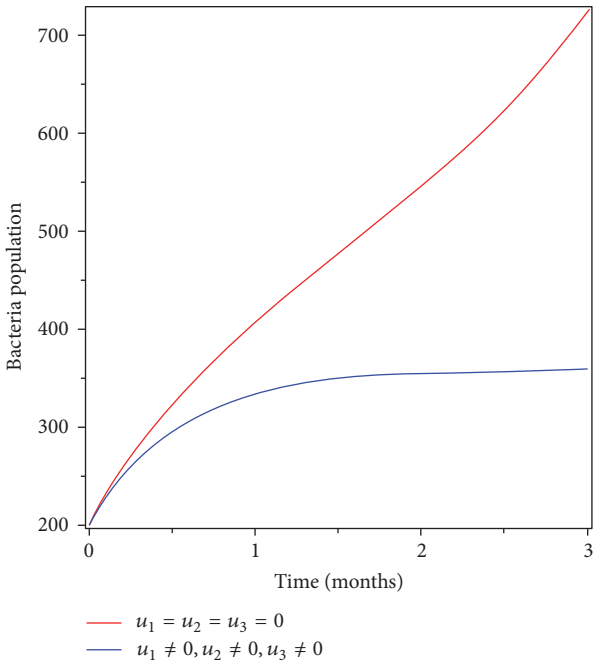

Figure 11: Simulations of the typhoid fever model with prevention, treatment, and screening controls on Salmonella bacteria populations.

Table 3: Number of infections averted and total cost of each strategy.

Strategies	Description	Total infections averted	Total cost (USD)
A	Prevention and screening	11,977	733.07
B	Treatment and screening	13,805	800
C	Prevention and treatment	19,699	531.19
D	Prevention, treatment, and screening	19,987	1104.5

We used parameter values in Table 2 to estimate the total cost and total infections averted in Table 3.

First we compared the cost-effectiveness of strategies A and B: ICER(A) = 733.07/11,977 = 0.06, ICER(B) = (733.07 − 800)/(11,977 − 13,805) = 0.037.

This shows that strategy B is cheaper than strategy A by saving 0.037. That means strategy A needs higher money than strategy B. Therefore, we exclude strategy A and continue to compare strategies B and C.

$$\text{ICER (B)} = \frac{800}{13{,}805} = 0.058,$$
$$\text{ICER (C)} = \frac{800 - 573.19}{13{,}805 - 19{,}699} = -0.039. \tag{56}$$

Strategy C (prevention and treatment)

Strategy D (prevention, treatment, and screening)

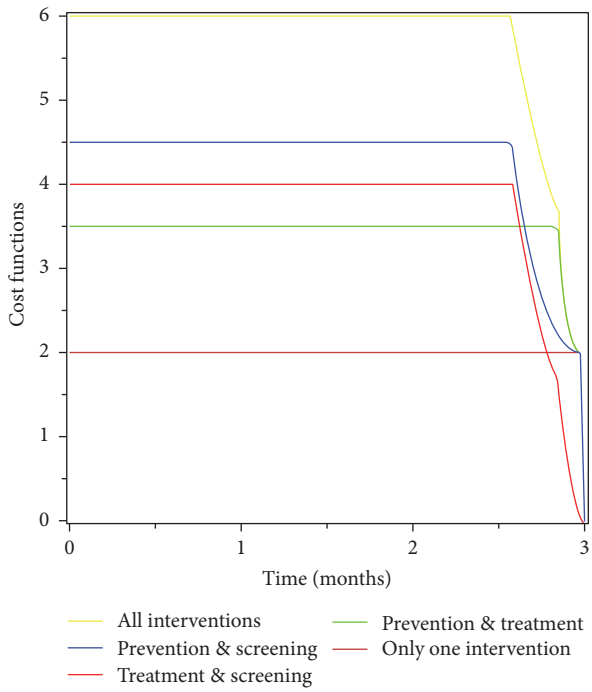

FIGURE 12: Cost function of the intervention strategies for the period of 3 months.

Similarly, this comparison indicates that strategy C is cheaper than strategy B by saving 0.039. Therefore, strategy B is rejected and continues to compare strategy C with the last strategy which is D.

$$\text{ICER (C)} = \frac{573.19}{19{,}699} = 0.029,$$
$$\text{ICER (D)} = \frac{573.19 - 1{,}104.5}{19{,}699 - 19{,}987} = 1.845. \quad (57)$$

Finally, the comparison result reveals that strategy C is cheaper than strategy D by saving 0.029. Therefore, strategy C (combination of prevention and treatment) is the best strategy from all compared strategies due to its cost-effectiveness and healthy benefit.

Moreover, Figure 12 shows that applying only one intervention is cheapest. But we do not consider this because a single intervention is not effective in eradicating the disease. A combination of prevention and treatment strategy is the cheapest of all other combined intervention strategies. The combination of all the three interventions (prevention, treatment, and screening) is the most expensive strategy compared to other strategies.

8. Discussions and Conclusions

In this study, a deterministic model for the dynamics of typhoid fever disease is proposed. The qualitative analysis of the model shows that the solution of the model is bounded and positive and also the equilibria points of the model are obtained and their local as well as global stability condition is established. The study also obtained the basic reproduction number and it reveals that for $\mathfrak{R}_0 < 1$ there is no possibility of having backward bifurcation. In Section 4, sensitivity analysis of the reproductive number has been carried out. Results from the sensitivity analysis of the reproductive number suggest that an increase in ν, K, σ_1, and σ_2 has the greatest influence on increasing the magnitude of the associated reproductive number which results in the endemicity of typhoid fever.

In Section 5, using Pontryagin's maximum principle, the optimal control problem is formulated and the conditions for optimal control of the disease are analyzed with effective preventive measures (sanitation and proper hygiene controls), treatment regime, and screening. Existence conditions for optimal control are established and the optimality system is developed. Seven intervention strategies are proposed for examining each strategy on the eradication of typhoid. In Section 6, the proposed strategies are investigated numerically and their results are displayed graphically. Cost-effectiveness analysis of the main strategies is done in Section 7, and the results indicate that prevention and the cost put into treatment have a strong impact on the disease control. Effective treatment only without prevention is not the best option in controlling the spread of typhoid fever. Therefore, this finding conclude that adequate control measures which adhered to these control strategies (preventive and treatment) would be a very effective way for fighting the disease and also for cost-effectiveness.

Conflicts of Interest

The authors declare that there are no conflicts of interest regarding the publication of this paper.

References

[1] World Health Organization, "Typhoid fever fact sheet," 2000, http://www.who.int/mediacentre/factsheets/.

[2] World Health Organization (WHO), *The Diagnosis,Treatment and Prevention of Typhoid Fever*, 2003.

[3] O. D. Makinde and K. O. Okosun, "Impact of chemo-therapy on optimal control of malaria disease with infected immigrants," *BioSystems*, vol. 104, no. 1, pp. 32–41, 2011.

[4] K. O. Okosun and O. D. Makinde, "On a drug-resistant malaria model with susceptible individuals without access to basic amenities," *Journal of Biological Physics*, vol. 38, no. 3, pp. 507–530, 2012.

[5] K. O. Okosun and O. D. Makinde, "Optimal control analysis of malaria in the presence of non-linear incidence rate," *Applied and Computational Mathematics. An International Journal*, vol. 12, no. 1, pp. 20–32, 2013.

[6] K. O. Okosun and O. D. Makinde, "Optimal control analysis of hepatitis C virus with acute and chronic stages in the presence of treatment and infected immigrants," *International Journal of Biomathematics*, vol. 7, no. 2, Article ID 1450019, 23 pages, 2014.

[7] K. O. Okosun and O. D. Makinde, "A co-infection model of malaria and cholera diseases with optimal control," *Mathematical Biosciences*, vol. 258, pp. 19–32, 2014.

[8] I. A. Adetunde, "Mathematical models for the dynamics of typhoid fever in kassena-nankana district of upper east region of Ghana," *Modern Mathematics and Statistics*, 2008.

[9] S. Mushayabasa and C. P. Bhunu, "Prostitution and drug (alcohol) misuse: the menacing combination," *Journal of Biological Systems*, vol. 20, no. 2, Article ID 1250005, pp. 177–193, 2013.

[10] K. R. Adeboye and M. Haruna, "A mathematical model for the transmission and control of malaria and typhoid co-infection using sirs approach," *Nigeria Research Journal of Mathematics*, 2015.

[11] A. Omame, R. A. Umana, N. O. Iheonu, and S. Chioma, "On the existence of a stochastic model of typhoid fever," *Mathematical Theory and Modeling*, vol. 5, no. 8, 2015.

[12] M. A. Khan, M. Parvez, S. Islam, I. Khan, S. Shafie, and T. Gul, "Mathematical analysis of typhoid model with saturated incidence rate," *Advanced Studies in Biology*, vol. 7, pp. 65–78, 2015.

[13] O. C. Akinyi, J. Y. T. Mugisha, A. Manyonge, and C. Ouma, "A model on the impact of treating typhoid with anti-malarial: Dynamics of malaria concurrent and co-infection with typhoid," *International Journal of Mathematical Analysis*, vol. 9, no. 9-12, pp. 541–551, 2015.

[14] M. Gosh, P. Chandra, P. Sinha, and J. B. Shukla, "Modelling the spread of bacterial infectious disease with environmental effect in a logistically growing human population," *Non-linear - Analysis: Real World Applications*, vol. 7, pp. 341–363, 2006.

[15] P. van den Driessche and J. Watmough, "Reproduction numbers and sub-threshold endemic equilibria for compartmental models of disease transmission," *Mathematical Biosciences*, vol. 180, pp. 29–48, 2002.

[16] J. P. LaSalle, *The Stability of Dynamical Systems*, SIAM, Philadelphia, Pa, USA, 1976.

[17] N. Chitnis, J. M. Cushing, and J. M. Hyman, "Bifurcation analysis of a mathematical model for malaria transmission," *SIAM Journal on Applied Mathematics*, vol. 67, no. 1, pp. 24–45, 2006.

[18] S. M. Blower and H. Dowlatabadi, "Sensitivity and Uncertainty Analysis of Complex Models of Disease Transmission: an HIV Model as an Example," *International Statistical Institute, Great-Britain*, vol. 62, pp. 229–243, 1994.

[19] S. Baba and O. D. Makinde, "Optimal control of HIV/AIDS in the workplace in the presence of careless individuals," *Computational and Mathematical Methods in Medicine*, vol. 2014, Article ID 831506, 2014.

[20] W. H. Fleming and R. W. Rishel, *Deterministic and Stochastic Optimal Control*, vol. 1, Springer, New York, NY, USA, 1975.

[21] L. S. Pontryagin, V. G. Boltyanskii, R. V. Gamkrelidze, and E. F. Mishchenko, *The Mathematical Theory of Optimal Processes*, John Wiley & Sons, London, UK, 1962.

[22] K. R. Fister, S. Lenhart, and J. S. McNally, "Optimizing chemotherapy in an HIV model," *Electronic Journal of Differential Equations*, vol. 1998, 12 pages, 1998.

[23] S. M. Lenhart and J. T. Workman, *Optimal Control Applied to Biological Models*, CRC Press, 2007.

Hindawi
Computational and Mathematical Methods in Medicine
Volume 2017, Article ID 4253167, 11 pages
https://doi.org/10.1155/2017/4253167

Research Article

Hamiltonian Analysis of Subcritical Stochastic Epidemic Dynamics

Lee Worden,[1] Ira B. Schwartz,[2] Simone Bianco,[3] Sarah F. Ackley,[1,4] Thomas M. Lietman,[1,4] and Travis C. Porco[1,4]

[1]*Francis I. Proctor Foundation, University of California, San Francisco, San Francisco, CA, USA*
[2]*Nonlinear Systems Dynamics Section, Plasma Physics Division, U.S. Naval Research Laboratory, Washington, DC, USA*
[3]*Department of Industrial and Applied Genomics, IBM Accelerated Discovery Lab, IBM Almaden Research Center, 650 Harry Rd, San Jose, CA 95120-6099, USA*
[4]*Department of Epidemiology and Biostatistics, University of California, San Francisco, San Francisco, CA, USA*

Correspondence should be addressed to Lee Worden; lee.worden@ucsf.edu

Received 31 January 2017; Revised 7 June 2017; Accepted 12 June 2017; Published 28 August 2017

Academic Editor: Anwar Zeb

We extend a technique of approximation of the long-term behavior of a supercritical stochastic epidemic model, using the WKB approximation and a Hamiltonian phase space, to the subcritical case. The limiting behavior of the model and approximation are qualitatively different in the subcritical case, requiring a novel analysis of the limiting behavior of the Hamiltonian system away from its deterministic subsystem. This yields a novel, general technique of approximation of the quasistationary distribution of stochastic epidemic and birth-death models and may lead to techniques for analysis of these models beyond the quasistationary distribution. For a classic SIS model, the approximation found for the quasistationary distribution is very similar to published approximations but not identical. For a birth-death process without depletion of susceptibles, the approximation is exact. Dynamics on the phase plane similar to those predicted by the Hamiltonian analysis are demonstrated in cross-sectional data from trachoma treatment trials in Ethiopia, in which declining prevalences are consistent with subcritical epidemic dynamics.

1. Introduction

Stochastic models are a common tool in epidemiological research, where public health interventions aim at the reduction of fluctuating counts of infected or infective individuals [1], and models are used in explaining, predicting, and responding to acute and chronic diseases of public health significance.

A fundamental result is the presence of a critical value of the basic reproduction number R_0, defined as the expected number of secondary cases resulting from a single infective case in an otherwise susceptible population. Supercritical diseases, those with $R_0 > 1$, tend to stabilize around a positive number of infective cases that can persist for very long times, while in subcritical cases ($R_0 < 1$) the infective count declines to zero on a relatively short timescale. In either case, the long-term, stationary probability distribution of number of infective cases is trivial, as all epidemics in finite population stochastic transmission models must eventually die out due to chance fluctuations, but the quasistationary distribution—the distribution conditional on nonextinction of the disease—can be very informative about the behavior of the system within finite time intervals.

When $R_0 < 1$, the quasistationary distribution of number of infective cases in simple transmission models is often approximately geometric, with probability of I infective cases proportional to $(R_0)^I$ [2, 3]. Prevalences consistent with the geometric distribution, when analyzed statistically across multiple locations simultaneously, have been observed in trachoma elimination trials at times in which the disease's dynamics are subcritical [4–6].

Such statistics of case count distributions observed in multiple communities at a single time may be able to help provide an assessment of the dynamics of a disease, possibly

of its basic reproductive number and, hence, of the future time course of the disease. An approximately geometric distribution of prevalences also implies that there will be more high-prevalence communities than there would be in a lighter-tailed distribution, even when the mean prevalence is low and declining. This suggests that an exceptionally high-prevalence community may be simply a statistical outlier, which can be expected to regress to the mean without intervention, rather than a "transmission hotspot" calling for intensified intervention [5].

While the quasistationary distribution of a specific stochastic model can be calculated as an eigenvector of a Markov transition matrix, since the equations for the entries of that vector cannot be solved explicitly for even very simple models, research has focused on approximations ([2, 7–9], e.g.). Barbour and Pollett [10] established that the quasistationary distribution is a fixed point of a given map defined on probability mass functions, allowing efficient approximation techniques [11]. The fixed point of that map can also be found using a "ratio of means" approach built on waiting times rather than transition rates [12] that can aid in calculation. Quasistationary approximations for diffusion processes and branching processes are also well developed and are the subject of active research and development [3, 11, 13].

In this paper we introduce a method of approximating the quasistationary distribution of a stochastic model in the subcritical regime, using a technique that has been used previously to approximate rare large-deviation events in supercritical dynamics [14–16]. This technique takes a large-population limit of the model dynamics in a way that yields a Hamilton-Jacobi equation, which can be understood by analyzing the geometry of an associated Hamiltonian ODE system.

This Hamiltonian approach to stochastic mechanics, innovated by Graham and Tél [17] for diffusion equations and extended by Hu [18] to master equations, has primarily been used to study stationary solutions of the limiting stochastic process, by locating special solutions of the Hamiltonian ODE system, characterized by $H = 0$, where H is the Hamiltonian. The Hamiltonian ODE system includes the deterministic limit of the stochastic model as an invariant subsystem within the equipotential ($H = 0$) set, and at each limit set of the deterministic system, the equipotential set extends outwards into the nondeterministic regions of the Hamiltonian system's phase space. Those extensions reveal quantitative information about the system's stochastic behavior near attractors. Thus they are used to analyze stationary probability densities associated with attractors and other limit sets of the deterministic system and the frequencies and paths of rare escape events from one attractor to another [15, 19–22]. This geometric structure, which encodes characteristics of the deterministic limit of the stochastic system and the probability distribution of deviations from the deterministic limit, is strange in comparison to the structures seen in Hamiltonian systems from physics and is much less well understood.

Here we investigate the use of structures within the equipotential set, but at a distance from the deterministic subsystem, to analyze a stochastic model's behavior. We identify such a structure far from the deterministic subsystem with the quasistationary behavior of an epidemic model, in contrast to the use of structures intersecting the deterministic subsystem to analyze stationary behavior.

2. Limiting Behavior of Birth-Death Process

Many models of stochastic epidemic dynamics, biological population dynamics more generally, and branching processes are included in the category of birth-death processes. Here we apply the analysis of Hu [18] to this class of processes, and below we will apply it to specific example models.

A stochastic birth-death process models the size of a single population, altered by events in which the size either increases by one or decreases by one. The rate of increase from size k is labeled $B(k)$ and the rate of decrease from size k is labeled $D(k)$. Writing $P(k,t)$ for the probability that the size is k at time t, the change in probability over time is governed by a master equation:

$$\begin{aligned}\frac{dP(k,t)}{dt} &= B(k-1)P(k-1,t) \\ &\quad + D(k+1)P(k+1,t) - B(k)P(k,t) \\ &\quad - D(k)P(k,t) \quad \text{for each } k.\end{aligned} \tag{1}$$

Taking $D(0) = 0$ and $B(-1)P(-1,t) = 0$ for all t, the dynamics of the master equation is confined to nonnegative values of k. In order to take a large-system-size limit, let Ω be a measure of system size such as, for example, a maximum population size, such that, as we consider increasingly large birth-death systems in which both Ω and k become unboundedly large, the ratio k/Ω remains finite. For example, in a system with finite population size N, we can use $\Omega = N$, as we will see below. Then letting $x = k/\Omega$, we obtain a transformed master equation

$$\begin{aligned}\frac{1}{\Omega}\frac{dP(x,t)}{dt} &= b\left(x-\frac{1}{\Omega}\right)P\left(x-\frac{1}{\Omega},t\right) \\ &\quad + d\left(x+\frac{1}{\Omega}\right)P\left(x+\frac{1}{\Omega},t\right) \\ &\quad - b(x)P(x,t) - d(x)P(x,t),\end{aligned} \tag{2}$$

where $b(x) = (1/\Omega)B(\Omega x)$ and $d(x) = (1/\Omega)D(\Omega x)$. Let the functions b and d be smooth functions of x for each Ω, with a smooth limit as $\Omega \to \infty$.

Additionally, let $\phi(x,t)$ be a probability density function that is smooth in x and t, such that $\phi(k/\Omega,t) = \Omega P(k/\Omega,t)$. Following Hu [18], this allows construction of a Kramers-Moyal expansion of the dynamics, by substituting and Taylor expanding the master equation around x so that it is expressed using only values at x:

$$\begin{aligned}\frac{1}{\Omega}\frac{\partial\phi(x,t)}{\partial t} &= \sum_{n=1}^{\infty}\frac{1}{n!}\left(-\frac{1}{\Omega}\right)^n\frac{\partial^n}{\partial x^n}\left(b(x)\phi(x,t)\right) \\ &\quad + \sum_{n=1}^{\infty}\frac{1}{n!}\left(\frac{1}{\Omega}\right)^n\frac{\partial^n}{\partial x^n}\left(d(x)\phi(x,t)\right).\end{aligned} \tag{3}$$

To derive a partial differential equation in the large-system limit, we rewrite the density as an exponential expression:

$$\phi(x,t) = \Omega e^{-\Omega U(x,t)}. \tag{4}$$

Assume that the function U can be expanded in powers of Ω on $0 < x < 1$,

$$U(x,t) = u(x,t) + \frac{1}{\Omega}u_1(x,t) + \frac{1}{\Omega^2}u_2(x,t) + \cdots, \tag{5}$$

and that the terms of that expansion other than $u(x,t)$ vanish asymptotically as Ω approaches infinity. This *ansatz*, known as the WKB approximation [18, 26], makes it possible to generate a partial differential equation in u.

With these assumptions, derivatives of products of ϕ take on a simplified form,

$$\begin{aligned}&\left[-\frac{1}{\Omega}\right]^n \frac{\partial^n}{\partial x^n} F(x,t)\, e^{-\Omega U(x,t)} \\ &\quad = e^{-\Omega U(x,t)} F(x,t) \left(\frac{\partial u}{\partial x}\right)^n + \mathcal{O}\left(\frac{1}{\Omega}\right).\end{aligned} \tag{6}$$

Substituting, the expansion of (3) to first order is

$$\begin{aligned}\frac{1}{\Omega}\frac{\partial \phi(x,t)}{\partial t} = \Omega \Bigg[& e^{-\Omega U(x,t)} \left(b(x) \sum_{n=1}^{\infty} \frac{1}{n!} \left(\frac{\partial u}{\partial x}\right)^n + d(x) \right. \\ & \left. \cdot \sum_{n=1}^{\infty} \frac{1}{n!} \left(-\frac{\partial u}{\partial x}\right)^n \right) + \mathcal{O}\left(\frac{1}{\Omega}\right) \Bigg].\end{aligned} \tag{7}$$

Thus, in the large size limit, (3) becomes a partial differential equation for u:

$$\begin{aligned}&\frac{\partial u(x,t)}{\partial t} \\ &\quad = -\left(b(x) \left(e^{\partial u/\partial x} - 1 \right) + d(x) \left(e^{-\partial u/\partial x} - 1 \right) \right).\end{aligned} \tag{8}$$

2.1. The Associated Hamiltonian System. Because the right hand side of (8) contains only first partial derivatives of u, it has the form of a Hamilton-Jacobi equation of classical mechanics [27],

$$\frac{\partial u(x,t)}{\partial t} = -H\left(x, \frac{\partial u}{\partial x}\right), \tag{9}$$

with the consequence that it can be analyzed using characteristic curves described by an associated system of ordinary differential equations [18]. This analysis is based on the Hamiltonian function

$$H\left(x, \frac{\partial u}{\partial x}\right) = b(x)\left(e^{\partial u/\partial x} - 1\right) + d(x)\left(e^{-\partial u/\partial x} - 1\right). \tag{10}$$

From that Hamiltonian a two-dimensional dynamical system can be written, whose state variables are x, the scaled population size, and a conjugate variable p, which takes the place of $\partial u/\partial x$ in the Hamiltonian. The associated Hamiltonian dynamical system is

$$\begin{aligned}\frac{dx}{dt} &= \frac{\partial}{\partial p} H(x,p) = b(x)\, e^{p} - d(x)\, e^{-p}, \\ \frac{dp}{dt} &= -\frac{\partial}{\partial x} H(x,p) \\ &= -b'(x)\left(e^{p} - 1\right) - d'(x)\left(e^{-p} - 1\right).\end{aligned} \tag{11}$$

Trajectories of this system do not correspond to realizations of the stochastic birth-death process but rather trace out curves along the surface of u versus x and t, which can be used to analyze the behavior of u over time.

Thus we can gain information about birth-death processes in the large size limit by using this associated system to analyze the Hamilton-Jacobi equation (8). Stationary solutions of the master equation, characterized by the equilibrium condition $d\phi(x,t)/dt = 0$, are identified with curves on the (x, p) plane on which $H(x, p) = 0$.

In the case of this one-dimensional system, though not in the general master equation case, the Hamiltonian has two factors,

$$H(x,p) = \left(b(x) - d(x)\, e^{-p}\right)\left(e^{p} - 1\right), \tag{12}$$

which contribute two solution sets to the solution of $H = 0$.

The flat subspace $p = 0$ is always a solution set for $H = 0$ in Hamiltonian systems constructed from master equations in this way [18]. The dynamics within this set are the dynamics of the ODE approximation to the stochastic dynamics, and fixed points and other limit sets of the Hamiltonian system located in this set correspond to fixed points and other limit sets of this deterministic subsystem. Other solutions to the equation $H = 0$ pass transversely through those limit sets and can reveal information about the stochastic behavior of the master equation system, as we will see in the treatment of the supercritical SIS model, below.

In the birth-death systems we consider here, in which $k = 0$ is an absorbing state, a common factor of x can be taken out of $b(x)$ and $d(x)$, allowing us to describe three components of the solution set in all.

3. The SIS Model

The SIS (susceptible-infective-susceptible) model provides a simple representation of infectious disease processes in the absence of immunity [28]. Classically, this model describes the number of susceptibles S and infective cases I in a population of fixed size, where increase in the infective class is driven by infective-susceptible contact events, and infective cases return to the susceptible class at a rate independent of contact with others. SIS models have been used to describe a range of diseases, including trachoma [29] and sexually transmitted infections [30]. In population biology, a model identical in form to this one is known as a stochastic logistic model [31].

In the basic SIS model, the infective class increases at a rate $\beta S(I/N)$, which is proportional to a quadratic

susceptible-infective contact rate, and decreases at a per capita constant rate γI, with $S = N - I$, and total population N held fixed. Thus it is the number of infective cases, I, that is the stochastically varying state variable of the model. Infective cases are added by transmission events, at rate $\beta(S/N)I$, where β is the transmission rate per susceptible-infective pair [1]. Cases return to the susceptible class at rate γI, where γ is the per capita removal rate. The parameters can be combined into one nondimensional value by rescaling the time variable by a factor of γ, after which the birth and death rates are

$$\begin{aligned} B(I) &= R_0\left(1 - \frac{I}{N}\right)I, \\ D(I) &= I, \end{aligned} \tag{13}$$

where $R_0 = \beta/\gamma$ is the basic reproduction number [28].

Using system size $\Omega = N$, the analysis we have presented for birth-death systems applies to the SIS model, with Hamiltonian

$$H(x, p) = R_0(1 - x)x\left(e^p - 1\right) - x\left(e^{-p} - 1\right), \tag{14}$$

where $x = I/N$ is the infective fraction of the population.

3.1. The Supercritical Case. In the supercritical ($R_0 > 1$) case, the SIS process is attracted to a positive, or endemic, equilibrium value $x = 1 - 1/R_0$, at which the birth and death rates are equal. The probability density of the fraction infective case concentrates around that value. On very long time scales, however, in finite systems, stochastic fluctuation will bring the fraction infective case to zero, which is an absorbing state from which the epidemic cannot return. Thus the stationary distribution of the process is a point mass at $x = 0$, and the density function concentrated around the endemic equilibrium, while it is a stationary distribution in the infinite-size limit and is the quasistationary distribution in the finite cases.

The Hamiltonian analysis of the supercritical SIS model has been treated exactly elsewhere [16, 20]. The phase plane of the Hamiltonian system is shown in Figure 1.

Stationary solutions of the PDE correspond to solutions of $H(x, p) = 0$ on this plane, when p is interpreted as $\partial u/\partial x$. The Hamiltonian factors into three parts:

$$H(x, p) = x\left(R_0(1 - x) - e^{-p}\right)\left(e^p - 1\right), \tag{15}$$

which directly identifies the three solution curves of $H = 0$ in the plane: two trivial solutions,

$$\begin{aligned} x &= 0, \\ p &= 0, \end{aligned} \tag{16}$$

and one nontrivial solution,

$$p = -\ln\left(R_0(1 - x)\right), \tag{17}$$

shown in Figure 1. These curves are trajectories of the Hamiltonian dynamical system (11).

The horizontal axis of the phase plane, which is the $p = 0$ solution, is isomorphic to the deterministic SIS system.

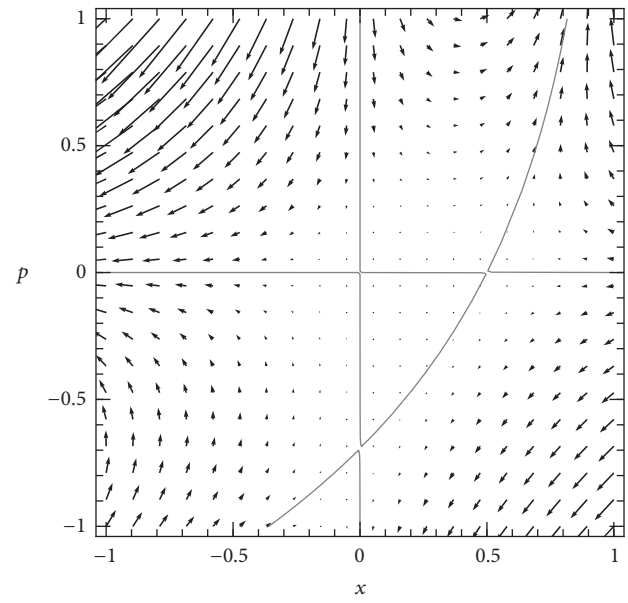

Figure 1: *Phase plane of the Hamiltonian dynamical system (11), for a supercritical SIS model* ($R_0 = 2$). Arrows depict the flow of the dynamics of x and p. The three invariant curves of the dynamics (solution curves of $H = 0$) are shown in gray: the two axes of the space and one nontrivial curve. The nontrivial curve corresponds to the quasistationary solution of the stochastic SIS model, as discussed in the text.

Two of the fixed points of the Hamiltonian system are the fixed points of that deterministic system—the disease-free equilibrium at $(0, 0)$ and the endemic equilibrium at $(1 - 1/R_0, 0)$. They are located at the points where the horizontal axis intersects the other two solution curves. A third fixed point, at $(0, -\ln R_0)$, also corresponds to the disease-free state ($x = 0$) but is at the intersection of solution curves away from the horizontal axis.

The nontrivial solution curve (17) corresponds to the stationary solution of $u(x)$ on which probability concentrates around the endemic equilibrium, and the fixed points on it describe the probability density at the endemic and disease-free equilibria. That solution is a function $u(x)$ that solves

$$\frac{\partial u(x)}{\partial x} = -\ln\left(R_0(1 - x)\right). \tag{18}$$

Changing variables to $s = 1 - x$ and integrating produce a closed-form solution,

$$u(s) = s\ln\left(R_0 s\right) - s + C_0. \tag{19}$$

This provides a closed-form solution for the quasistationary probability density:

$$\phi(s) = Ne^{-Nu(s)} = C_1\left(\frac{e}{R_0 s}\right)^{Ns}. \tag{20}$$

The constant C_1 is determined by the constraint that $\int_0^1 \phi(s)ds = 1$.

In supercritical models in general, the equipotential surfaces (solutions of $H = 0$) near the nontrivial solution

of the deterministic subsystem describe the behavior of the probability distribution of rare events, which are located in the tail of the stationary distribution.

The above stationary solution approximates the quasistationary density in the finite-N SIS system, in which extinction is a rare event given large N.

It provides an approximation for the time to extinction in the stochastic dynamics. The function u is the *action* of classical mechanics. The most probable path to extinction can be obtained by maximizing the function $u(x)$, which produces the equipotential surfaces $H = 0$. The path is explicitly calculated by integrating along the $H = 0$ curves, both in this SIS case and in more complex models (e.g., [16]).

4. Subcritical Dynamics

In the deterministic SIS system in the subcritical case, x relaxes to zero for all initial conditions $0 \le x \le 1$. The master equation solution also relaxes to $x = 0$, with probability mass declining to zero at all other values of x [2]. In this case, the quasistationary distribution is not stationary even in the large-N limit due to the deterministic attraction of the origin. The WKB hypothesis that the probability current near the absorbing state $x = 0$ vanishes when the system size N grows without bound is not satisfied, and we do not use the stationary behavior of the PDE (which relaxes to a point mass) to analyze the quasistationary behavior of the master equations. Instead we use the transient behavior of the PDE to identify the equilibrium structure in the Hamiltonian phase plane that describes the master equation's quasistationary solution.

4.1. Using the Phase Plane to Analyze Dynamics of the Hamilton-Jacobi Equation. In the Hamiltonian phase plane for the subcritical model, the same three solution curves for $H = 0$ are present as in the supercritical case, but they fall in different places on the phase plane, as shown in Figure 2. In this case, the point of intersection of the nontrivial curve (17) and the horizontal axis is shifted to the left of the origin. The endemic equilibrium represented by that point is lost in a transcritical bifurcation when R_0 declines below 1, and the origin becomes the attracting solution for the stochastic SIS system. The intercept where the nontrivial curve (17) meets the vertical axis, at $p = -\ln R_0$, is now above $p = 0$.

Because of this bifurcation, in the subcritical case we cannot apply the analysis used for the supercritical case, as the system is drawn to a singular value of x at which the $H = 0$ curve crossing the horizontal axis is vertical and cannot be translated to values of $\partial u/\partial x$ as a function of x. To study the quasistationary distribution of this system requires further analysis.

Any smooth initial distribution $\phi(x)$ can be mapped onto a curve in the (x, p) plane on which $p = \partial u/\partial x$ at every value of x, where u is defined by $\phi(x) = Ne^{-Nu(x)}$ as above. This curve for an example initial distribution is plotted in Figure 3.

Integrating points of this curve forward along trajectories of this system produces a geometric representation of the time evolution of the system as a moving curve in the phase plane, on which the changing shape of $\partial u/\partial x$ is visible, and that

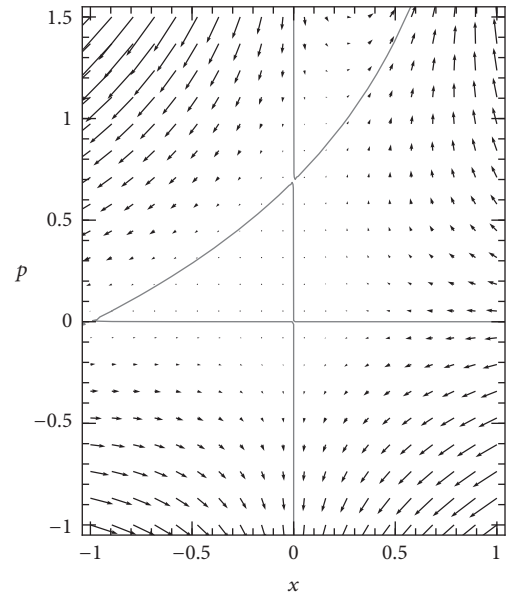

Figure 2: *Phase plane of Hamiltonian dynamical system for subcritical SIS system* ($R_0 = 0.5$). Flow is represented by arrows and the three invariant curves of the dynamics (solution curves of $H = 0$) are shown in gray, as in Figure 1. In this case, the nontrivial curve is shifted to a different position, and its intersections with the axes are located above and to the left of the origin, where in the supercritical case (Figure 1) they are below and to the right of the origin. This leads to qualitatively different dynamics, requiring a different analysis to explain the quasistationary behavior of the model.

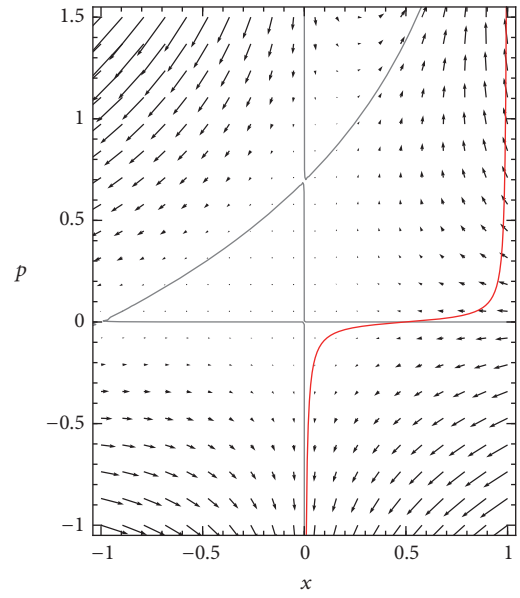

Figure 3: *Initial condition for the subcritical SIS system* on the Hamiltonian phase plane, represented by a curve of p values as a function of x. In this and following figures, the initial condition used is a β distribution with $\alpha = \beta = 2$ (i.e., $\phi_0(x) = 6x(1 - x)$) and using $N = 100$, transformed to a curve in the x-p plane using the relations $u(x) = -\ln(\phi_0(x)/N)/N$ and $p = \partial u/\partial x$.

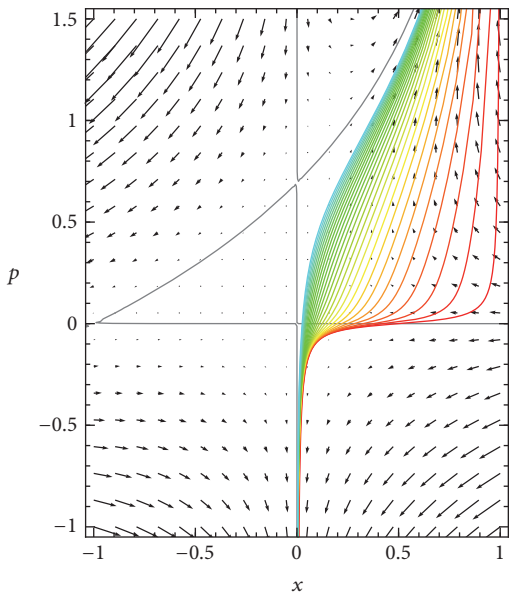

FIGURE 4: *Transient dynamics of the subcritical SIS system* on the Hamiltonian phase plane, evolving from the initial condition depicted in Figure 3 (red) toward later states (yellow, green, and blue), as each point of the initial curve moves according to the Hamiltonian dynamics (11).

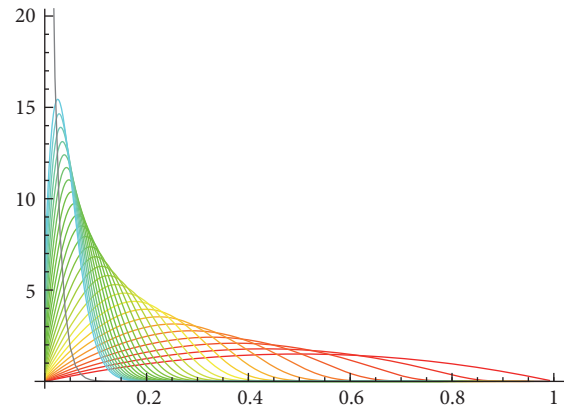

FIGURE 5: *Transient dynamics of probability density* in the subcritical SIS system, displayed as $\phi(x,t) = Ce^{-Nu(x,t)}$ versus x using the same data points as in Figure 4, with $N = 100$. Each curve is normalized to total probability one. The quasistationary distribution (23) is plotted in gray.

relation between $\partial u/\partial x$ and x provides information about the form of the function $u(x)$.

In terms of Hamiltonian dynamics, the function $u(x,t)$ is the *action* of the system, a scalar quantity that can be evaluated by integrating along its trajectories:

$$\frac{du(x,t)}{dt} = \frac{\partial u}{\partial x}\frac{dx}{dt} + \frac{\partial u}{\partial t} = p\frac{\partial H}{\partial p} - H. \tag{21}$$

For convenience, it is possible to calculate u directly when integrating the Hamiltonian dynamics numerically, by extending the dynamical system to include u as a state variable:

$$\frac{\partial}{\partial t}\begin{pmatrix} x \\ p \\ u \end{pmatrix} = \begin{pmatrix} \dfrac{\partial H}{\partial p} \\ -\dfrac{\partial H}{\partial x} \\ p\dfrac{\partial H}{\partial p} - H \end{pmatrix}. \tag{22}$$

Integrating this system, with initial conditions $u(x,0) = u_0(x)$ at selected points of the initial curve, then yields values of $u(x,t)$ explicitly for positive t.

4.2. Evolution of the Subcritical System from Initial Conditions. As time passes, each point of the p-versus-x curve moves on the phase plane according to the Hamiltonian dynamics. Their evolution stretches and translates the curve across the phase plane, as shown in Figure 4. While any given point may move in somewhat strange ways, including many that tend to infinity in the upper right direction, the curve moves smoothly to the left, approaching the vertical line $x = 0$ and the gray curve that extends into the first quadrant.

From the moving points (x, p, u) of this curve, a plot of u versus x can be constructed, or of $\phi = Ne^{-Nu}$ versus x, at each time t. Figure 5 presents this plot of ϕ versus x in time. The peak of the probability density moves asymptotically toward $x = 0$, and there is a declining tail to the right of the peak.

A number of features of the evolution of $u(x,t)$ versus x are visible in this view of the dynamics. As discussed above, the dynamics on the horizontal axis of the phase plane is identical to the usual deterministic ODE for the SIS system. When p is read as $\partial u/\partial x$, it follows that horizontal axis, where $p = 0$, corresponds to the extrema of the potential function $u(x,t)$ with respect to x. In the case pictured in these figures, the only extremum is a minimum of $u(x,t)$, which is a maximum of $\phi(x,t)$. This implies that the maximum point of the probability density function ϕ, which is the mode of the probability distribution, in the large-system approximation we are using (8), moves in exact accordance with the deterministic SIS dynamics.

Regions of x values for which a curve in the x-p plane is below the horizontal axis are regions where $\partial u/\partial x < 0$ and equivalently on which $\phi(x,t)$ is increasing in x, and regions where the curve is above the axis are where $\phi(x,t)$ is decreasing in x. Near the vertical axis, the p-versus-x curve diverges to $p = -\infty$. The fact that p, representing $\partial u/\partial x$, becomes negatively infinite there strongly suggests that $u(x)$ is divergent to $+\infty$ at $x = 0$, and so $\lim_{x\to 0^+}\phi(x,t) = 0$, at least in cases like the one illustrated in which $\phi(0)$ is zero in the initial conditions.

If the Hamilton-Jacobi PDE (8) is used to approximate any finite-N system, by grouping the probability density into bins of width $1/N$, the result will be that probability mass accumulates in the bin that includes $x = 0$, and all the other bins contain a tail that is decreasing in x, and whose total mass declines asymptotically to zero as $t \to \infty$.

Figure 4 demonstrates that, in the long term, the p-versus-x curve becomes asymptotically close to the union of the vertical axis below the positive-p equilibrium and the nontrivial $H = 0$ curve (17) at and above that equilibrium.

We conclude that as the probability density accumulates near $x = 0$, the shape of the tail of the density on $x > 0$ approaches a function described by the diagonal curve, which is the nontrivial solution (17) of $H = 0$. That tail defines the conditional distribution of x given $x > 0$, and therefore the limiting curve (17) should provide an approximation for the quasistationary distribution of the SIS master equations.

4.3. Explicit Approximation for the Quasistationary Distribution. From the above analysis we conclude that the quasistationary probability density function of the master equation system (1) is approximated by the density function represented by the nontrivial $H = 0$ curve (17). This is solved in the same way as in the supercritical case:

$$\phi(s) = C_1 \left(\frac{e}{R_0 s}\right)^{Ns}, \tag{23}$$

where $s = 1 - x$.

While in the supercritical case this density function has a mode at the endemic value $s = 1/R_0$, in this case the density is greatest at $x = 0$ ($s = 1$), as the function is monotonic decreasing on the interval $0 < x < 1$.

Changing variables back to the number of infective cases, $I = Nx = N(1 - s)$, the quasistationary approximation becomes

$$P(I) = \frac{1}{N}\phi\left(1 - \frac{I}{N}\right) = C_2 \left(\frac{eN}{R_0 (N - I)}\right)^{N-I}, \tag{24}$$

using the appropriate normalizing factor C_2 for this discrete probability mass function.

This quasistationary approximation is closely related to the classical approximation $p^{(1)}$ of Kryscio et al. [2, 8] (see also [32]): their approximation,

$$p^{(1)}(I) = C_3 \frac{1}{(N - I)!} \left(\frac{R_0}{N}\right)^I, \tag{25}$$

when transformed using Stirling's approximation for factorials,

$$\ln n! \approx n \ln n - n, \tag{26}$$

yields the approximation we have derived:

$$\begin{aligned} p^{(1)}(I) &\approx C_3 \left(\frac{e}{N - I}\right)^{(N-I)} \left(\frac{N}{R_0}\right)^{-I} \\ &\approx C_4 \left(\frac{eN}{R_0 (N - I)}\right)^{N-I}, \end{aligned} \tag{27}$$

(where C_3, C_4 are normalizing constants).

Previous approximations and numeric evaluation have established [2, 7, 8] that the quasistationary distribution of the subcritical SIS system is approximately geometric near $I = 0$, with the probabilities of successive values of I having ratio R_0.

Thus the approximating geometric distribution has the form

$$\Gamma(I) = C_5 (R_0)^I. \tag{28}$$

The geometric distribution is characterized by the constant slope of its logarithm:

$$\frac{d}{dI} \ln \Gamma(I) = \frac{d}{dI} \left[\ln C_5 + I \ln R_0\right] = \ln R_0. \tag{29}$$

Comparing to our approximation p, the slope of $\ln p$ is not constant:

$$\begin{aligned} \frac{d}{dI} \ln P(I) = \frac{d}{dI} \Big[&\ln C_2 \\ &+ (N - I)\left(1 + \ln N - \ln R_0 - \ln (N - I)\right)\Big] = -\Big(1 \\ &+ \ln N - \ln R_0 - \ln (N - I)\Big) + (N - I)\left(\frac{1}{N - I}\right) \\ &= \ln R_0 + \ln \frac{N - I}{N}. \end{aligned} \tag{30}$$

However, near $I = 0$, the nonconstant term is approximately zero, and the slope of the logarithm is approximately $\ln R_0$, with the consequence that the distribution is approximately geometric with the desired ratio when $I \ll N$.

Since the ratio $(N - I)/N$ is smaller than one when $0 < I < N$ and thus its logarithm is negative, it follows that the probability mass function p decreases to zero more rapidly than the geometric function Γ does as I increases.

In an appendix we compare the SIS process to a birth-death process that has the transmission and removal rates of the SIS model without the effect of depletion of susceptibles and whose quasistationary distribution is exactly the geometric distribution that approximates the above distribution. The phase plane analysis of the birth-death process provides visual evidence that the parameter characterizing the approximating geometric distribution by its rate of decay is determined by the intercept where the nontrivial curve (17) crosses the vertical axis.

5. Application of SIS Model Analysis to Trachoma Case Counts

Trachoma is a common subclinical childhood infection in certain regions of the less-developed world. Repeated infection results in scarring of the eyelid and trichiasis (turning inward of the eyelashes, so that the eyelids scrape against the cornea). Millions of cases of blindness have resulted. The causative agent, *Chlamydia trachomatis*, can be cleared with high efficacy with a single dose of azithromycin [33]. The World Health Organization currently recommends annual mass treatment in affected communities as a public health control measure [33, 34].

During a clinical trial of timing of mass administration of azithromycin in the Amhara Region of Ethiopia [23, 34, 35], village-level prevalence data were collected. At baseline the probability distribution of village-level prevalences, omitting zero values, had a mean of 0.39 (range 0.08–0.62) (Figure 6, top plot). After the initiation of mass treatment at or exceeding recommended WHO levels, the mean prevalence declined, and the distributions became indistinguishable from exponential [5] (Figure 6, subsequent

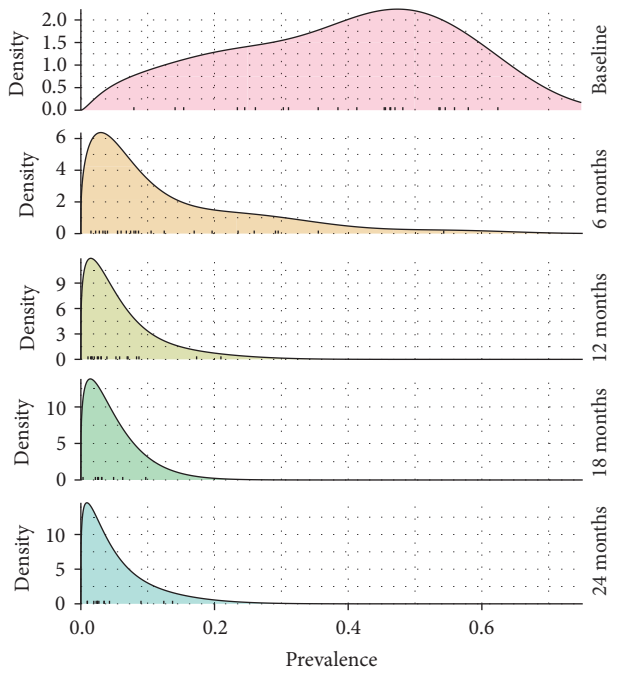

Figure 6: *Changing trachoma prevalence* at baseline and at 6-month intervals during the TANA trial of mass administration of azithromycin [23]. As the trial progresses, the prevalences become smaller and become more closely approximated by the exponential [5]. (Individual village prevalences are shown in tick marks on the horizontal axis. Curves result from beta distribution kernel density smoothing [24], with smoothing parameter determined from leave-one-out cross-validation [25].)

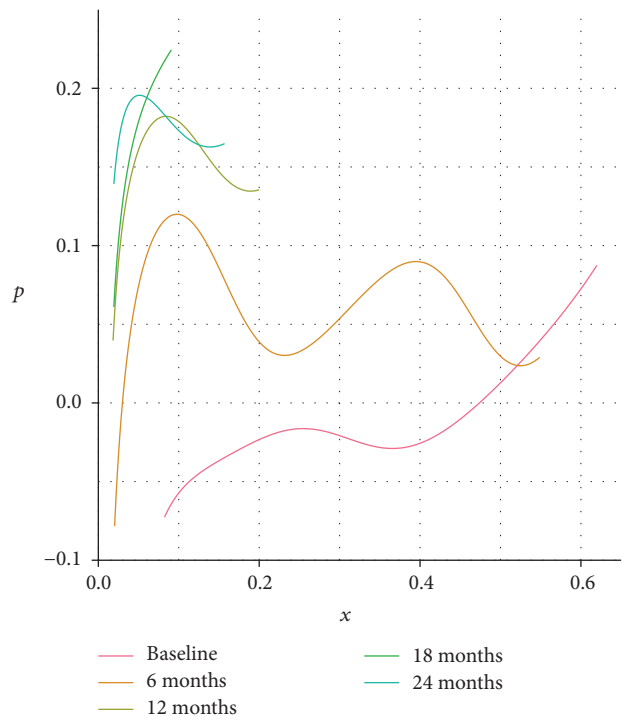

Figure 7: *Phase plane representation of changing trachoma prevalence* data from TANA trial shown in Figure 6. Each curve on the plot corresponds to one of the distributions shown in Figure 6, transformed to the x-p plane as in earlier figures (see text for details). Over time the curves shift upward and to the left, moving close to the vertical axis for smaller values of p and diverging from it at larger values of p, similar to the motion seen in the Hamiltonian analysis of the SIS model (Figure 4). Each curve in this figure is restricted to the range of the nonzero prevalence values.

plots). This finding is consistent with the approximately exponential distributions predicted by simple epidemic models, as discussed above. The matter is of more than theoretical interest, as mentioned in our introduction: the long tail of the exponential distribution implies that, during an elimination campaign, some communities may have unexpectedly large prevalence and appear to be outliers when in fact they are entirely consistent with the variation expected.

The SIS model has been used in practice to assess treatment frequency needed for elimination of trachoma [4, 29, 36].

Figure 7 displays these probability density functions $\phi(x)$ transformed to the phase plane representation defined above, $p(x) = -(d/dx)\ln(\phi(x)/N)/N$. We assume a population size $N = 100$ per village, which is approximately the number of children at risk in one of these villages [23]. In this plot, the same motion from lower right to upper left is visible, with convergence to the vertical axis and possibly to a curve leaving that axis in the positive quadrant. More abundant data may permit location of such a limiting curve that would intersect the vertical axis in this representation of the data. That curve would provide an estimate of the quasistationary behavior of the disease, and its intercept would provide an estimate of the disease's R_0.

6. Summary

Hamiltonian structures describing master equation and diffusion equation systems are the subject of ongoing exploration in stochastic processes research, where the solution sets of $H = 0$ near the deterministic subspace are used to model quasistationary behaviors and rare transition events, such as switching between states or noise-induced extinctions. We have presented an application of these structures far away from the deterministic subsystem, to approximate the probability distribution of a process near an absorbing singular point, where the WKB hypothesis does not hold and transient dynamics of the limiting PDE rather than its large-time limit behavior must be used to identify the structure corresponding to the quasistationary probability distribution of the finite-size system.

Quasistationary solutions in epidemic models can generally not be solved exactly, so approximation techniques are crucial in analysis of these processes. We present an alternative approach to this approximation problem, which may be extensible to other similar model settings and whose full usefulness is yet to be discovered. The WKB approximation and the Hamiltonian and Lagrangian techniques of analysis that it makes available are powerful and flexible and may have

applications in subcritical disease settings that go well beyond the quasistationary distribution.

Our exploration of cross-sectional prevalence data from trachoma trials, when the prevalence distributions are represented as curves on the Hamiltonian phase plane, reveals a pattern of motion consistent with the motion on the phase plane predicted by this analysis for a subcritical transmission model. Thus it is consistent, at least qualitatively, with a hypothesis that trachoma transmission in that trial setting is in fact subcritical and stochastic. This analysis fails to disconfirm that hypothesis, though other explanations are possible. In epidemiological settings where more data are available, it may become possible to observe an upper limiting curve in such a plot as well as the convergence to the vertical axis. By revealing an emerging shape of the tail of the prevalence distribution, information about that curve could contribute to description of the quasistationary behavior of the disease. Such information also may contribute to an estimate of its basic reproduction number, arrived at independently of any estimate based on temporal change in prevalences.

Beyond the one-variable birth-death models that we have analyzed, the techniques that we explore here for study of quasistationary dynamics may be of use with models with more stages of disease progression or differing transition rates, multitype models, models with patch or network structure (cf. [37]), and other cases that are more complex than the simple models presented here. In population biology, the SIS model we have discussed is also known as a stochastic logistic model [38], and this analysis has promise for population biology models that are similar but not identical to this model. While the primary goal in conservation biology is to preserve the populations in question, rather than to eradicate them as in epidemiology, declining populations are clearly of interest and the models in use may benefit from a similar analysis. This analysis may be of use in other applications as well, where quasistationary dynamics near an absorbing state is of interest.

Appendix

Comparison to Poisson Birth-Death Process

The close approximation to the geometric by the SIS and other transmission models when infective counts are small can also be explained by comparing the transmission model to a Poisson birth-death process, that is, a process in which depletion of the susceptible class is not accounted for [1]. The quasistationary limit of this process is the Yaglom limit of its associated branching process [39, 40] and is exactly geometric.

Here we use the above Hamiltonian phase plane analysis to approximate the quasistationary limit of a Poisson birth-death process with the same basic reproduction number R_0, for comparison to the above results.

In the Poisson birth-death process, the birth and death rates are the same as in the SIS model, except for the absence of the nonlinear S factor in the birth rate:

$$B(I) = R_0 I,$$
$$D(I) = I. \tag{A.1}$$

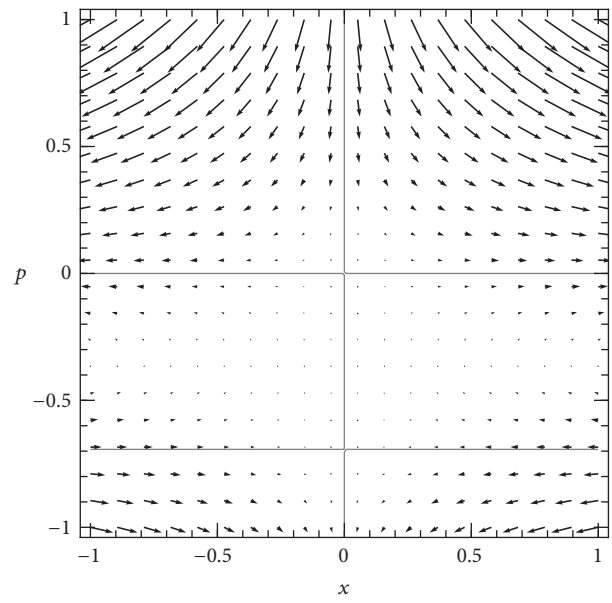

Figure 8: *Phase plane for supercritical Poisson birth-death process* ($R_0 = 2$).

It follows that the resulting Hamiltonian also is the same except for the absence of that factor:

$$\begin{aligned} H(x,p) &= R_0 x\left(e^{p}-1\right) + x\left(e^{-p}-1\right) \\ &= x\left(R_0 - e^{-p}\right)\left(e^{p}-1\right). \end{aligned} \tag{A.2}$$

As in the SIS case, the Hamiltonian factors into three parts, corresponding to three intersecting components of the solution set of $H = 0$. Again, two components are the vertical and horizontal axis. The third, nontrivial solution in this case is a horizontal line rather than a rising curve. Unlike the SIS case, here the nontrivial curve does not intersect the horizontal subsystem (except in the critical case, which we will leave aside in this discussion).

In the supercritical case (Figure 8), the dynamics on the horizontal axis (the deterministic subsystem) is similar to the SIS model in that positive values rise away from zero, but with the difference that they increase to infinity rather than to a finite endemic equilibrium value. In the subcritical case (Figure 9), in which the birth-death process tends to extinction, the behavior of the Hamiltonian system in the $x \geq 0$ half-plane is qualitatively the same as for the subcritical SIS. The only difference is in the form of the nontrivial curve that specifies the quasistationary distribution.

The quasistationary curve is specified by the equation $R_0 = e^{-p}$, or $p = -\ln R_0$. Substituting $\partial u/\partial x$ for p produces the quasistationary solution for the action, $u(x) = -x \ln R_0$, and for the probability density, $\phi(x) = Ce^{-Nu(x)} = C(R_0)^I$. This is equivalent to the geometric distribution with parameter R_0, which is well known to be the quasistationary distribution of this process.

We note that we can relate the geometric approximation to the geometry of the Hamiltonian phase plane. As discussed

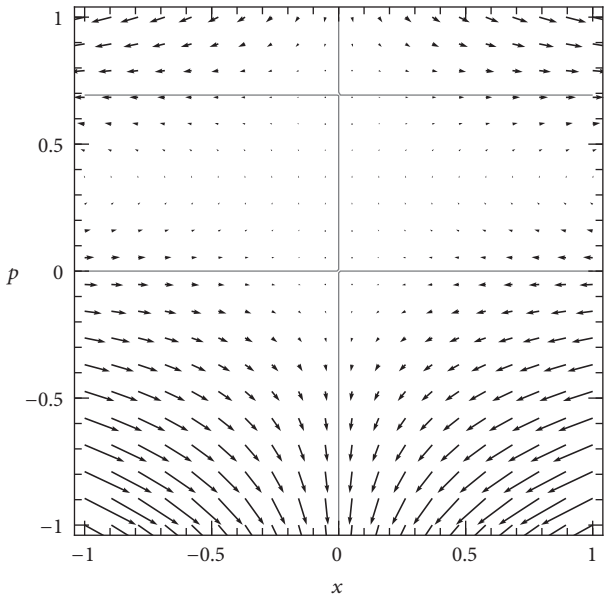

Figure 9: *Phase plane for subcritical Poisson birth-death process* ($R_0 = 1/2$).

above, the geometric approximation to the quasistationary distribution is characterized by the logarithmic slope $(\partial/\partial I) \ln P(I,t)$. The density function in terms of the fraction x is $\phi(x,t) = \Omega P(I,t)$, and the action u is defined by $\phi(x,t) = \Omega e^{-\Omega u(x,t)}$, or $u(x,t) = -\ln(\phi(x,t)/\Omega)/\Omega$. Combining,

$$u(x,t) = -\frac{\ln P(I,t)}{\Omega}, \tag{A.3}$$

so that

$$\frac{\partial}{\partial x} u(x,t) = \Omega \frac{\partial}{\partial I}\left(-\frac{\ln P(I,t)}{\Omega}\right) = -\frac{\partial}{\partial I} \ln P(I,t). \tag{A.4}$$

But note that, on the phase plane, the vertical coordinate p is identified with $\partial u/\partial x$; so it follows that the parameter of the geometric distribution approximating the quasistationary distribution near $I = 0$ is revealed by the value of the nontrivial solution for p at $x = 0$, that is, the intercept where the limiting curve describing the quasistationary distribution crosses the vertical axis. That intercept is equal to $-\ln R$, where R is the parameter of the approximating geometric distribution.

We note that the horizontal line found in the Poisson birth-death model's phase plane and the SIS process's limiting curve converge on the same value $p = -\ln R_0$ at $x = 0$, confirming visually that this birth-death process is a good approximation for the SIS process when its infective count is much smaller than N.

Conflicts of Interest

The authors declare they each have no conflicts of interest.

Acknowledgments

This study was supported by a Models of Infectious Disease Agent Study (MIDAS) grant from the US NIH/NIGMS to the University of California, San Francisco (U01GM087728), by US NEI R01-EY025350 and by a Research to Prevent Blindness Award. Ira B. Schwartz was supported by NRL base funding (N0001414WX00023) and Office of Naval Research (N0001414WX20610).

References

[1] N. T. J. Bailey, *The Mathematical Theory of Infectious Diseases*, Griffin, London, UK, 1975.

[2] I. Nåsell, "The quasi-stationary distribution of the closed endemic SIS model," *Advances in Applied Probability*, vol. 28, no. 3, pp. 895–932, 1996, http://www.jstor.org/stable/1428186.

[3] A. Lambert, "Population dynamics and random genealogies," *Stochastic Models*, vol. 24, no. 1, pp. 45–163, 2008.

[4] T. M. Lietman, T. Gebre, B. Ayele et al., "The epidemiological dynamics of infectious trachoma may facilitate elimination," *Epidemics*, vol. 3, no. 2, pp. 119–124, 2011.

[5] T. M. Lietman, T. Gebre, A. Abdou et al., "The distribution of the prevalence of ocular chlamydial infection in communities where trachoma is disappearing," *Epidemics*, vol. 11, pp. 85–91, 2015.

[6] S. A. Rahman, S. K. West, H. Mkocha et al., "The distribution of ocular Chlamydia prevalence across Tanzanian communities where trachoma is declining," *PLoS Neglected Tropical Diseases*, vol. 9, no. 3, Article ID e0003682, 2015.

[7] J. A. Cavender, "Quasi-stationary distributions of birth-and-death processes," *Advances in Applied Probability*, vol. 10, no. 3, pp. 570–586, 1978.

[8] R. J. Kryscio and C. Lefèvre, "On the extinction of the SIS Stochastic logistic epidemic," *Journal of Applied Probability*, vol. 26, no. 4, pp. 685–694, 1989.

[9] I. Nåsell, "Moment closure and the stochastic logistic model," *Theoretical Population Biology*, vol. 63, no. 2, pp. 159–168, 2003.

[10] A. D. Barbour and P. K. Pollett, "Total variation approximation for quasi-stationary distributions," *Journal of Applied Probability*, vol. 47, no. 4, pp. 934–946, 2010.

[11] E. A. Van Doorn and P. K. Pollett, "Quasi-stationary distributions for discrete-state models," *European Journal of Operational Research*, vol. 230, no. 1, pp. 1–14, 2013.

[12] J. R. Artalejo and M. J. Lopez-Herrero, "Quasi-stationary and ratio of expectations distributions: a comparative study," *Journal of Theoretical Biology*, vol. 266, no. 2, pp. 264–274, 2010, http://www.sciencedirect.com/science/article/pii/S0022519310003206.

[13] S. Méléard and D. Villemonais, "Quasi-stationary distributions and population processes," *Probability Surveys*, vol. 9, pp. 340–410, 2012.

[14] M. I. Dykman, I. B. Schwartz, and A. S. Landsman, "Disease extinction in the presence of random vaccination," *Physical Review Letters*, vol. 101, no. 7, Article ID 078101, 2008.

[15] O. Ovaskainen and B. Meerson, "Stochastic models of population extinction," *Trends in Ecology & Evolution*, vol. 25, no. 11, pp. 643–652, 2010, http://linkinghub.elsevier.com/retrieve/pii/S0169534710001801.

[16] I. B. Schwartz, E. Forgoston, S. Bianco, and L. B. Shaw, "Converging towards the optimal path to extinction," *Journal*

of the Royal Society Interface, vol. 8, no. 65, pp. 1699–1707, 2011, http://rsif.royalsocietypublishing.org/cgi/doi/10.1098/rsif.2011.0159.

[17] R. Graham and T. Tél, "On the weak-noise limit of Fokker-Planck models," *Journal of Statistical Physics*, vol. 35, no. 5-6, pp. 729–748, 1984, http://link.springer.com/article/10.1007/BF01010830.

[18] G. Hu, "Stationary solution of master equations in the large-system-size limit," *Physical Review A*, vol. 36, no. 12, pp. 5782–5790, 1987.

[19] A. J. Black and A. J. McKane, "WKB calculation of an epidemic outbreak distribution," *Journal of Statistical Mechanics: Theory and Experiment*, vol. 2011, no. 12, Article ID P12006, 2011, http://iopscience.iop.org/1742-5468/2011/12/P12006.

[20] E. Forgoston, S. Bianco, L. B. Shaw, and I. B. Schwartz, "Maximal sensitive dependence and the optimal path to epidemic extinction," *Bulletin of Mathematical Biology*, vol. 73, no. 3, pp. 495–514, 2011.

[21] B. S. Lindley and I. B. Schwartz, "An iterative action minimizing method for computing optimal paths in stochastic dynamical systems," *Physica D. Nonlinear Phenomena*, vol. 255, pp. 22–30, 2013, http://linkinghub.elsevier.com/retrieve/pii/S0167278913001085.

[22] B. S. Lindley, L. B. Shaw, and I. B. Schwartz, "Rare-event extinction on stochastic networks," *EPL (Europhysics Letters)*, vol. 108, no. 5, Article ID 58008, 2014, http://stack.iop.org/0295-5075/108/i=5/a=58008?key=crossref.7e6261f502857111feecb75a4fbe14c2.

[23] T. Gebre, B. Ayele, M. Zerihun et al., "Comparison of annual versus twice-yearly mass azithromycin treatment for hyperendemic trachoma in Ethiopia: a cluster-randomised trial," *The Lancet*, vol. 379, no. 9811, pp. 143–151, 2012.

[24] S. X. Chen, "Beta kernel estimators for density functions," *Computational Statistics and Data Analysis*, vol. 31, no. 2, pp. 131–145, 1999.

[25] K. P. Burnham and D. R. Anderson, *Model Selection and Inference: A Practical Information-Theoretic Approach*, Springer, New York, NY, USA, 1998.

[26] C. M. Bender and S. A. Orszag, *Advanced Mathematical Methods for Scientists and Engineers*, International Series in Pure and Applied Mathematics, McGraw-Hill, New York, NY, USA, 1978.

[27] R. Courant and D. Hilbert, *Methods of Mathematical Physics*, vol. 2, Wiley Classics Library, Interscience Publishers, New York, NY, USA, 1989.

[28] H. W. Hethcote, "The mathematics of infectious diseases," *SIAM Review*, vol. 42, no. 4, pp. 599–653, 2000.

[29] T. Lietman, T. Porco, C. Dawson, and S. Blower, "Global elimination of trachoma: How frequently should we administer mass chemotherapy?" *Nature Medicine*, vol. 5, no. 5, pp. 572–576, 1999.

[30] H. W. Hethcote and J. A. Yorke, *Gonorrhea Transmission Dynamics and Control*, Springer-Verlag, New York, NY, USA, 1984.

[31] I. Nåsell, *Extinction and Quasi-Stationarity in the Stochastic Logistic SIS Model*, vol. 2022 of *Lecture Notes in Mathematics*, Springer Heidelberg, Berlin, Germany, 2011.

[32] T. G. Kurtz, "Limit theorems for sequences of jump Markov processes approximating ordinary differential processes," *Journal of Applied Probability*, vol. 8, pp. 344–356, 1971.

[33] A. W. Solomon, World Health Organization, London School of Hygiene and Tropical Medicine, and International Trachoma Initiative, *Trachoma Control: A Guide for Programme Managers*, World Health Organization, Geneva, Switzerland, 2006, http://apps.who.int/iris/bitstream/10665/43405/1/9241546905_eng.pdf.

[34] J. I. House, B. Ayele, T. C. Porco et al., "Assessment of herd protection against trachoma due to repeated mass antibiotic distributions: a cluster-randomised trial," *The Lancet*, vol. 373, no. 9669, pp. 1111–1118, 2009.

[35] N. E. Stoller, T. Gebre, B. Ayele et al., "Efficacy of latrine promotion on emergence of infection with ocular Chlamydia trachomatis after mass antibiotic treatment: A cluster-randomized trial," *International Health*, vol. 3, no. 2, pp. 75–84, 2011.

[36] D. Gao, T. M. Lietman, C.-P. Dong, and T. C. Porco, "Mass drug administration: the importance of synchrony," *Mathematical Medicine and Biology*, vol. 34, no. 2, pp. 241–260, 2016.

[37] J. Hindes and I. B. Schwartz, "Epidemic extinction and control in heterogeneous networks," *Physical Review Letters*, vol. 117, no. 2, Article ID 028302, 2016, http://link.aps.org/doi/10.1103/PhysRevLett.117.028302.

[38] I. Nåsell, "On the quasi-stationary distribution of the stochastic logistic epidemic," *Mathematical Biosciences*, vol. 156, no. 1-2, pp. 21–40, 1999.

[39] A. M. Yaglom, "Certain limit theorems of the theory of branching random processes," vol. 56, pp. 795–798, 1947.

[40] T. E. Harris, *The Theory of Branching Processes*, Springer-Verlag, Berlin, Germany, 1963.

Hindawi
Computational and Mathematical Methods in Medicine
Volume 2017, Article ID 1975780, 6 pages
https://doi.org/10.1155/2017/1975780

Research Article

Mathematical Modeling for Inherited Diseases

Saima Anis,[1] Madad Khan,[1] and Saqib Khan[2]

[1]*Department of Mathematics, COMSATS Institute of Information Technology, Abbottabad, Pakistan*
[2]*Department of Mathematics, Government Postgraduate College, Abbottabad, Pakistan*

Correspondence should be addressed to Madad Khan; madadmath@yahoo.com

Received 22 December 2016; Revised 7 April 2017; Accepted 24 May 2017; Published 9 July 2017

Academic Editor: Delfim F. M. Torres

We introduced a new nonassociative algebra, namely, left almost algebra, and discussed some of its genetic properties. We discussed the relation of this algebra with flexible algebra, Jordan algebra, and generalized Jordan algebra.

1. Introduction

We introduced a new nonassociative and noncommutative algebra which has several properties similar to nonassociative and commutative algebras. The relation of the left almost algebra with other nonassociative algebras is useful and interesting to be known; in this regard, we found some relations with known algebras, namely, flexible, alternative, and Jordan algebras. We discussed some characteristics of this algebra which is similar to a commutative and associative algebra. We discussed some of the genetic properties of this algebra.

Some Basics from Genetics. Here, we discuss some simple ideas in genetics for nongeneticists and for those who are purely related to mathematics. Each cell of an organism contains long thread-like structures called chromosomes which are located inside the nucleus of animals and plants. Chromosomes are made of protein and a single molecule of deoxyribonucleic acid (DNA). After cell division, chromosomes pass from parent cells to the newborn cells. The particular intersections that the DNA carries make each living creature unique from others. The molecules of the DNA are too long, which can be fitted inside the cells only by chromosomes. Moreover, chromosomes play an important role in copying and distributing DNA accurately in the whole process of cell division. Problems in chromosomes in new cells can create serious issues like leukemia and some types of cancer. Males and females have different chromosomes; that is, females have two X chromosomes in their cells whereas males have one X and one Y chromosome. Humans have 23 pairs of chromosomes, with a total of 46 chromosomes. A gene is a unit of hereditary information and lies on chromosomes. A gene can take different forms which are called alleles. In these 23 pairs, one represents the sexual character in males; a locus which occurs on 22 pairs of chromosomes is called autosomal, whereas a locus on one pair is called sex-linked. Diploid cells are those which carry a double set of chromosomes and haploid cells are those which carry a single set of chromosomes. Diploid cells produce sex cells called gametes through a process called meiosis. Mitosis is the process of reproduction in haploid cells. The gametes cells meet each other and give a zygote which is again a diploid cell.

Basics of Genetic Algebra. After the theory of Charles Darwin, it was Gregor Mendel who studied the natural laws of genetic inheritance and tried to express them in a mathematical language. In [1–3], Etherington introduced a new method of nonassociative algebras to study genetics. Holgate studied these algebras with genetic realizations in [4–7]. Reed discussed the nonassociative algebraic structure of genetic inheritance in [8]. The genetic algebra with mutation has been discussed in [9, 10]. Several other authors studied nonassociative algebras with genetic realizations (for details, see [10–14]).

Let R be a nonempty set together with two binary operations "+" and "$\cdot$" which satisfies all the axioms of an associative ring (algebra) except an associative property with respect to multiplication; then, it is known as a nonassociative ring (algebra). Lie ring was introduced by defining and replacing a new binary operation $[a, b] = ab - ba$, for all a, b,

with ordinary multiplication of an associative ring (algebra); obviously, it is a nonassociative ring (algebra). By defining a new binary operation $a \cdot b = (1/2)(ab + ba)$ on an associative algebra over a field whose characteristic is not equal to 2, we obtain another important nonassociative algebra known as Jordan algebra. It is worth mentioning here that the theory of nonassociative algebras is a fruitful branch of algebra. Most importantly, the class of nonassociative algebras has closed connections with other branches of mathematics; also, it has closed connections with quantum mechanics, physics, biology, and other sciences. The crucial part of this theory is the theory of nearly associative rings and algebras: Lie, alternative, and Jordan algebras. In short, considering nonassociative algebras over real number fields has several applications in biology especially in genetics. Moreover, there are some other classes of nonassociative algebras closely related to genetics which are popular among mathematicians and geneticists for their usefulness in genetics. Generally, these types of algebras are commutative and nonassociative. In fact, one can study the properties of genetics by making the mathematical models using nonassociative, commutative algebras. To visualize the concept of such algebras, let us pay attention to some specific classes of algebras like gametic, zygotic, and copular algebras.

Here, we will discuss some simple algebras with genetic realizations. In order to understand the algebraic properties in genetics, simple Mendelian inheritance has been considered in [10]. If we consider a single gene with two alleles x_1 and x_2, after mating of alleles x_1 and x_2, we get the zygotes x_1x_1, x_1x_2, x_2x_1, and x_2x_2, where x_1x_1, x_2x_2 are known as homozygotes while x_1x_2, x_2x_1 are called heterozygotes. In particular, $x_1x_2 = x_2x_1$, which means that the commutative law holds in this case, which genetically represents the notion that mating of allele x_1 with allele x_2 is the same as mating of x_2 with x_1. Let us consider the equation $x_1x_2 = (1/2)(x_1 + x_2)$. This linear equation represents the notion that $x_1x_1 = x_1$ and $x_2x_2 = x_2$. The algebra with the multiplication table above is known as gamete algebra. Moreover, the zygotic algebra can be obtained from the gametic algebra by commutative duplication. From mathematical perspectives, the juxtaposition between x_1 and x_2 shows a binary operation which is not associative because $(x_1x_2)x_2 \neq x_1(x_2x_2)$ or equivalently $(x_1x_2)x_2 = x_1(x_2x_2)$ says that both alleles x_1 and x_2 are the same. Therefore, the associative law does not hold for the gametic algebra and it also does not hold for the zygotic algebra. Generally, algebras associated with genetics are commutative but nonassociative. In [3], Etherington proved that the zygotic algebra can be obtained from the gametic algebra through a commutative duplication process. Now, it is interesting to note that there is a class of algebras which is nonassociative and noncommutative but possesses many characteristics similar to commutative and associative algebras and has close relations with commutative algebras. Using notions from these algebras, we give a more general definition of gametic and zygotic algebras. Moreover, this nonassociative and noncommutative algebra has closed connections with Jordan and flexible algebras. In addition to this, if it contains a left identity, then it satisfies the famous Jordan identity and the generalized Jordan identity. This algebra works mostly like a commutative algebra; for instance, $x^2y^2 = y^2x^2$, for all x, y, holds in a commutative algebra while this equation also holds for a left almost algebra, and if a left almost algebra contains a left identity e, then $xy = (yx)e$, for any x, y. In fact, the structure is nonassociative and noncommutative but it possesses many properties which usually hold in associative and commutative algebraic structures. Also, defining a new operation on this algebra gives a commutative and associative algebra.

In this paper, we will discuss those algebras which are nonassociative and noncommutative but have close connections with nonassociative and commutative algebras. We generalized the definition available in [8] and introduced a new generalized definition for gamete algebras. Moreover, we introduce a new class of a nonassociative algebra called left almost algebra.

We restrict ourselves by considering a gene on a particular locus on a chromosome. Here, we begin with the definition of gametic algebra [8]. Consider n gametes $a_1, a_2, \ldots, a_n$ as basis elements of an n-dimensional real vector space. Multiplication is defined by

$$a_i a_j = \sum_{k=1}^{n} \gamma_{ijk} a_k, \quad \text{such that } 0 \leq \gamma_{ijk} \leq 1,\ i, j, k = 1, 2, \ldots, n,\ \sum_{k=1}^{n} \gamma_{ijk} = 1,\ i, j, k = 1, 2, \ldots, n,\ \gamma_{ijk} = \gamma_{jik},\ i, j, k = 1, 2, \ldots n, \tag{1}$$

where γ_{ijk} represent the relative gene frequencies.

The resulting algebra $\mathfrak{C}$ is called an n-dimensional gametic algebra.

Some Basic Notions of Nonassociative Algebras. A groupoid S is called a left almost semigroup if it satisfies the following left invertive law, $(ab)c = (cb)a$, for all $a, b, c \in S$. Holgate called it a left invertive groupoid [4]. An element e of a groupoid S is called left (right) identity if $ex = x (xe = x)$ for all x in S. A left identity in a left almost semigroup is unique.

Let $a, b, c \in S$, where S is a left almost semigroup with left identity e. Then,

$$a(bc) = b(ac), \quad \forall a, b, c \in S. \tag{2}$$

But the converse of the above statement is not true.

If a left almost semigroup contains a right identity, then it becomes a commutative semigroup. A left almost semigroup S is a mid structure between a groupoid and a commutative semigroup.

From the discussion above, it is easy to conclude that this nonassociative structure with left identity has a closed connection with a commutative semigroup.

A nonassociative algebra $\mathfrak{A}$ is a vector space over a field $\mathfrak{F}$ along with the bilinear multiplication from $\mathfrak{A} \times \mathfrak{A} \to \mathfrak{A}$, satisfying the following distributive properties:

$$\begin{aligned} &(\alpha a + \beta b)\, c = \alpha\,(ac) + \beta\,(bc),\\ &a\,(\alpha b + \beta c) = \alpha\,(ab) + \beta\,(ac), \qquad \forall \alpha, \beta \in \mathfrak{F},\ a, b, c \in \mathfrak{A}. \end{aligned} \tag{3}$$

A nonassociative algebra $\mathfrak{A}$ is called left almost algebra over a field $\mathfrak{F}$ if it satisfies the left invertive property with respect to multiplication.

Several authors discussed mostly commutative and nonassociative algebras with genetic realizations. There are some cases of noncommutative, nonassociative algebraic structures which were discussed in [2, 10, 14]. Moreover, Mendel's algebra is interesting to discuss. To study such cases of Mendel's algebra with mutation, we introduce a new class of nonassociative and noncommutative algebras known as left almost algebras. These algebras possess many characteristics which are similar to those of commutative nonassociative algebras with genetic realizations. Here, we give the generalized definition for gametic algebra; consider n gametes $a_1, a_2, \ldots, a_n$ as basis elements of an n-dimensional left almost vector space over $\mathbb{R}$. If we define multiplication by

$$\begin{aligned} &a_i a_j = \gamma_{ij1} a_1 + \gamma_{ij2} a_2 + \gamma_{ij3} a_3 + \cdots + \gamma_{ijn} a_n,\\ &\text{such that } 1 = \gamma_{ij1} + \gamma_{ij2} + \gamma_{ij3} + \cdots + \gamma_{ijn},\ i, j, k = 1, 2, \ldots, n, \end{aligned} \tag{4}$$

where $0 \le \gamma_{ijk} \le 1$ for all $i, j, k = 1, 2, \ldots, n$, γ_{ijk} represent the relative gene frequencies.

Then, the resulting algebra $\mathfrak{A}$ is called an n-dimensional nonassociative and noncommutative left almost gametic algebra.

Let $(a_1, \ldots, a_n)$ be a basis representing the n alleles generating a gametic left almost algebra and the multiplication defined as $a_i a_j = (1/2)(a_i + a_j)$. Consider the mapping $\omega : \mathfrak{B} \to \mathbb{R}$ and let w be the weight function defined as $\omega(a_i) = 1$. For any element x of $\mathfrak{A}$, $x = \sum \alpha_i a_i$. Thus,

$$\begin{aligned} x^2 = xx &= \sum_{i=1}^{n} (\alpha_i a_i) \sum_{i=1}^{n} (\alpha_i a_i) = \sum_{i=1}^{n} \sum_{i=1}^{n} (\alpha_i a_i)(\alpha_i a_i)\\ &= \sum_{i=1}^{n} \sum_{i=1}^{n} (\alpha_i \alpha_i)(a_i a_i) = \sum_{i=1}^{n} \sum_{i=1}^{n} (\alpha_i \alpha_i) a_i\\ &= \sum_{i=1}^{n} \sum_{i=1}^{n} (\alpha_i \alpha_i)(a_i) = \sum_{i=1}^{n} (\alpha_i) \sum_{i=1}^{n} (\alpha_i a_i) = x, \end{aligned} \tag{5}$$

$$\text{Provided } \sum_{i=1}^{n} (\alpha_i) = 1.$$

Now, in a similar way, we can define the zygotic algebra and for this we consider n gametes $a_{ij} = a_i a_j$ (considering only $i \le j$), and then random mating of zygotes a_{ij} with a_{pq} will produce zygotes a_{ks} with a particular ratio, say $\gamma_{ij,pq,ks}$. Thus, we define the following generalized zygotic multiplication as

$$a_{ij} a_{pq} = \sum_{k \le s} \gamma_{ij,pq,ks} a_{ks}, \quad \text{such that } \sum_{k \le s} \gamma_{ij,pq,ks} = 1,\ i, j, k = 1, 2, \ldots, n \text{ such that } 0 \le \gamma_{ij,pq,ks} \le 1\ \forall i, j, k = 1, 2, \ldots, n, \tag{6}$$

where $\gamma_{ij,pq,ks}$ are the relative gene frequencies.

An element x in our noncommutative, nonassociative algebra $\mathfrak{A}$ indicates a population or a gene pool and it can be expressed as a linear combination of the basis elements $a_1, a_2, \ldots, a_n$ as $x = \lambda_1 a_1 + \lambda_2 a_2 + \lambda_3 a_3 + \cdots + \lambda_n a_n$ and $\lambda_1 + \lambda_2 + \lambda_3 + \cdots + \lambda_n = 1$, where $\lambda_l \in \mathfrak{F}$, for all $l = 1, 2, \ldots, n$.

The algebra with genetic realization arising from expression (4) is more general than the one arising from (1) because the algebra is both nonassociative and noncommutative.

An algebra $\mathfrak{A}$ is called flexible if it satisfies the following property:

$$(xy)\, x = x\,(yx), \quad \forall x, y \text{ in } \mathfrak{A}. \tag{7}$$

An algebra $\mathfrak{A}$ is called a generalized Jordan algebra if it satisfies the following property:

$$(xy)\,(xx) = x\,(y\,(xx)), \quad \forall x, y \text{ in } \mathfrak{A}. \tag{8}$$

It is obvious that both flexible and generalized Jordan algebras are different but if $x = x^2$ for all x then both become identical.

2. Mutation Algebra

In [9], the author considered mutation algebra with mutation rates r and s, the gametic algebra having the basis with elements D and R, where the multiplication table is defined as

$$\begin{aligned} D^2 &= (1 - r)\, D + rR,\\ R^2 &= sD + (1 - s)\, R \end{aligned} \tag{9}$$

$$DR = \frac{1}{2}(1 - r + s)\, D + \frac{1}{2}(1 - s + r)\, R. \tag{10}$$

Then, the author chose another basis with elements $a = D$ and $b = D - R$, and thus

$$\begin{aligned} a^2 &= a - rb,\\ ab &= \frac{1}{2}(1 - r - s)\, b,\\ b^2 &= 0. \end{aligned} \tag{11}$$

Let us define an abstract algebra $\mathfrak{A}$ generated by $\{a_i : 1 \leq i \leq n\}$ over a finite field $\mathfrak{F}$. If we define the binary operation "$\star$" on $\mathfrak{A}$ as $a_i \star a_j = \alpha a_i + \alpha^2 a_j (\alpha + \alpha^2 = 1)$, then this algebra satisfies (10) but $a_i \star a_i = a_i$. Therefore, it is important to mention here that the algebra defined by this operation is not totally consistent with the mutation algebra introduced by Gonshor above. This simply implies that there is a lack of one hundred correspondences between this algebra and the algebra defined in (10) but there are still several similarities existing between the ideas of the mutation algebra and the algebra we introduced. In the next theorem, we will prove that this algebra is a left almost algebra. We denote this algebra by $\mathscr{M}_{\mathfrak{n}}(\alpha_{\mathfrak{F}})$.

Theorem 1. *$\mathscr{M}_{\mathfrak{n}}(\alpha_{\mathfrak{F}})$ is a noncommutative and nonassociative left almost algebra.*

Proof. Obviously, $\mathscr{M}_{\mathfrak{n}}(\alpha_{\mathfrak{F}})$ is closed. Next, we will show that $\mathscr{M}_{\mathfrak{n}}(\alpha_{\mathfrak{F}})$ satisfies the left invertive property, for this left $X, Y, Z \in \mathscr{M}_{\mathfrak{n}}(\alpha_{\mathfrak{F}})$. Then, $X = \sum_{j=1}^{n} \beta_j a_j$, $Y = \sum_{k=1}^{n} \gamma_k a_k$ and $Z = \sum_{l=1}^{n} \delta_l a_l$. To prove $(X \star Y) \star Z = (Z \star Y) \star X$, we need to prove $(a_j \star a_k) \star a_l = (a_l \star a_k) \star a_j$.

$$\begin{aligned}
\left(a_j \star a_k\right) \star a_l &= \alpha\left(\alpha a_j + \alpha^2 a_k\right) + \alpha^2 a_l \\
&= \alpha^2 a_j + \alpha^3 a_k + \alpha^2 a_l, \\
\left(a_l \star a_k\right) \star a_j &= \alpha\left(\alpha a_l + \alpha^2 a_k\right) + \alpha^2 a_j \\
&= \alpha^2 a_l + \alpha^3 a_k + \alpha^2 a_j \\
&= \alpha^2 x + \alpha^3 y + \alpha^2 z.
\end{aligned} \tag{12}$$

It is not associative because

$$\begin{aligned}
a_j \star \left(a_k \star a_l\right) &= \alpha a_j + \alpha^2\left(\alpha a_k + \alpha^2 a_l\right) \\
&= \alpha a_j + \alpha^3 a_k + \alpha^4 a_l.
\end{aligned} \tag{13}$$

Moreover, $a_j \star a_k = \alpha a_j + \alpha^2 a_k$ and $a_k \star a_j = \alpha a_k + \alpha^2 a_j$. Thus, $XY \neq YX$, for some X, Y. □

If we consider this theorem for a finite field of cardinality 4 which is the extension of $\mathbb{Z}_2$, then $t^2 + t = 1$ gives $t^2 + t + 1 = 0$. More generally, $x^2 + x + 1 = 0$ is the quadratic equation representing the irreducible polynomial in $\mathbb{Z}_2 = \{0, 1\}$. Thus, $GF(2^2) = \{0, 1, t, t^2\}$, and thus $GF(2^2) \setminus \{0\} = \mathfrak{F} \setminus \{0\} = \langle t : t^3 = 1\rangle = \{1, t, t^2\}$. We denote this algebra by $\mathscr{M}_4(\mathfrak{t}_{\mathfrak{F}})$. Roots of the equation $x^2 + x = 1$ are $(-1 + \sqrt{5})/2$ and $(-1 - \sqrt{5})/2$. Thus,

$$\begin{aligned}
a_k \star a_j &= \alpha a_k + \alpha^2 a_j \\
&\left(\alpha + \alpha^2 = 1, \text{ where } \alpha = \frac{-1 \pm \sqrt{5}}{2}\right).
\end{aligned} \tag{14}$$

Obviously, $a_j \star a_j = \alpha a_j + \alpha^2 a_j = (\alpha + \alpha^2) a_j = a_j$.

Theorem 2. *The algebra $\mathscr{M}_4(\mathfrak{t}_{\mathfrak{F}})$ is a generalized Jordan algebra.*

Proof. Clearly, $\mathscr{M}_4(\mathfrak{t}_{\mathfrak{F}})$ is a left almost algebra. Next, we will prove that it satisfies the property of flexible algebra. We have $a_j \star a_j = \alpha a_j + \alpha^2 a_j = (\alpha + \alpha^2) a_j = a_j$. Therefore,

$$\begin{aligned}
X \star X &= \sum_{j=1}^{n} \beta_j a_j \star \sum_{j=1}^{n} \beta_j a_j = \sum_{j=1}^{n} \sum_{j=1}^{n} \beta_j \beta_j \left(a_j \star a_j\right) \\
&= \sum_{j=1}^{n} \sum_{j=1}^{n} \beta_j \beta_j a_j = \sum_{j=1}^{n} \beta_j \sum_{j=1}^{n} \beta_j a_j = \sum_{j=1}^{n} \beta_j a_j.
\end{aligned} \tag{15}$$

Thus,

$$\begin{aligned}
(X \star Y) \star (X \star X) &= [(X \star X) \star Y] \star X \\
&= [(Y \star X) \star X] \star X \\
&= (X \star X) \star (Y \star X) \\
&= X \star (Y \star X) \\
&= X \star [Y \star (X \star X)].
\end{aligned} \tag{16}$$

□

Corollary 3. *The algebra $\mathscr{M}_4(\mathfrak{t}_{\mathfrak{F}})$ is a flexible algebra.*

It is obvious from Theorem 2 that $\mathscr{M}_4(\mathfrak{t}_{\mathfrak{F}})$ contains idempotent elements and we know that idempotent elements in nonassociative algebras have their own importance. Thus, we arrived at the following remark.

Remark 4. From the biological point of view, the idempotents in the algebra $\mathscr{M}_4(\mathfrak{t}_{\mathfrak{F}})$ have their own usefulness. Since this algebra has several characteristics similar to a nonassociative algebra arising in genetics, the idempotent elements of this algebra may be used for equilibria of a population described by some nonassociative algebras with genetic realizations.

In the following, we will consider some other nonassociative algebras and will discuss their relations with the left almost algebra mathematically.

An alternative algebra $\mathfrak{A}$ is a nonassociative algebra satisfying the following properties:

$$\begin{aligned}
&x(xy) = (xx)\, y, \\
&(yx)\, x = y\,(xx), \\
&\qquad \forall x, y \text{ in } \mathfrak{A}.
\end{aligned} \tag{17}$$

Lemma 5. *If $\mathfrak{A}$ is a left almost alternative algebra, then $x(xy) = (xx)y = (yx)x = y(xx)$ and $x^2 y = yx^2$, for all x and y in $\mathfrak{A}$.*

Proof. Let x and y belong to $\mathfrak{A}$; then, $x(xy) = (xx)y = (yx)x = y(xx)$, so $x^2 y = yx^2$, for all x and y. □

It is proved above that $x^2 y = yx^2$ for all x and y in $\mathfrak{A}$. Thus, $x^2 x = xx^2$ for x in $\mathfrak{A}$. Therefore, we can define powers of an element in $\mathfrak{A}$.

Lemma 6. *If $\mathfrak{A}$ is a left almost alternative algebra that contains a left identity $\mathfrak{e}$, then $\mathfrak{A}$ becomes commutative and associative with identity.*

Proof. Since $x^2y = yx^2$, for all x and y, therefore $x = \mathfrak{e}x = \mathfrak{e}^2x = x\mathfrak{e}^2 = x\mathfrak{e}$. Then,

$$xy = (xy)\,\mathfrak{e} = (\mathfrak{e}y)\,x = yx. \tag{18}$$

It is easy to see that commutativity and the left invertive law give associativity. □

For the rest of the paper, by $\mathfrak{A}$, we shall mean the left almost alternative algebra satisfying (2).

Lemma 7. *$yx^n = x^n y$, for all x, y in $\mathfrak{A}$ and for $n \geq 2$.*

Proof. We already proved that $x^2y = yx^2$, for all x, y in $\mathfrak{A}$. Then,

$$\begin{aligned}\left(x^2y\right)x &= \left(yx^2\right)x = \left(x^2y\right)x = (xy)\,x^2 = x^2\,(yx)\\ &= y\left(x^2x\right) = yx^3,\\ \left(yx^2\right)x &= \left(xx^2\right)y = x^3y.\end{aligned} \tag{19}$$

Thus, $yx^3 = x^3y$. Let us assume that let $yx^k = x^ky$, for $k \geq 3$. Then,

$$\begin{aligned}\left(x^ky\right)x &= (xy)\,x^k = x^k\,(yx) = y\left(x^kx\right) = yx^{k+1},\\ \left(yx^k\right)x &= \left(xx^k\right)y = x^{k+1}y.\end{aligned} \tag{20}$$

□

Theorem 8. *Every $\mathfrak{A}$ becomes a generalized Jordan algebra.*

Proof. Let $x, y \in \mathfrak{A}$. Then,

$$(xy)\,x^2 = x^2\,(yx) = y\left(x^2x\right) = y\left(xx^2\right) = x\left(yx^2\right). \tag{21}$$

Hence, $(xy)x^2 = x(yx^2)$. □

Lemma 9. *$(x^2y)x = x^2(yx)$, for all x, y in $\mathfrak{A}$.*

Proof. Using $x^2y = yx^2$, we get

$$\left(x^2y\right)x = (xy)\,x^2 = x^2\,(xy) = (yx)\,x^2 = x^2\,(yx). \tag{22}$$

□

We get a more generalized form of generalized Jordan algebra which is available in the following crucial theorem.

Theorem 10. *$(x^2y)z = x^2(yz)$, $x^2(yz) = x^2(zy)$, for all x, y, z in $\mathfrak{A}$.*

Proof. Using $x^2y = yx^2$, we get

$$\left(x^2y\right)z = (zy)\,x^2 = x^2\,(zy) = (yz)\,x^2 = x^2\,(yz). \tag{23}$$

□

This theorem represents a mathematical model showing that mating of x^2 with yz is the same as mating of x^2 with zy.

Proposition 11. *$(ab)(cd) = (db)(ca) = (dc)(ba)$, for all a, b, c, d in $\mathfrak{A}$.*

Proof. The proof is easy. □

For any a in S, we put $a^1 = a$ and $a^{n+1} = a^na$, where n is a positive integer.

Proposition 12. *$\mathfrak{A}$ has associative powers.*

Proof. The proof is easy. □

Proposition 13. *$a^ma^n = a^{m+n}$, for all $a \in \mathfrak{A}$ and positive integers m, n.*

Proof. According to Proposition 12, the result is true for $m \geqslant 1$. Again, by Lemma 7, we obtain

$$\begin{aligned}a^{m+1}a^n &= \left(a^ma\right)a^n = \left(aa^m\right)a^n = \left(a^ma^n\right)a = a^{m+n}a\\ &= a^{m+n+1}.\end{aligned} \tag{24}$$

Hence, $a^ma^n = a^{m+n}$ $\forall a \in \mathfrak{A}$. □

Proposition 14. *$(a^m)^n = a^{mn}$ for all $a \in A$ and positive integers m, n.*

Proof. The result is true for $n = 1$. Suppose it is true for $n > 1$. Then, we obtain

$$\left(a^m\right)^{n+1} = \left(a^m\right)^n a^m = a^{mn}a^m = a^{mn+m} = a^{m(n+1)}. \tag{25}$$

Hence, by induction on n, $(a^m)^n = a^{mn}$ for all a in S and positive integers m, n. □

Proposition 15. *$(ab)^n = a^nb^n$, for all a, b in $\mathfrak{A}$ and for positive integer $n \geq 1$.*

Proof. The result is true for $n = 1$. If $n = 2$, then

$$(ab)^2 = (ab)\,(ab) = (aa)\,(bb) = a^2b^2. \tag{26}$$

Suppose that the result is true for $n = k$. Then, we get

$$\begin{aligned}(ab)^{k+1} &= (ab)^k\,(ab) = \left(a^kb^k\right)(ab) = \left(a^ka\right)\left(b^kb\right)\\ &= a^{k+1}b^{k+1}.\end{aligned} \tag{27}$$

Hence, the result is true for all positive integers. □

Theorem 16. *$x^ny^m = y^mx^n$, for $n \geq 1$, $m \geq 2$, for all x, y in $\mathfrak{A}$.*

Proof. The proof follows from Lemma 7. □

Theorem 17. *$(x^nx^m)y = y(x^mx^n)$, for $m \geq 2$, $n \geq 1$.*

Proof. Let $x, y \in \mathfrak{A}$. Then,

$$\begin{aligned}(x^n x^m)\, y &= (x^m x^n)\, y = (x^n y)\, x^m = x^m\, (y x^n) \\ &= y\, (x^m x^n)\,.\end{aligned} \tag{28}$$

□

Theorem 18. *Every* $\mathfrak{A}$ *satisfies the generalized Jordan identity* $(x^m y)x^n = x^m(yx^n)$ *for* $m \geq 1,\ n \geq 2$.

Proof. We will use induction. For $m = 1$ and $n = 2$, it is the same as in Theorem 17.

$$\begin{aligned}(x^m y)\, x^n &= (y x^m)\, x^n = (x^n x^m)\, y = y\, (x^m x^n) \\ &= x^m\, (y x^n)\,.\end{aligned} \tag{29}$$

□

It is obvious from the above that the left almost algebra has closed connections with generalized Jordan algebra and flexible algebra.

It is interesting to note that genetic algebras (gametic, zygotic, copular, train, Bernstein, etc.) do not satisfy the properties of Jordan algebra but the left almost algebra becomes a Jordan algebra. Moreover, this algebra is power associative and satisfies the generalized identity $(x^m y)x^n = x^m(yx^n)$ introduced by Jordan. It also satisfies $x^n y^m = y^m x^n$ for $m, n \geq 2$. This algebra is the generalization of the Jordan algebra. It is noncommutative and nonassociative but possesses many characteristics similar to Jordan algebra. Since Jordan algebra has many applications in genetics, it is concluded that our new generalized algebra will give direction for applications in genetics.

3. Conclusion

In this paper, we introduced a new nonassociative and noncommutative algebra with genetic realizations. We discussed its link with flexible, alternative, and Jordan algebras. This algebra possesses many characteristics similar to a commutative and associative algebra. We discussed some of the genetic properties of this algebra. In our future work, we will focus on some other nonassociative algebras. We conclude that this research will give a new direction for applications in genetics.

Conflicts of Interest

The authors declare that there are no conflicts of interest regarding the publication of this paper.

References

[1] I. M. H. Etherington, "Genetic algebras," *Proceedings of the Royal Society of Edinburgh*, vol. 59, pp. 242–258, 1939.

[2] I. M. H. Etherington, "Non-commutative train algebras of ranks 2 and 3," Mathematical Institute, University of Edinburgh, 241-252.

[3] I. M. Etherington, "Duplication of linear algebras," *Proceedings of the Edinburgh Mathematical Society. Series II*, vol. 6, pp. 222–230, 1941.

[4] P. Holgate, "Groupoids satisfying a simple invertive law," *The Mathematics Student*, vol. 61, no. 1-4, pp. 101–106, 1992.

[5] P. Holgate, "Sequences of powers in genetic algebras," *Journal of the London Mathematical Society*, vol. 42, pp. 489–496, 1967.

[6] P. Holgate, "Genetic algebras associated with sex linkage," *Proceedings of the Edinburgh Mathematical Society*, vol. 17, pp. 113–120, 1970.

[7] P. Holgate, "Jordan algebras arising in population genetics," *Proceedings of the Edinburgh Mathematical Society. Series II*, vol. 15, pp. 291–294, 1967.

[8] M. L. Reed, "Algebraic structure of genetic inheritance," *American Mathematical Society. Bulletin. New Series*, vol. 34, no. 2, pp. 107–130, 1997.

[9] H. Gonshor, "Special train algebras arising in genetics," *Proceedings of the Edinburgh Mathematical Society*, vol. 12, no. 1, pp. 41–53, 1960.

[10] A. Wörz-Busekros, *Algebras in Genetics*, vol. 36 of *Lecture Notes in Biomathematics*, Springer, New York, NY, USA, 1980.

[11] T. Cortes, "Modular Bernstein algebras," *Journal of Algebra*, vol. 163, no. 1, pp. 191–206, 1994.

[12] D. L. Hartl, *Essential Genetics: A Genomics Perspecive*, John and Bartlett Publishers, Inc., Barnstable, Mass, USA, 2002.

[13] R. D. Schafer, "Structure of genetic algebras," *American Journal of Mathematics*, vol. 71, pp. 121–135, 1949.

[14] D. Towers, "Nonassociative algebraic structures arising in genetics," *The Mathematical Gazette*, vol. 70, no. 454, pp. 281–286, 1986.

Hindawi
Computational and Mathematical Methods in Medicine
Volume 2017, Article ID 4820183, 10 pages
https://doi.org/10.1155/2017/4820183

Research Article

Threshold Dynamics of a Stochastic *SIR* Model with Vertical Transmission and Vaccination

Anqi Miao,[1] Jian Zhang,[1] Tongqian Zhang,[1,2] and B. G. Sampath Aruna Pradeep[3]

[1]*College of Mathematics and Systems Science, Shandong University of Science and Technology, Qingdao 266590, China*
[2]*State Key Laboratory of Mining Disaster Prevention and Control Co-Founded by Shandong Province and the Ministry of Science and Technology, Shandong University of Science and Technology, Qingdao 266590, China*
[3]*Department of Mathematics, University of Ruhuna, 81000 Matara, Sri Lanka*

Correspondence should be addressed to Tongqian Zhang; zhangtongqian@sdust.edu.cn

Received 25 March 2017; Accepted 4 June 2017; Published 6 July 2017

Academic Editor: Gul Zaman

A stochastic *SIR* model with vertical transmission and vaccination is proposed and investigated in this paper. The threshold dynamics are explored when the noise is small. The conditions for the extinction or persistence of infectious diseases are deduced. Our results show that large noise can lead to the extinction of infectious diseases which is conducive to epidemic diseases control.

1. Introduction

The history of mankind is filled with struggle with diseases. Infectious diseases such as smallpox, cholera, plague of leprosy, diphtheria, syphilis, typhus fever, malaria, rabies, and tuberculosis have threatened the health of human beings. People have realized the importance of quantitative studies on the spread of infectious diseases to predict and to control them. It can be known from referring to the literature [1–4] that, with the aid of the establishment of infectious disease models, people can understand the crucial laws of infectious diseases and provide reliable and enough information to predict and control infectious diseases. For example, as early as 1760, Bernoulli and Blower [5] proposed the first mathematical model in epidemiology for studying the spread and inoculation of smallpox. Further, in 1927, Kermack and McKendrick [6] proposed the concept of the so-called "compartmental model," in which all the population was classified into three compartments: susceptible compartment S, infected compartment I, and removed compartment R. It is assumed in the model that the susceptible class can transform into the infective class through contact with infected individuals, and the infectives can recover through treatment so that they have permanent immunity. Therefore, it is now well known that many scholars have paid attention to *SIR* models; as a result, it can be seen in the literature that a large number of mathematical models of ordinary differential equations, delay differential equations, and partial differential equations have been constructed to study the spread of infectious diseases (see, e.g., [7–23]). In the last decades, we observed that scholars published few papers in scientific journals related to mathematics considering infectious diseases with vertical transmission which are transmitted from parents to their offspring (e.g., [1, 24–26]). Although scholars neglect the effect of vertical transmission, it is very important to study the real situation of the transmission of infectious diseases. The current diseases affecting humanity such as AIDS [27–31], Chagas' disease [32–34], hepatitis B [35, 36], and hepatitis C [37] are vertically transmitted. From this, it can be clearly seen that mathematical modeling including vertical transmission, horizontal transmission, and vaccination [38, 39] is more realistic than without them. Therefore, in this study, we have focused our attention on this and an *SIR* epidemic model involving vertical transmission and vaccination was proposed as follows [1, 24] (see Figure 1):

$$\begin{aligned}
\dot{S}(t) &= -\beta S(t) I(t) + (1-m) b (S(t) + R(t)) \\
&\quad + pb' I(t) - bS(t), \\
\dot{I}(t) &= \beta S(t) I(t) + qb' I(t) - b' I(t) - \gamma I(t), \\
\dot{R}(t) &= \gamma I(t) - bR(t) + mb (S(t) + R(t)),
\end{aligned} \tag{1}$$

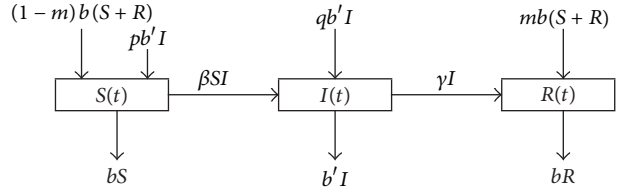

Figure 1: The compartmental diagram for the *SIR* model with vertical transmission and vaccination.

where $S(t)$, $I(t)$, and $R(t)$ represent the members of the susceptible, the infectious, and the removed or the recovered members from infection, respectively. b is the birth and death rate of $S(t)$ and $R(t)$, b' is the birth and death rate of $I(t)$, β is the contact rate, and m $(0 < m < 1)$ is the vaccination proportion to the newborn from $S(t)$ and $R(t)$. Then, constant p $(0 < p < 1)$ is the proportion of the offspring of infective parents that are susceptible individuals and $p + q = 1$. γ is the recovery rate of the infective individuals. Obviously, the total population size is normalized to one, and the basic reproductive number of system (1) is $R_0 = \beta(1-m)/(pb' + \gamma)$. By constructing a Lyapunov function and using the LaSalle invariance principle, we can show that if $R_0 < 1$, the infection-free equilibrium $P_0(1 - m, 0, m)$ is globally asymptotically stable, while if $R_0 > 1$, the infection-free equilibrium P_0 is unstable and the endemic equilibrium $P^*(S^*, I^*, R^*)$ is globally asymptotically stable.

In fact, the spread of diseases is inevitably disturbed by the influence of random factors; the stochastic epidemic system is more in line with the actual situation. Therefore, epidemic systems described by stochastic differential equations have been paid extensive attention in recent years (see, e.g., [40–46]). Various stochastic perturbation approaches have been introduced into epidemic systems and excellent results have been obtained. In this study, our main objective is to introduce four approaches. The first one is to analyze epidemic systems including the environment noise by using the method of time Markov chain (see, e.g., [47–51]). The second one is to consider the parameters' perturbation (see, e.g., [52–72]). The third one is to introduce Lévy jump noise into the system [73–75]. The fourth one is to investigate stochastic perturbation around the positive equilibria of deterministic systems (see, e.g., [41, 42, 76–78]).

Parameter perturbation induced by white noises is an important and common form to describe the effect of stochasticity. In this paper, we adopt the perturbation with white noises, that is, $\beta \to \beta + \sigma\dot{B}(t)$, where $B(t)$ is a standard Brownian motion with intensity $\sigma^2 > 0$. Then, the resultant system transforms into the following form:

$$\begin{aligned} dS(t) &= \left(-\beta S(t) I(t) + (1-m) b (S(t) + R(t)) \right. \\ &\quad \left. + pb' I(t) - bS(t)\right) dt - \sigma S(t) I(t) dB(t), \\ dI(t) &= \left(\beta S(t) I(t) + qb' I(t) - b' I(t) - \gamma I(t)\right) dt \\ &\quad + \sigma S(t) I(t) dB(t), \\ dR(t) &= \left(\gamma I(t) - bR(t) + mb (S(t) + R(t))\right) dt. \end{aligned} \tag{2}$$

This paper is organized as follows. In Section 3, we will discuss the extinction of infectious diseases and explore the conditions leading to the extinction of infectious diseases. In Section 4, we will deduce the condition for a disease in order to be persistent.

2. Preliminaries

Throughout this paper, we let $\mathbb{R}^d$: be the d-dimensional Euclidean space. $\mathbb{R}^d_+ := \{x \in \mathbb{R}^d : x_i > 0,\ 1 \le i \le d\}$, that is, the positive cone.

Let $\{B_t\}_{t\ge 0}$ be a one-dimensional Brownian motion defined on the complete probability space $(\Omega, \mathcal{F}, \mathcal{P})$ adapted to the filtration $\{\mathcal{F}\}_{t\ge 0}$. Let $\mathcal{L}^1(\mathbb{R}_+; \mathbb{R}^d)$ denote the family of all $\mathbb{R}^d$-valued measurable $\{\mathcal{F}_t\}$-adapted processes $f = \{f(t)\}_{t\ge 0}$ such that

$$\int_0^T \left|f(t)\right| dt < \infty \quad \text{a.s. for every } T > 0. \tag{3}$$

Let $C^{2,1}(\mathbb{R}^d \times \mathbb{R}_+; \mathbb{R})$ denote the family of all real-valued functions $V(x,t)$ defined on $\mathbb{R}^d \times \mathbb{R}_+$ such that they are continuously twice differentiable in x and once in t. We set

$$\begin{aligned} V_t &= \frac{\partial V}{\partial t}, \\ V_x &= \left(\frac{\partial V}{\partial x_1}, \frac{\partial V}{\partial x_2}, \ldots, \frac{\partial V}{\partial x_d}\right), \\ V_{xx} &= \left(\frac{\partial^2 V}{\partial x_i \partial x_j}\right)_{d\times d} = \begin{pmatrix} \frac{\partial^2 V}{\partial x_1 \partial x_1} & \cdots & \frac{\partial^2 V}{\partial x_1 \partial x_d} \\ \vdots & & \vdots \\ \frac{\partial^2 V}{\partial x_d \partial x_1} & \cdots & \frac{\partial^2 V}{\partial x_d \partial x_d} \end{pmatrix}. \end{aligned} \tag{4}$$

Clearly, when $V \in C^{2,1}(R \times R_+; R)$, we have $V_x = \partial V/\partial x$, $V_{xx} = \partial^2 V/\partial x^2$. Then, we have the following.

Lemma 1 (one-dimensional Itô's formula [40, 79, 80]). *Let $x(t)$ be an Itô process on $t \ge 0$ with the stochastic differential*

$$dx(t) = f(t)\, dt + g(t)\, dB_t, \tag{5}$$

where $f \in \mathcal{L}^1(\mathbb{R}_+; \mathbb{R})$ and $g \in \mathcal{L}^2(\mathbb{R}_+; \mathbb{R})$. Let $V \in C^{2,1}(\mathbb{R}^d \times \mathbb{R}_+; \mathbb{R})$. Then, $V(x(t), t)$ is again an Itô process with the stochastic differential given by

$$\begin{aligned} dV(x(t), t) &= \left[V_t(x(t), t) + V_x(x(t), t) f(t) \right. \\ &\quad \left. + \frac{1}{2} V_{xx}(x(t), t) g^2(t)\right] dt + V_x(x(t), t) \\ &\quad \cdot g(t)\, dB_t, \end{aligned} \tag{6}$$

almost surely.

By using the methods from Lahrouz and Omari [81], we can prove the following lemma.

Lemma 2. *For any initial value* $(S(0), I(0), R(0)) \in R_+^3$*, there exists a unique solution* $(S(t), I(t), R(t))$ *to system (2) on* $t \geq 0$*, and the solution will remain in* R_+^3 *with probability one, namely.*

Lemma 3. *On the basis of Lemma 2, if* $S(0) + I(0) + R(0) \leq 1$*, then* $S(t) + I(t) + R(t) \leq 1$*, almost surely. Thus, the region* $\Gamma = \{(S, I, R) \in R_+^3 : S > 0, I \geq 0, R > 0, S + I + R \leq 1\}$ *is a positively invariant set of system (2).*

3. Extinction

In this section, we deduce the condition which will cause a disease to die out.

Definition 4. For system (2), the infected individual $I(t)$ is said to be extinctive if $\lim_{t\to+\infty} I(t) = 0$, almost surely.

Let us introduce

$$R^* = \frac{R_0}{1-m} - \frac{\sigma^2}{2\left(pb' + \gamma\right)} \tag{7}$$

for convenience; then, we have the following results that we have mentioned in the following theorem.

Theorem 5. *If* $\sigma^2 > \max\{\beta, \beta^2/2(pb'+\gamma)\}$ *or* $\sigma^2 < \beta$ *and* $R^* < 1$*, then the infected individual of system (2) goes to extinction almost surely.*

Proof. Let $(S(t), I(t), R(t))$ be a solution of system (2) with initial value $(S(0), I(0), R(0)) \in R_+^3$. Applying Itô's formula to the second equation of system (2) leads to

$$\begin{aligned} \mathrm{d}\ln I(t) = &\left(\beta S(t) - \left(pb' + \gamma\right) - \frac{\sigma^2}{2} S^2(t)\right)\mathrm{d}t \\ &+ \sigma S(t)\,\mathrm{d}B(t). \end{aligned} \tag{8}$$

Integrating both sides of (8) from 0 to t gives

$$\begin{aligned} \ln I(t) = &\int_0^t \left(\beta S(\tau) - \frac{\sigma^2}{2} S^2(\tau)\right)\mathrm{d}\tau - \left(pb' + \gamma\right)t \\ &+ M(t) + \ln I(0), \end{aligned} \tag{9}$$

where $M(t) = \int_0^t \sigma S(\tau)\mathrm{d}B(\tau)$ and $M(t)$ is the local continuous martingale with $M(0) = 0$. Next, we have two cases to be discussed, depending on whether $\sigma^2 > \beta$.

If $\sigma^2 > \beta$, we can easily see from (9) that

$$\ln I(t) \leq \left(\frac{\beta^2}{2\sigma^2} - \left(pb' + \gamma\right)\right)t + M(t) + \ln I(0). \tag{10}$$

Dividing both sides of (10) by $t > 0$, we have

$$\frac{\ln I(t)}{t} \leq -\left(pb' + \gamma - \frac{\beta^2}{2\sigma^2}\right) + \frac{M(t)}{t} + \frac{\ln I(0)}{t}. \tag{11}$$

Since $\limsup_{t\to\infty}(\langle M(t), M(t)\rangle_t / t) < \sigma^2 < \infty$ almost surely, by the large number theorem for martingales (see, e.g., [53]), one can obtain that

$$\lim_{t\to+\infty} \frac{M(t)}{t} = 0. \tag{12}$$

Then, taking the limit superior on both sides of (11) leads to

$$\limsup_{t\to+\infty} \frac{\ln I(t)}{t} \leq -\left(pb' + \gamma - \frac{\beta^2}{2\sigma^2}\right) < 0, \tag{13}$$

when $\sigma^2 > \beta^2/2(pb' + \gamma)$, which implies $\lim_{t\to+\infty} I(t) = 0$.

If $\sigma^2 < \beta$, similarly, one can have that

$$\ln I(t) \leq \left(\beta - \left(pb' + \gamma\right) - \frac{\sigma^2}{2}\right)t + M(t) + \ln I(0). \tag{14}$$

Dividing both sides of (14) by $t > 0$, we have

$$\begin{aligned} \frac{\ln I(t)}{t} \leq &\left(pb' + \gamma\right)\left[\frac{\beta}{pb' + \gamma} - \frac{\sigma^2}{2\left(pb' + \gamma\right)} - 1\right] \\ &+ \frac{M(t)}{t} + \frac{\ln I(0)}{t}. \end{aligned} \tag{15}$$

By taking the superior limit on both sides of (15), one can have that

$$\limsup_{t\to+\infty} \frac{\ln I(t)}{t} \leq \left(pb' + \gamma\right)\left(R^* - 1\right). \tag{16}$$

Then, when $R^* < 1$, we obtain

$$\limsup_{t\to+\infty} \frac{\ln I(t)}{t} < 0, \tag{17}$$

which implies $\lim_{t\to+\infty} I(t) = 0$. This completes the proof of Theorem 5. □

Remark 6. Theorem 5 shows that when $\sigma^2 > \max\{\beta, \beta^2/2(pb' + \gamma)\}$, the infectious disease of system (2) goes to extinction almost surely; namely, large white noise stochastic disturbance is conducive to control infectious diseases. When the white noise is not large and $R^* < 1$, the infectious disease of system (2) also goes to extinction almost surely; then, R^* is the threshold associated with the extinction of infectious diseases.

4. Persistence in Mean

Definition 7. For system (2), the infected individual $I(t)$ is said to be permanent in mean if $\liminf_{t\to+\infty}\langle I(t)\rangle > 0$, almost surely, where $\langle I(t)\rangle$ is defined as $(1/t)\int_0^t I(\tau)\mathrm{d}\tau$.

Let us denote

$$\mathscr{R}^{**} = R_0 - \frac{\sigma^2}{2\left(pb' + \gamma\right)} \tag{18}$$

for convenience; then, we have the following results that we have mentioned in the following theorem.

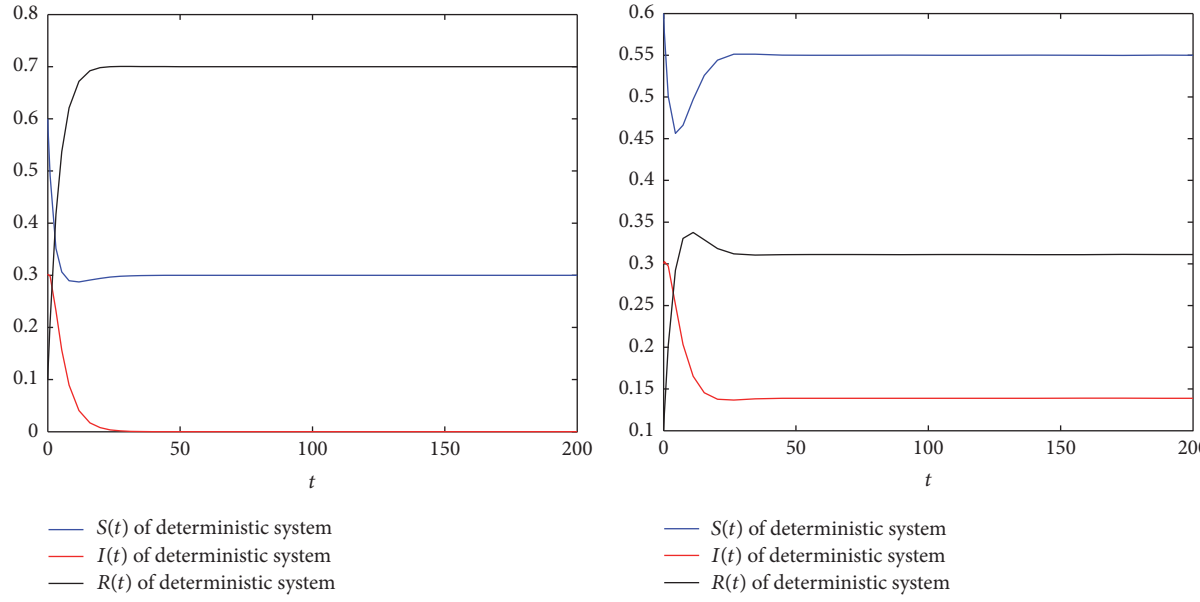

(a) Time series for $S(t), I(t), R(t)$ where $m = 0.7$ and $R_0 = 0.5455$

(b) Time series for $S(t), I(t), R(t)$ where $m = 0.2$ and $R_0 = 1.4545$

FIGURE 2: Illustration for the deterministic *SIR* system where $\beta = 0.8$, $p = 0.6$, $b = 0.2$, $b' = 0.4$, and $\gamma = 0.2$.

Theorem 8. *If $\mathscr{R}^{**} > 1$, then the infected individual $I(t)$ is persistent in mean; moreover, $I(t)$ satisfies*

$$\liminf_{t\to+\infty} \langle I(t)\rangle \geq \frac{\left(pb' + \gamma\right)}{\beta\left(1 - m + \gamma/b\right)}\left(R^{**} - 1\right), \tag{19}$$

almost surely.

Proof. Integrating from 0 to t and dividing by t $(t > 0)$ on both sides of the third equation of system (2) yield

$$\begin{aligned}\frac{R(t) - R(0)}{t} &= \gamma\langle I(t)\rangle + mb\langle S(t)\rangle \\ &\quad - (1-m)\, b\langle R(t)\rangle \triangleq \Theta(t).\end{aligned} \tag{20}$$

Note that $\langle S(t)\rangle + \langle I(t)\rangle + \langle R(t)\rangle = 1$; then, one can get

$$\langle S(t)\rangle = (1-m) + \frac{\Theta(t)}{b} - \left(1 - m + \frac{\gamma}{b}\right)\langle I(t)\rangle. \tag{21}$$

Applying Itô's formula gives

$$\begin{aligned}\mathrm{d}(\ln I(t)) &= \left[\beta S(t) - \left(pb' + \gamma\right) - \frac{\sigma^2}{2}S^2(t)\right]\mathrm{d}t \\ &\quad + \sigma S(t)\,\mathrm{d}B(t) \\ &\geq \left[\beta S(t) - \left(pb' + \gamma\right) - \frac{\sigma^2}{2}\right]\mathrm{d}t \\ &\quad + \sigma S(t)\,\mathrm{d}B(t).\end{aligned} \tag{22}$$

Integrating from 0 to t and dividing by t $(t > 0)$ on both sides of (22) yield

$$\begin{aligned}&\frac{\ln I(t) - \ln I(0)}{t} \\ &\geq \beta\langle S(t)\rangle - \left[\left(pb' + \gamma\right) + \frac{\sigma^2}{2}\right] + \frac{M(t)}{t} \\ &= \beta\left(1 - m + \frac{\Theta(t)}{b} - \left(1 - m + \frac{\gamma}{b}\right)\langle I(t)\rangle\right) \\ &\quad - \left(pb' + \gamma + \frac{\sigma^2}{2}\right) + \frac{M(t)}{t}.\end{aligned} \tag{23}$$

From (23), we obtain

$$\begin{aligned}\langle I(t)\rangle &\geq \frac{1}{\beta\left(1 - m + \gamma/b\right)}\left[\beta(1-m) - \left(pb' + \gamma\right)\right. \\ &\quad \left. - \frac{\sigma^2}{2}\right] + \frac{1}{\beta\left(1 - m + \gamma/b\right)}\left[\frac{\beta\Theta(t)}{b}\right. \\ &\quad \left. - \frac{\ln I(t) - \ln I(0)}{t} + \frac{M(t)}{t}\right].\end{aligned} \tag{24}$$

Since both $I(t) \leq 1$ and $R(t) \leq 1$, then one has $\lim_{t\to+\infty}(R(t)/t) = 0$, $\lim_{t\to+\infty}(\ln I(t)/t) = 0$, and $\lim_{t\to+\infty}\Theta(t) = 0$. Note

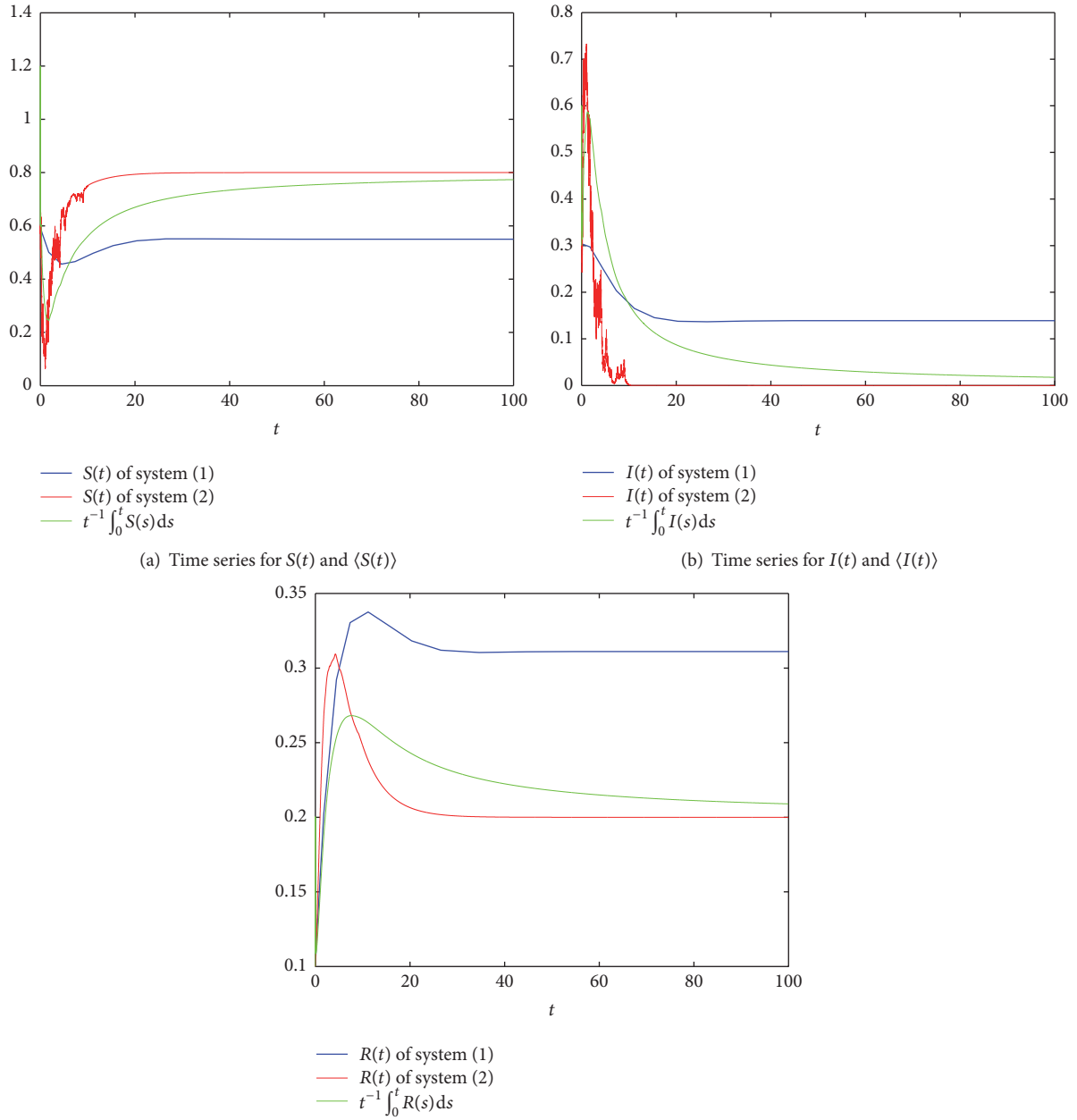

(a) Time series for $S(t)$ and $\langle S(t)\rangle$

(b) Time series for $I(t)$ and $\langle I(t)\rangle$

(c) Time series for $R(t)$ and $\langle R(t)\rangle$

FIGURE 3: Comparison of the deterministic system and stochastic system, where $m = 0.2$, $\beta = 0.8$, $p = 0.6$, $b = 0.2$, $b' = 0.4$, $\gamma = 0.2$, $\sigma = 0.9$, and $R_0 = 1.4545 > 1$.

that $\lim_{t\to+\infty}(M(t)/t) = 0$; by taking the inferior limit of both sides of (24), we have

$$\begin{aligned}
&\liminf_{t\to+\infty} \langle I(t)\rangle \\
&\geq \frac{1}{\beta(1-m+\gamma/b)}\left[\beta(1-m) - pb' - \gamma - \frac{\sigma^2}{2}\right] \qquad (25)\\
&= \frac{(pb'+\gamma)}{\beta(1-m+\gamma/b)}\left(R^{**}-1\right).
\end{aligned}$$

This completes the proof of Theorem 8. □

Remark 9. Theorems 5 and 8 show that the condition for the disease to die out or persist depends on the intensity of white noise disturbances strongly. And small white noise disturbances will be beneficial for long-term prevalence of the disease; conversely, large white noise disturbances may cause the epidemic disease to die out.

5. Conclusion and Numerical Simulation

In this paper, a stochastic *SIR* system with vertical transmission and vaccination is proposed. The threshold dynamics

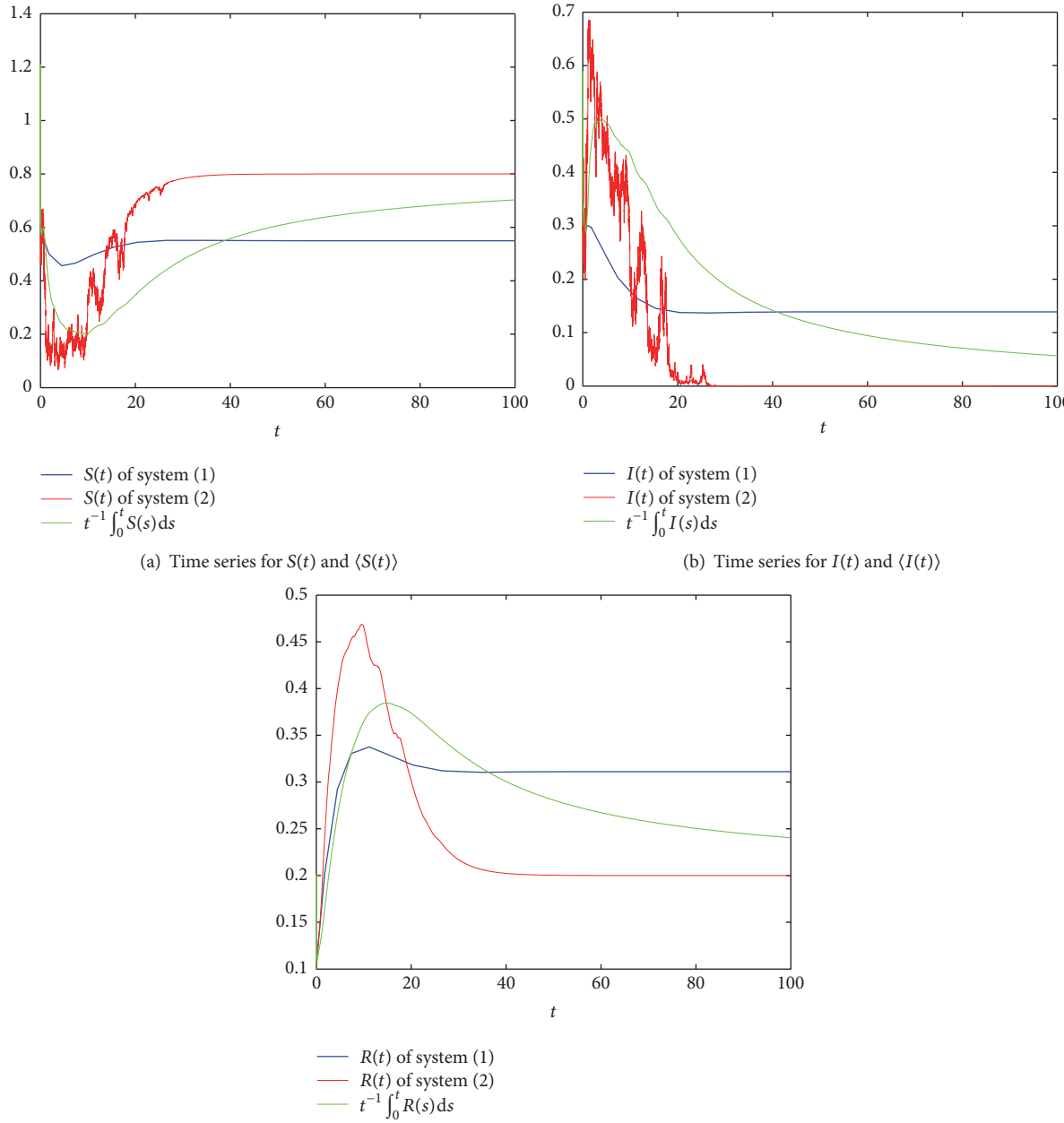

(a) Time series for $S(t)$ and $\langle S(t)\rangle$

(b) Time series for $I(t)$ and $\langle I(t)\rangle$

(c) Time series for $R(t)$ and $\langle R(t)\rangle$

FIGURE 4: Comparison of the deterministic system and stochastic system, where $m = 0.2$, $\beta = 0.8$, $p = 0.6$, $b = 0.2$, $b' = 0.4$, $\gamma = 0.2$, $\sigma = 0.85$, $R^* = 0.9972$, and $R_0 = 1.4545 > 1$.

depending on the stochastic perturbation are deduced by using the theory of stochastic differential equation and inequality technique. Our results show that the dynamics of the stochastic system are different with the deterministic case due to the effect of stochastic perturbation, and the persistent diseases in the deterministic system may be eliminated under the stochastic perturbation.

In the following, by employing the Euler Maruyama (EM) method [40], we perform some numerical simulations to illustrate the extinction and persistence of the diseases in the stochastic system and corresponding deterministic system for comparison.

For numerical simulations, we set parameters as $m = 0.7$, $\beta = 0.8$, $p = 0.6$, $b = 0.2$, $b' = 0.4$, and $\gamma = 0.2$ in system (1). A simple computation shows that $R_0 = 0.5455 < 1$, and then system (1) has a stable infection-free equilibrium $P_0(0.3, 0, 0.7)$, which implies that the disease of system (1) will be eliminated ultimately (see Figure 2(a)). If we change $m = 0.7$ to $m = 0.2$, in this case, $R_0 = 1.4545 > 1$, and then system (1) has a stable infection equilibrium $P^*(0.55, 0.3111, 0.1389)$,

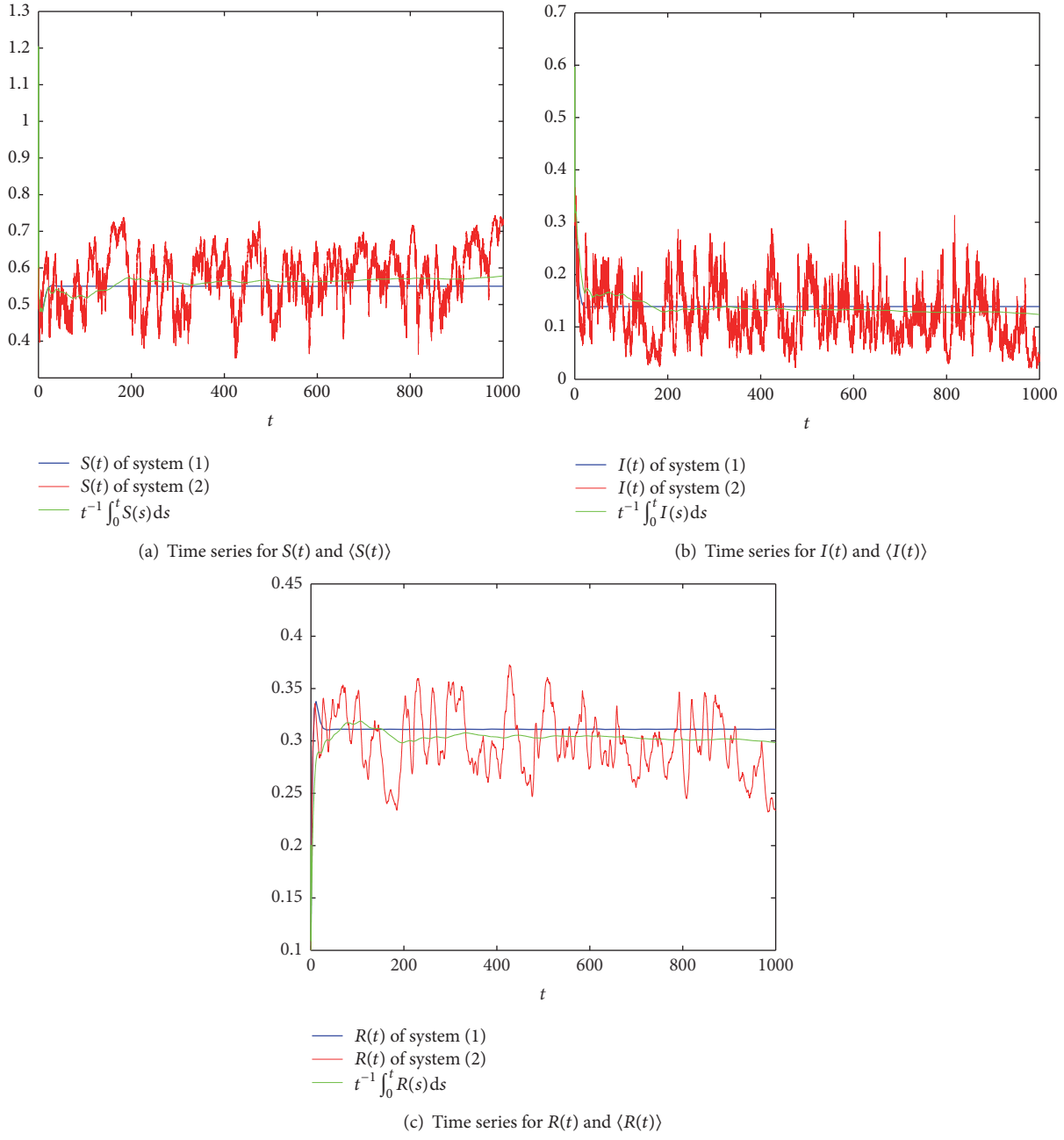

(a) Time series for $S(t)$ and $\langle S(t)\rangle$

(b) Time series for $I(t)$ and $\langle I(t)\rangle$

(c) Time series for $R(t)$ and $\langle R(t)\rangle$

FIGURE 5: Comparison of the deterministic system and stochastic system, where $m = 0.2$, $\beta = 0.8$, $p = 0.6$, $b = 0.2$, $b' = 0.4$, $\gamma = 0.2$, $\sigma = 0.2$, $R^{**} = 1.4091$, and $R_0 = 1.4545 > 1$.

which implies that the disease of system (1) will be persistent ultimately (see Figure 2(b)).

Next, we consider the effect of stochastic white noise based on the persistent system. Let $\sigma = 0.9$, and obviously, $\sigma^2 > \max\{\beta, \beta^2/2(pb' + \gamma)\}$; by Theorem 5, the disease dies out under a large white noise disturbance (see Figure 3). If we change σ to 0.85, in this case, $\sigma^2 < \beta^2/2(pb' + \gamma)$ and $R^* = 0.9972 =< 1$; then, by Theorem 5, the disease dies out (see Figure 4). If we reduce the intensity of noise σ to 0.2, obviously, $R^{**} = 1.4091 > 1$; by Theorem 8, the disease is persistent (see Figure 5).

Conflicts of Interest

The authors declare that there are no conflicts of interest regarding the publication of this paper.

Acknowledgments

This work is supported by Shandong Provincial Natural Science Foundation of China (no. ZR2015AQ001), the National Natural Science Foundation of China (no. 11371230), and Research Funds for Joint Innovative Center for Safe and Effective Mining Technology and Equipment

of Coal Resources by Shandong Province and SDUST (2014TDJH102).

References

[1] R. Anderson and R. May, *Infectious Diseases in Humans: Dynamics and Control*, Oxford University Press, Oxford, UK, 1992.

[2] C. V. De-León, "On the global stability of SIS, SIR and SIRS epidemic models with standard incidence," *Chaos, Solitons & Fractals*, vol. 44, no. 12, pp. 1106–1110, 2011.

[3] F. Brauer, *Epidemic Models in Populations of Varying Size*, Springer, Berlin, Germany, 1989.

[4] H. W. Hethcote, "The mathematics of infectious diseases," *SIAM Review*, vol. 42, no. 4, pp. 599–653, 2000.

[5] D. Bernoulli and S. Blower, "An attempt at a new analysis of the mortality caused by smallpox and of the advantages of inoculation to prevent it," *Reviews in Medical Virology*, vol. 14, no. 5, pp. 275–288, 2004.

[6] W. O. Kermack and A. G. McKendrick, "A contribution to the mathematical theory of epidemics," *Proceedings of the Royal Society of London A: Mathematical, Physical and Engineering Sciences*, vol. 115, no. 772, pp. 700–721, 1927.

[7] G. Huang and Y. Takeuchi, "Global analysis on delay epidemiological dynamic models with nonlinear incidence," *Journal of Mathematical Biology*, vol. 63, no. 1, pp. 125–139, 2011.

[8] G. Huang, Y. Takeuchi, W. Ma, and D. Wei, "Global stability for delay SIR and SEIR epidemic models with nonlinear incidence rate," *Bulletin of Mathematical Biology*, vol. 72, no. 5, pp. 1192–1207, 2010.

[9] Z. Hu, W. Ma, and S. Ruan, "Analysis of SIR epidemic models with nonlinear incidence rate and treatment," *Mathematical Biosciences*, vol. 238, no. 1, pp. 12–20, 2012.

[10] B. G. Pradeep and W. Ma, "Global stability of a delayed mosquito-transmitted disease model with stage structure," *Electronic Journal of Differential Equations*, vol. 10, pp. 1–19, 2015.

[11] Z. Jiang and W. Ma, "Permanence of a delayed SIR epidemic model with general nonlinear incidence rate," *Mathematical Methods in the Applied Sciences*, vol. 38, no. 3, pp. 505–516, 2015.

[12] T. Zhang, X. Meng, T. Zhang, and Y. Song, "Global dynamics for a new high-dimensional SIR model with distributed delay," *Applied Mathematics and Computation*, vol. 218, no. 24, pp. 11806–11819, 2012.

[13] W. Zhao, T. Zhang, Z. Chang, X. Meng, and Y. Liu, "Dynamical analysis of SIR epidemic models with distributed delay," *Journal of Applied Mathematics*, vol. 2013, Article ID 154387, 15 pages, 2013.

[14] K. I. Kim, Z. Lin, and L. Zhang, "Avian-human influenza epidemic model with diffusion," *Nonlinear Analysis: Real World Applications*, vol. 11, no. 1, pp. 313–322, 2010.

[15] G. Zaman, Y. Han Kang, and I. H. Jung, "Stability analysis and optimal vaccination of an SIR epidemic model," *BioSystems*, vol. 93, no. 3, pp. 240–249, 2008.

[16] L. Zhang, Z.-C. Wang, and X.-Q. Zhao, "Threshold dynamics of a time periodic reaction-diffusion epidemic model with latent period," *Journal of Differential Equations*, vol. 258, no. 9, pp. 3011–3036, 2015.

[17] W. Wang and X.-Q. Zhao, "An epidemic model with population dispersal and infection period," *SIAM Journal on Applied Mathematics*, vol. 66, no. 4, pp. 1454–1472, 2006.

[18] W. Wang, W. Ma, and X. Lai, "Repulsion effect on superinfecting virions by infected cells for virus infection dynamic model with absorption effect and chemotaxis," *Nonlinear Analysis: Real World Applications*, vol. 33, pp. 253–283, 2017.

[19] W. Wang, W. Ma, and X. Lai, "A diffusive virus infection dynamic model with nonlinear functional response, absorption effect and chemotaxis," *Communications in Nonlinear Science and Numerical Simulation*, vol. 42, pp. 585–606, 2017.

[20] G. Zaman, Y. H. Kang, and I. H. Jung, "Optimal treatment of an SIR epidemic model with time delay," *BioSystems*, vol. 98, no. 1, pp. 43–50, 2009.

[21] X. Meng, Y. Yang, and S. Zhao, "Adaptive evolution of virulence-related traits in a susceptible-infected model with treatment," *Abstract and Applied Analysis*, vol. 2014, Article ID 891401, 10 pages, 2014.

[22] W. Zhao, J. Li, and X. Meng, "Dynamical analysis of SIR epidemic model with nonlinear pulse vaccination and lifelong immunity," *Discrete Dynamics in Nature and Society*, vol. 2015, Article ID 848623, 10 pages, 2015.

[23] S. Guo and W. Ma, "Global behavior of delay differential equations model of HIV infection with apoptosis," *Discrete and Continuous Dynamical Systems. Series B*, vol. 21, no. 1, pp. 103–119, 2016.

[24] X. Meng and L. Chen, "The dynamics of a new SIR epidemic model concerning pulse vaccination strategy," *Applied Mathematics and Computation*, vol. 197, no. 2, pp. 582–597, 2008.

[25] Z. Lu, X. Chi, and L. Chen, "The effect of constant and pulse vaccination on SIR epidemic model with horizontal and vertical transmission," *Mathematical and Computer Modelling*, vol. 36, no. 9-10, pp. 1039–1057, 2002.

[26] Y. Chen, J. Evans, and M. Feldlaufer, "Horizontal and vertical transmission of viruses in the honey bee, Apis mellifera," *Journal of Invertebrate Pathology*, vol. 92, no. 3, pp. 152–159, 2006.

[27] S. Sprecher, G. Soumenkoff, F. Puissant, and M. Degueldre, "Vertical transmission of hiv in 15-week fetus," *The Lancet*, vol. 328, no. 8501, pp. 288-289, 1986.

[28] A. B. Van't Wout, N. A. Kootstra, G. A. Mulder-Kampinga et al., "Macrophage-tropic variants initiate human immunodeficiency virus type 1 infection after sexual, parenteral, and vertical transmission," *Journal of Clinical Investigation*, vol. 94, no. 5, pp. 2060–2067, 1994.

[29] T. Zhang, X. Meng, and T. Zhang, "Global dynamics of a virus dynamical model with cell-to-cell transmission and cure rate," *Computational and Mathematical Methods in Medicine*, vol. 2015, Article ID 758362, 8 pages, 2015.

[30] T. Zhang, X. Meng, and T. Zhang, "Global analysis for a delayed SIV model with direct and environmental transmissions," *The Journal of Applied Analysis and Computation*, vol. 6, no. 2, pp. 479–491, 2016.

[31] K. Hattaf, N. Yousfi, and A. Tridane, "Mathematical analysis of a virus dynamics model with general incidence rate and cure rate," *Nonlinear Analysis: Real World Applications*, vol. 13, no. 4, pp. 1866–1872, 2012.

[32] J. R. Coura and P. A. Vĩas, "Chagas disease: a new worldwide challenge," *Nature*, vol. 465, no. 7301, pp. S6–S7, 2010.

[33] J. A. Pérez-Molina, A. M. Perez, F. F. Norman, B. Monge-Maillo, and R. López-Vélez, "Old and new challenges in chagas disease," *The Lancet Infectious Diseases*, vol. 15, no. 11, pp. 1347–1356, 2015.

[34] A. L. Ribeiro, M. P. Nunes, M. M. Teixeira, and M. O. Rocha, "Diagnosis and management of Chagas disease and cardiomyopathy," *Nature Reviews Cardiology*, vol. 9, no. 10, pp. 576–589, 2012.

[35] R. P. Beasley, C. Trepo, C. E. Stevens, and W. Szmuness, "The e antigen and vertical transmission of hepatitis B surface antigen," *The American Journal of Epidemiology*, vol. 105, no. 2, pp. 94–98, 1977.

[36] K. Hattaf and N. Yousfi, "A generalized HBV model with diffusion and two delays," *Computers and Mathematics with Applications*, vol. 69, no. 1, pp. 31–40, 2015.

[37] M. M. Thaler, D. W. Wara, G. Veereman-Wauters et al., "Vertical transmission of hepatitis C virus," *The Lancet*, vol. 338, no. 8758, pp. 17-18, 1991.

[38] X. Meng, L. Chen, and B. Wu, "A delay SIR epidemic model with pulse vaccination and incubation times," *Nonlinear Analysis: Real World Applications*, vol. 11, no. 1, pp. 88–98, 2010.

[39] T. Zhang, X. Meng, and T. Zhang, "SVEIRS: a new epidemic disease model with time delays and impulsive effects," *Abstract and Applied Analysis*, vol. 2014, Article ID 542154, 15 pages, 2014.

[40] X. Mao, *Stochastic Differential Equations and Applications*, Horwood Publishing, Chichester, UK, 2nd edition, 1997.

[41] E. Beretta, V. Kolmanovskii, and L. Shaikhet, "Stability of epidemic model with time delays influenced by stochastic perturbations," *Mathematics and Computers in Simulation*, vol. 45, no. 3-4, pp. 269–277, 1998.

[42] J. Yu, D. Jiang, and N. Shi, "Global stability of two-group SIR model with random perturbation," *Journal of Mathematical Analysis and Applications*, vol. 360, no. 1, pp. 235–244, 2009.

[43] N. Bacaër, "On the stochastic SIS epidemic model in a periodic environment," *Journal of Mathematical Biology*, vol. 71, no. 2, pp. 491–511, 2015.

[44] C. Ji and D. Jiang, "Threshold behaviour of a stochastic SIR model," *Applied Mathematical Modelling*, vol. 38, no. 21-22, pp. 5067–5079, 2014.

[45] T. Feng, X. Meng, L. Liu, and S. Gao, "Application of inequalities technique to dynamics analysis of a stochastic eco-epidemiology model," *Journal of Inequalities and Applications*, vol. 1, article 327, 2016.

[46] X. Meng, "Stability of a novel stochastic epidemic model with double epidemic hypothesis," *Applied Mathematics and Computation*, vol. 217, no. 2, pp. 506–515, 2010.

[47] A. Gray, D. Greenhalgh, X. Mao, and J. Pan, "The SIS epidemic model with Markovian switching," *Journal of Mathematical Analysis and Applications*, vol. 394, no. 2, pp. 496–516, 2012.

[48] H. C. Tuckwell and R. J. Williams, "Some properties of a simple stochastic epidemic model of SIR type," *Mathematical Biosciences*, vol. 208, no. 1, pp. 76–97, 2007.

[49] X. Zhang, D. Jiang, A. Alsaedi, and T. Hayat, "Stationary distribution of stochastic SIS epidemic model with vaccination under regime switching," *Applied Mathematics Letters*, vol. 59, pp. 87–93, 2016.

[50] Y. Cai, Y. Kang, M. Banerjee, and W. Wang, "A stochastic SIRS epidemic model with infectious force under intervention strategies," *Journal of Differential Equations*, vol. 259, no. 12, pp. 7463–7502, 2015.

[51] W. Zhao, J. Li, T. Zhang, X. Meng, and T. Zhang, "Persistence and ergodicity of plant disease model with Markov conversion and impulsive toxicant input," *Communications in Nonlinear Science and Numerical Simulation*, vol. 48, pp. 70–84, 2017.

[52] E. Tornatore, S. M. Buccellato, and P. Vetro, "Stability of a stochastic SIR system," *Physica A: Statistical Mechanics and Its Applications*, vol. 354, no. 1-4, pp. 111–126, 2005.

[53] A. Gray, D. Greenhalgh, L. Hu, X. Mao, and J. Pan, "A stochastic differential equation SIS epidemic model," *SIAM Journal on Applied Mathematics*, vol. 71, no. 3, pp. 876–902, 2011.

[54] Y. Zhao and D. Jiang, "The threshold of a stochastic SIS epidemic model with vaccination," *Applied Mathematics and Computation*, vol. 243, pp. 718–727, 2014.

[55] Y. Lin and D. Jiang, "Long-time behaviour of a perturbed SIR model by white noise," *Discrete and Continuous Dynamical Systems. Series B*, vol. 18, no. 7, pp. 1873–1887, 2013.

[56] H. Schurz and K. Tosun, "Stochastic asymptotic stability of SIR model with variable diffusion rates," *Journal of Dynamics and Differential Equations*, vol. 27, no. 1, pp. 69–82, 2015.

[57] Q. Lu, "Stability of SIRS system with random perturbations," *Physica A. Statistical Mechanics and Its Applications*, vol. 388, no. 18, pp. 3677–3686, 2009.

[58] X. Meng, S. Zhao, T. Feng, and T. Zhang, "Dynamics of a novel nonlinear stochastic SIS epidemic model with double epidemic hypothesis," *Journal of Mathematical Analysis and Applications*, vol. 433, no. 1, pp. 227–242, 2016.

[59] F. Wei and J. Liu, "Long-time behavior of a stochastic epidemic model with varying population size," *Physica A: Statistical Mechanics and Its Applications*, vol. 470, pp. 146–153, 2017.

[60] N. Dalal, D. Greenhalgh, and X. Mao, "A stochastic model of AIDS and condom use," *Journal of Mathematical Analysis and Applications*, vol. 325, no. 1, pp. 36–53, 2007.

[61] C. Xu, "Global threshold dynamics of a stochastic differential equation SIS model," *Journal of Mathematical Analysis and Applications*, vol. 447, no. 2, pp. 736–757, 2017.

[62] A. Lahrouz and A. Settati, "Necessary and sufficient condition for extinction and persistence of SIRS system with random perturbation," *Applied Mathematics and Computation*, vol. 233, pp. 10–19, 2014.

[63] A. Lahrouz and A. Settati, "Qualitative study of a nonlinear stochastic SIRS epidemic system," *Stochastic Analysis and Applications*, vol. 32, no. 6, pp. 992–1008, 2014.

[64] D. Zhao, T. Zhang, and S. Yuan, "The threshold of a stochastic SIVS epidemic model with nonlinear saturated incidence," *Physica A. Statistical Mechanics and Its Applications*, vol. 443, pp. 372–379, 2016.

[65] Y. Zhao, Y. Lin, D. Jiang, X. Mao, and Y. Li, "Stationary distribution of stochastic SIRS epidemic model with standard incidence," *Discrete and Continuous Dynamical Systems. Series B*, vol. 21, no. 7, pp. 2363–2378, 2016.

[66] Q. Liu, D. Jiang, N. Shi, T. Hayat, and A. Alsaedi, "Stationary distribution and extinction of a stochastic SIRS epidemic model with standard incidence," *Physica A. Statistical Mechanics and Its Applications*, vol. 469, pp. 510–517, 2017.

[67] D. Jiang, Q. Liu, N. Shi, T. Hayat, A. Alsaedi, and P. Xia, "Dynamics of a stochastic HIV-1 infection model with logistic growth," *Physica A. Statistical Mechanics and Its Applications*, vol. 469, pp. 706–717, 2017.

[68] Y. Cai, Y. Kang, M. Banerjee, and W. Wang, "A stochastic epidemic model incorporating media coverage," *Communications in Mathematical Sciences*, vol. 14, no. 4, pp. 893–910, 2016.

[69] N. T. Dieu, D. H. Nguyen, N. H. Du, and G. Yin, "Classification of asymptotic behavior in a stochastic SIR model," *SIAM Journal on Applied Dynamical Systems*, vol. 15, no. 2, pp. 1062–1084, 2016.

[70] N. H. Du and N. N. Nhu, "Permanence and extinction of certain stochastic SIR models perturbed by a complex type of noises," *Applied Mathematics Letters*, vol. 64, pp. 223–230, 2017.

[71] Q. Liu and Q. Chen, "Analysis of the deterministic and stochastic SIRS epidemic models with nonlinear incidence," *Physica A. Statistical Mechanics and Its Applications*, vol. 428, pp. 140–153, 2015.

[72] Z. Chang, X. Meng, and X. Lu, "Analysis of a novel stochastic SIRS epidemic model with two different saturated incidence rates," *Physica A. Statistical Mechanics and Its Applications*, vol. 472, pp. 103–116, 2017.

[73] X. Zhang, D. Jiang, T. Hayat, and B. Ahmad, "Dynamics of a stochastic SIS model with double epidemic diseases driven by Lévy jumps," *Physica A. Statistical Mechanics and Its Applications*, vol. 471, pp. 767–777, 2017.

[74] Y. Zhou, S. Yuan, and D. Zhao, "Threshold behavior of a stochastic SIS model with Lévy jumps," *Applied Mathematics and Computation*, vol. 275, pp. 255–267, 2016.

[75] C. Li, Y. Pei, X. Liang, and D. Fang, "A stochastic toxoplasmosis spread model between cat and oocyst with jumps process," *Communications in Mathematical Biology and Neuroscience*, 2016.

[76] D. Jiang, C. Ji, N. Shi, and J. Yu, "The long time behavior of DI SIR epidemic model with stochastic perturbation," *Journal of Mathematical Analysis and Applications*, vol. 372, no. 1, pp. 162–180, 2010.

[77] M. Liu, C. Bai, and K. Wang, "Asymptotic stability of a two-group stochastic SEIR model with infinite delays," *Communications in Nonlinear Science and Numerical Simulation*, vol. 19, no. 10, pp. 3444–3453, 2014.

[78] Q. Liu, D. Jiang, N. Shi, T. Hayat, and A. Alsaedi, "Asymptotic behavior of a stochastic delayed SEIR epidemic model with nonlinear incidence," *Physica A. Statistical Mechanics and Its Applications*, vol. 462, pp. 870–882, 2016.

[79] X. Li, X. Lin, and Y. Lin, "Lyapunov-type conditions and stochastic differential equations driven by G-brownian motion," *Journal of Mathematical Analysis and Applications*, vol. 439, no. 1, pp. 235–255, 2016.

[80] H. Ma and Y. Jia, "Stability analysis for stochastic differential equations with infinite Markovian switchings," *Journal of Mathematical Analysis and Applications*, vol. 435, no. 1, pp. 593–605, 2016.

[81] A. Lahrouz and L. Omari, "Extinction and stationary distribution of a stochastic SIRS epidemic model with non-linear incidence," *Statistics and Probability Letters*, vol. 83, no. 4, pp. 960–968, 2013.